FCT
Fundação para a Ciência e a Tecnologia
MINISTÉRIO DA EDUCAÇÃO E CIÊNCIA

POPH
QUALIFICAR É CRESCER.

QREN
QUADRO DE REFERÊNCIA ESTRATÉGICO NACIONAL
PORTUGAL 2007.2013

Governo da República Portuguesa

UNIÃO EUROPEIA
Fundo Social Europeu

Antibacterial Glass and Glass-Biodegradable Matrix Composites for Bone Tissue Engineering
João Pedro Silva Fernandes
UMinho | 2017

Universidade do Minho
Escola de Engenharia

João Pedro Silva Fernandes

Antibacterial Glass and Glass-Biodegradable Matrix Composites for Bone Tissue Engineering

January 2017

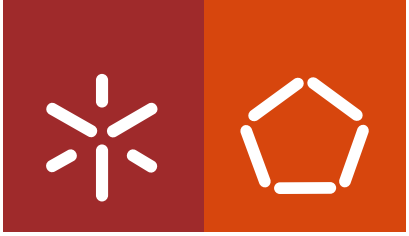

Universidade do Minho
Escola de Engenharia

João Pedro Silva Fernandes

Antibacterial Glass and Glass-Biodegradable Matrix Composites for Bone Tissue Engineering

PhD thesis in Materials Engineering

Supervisors:
Professor Rui Luís Gonçalves Reis
Doutor Ricardo Alexandre Rodrigues Pires

January 2017

STATEMENT OF INTEGRITY

I hereby declare having conducted my thesis with integrity. I confirm that I have not used plagiarism or any form of falsification of results in the process of the thesis elaboration.
I further declare that I have fully acknowledged the Code of Ethical Conduct of the University of Minho.

University of Minho, January 3rd, 2017

Full name: João Pedro Silva Fernandes

Signature: _____.

"Meu sono é de armas e mar

Minha força é navegar

Meu norte em contraluz

Meu fado é vento que leva

E conduz."

Tiago Bettencourt

À minha Família.

ACKNOWLEDGEMENTS

This PhD was an outstanding experience. Along with the scientific knowledge acquired, it comprised a journey of personal and cultural development that resulted in a unique and memorable step in my life. The work described here would not be possible without the support and contribution of several people and institutions. To them, I would like to genuinely express my gratitude and dedicate this PhD thesis.

First of all, I would like to express my gratitude to my supervisor, Professor Rui L. Reis, which allowed me to be part of the 3B's Research Group and to achieve this great life project, my PhD. His strength of character and motivation, which are continuous driving force that places 3B's Research Group in the cutting-edge of tissue engineering research worldwide served as example and mentoring during this project. A special thanks goes to my co-supervisor, Dr Ricardo A. Pires, who believe me at first. In which his patience and his encouragement guided me trough the development of my PhD. He was there to meet and discuss about new ideas, to proofread papers and improve its contents.

I would like to acknowledge Professor Paul Vincent Hatton. I am profoundly grateful for welcomed me as part of the group, Bioengineering and Health Technologies Research Group, School of Clinical Dentistry at University of Sheffield. He taught me how to ask questions and express my ideas. I thank you for the support and mentoring. I would also like to acknowledge: Dr Piergiorgio Gentile, who received and guided me trough the scientific adventure at UK. For all your scientific support, the incentives, creativity and your kindness. Dr Cheryl Miller, Dr Aileen Crawford and Robert Moorehead for sharing your knowledge with me. It was a privilege to work in such an environment and team.

To the Portuguese Foundation for Science and Technology for the financial support through my PhD grant (BD/73162/2010). This work was also partially supported by the European Union's Seventh Framework Programme (FP7/2007–2013) under Grant No. REGPOT-CT2012-31633-POLARIS and UK EPSRC Centre for Innovative Manufacturing of Medical Devices-MeDe Innovation (EPSRC grant EP/K029592/1).

To Professor Maria Helena V. Fernandes for welcoming me at her group Biomedical and Biomimetic Materials, Department of Materials and Ceramic Engineering, University of

Aveiro. Thank you for the opportunity and availability. Thank you Margarida Martins for her special care and availability to collaborate and helping improve my work.

Thanks to all the friends I made and colleagues that I had the pleasure to met at the 3B's Group, especially to those who shared a lab bench, a lab space or an awkward moment. To Diana, Ana, Clarinha, Dianinha, Tininha, Ivo, Alex and Pedro for all the amazing moments we spent together, for the friendship, understanding and support; and the brainstorming's, which made our ideas clearer (or not). Thanks to the group F&FCB&K for the out of the "box" problems solving, which made daily science discussions alive!

Thanks to all the friends and colleagues from Sheffield, which helped me and made my life happier. A special thanks to Saima, Sarah, Raghu, Cristina, Diana, Priyanka, Sofia, Rob and Saleem…

We sometimes forget people who were essential for the achievement of our project. I would not be here without their work and their help from the beginning to the end. For these reasons, I would like to thank all the staff members and technicians I had the pleasure to work with. The lab would not turn round if you were not there, you rock!

Diana and Ana. For all, just because it is easily converted in "For-ever".

E por fim, quero agradecer à minha família e amigos, apenas por serem Família e Amigos. Quero partilhar o sentimento especial à **Mãe**, ao **Pai** e à **Diana**. Simplesmente porque são e serão sempre parte de mim e com toda a certeza passaram comigo por todos os (maus e bons) momentos que eu passei durante este projeto da minha vida.

ABSTRACT

Multiple joint and bone diseases affect millions of people worldwide. In fact the Bone and Joint Decade's association predicted that the percentage of people over 50 years of age affected by bone diseases will double by 2020. Bone diseases commonly require the need for surgical intervention, often involving partial or total bone substitution. Therefore biodegradable biomaterials designed as bone tissue engineered (BTE) devices to be implanted into the human body, function as a short-term template for regeneration of bone defects. They should be biologically active, osteoconductive, strongly bonding to bone tissue, while being osteoinductive, stimulating cell ingrowth and extra cellular matrix (ECM) deposition, leading to bone formation. The huge increase in surgeries to the joint and bone to implant biomedical devices led to an increase on MDAIs. This can lead to the failure of the device, frequently demanding for prolonged usage of antibiotic therapies. Currently, there is a pressing clinical need to develop innovative biomaterials or device surfaces that provide a dual functionality: bone tissue regeneration and inhibition of the proliferation of pathogenic microorganisms.

In this thesis it is proposed the development of a system that could be efficiently, and successfully applied as a BTE device. Due to its great potential, the emphasis of the work was on the design of BBGs presenting osteoconductive, osteoinductive and antibacterial properties. BBGs incorporating different divalent cations (i.e. Mg^{2+}, Ca^{2+}, Sr^{2+}) were synthesised and consistently evaluated the influence of the different divalent cations on their cytotoxicity (Chapter III), bioactive and antibacterial (Chapter IV), and osteogenic (Chapter V) potential. It was demonstrated that: i) the controlled crystallisation of BBGs produce glass-ceramics with less cytotoxic effects on cells (i.e. L929 cells); ii) the BBG-Ca and BBG-Sr glasses are osteoconductive, presenting the ability to form an apatite layer at their surface, whereas the BBG-Mg and BBG-Sr glasses (9, to 72 $mg \cdot ml^{-1}$) present antibacterial properties (specially, BBG-Sr, that was able to eradicate *Pseudomonas aeruginosa* at concentrations $\geq$ 18 $mg \cdot ml^{-1}$); and iii) the BBG-Mg and BBG-Sr induced an overexpression of bone-specific proteins (i.e. ALP, OP and OC) and high mineralisation of bone marrow mesenchymal stem cells (BM-MSCs) culture under osteogenic media for glass concentrations between 20 and 50 $mg \cdot ml^{-1}$. Outstandingly,

BBG-Sr at a concentration of 50 $mg \cdot ml^{-1}$ was able to increase the mineralisation and expression of bone-specific proteins even under basal media conditions.

After demonstrating the potential of BBGs to promote the osteogenic differentiation of stem cells and their proliferation, as well as the antibacterial activity of these glass compositions, BBG glass particles were combined with a biodegradable matrix of poly L lactic acid (PLLA) to generate three-dimensional (3D) composite scaffolds as BTE devices. Specifically, the the incorporation of those BBG glass particles into a PLLA fibrous by the wet spinning technique was tested to form PLLA-BBG scaffolds (Chapter IV). It was demonstrated that these composites were biodegradable, bioactive and non-cytotoxicity towards human osteosarcoma cell line (SaOs-2) and human adipose-derived stem cells (hASCs). The last experimental chapter (Chapter VII), reports the fabrication of PLLA- strontium containing- BBG (PLLA-BBG-Sr) composite membranes by electrospinning. From this study we verified that the incorporation of BBG-Sr into the PLLA membranes enhanced their mechanical properties (improving Young modulus and tensile strength) and increased the degradability with a continuous release of ions and water uptake. Furthermore, cellular *in vitro* evaluation with BM-MSCs demonstrated that the develop PLLA-BBG-Sr membranes stimulated alkaline phosphatase (ALP) activity and up-regulated osteogenic related gene expression (i.e. *Alpl*, *Sp7* and *Bglap*) under osteogenic culture conditions promoting the osteogenic differentiation of BM-MSCs.

The results presented in thesis show that BBGs and the biodegradable PLLA-BBG composites present the capacity of actively enhancing cell adhesion, proliferation and osteogenic differentiation, as well as controlling bacterial infections. Moreover, the reinforcement of PLLA membranes with BBG show great potential to achieve an effective biomedical device for bone regeneration.

BIOVIDROS E COMPÓSITOS BIOVIDRO-POLÍMEROS BIODEGRADÁVEIS PARA ENGENHARIA DE TECIDOS ÓSSEOS

RESUMO

Doenças ósseas e de articulações afectam milhões de pessoas por tudo o mundo. De facto, a associação Bone and Joint Decade's prevê que o número de pessoas com idades superiores a 50 anos afectadas por doenças ósseas vá aumentar para o dobro até 2020. Este tipo de doenças requer normalmente intervenção cirúrgica com substituição parcial ou total do osso. A engenharia de tecidos ósseos (ETO) utiliza materiais biodegradáveis para criar dispositivos implantáveis no corpo humano, funcionando como suporte temporário ao passo que regeneram o osso. Estes biomateriais devem ser: osteocondutores, ligando-se fortemente aos tecidos ósseos; e osteoindutores, estimulando o crescimento celular e deposição de matriz extra celular para a formação de novo osso. O aumento do número de intervenções cirúrgicas está diretamente relacionado com um elevado número de infecções associadas a implantes ósseos (IAIO), que pode levar ao uso prolongado de antibióticos ou à rejeição do implante. Atualmente existe uma grande necessidade de desenvolver biomateriais e dispositivos médicos que possuam a dupla funcionalidade: regeneração óssea e inibição de proliferação de microrganismos.

O objectivo deste projeto de doutoramento é desenvolver um dispositivo médico baseado nos princípios ETO. Devido ao seu grande potencial, o enfâse deste trabalho focou no desenvolvimento de vidros bioactivos com matriz de borossilicatos (BBGs) dotados com propriedades osteocundutoras, onsteoindutoras e antibacterianas. BBGs com diferentes catiões bivalentes incorporados (ex. Mg^{2+}, Ca^{2+}, Sr^{2+}) foram sintetizados e sistematicamente avaliados quanto à sua influência relativamente ao seu potencial citotóxico (Capítulo III), antibacteriano (Capítulo IV) e osteogénico (Capítulo V). Foi demostrado: i) que uma cristalização controlada dos vidros origina vidro-cerâmicos com menores efeitos citotóxicos para as células (ex. L929); ii) que BBG-Ca e BBG-Sr revelaram grande capacidade osteocondutora, apresentando a formação de camadas de apatite na sua superfícies, e que BBG-Mg e BBG-Sr (9–72 $mg \cdot ml^{-1}$) exibiram propriedades antibacterianas (especialmente, BBG-Sr que foi capaz de erradicar *Pseudomonas aeruginosa* para concentrações $\geq$ 18 $mg \cdot ml^{-1}$); e iii) BBG-Mg e BBG-Sr induziram a superexpressão de proteínas específicas do osso (ex. ALP, OP e OC) com

elevada mineralização das células estaminais da medula óssea (BM-MSCs) cultivadas em meio osteogénico com concentrações entre 20 e 50 $mg \cdot ml^{-1}$. De forma extraordinária, BBG-Sr a concentrações de 50 $mg \cdot ml^{-1}$ demonstrou capacidade de mineralização e expressão de proteínas específicas do osso mesmo em meio de cultura basal.

Após demonstrada a capacidade antibacteriana, de promover a diferenciação osteogénica de células estaminais e a sua proliferação; as partículas de BBG foram combinadas com uma estrutura polimérica degradável de ácido poli-L-láctico (PLLA) para o fabrico de compósitos tridimensionais (3D). A incorporação dessas partículas BBG numa estrutura fibrosa de PLLA através de técnica extrusão húmida foi testada para o fabrico de compósitos PLLA-BBG (capítulo IV). Foi demonstrado também que estes compósitos são biodeagradáveis, com grande capacidades bioactivas, não apresentando citotoxicidade em cultura com células osteoblásticas derivadas de osteossarcoma humano (SaOS-2), bem como com células humanas estaminais derivadas de tecido adiposo (hASCs). O último capítulo experimental (Capítulo VII), descreve o fabrico de membranas compostas por PLLA – vidros bioactivos borossilicatos com estrôncio (PLLA-BBG-Sr) através da técnica de electro-fiação. Após este estudo verificamos que a incorporação de partículas de vidro BBG-Sr nas membranas PLLA provoca um incremento das suas propriedades mecânicas (aumento de módulo de Young e da resistência à tração) bem como um aumento da degradabilidade com uma contínua libertação de iões e absorção de água. Para além disso, estudos *in vitro* com BM-MSCs demonstraram que as membranas de PLLA-BBG-Sr tem a capacidade de estimular a atividade da fosfatase alcalina (ALP) e superexpressar genes específicos do osso (ex. *Alpl*, *Sp7* e *Bglap*) em condições de culturas osteogénicas, promovendo a diferenciação osteogénica das BM-MSCs

Os resultados deste projeto de doutoramento demonstram que partículas de vidro BBG e os compósitos biodegradáveis PLLA-BBG têm uma enorme capacidade de suportar e ativamente aumentar a adesão, proliferação celular e diferenciação osteogénica, bem como controlar infecções bactérias ósseas. Além do mais, o reforço das membranas de um PLLA com a adição de partículas de vidro BBG demonstrou enorme potencial para o desenvolvimento de dispositivos biomédicos para a regeneração de tecidos ósseos.

TABLE OF CONTENTS

LIST OF ABBREVIATIONS

1-10

2D: two-dimensional

2θ: diffraction angle

3D: three-dimensional

A

≈: approximate

αMEM: α-minimum essential medium

Ag^{+}: silver

Al_2O_3: aluminium oxide

ALP: alkaline phosphatase

Alpl: alkaline phosphatase gene

ACP: amorphous calcium phosphate

Å: Angstrom

ASTM: Standard Test Method for Tensile Properties of Plastics

ATCC: American Type Culture Collection

ATR-FTIR: attenuated total reflection Fourier transform infrared spectroscopy

B

$(BO_3)^{3-}$: borate

B: boron

B_2O_3: di-boron trioxide

BBGs: borosilicate bioactive glasses

BBGC: borosilicate bioactive glass-ceramic

BBG-Mg, -Ca, -Sr: borosilicate bioactive glasses containing –magnesium, -calcium, and –strontium

BD: broth dilution method

BBG-Cu: copper doped borosilicate glasse

Bglap: bone gamma-carboxyglutamate protein gene

BGs: bioactive glasses

BM-MSCs: bone marrow mesenchymal stem cells

BTE/ ETO: bone tissue engineering/ engenharia de tecidos ósseos

C

Ca: calcium

$Ca(BO_2)_2$: calcium borate

$Ca_3(PO_4)_2$: tricalcium phosphate

$CaCO_3$: calcium carbonate

CaF_2: calcium fluoride

CaO: calcium oxide

$CaSiO_3$: wollastonite-2M

CDDEP: Center for Disease Dynamics, Economics & Policy

cDNA: complementary DNA

CECT: Colección Española de Cultivos Tipo

CFU: colony forming Uunits

cm: centimetres

CO_2: carbon dioxide

Cu: copper

D

º: degrees

ºC: degrees Celsius

Ø: diameter

DAPI: *4',6'*-diamidino-*2*-phenylindole

DD: disc diffusion method

Df: dilution factor

DMEM: dulbecco's modified eagle medium

DNA: deoxyribonucleic acid

DSC: differential scanning calorimetry

dsDNA: double-stranded deoxyribonucleic acid

DTA: differential thermal analysis

E

ECM: extra cellular matrix

EDS: energy dispersive X-ray spectroscopy

EDTA: ethylenediaminetetraacetic acid

F

FBS: fetal bovine serum

FDA: Food and Drug Administration

G

Gapdh: glyceraldehyde-3-phosphate dehydrogenase gene

G: gauge

GIC: glass-ionomer cements

G: grams

H

h: hour

HA: hydroxyapatite

hASCs: human adipose-derived stem cells

HR: humidity relative

I

ICP-AES: inductively coupled plasma-atomic emission spectrometry

ISO: International Organization for Standardization

J

JCPDS: Joint Commission on Powder Diffraction Standards

K

kN: kiloNewton

kPa: kiloPascal

kv: kiloVolt

L

l: litre

L929: mouse fibroblast-like cell line

λ: wavelength

M

M: molar

mA: miliAmpere

µA: microAmpere

µCT: micro-computed tomography

MDAI/ IAIO: medical-device associated infections/ infecções associadas a implantes ósseos

m_f: is the mass of the dried specimen after its immersion in water

m_f: initial mass of the specimen

mg: milligrams

µg: micrograms

Mg: magnesium

$Mg_2(SiO_3)_2$: magnesium silicate

$Mg_2B_2O_5$: magnesium borate

$Mg_3(PO_4)_2$: magnesium phosphate

MgO: magnesium oxide

MH: Muller Hinton media

min: minute

ml: millilitres

µl: microliters

Mm: millimetre

mM: milimolar

μm: micrometres

MPa: megaPascal

ms: milliseconds

m_{tp}: wet mass of the specimen

MTS: 3-(4,5-dimethylthiazol-2-yl)-5-(3-carboxymethoxyphenyl)-2-(4-sulfofenyl)-2H-tetrazolium

N

Na: sodium

Na_2O: sodium oxide

$NaHCO_3$: sodium bicarbonate

NEAA: non-essential amino acids

ng: nanogram

nm: nanometre

nM: nanomolar

O

OH-: hydroxyl

OC: osteocalcin

OP: osteopontin

O: oxygen

P

%: percentage

P: phosphorus

P_2O_5: phosphorus pentoxide

PBS: phosphate-buffered saline

PCL: polycaprolactone

pg: pictogram

PLDL: poly D lactic acid

PLA: poly lactic acid

PLLA-BBG: poly-L-lactic acid-borosilicate bioactive glasses

PLLA-BBG-Mg, -Ca, or -Sr: poly-L-lactic acid-borosilicate bioactive glasses containing -magnesium, -calcium, or -strontium

PLLA: poly-L-lactic acid

pNPP: p-nitrophenyl phosphatase

ppm: parts-per million

R

RNA: ribonucleic acid

ROS: reactive oxygen species

rpm: rotations per minute

RT: room temperature

rtPCR: real-time quantitative polymerase chain reaction

Runx2: runt-related transcription factor 2

S

s: seconds

Saos-2: human osteosarcoma cell line

SBF: simulated body fluid

SD: standard deviation

SEM: scanning electron microscopy

Si: silicon

SiO_2: silicon dioxide

Sp7: Sp7 transcription factor gene

Spp1: secreted phosphoprotein 1 gene

Sr: strontium

$Sr_2B_2O_5$: strontium borate

$SrCO_3$: strontium carbonate

Sr-HA: strontium-substituted bone-like apatite

$SrSiO_3$: strontium silicate

SrO: strontium oxide

T

T_c: crystallisation temperature

T_g: The mid point of glass transition temperature

TGA: thermogravimetric analysis

T_m: The mid point of glass crystallisation temperature

TSA: tryptone soya agar

U

U: units

V

v/v: volume per volume

V_E: volume of samples/ALP standard solution

V_F: volume of final solution

W

w/v: weight per volume

w/w: weight per weight

WL: weight loss

WD: working distance

WU: water uptake

X

XRD: X-ray powder diffraction

XRF: X-ray fluorescence

Z

Zn: zinc

LIST OF FIGURES

LIST OF TABLES

SHORT CURRICULUM VITÆ

João Pedro Silva Fernandes was born in Braga, Portugal, in 1984. He is a PhD student at the 3B's Research Group (Biomaterials, Biodegradables and Biomimetics), University of Minho, Braga, Portugal. His work is supervised by Professor Rui L. Reis, Director of the 3B's Research Group, Professor Paul V. Hatton, from the Centre for Biomaterials and Tissue Engineering, University of Sheffield, United Kingdom and Dr. Ricardo A. Pires from 3B's Research Group.

He has a integrated Master degree in Biological Engineering (Chemistry and Food Specialisation) from the Biological Department of the University of Minho, Portugal that he finished with a final graduation mark of 15 (0-20 scale). In the final stage of his degree, he was a research trainee at the Fluxome A/S, a biotechnology research company from Copenhagen, Denmark working in the research and development of a project to produce and purify polyunsaturated fatty acids (PUFA) under the supervision of Professor Isabel Rocha, Assistant Professor at Department of Biological Engineering and Jochen Forster Co-Founder and Senior Scientist at Fluxome A/S, where he received a traineeship mark of 17 (0- 20 scale).

In January 2010, he began his career as scientific researcher in a project based on a collaboration between the 3B's Research Group and Corticeira Amorim regarding the recovery of by-products from cork industry. He formally started his PhD at the 3B's Research Group with a main focus on bone tissue engineering. In September 2011, he received a grant from the Portuguese Foundation for Science and Technology (FCT) that enabled him to perform work at the University of Sheffield, UK. During the course of his PhD research he has participated with oral presentations at UK Society for Biomaterials (UKSB) 2015, Belfast, United Kingdom and at 27th European Conference on Biomaterials (ESB) Conference 2015, Krakow, Poland. He has been an invited reviewer for Biomatter: A new journal in Biomaterials and Tissue Engineering. Currently he is a Research Associate at CURAM, NUI Galway, Ireland enrolled into a industrial project with Collagen Solutions plc, UK.

As a researcher in the 3B's Research Group, he has been involved in several management activities from the very beginning involved in the writing, preparation, and supporting management of several academic and industrial reports. He was a member of the organising committees of 11th Delegates Assembly 2016, from European chemical Sciences / European Young Chemist Network.

As results of his research work, he attended several important international meetings in his field of research mostly with oral communications. Presently, he is author of 6 research papers (6 as first author; 4 published and 2 submitted), and 7 international communications (oral and poster).

LIST OF PUBLICATIONS

The work performed during this PhD resulted in the following publications:

INTERNATIONAL JOURNAL WITH REFEREES

João S. Fernandes, Piergiorgio Gentile, Robert Moorehead, Aileen Crawford, Cheryl A. Miller, Ricardo A. Pires, Paul V. Hatton, Rui L. Reis; Design and Properties of Novel Borosilicate Bioactive Glasses for Bone Tissue Applications, Crystal Growth and Design 2016, 16 (7), pp 3731–3740

João S. Fernandes, Margarida Martins, Nuno M. Neves, Maria H. Fernandes, Rui Reis, Ricardo A. Pires; Intrinsic Antibacterial Borosilicate Glasses for Bone Tissue Engineering Applications, ACS Biomaterials Science & Engineering 2016, 2 (7), pp 1143–1150

João S. Fernandes, Rui Reis, Ricardo A. Pires; Poly-L-(Lactic Acid)-Borosilicate Bioactive Glass Scaffolds for Guided Bone Regeneration, Materials Science and Engineering: C 2016 (http://dx.doi.org/10.1016/j.msec.2016.10.007)

João S. Fernandes, Piergiorgio Gentile, Margarida Martins, Nuno M. Neves, Cheryl Miller, Aileen Crawford, Ricardo A. Pires, Paul Hatton, Rui L. Reis; Reinforcement of Poly L lactic acid Electrospun Membranes by Addition of Strontium Borosilicate Glasses for Bone Tissue Engineering, Acta Biomaterialia 2016 Oct 15;44:168-77

João S. Fernandes, Piergiorgio Gentile, Ricardo A. Pires, Rui L. Reis, Paul V. Hatton; Multi-functional Bioactive Glass and Glass-Ceramic Biomaterials with Antibacterial Properties for Repair and Regeneration of Bone Tissue (2016); under peer revision.

João S. Fernandes, Piergiorgio Gentile, Aileen Crawford, Ricardo A. Pires, Paul V. Hatton, Rui L. Reis; Substituted Borosilicate Glasses with Improved Osteogenic Properties for Bone Tissue Engineering (2016); under peer revision.

ORAL PRESENTATIONS IN INTERNATIONAL MEETINGS, AS FIRST AUTHOR

João S. Fernandes, Piergiorgio Gentile, Robert Moorehead, Aileen Crawford, Cheryl A. Miller, Ricardo A. Pires, Paul V. Hatton, Rui L. Reis; The Design and Properties of Novel Borosilicate Bioactive Glasses - UKSB, Belfast, UK, June, 2015.

João S. Fernandes, Margarida Martins, Rui L. Reis, Ricardo A. Pires; Antibacterial Borosilicate Bioactive Glasses for Bone Tissue Engineering – ESB, Krakow, Poland, August 2015.

POSTER PRESENTATIONS IN INTERNATIONAL MEETINGS, AS FIRST AUTHOR

João S. Fernandes, Margarida Martins, Rui L. Reis, Ricardo A. Pires; Antibacterial Silica-borate Glasses for Bone Tissue Engineering – 3rd ICVS-3B's Associated Laboratory Meeting, Braga, Portugal, June, 2013.

João S. Fernandes, Ricardo A. Pires, Rui L. Reis; Silica-Borate Glasses for Bone Tissue Engineering Applications - 1st POLARIS Workshop Conference, Porto, Portugal, October 2013.

João S. Fernandes, Margarida Martins, Ricardo A. Pires, Rui L. Reis; Antibacterial Silica-borate Glasses for Bone Tissue Engineering Applications TERM STEM, Porto, Portugal, October, 2013.

João S. Fernandes, Margarida Martins, Nuno M. Neves, Ricardo A. Pires, Rui L. Reis; Antibacterial Glass Formulation for Bone Tissue Engineering Applications – TERMIS-EU, Genova, Italy, June, 2014.

João S. Fernandes, Ricardo A. Pires, Rui L. Reis; PLA-Glass Composites for Bone Tissue Engineering - ESB, Liverpool, UK, September 2014.

João S. Fernandes, Ricardo A. Pires, Rui L. Reis; Borosilicate Glasses / PLA Composites for Bone Tissue Engineering – TERM STEM, Porto, Portugal, 2015.

João S. Fernandes, Margarida Martins, Nuno M. Neves, Ricardo A. Pires, Rui L. Reis; Antibacterial Glass Formulation for Bone Tissue Engineering Applications – 10th Biomaterials World Congress, Montreal, Canada, May, 2016.

INTRODUCTION TO THE THESIS STRUCTURE

The present thesis is organised in **four sections** comprising **eight different chapters**, with five of them being of experimental research. According to the 3B's Research Group internal policy, the thesis format is based on published or submitted papers, including the introduction section that consists of a review paper. The contents of each chapter are summarised below.

SECTION 1 (Chapter I) - Review

Chapter I present a comprehensive overview on modifications and compositional changes of glass and glass ceramic biomaterials to further enhance their osteogenic behaviour and/or antimicrobial properties for the regeneration of bone tissue. It includes a brief introduction regarding the joint and bone diseases and medical-device associated infections (MDAIs) followed by the concepts and strategies using glass and glass-ceramic biomaterials to improve the osteogenic and antimicrobial properties of biomedical devices. It is also included a detailed description of the currently available solution to overcome the MDAIs, as well as their modes for action.

SECTION 2 (Chapter II)

Chapter II presents the materials and experimental methods used within the scope of this thesis. Even tough each experimental chapter is comprised by it specific materials and methods section, this chapter intends to comprise and compile the relevant information on this matter.

SECTION 3 (Chapters III to VII)

These chapters describe the experimental work performed within the scope of this thesis.

Chapter III describes the design and properties of novel substituted borosilicate bioactive glasses (BBGs) synthesised by melt quenching and their potential cytotoxicity towards mouse fibroblast-like cell line (L929) cultures.

Chapter IV outlines the *in vitro* evaluation of BBGs as antibacterial agents against the main bone infection-related bacterial species. Furthermore, it reports the bioactivity character of BBGs.

Chapter V studies the capacity of BBGs to promote the osteogenic differentiation of bone marrow mesenchymal stem cells (BM-MSCs). The different BBGs were investigated regarding their biological activity in terms of viability, proliferation, and differentiation of BM-MSCs.

Chapter VI describes the development of poly-L-lactic acid-borosilicate bioactive glasses (PLLA-BBG) fibrous scaffolds by wet spinning, and the *in vitro* evaluation for their biodegradability, bioactivity and biological response using human osteosarcoma cell line (SaOs-2) and human adipose-derived stem cells (hASCs)

Chapter VII presents the final experimental study performed within the work of this thesis. This last study reports, for the first time, the combination of poly-L-lactic acid (PLLA) with a strontium BBG (BBG-Sr) using electrospinning to generate a composite bioactive membrane of PLLA loaded with BBG-Sr glass particles (PLLA-BBG-Sr). It was investigated the impact of the incorporation of BBG-Sr glass particles in to the PLLA fibre meshes on their tensile strength and degradation, as well as evaluated the response of BM-MSCs in the presence of PLLA-BBG-Sr fibres, namely in what regards their morphology, proliferation and ability to induce its differentiation.

SECTION 4 (Chapter VIII)

Chapter VIII contains a summary of the results achieved and the general conclusions from this thesis. Specific remarks and future prospects are also provided.

1. SECTION

I. CHAPTER

INTRODUCTION

Multifunctional Bioactive Glass and Glass-Ceramic Biomaterials with Antibacterial Properties for Repair and Regeneration of Bone Tissue

I. CHAPTER

Multifunctional Bioactive Glass and Glass-Ceramic Biomaterials with Antibacterial Properties for Repair and Regeneration of Bone Tissue[1]

Abstract

Bioactive glasses (BGs) and related glass-ceramic biomaterials have been used in bone tissue repair for over 30 years. Previous work in this field was comprehensively reviewed including by their inventor Larry Hench, and the key features and properties of BGs are well understood. More recently, attention has focused on their modification to further enhance the osteogenic behaviour, or further compositional changes that may introduce additional properties such as antimicrobial activity. Evidence is emerging that BGs and related glass-ceramics may be modified in such a way as to simultaneously introduce more than one desirable property. The aim of this review is therefore to consider the evidence that these more recent inorganic modifications to glass and glass-ceramic biomaterials are effective, and whether or not these new compositions represent sufficiently versatile systems to underpin the development of a new generation of truly multifunctional biomaterials to address pressing clinical needs in orthopaedic, craniofacial and dental surgery.

[1] This chapter is based on the following publication:

João S. Fernandes, Piergiorgio Gentile, Ricardo A. Pires, Rui L. Reis, Paul V. Hatton; Glass & Glass-ceramic Biomaterials with Intrinsic or Enhanced Antimicrobial Properties for Repair and Regeneration of Bone Tissue (2016); under peer revision.

1. Introduction

Multiple degenerative and inflammatory joint and bone diseases affect millions of people worldwide. In fact, in 2007 the Bone and Joint Decade's association predicted that the percentage of people over 50 years of age affected by bone diseases will double by 2020 [1, 2]. The huge increase in joint and bone implant surgeries parallels that of medical-device associated infections (MDAIs) [3-7]. Bacterial infections associated with contamination of implanted medical devices are a critical complication that often leads to the failure of the implant with significant impact concerning public health in developed countries [8-10]. Moreover, the management of MDAIs often requires the need for surgical intervention or/and prolonged usage of intravenous or oral antibiotic therapies leading to bone loss and significant morbidity resulting in severe limitations to the patients regarding normal life and wellbeing [7, 11, 12].

To summarise, there is now a pressing clinical need to develop innovative biomaterials or device surfaces that provide the dual functionality of both: bone tissue regeneration and inhibition of pathogenic microorganisms. Such a technology would contribute significantly to a surgical solution to the problem of increasing infection rates in the most vulnerable patient groups. Extensive research have led to the development of bioactive glasses (BGs) and related glass-ceramics with excellent biocompatibility and bioactivity [2, 13-20]. However, clinical applications have so far been limited to what bone bonding and integration concerns. Their range of uses can be extended significantly by a better understanding of the structural role of each component in the glass, allowing intelligent design of the glass and glass-ceramics and thus introducing multifunctionality.

The purpose of this review is to determine whether or not BGs and related glass-ceramic biomaterials have the potential to provide the first generation of multifunctional biomaterials for the manufacture of advanced medical devices for bone surgery in orthopaedic, craniofacial and dental surgery. In addition, the authors will consider how inorganic modifications to glass and glass-ceramics can be used to introduce greater multifunctionality to create a new generation of versatile, multifunctional materials for biomedical applications.

2. Bioactive glass and glass-ceramic biomaterials

Since 1969, Hench [21] and their co-workers were largely responsible for the development of bioactive glasses (BGs) and study their bone bonding properties. Later, the work in this field was comprehensively reviewed by Rees Rawlings [22] in 1993, which included a description of the key features and properties of BGs and their glass-ceramics derivatives. In this framework, remarkable developments in the glass and glass-ceramic biomaterials for bone and joint repair and replacement have been made in the last 5 decades. It began with the development of a "bioinert" material, only aiming to minimise the scar tissue formation at the surface of the host tissue. Then, after extensive research it evolved to a BG concept, such as Bioglass® 45S5 with extraordinary interfacial bond properties between implants and bone [23]. Later, a third generation of biomaterials that aiming functional properties such as enhanced cell proliferation and osteogenic properties or even more recently the antibacterial activity, either by inorganic modifications and/or by intelligent design of the glass and glass-ceramics [1, 18, 20, 21, 24-28]. BGs and in particular the mechanisms responsible for their behaviour in the body have been reviewed extensively by some of the leading figures in the field [29-31]. Their sections on BG science were comprehensive and the subject is therefore only covered briefly here. However, relatively little attention has been paid to the development of antimicrobial glasses, and this is therefore reviewed in far more detail in Section 3, as well as their mechanisms of action in Section 4.

Glass biomaterials can predominantly be fabricated either by the traditional melt-quench or sol-gel processes, where a number of simple compounds are able to mix and solidify as a glass [32-35]. The glass structure is composed of network formers (e.g. Si^{4+}, B^{3+} and P^{3+}), usually silica, which contributes to the network formation containing either intermediate oxides (e.g. Al^{3+}, Zn^{2+}, Mg^{2+}) and/or network modifiers (e.g. Sr^{2+}, Ca^{2+}, Na^{+}). Intermediate oxides, depending on the composition of the glass, may play a network or disrupting function, while network modifiers disrupt the network and produce non-bridging oxygen ions.

A second step of controlled heat treatment is necessary to obtain glass crystallisation forming glass-ceramics [36, 37]. This second heat treatment that leads to crystallisation involves two stages, first a nucleation and then a crystal growth stage, which promote the

re-arrangement of the glass structures generating a well-ordered and crystalline structure. Crystallisation can also be a key factor for the fabrication of multifunctional glass-ceramics, modulating theirs resorbability, cytotoxicity and bioactivity [16, 38-41]. However, not all glasses are able to undergo a controlled heat treatment and form glass-ceramics either because they are already too stable or too unstable and difficult to have a controlled heat treatment. Therefore, glasses and glass-ceramics possess the same building units just arranged in many different patterns, which leads to different final properties. The work in this field was comprehensively revised by Hench *et al.* [21, 42], Rawlings *et al.* [22] and Julian Jones [29].

Silicate glasses, the most used BGs, are well studied to form of a bone-like hydroxyapatite (HA) layer that is fundamental for a strong interfacial bond between the device and bone [21, 23]. The mechanism of bioactivity and bone bonding has been extensively studied *in vitro* (immersion in SBF) and *in vivo*, mainly for 45S5 bioglass® and was discussed elsewhere [43, 44]. Thus, the bonding ability of glass and glass-ceramics relies in the degradation process of the biomaterials and subsequent formation of a HA layer on their surface, which mimics the mineral bone composition, bonding firmly with living bone tissue. Briefly the process follows the succeeding steps, (1) dissolution of ions from the glass into the medium, (2) reaction of dissolved Ca^{2+} and $(PO_4)^{3-}$ from the media and consequent precipitation of amorphous calcium phosphate (ACP) layer, (3) the pH unbalance and increased dissolution of ions supports the growth of ACP, and (4) ACP layer incorporates $(OH)^-$ and $(CO3)^{2-}$ from the media and crystallises as HA layer. Figure I.1 shows a schematic of the steps involved in the formation of HA, as well as SEM micrographs of HA structures formed on the surface of glass particles after immersion of SBF.

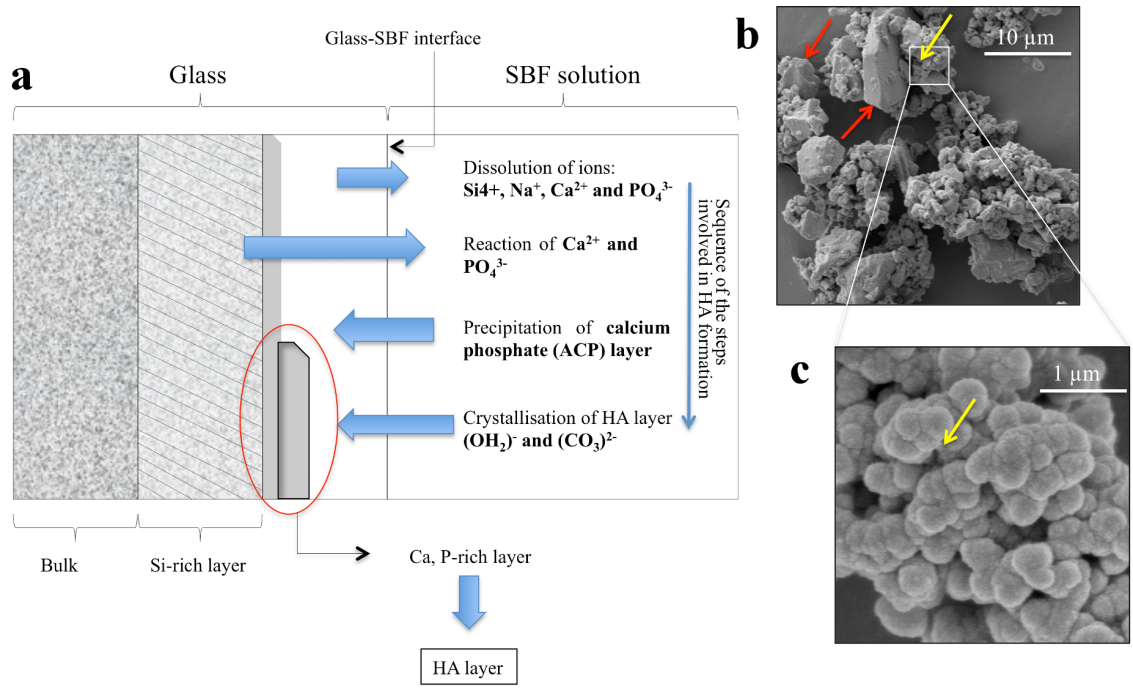

Figure I.1 - (a) Schematic view of the steps involved in the formation of a HA layer. (b) SEM micrographs of BG particles after immersion in SBF showing the apatite-like structures formed at their surface (5000x magnification); (c) detail of apatite-like surface layer (100000x magnification). The red arrows indicate the glass particles and yellow arrows indicate the formed apatite-like structures.

The silicate-based glasses and glass-ceramics are commonly associated with slow degradation rates and incomplete conversion to HA. This might result in a mismatch of the degradation rate with the rate of new tissue formation and the presence of long-term unconverted glass and glass-ceramics in the human body [44-47]. More recently, borate- and borosilicate-based glasses have been used with great potential to overcome the drawbacks of the silicate-based glasses [47-49]. Due to their lower chemical durability, borate and borosilicate bioactive (BBGs) glasses present increased biodegradation and more complete conversion to HA. BBGs offer a more controlled dissolution rate that triggers a range of biological responses required for the final biomaterial [50]. Furthermore, boron is associated with bone healing, stimulating bone formation and with the increase in bone resistance to fractures [51-53]. Thereby, the compositional flexibility is at most importance while designing glasses or glass-ceramics. A number of parameters might influence the design of the BGs. As already been shown a controlled release of ions promotes HA

formation leading to an osteointegration, while stimulating osteogenic functions of the surrounding cells [51, 54]. For instance, Maeno *et al.* and Santocildes-Romero *et al.* [55, 56] showed that ions such as Ca^{2+} and Sr^{2+} influenced both HA deposition and osteogenic behaviour of cells [55, 56]. In fact, Santocildes-Romero *et al.* [56] reported a strong evidence for upregulation of key genes as a mechanism for osteoconductivity or osseoinductivity in both conventional 45S5 and Sr-substituted BGs, which supported previously postulated theories for bioactivity of glasses. Specific trace amount of component ions (e.g. Ag^{+}, Cu^{+}, Sr^{2+}, Zn^{2+} and Ce^{3+}) incorporated and released in a controlled manner can trigger a range of different biological responses, in particularly antimicrobial activity [54, 57-59].

Glass and glass-ceramics are unique ion-containing matrices that recently are being investigated for the prevention and treatment of bone infections. As described above, they have excellent bioactive properties, strongly bonding to bone tissue through complex reactions [21] with good biocompatibility and great osteoinductive and osteoconductive properties [21, 23, 43, 60]. They have been used in the form of particles, porous or dense scaffolds for orthopaedic surgery and dentistry for bone repairing [23, 29, 61]. As a matter of fact, different inorganic modifications have been introduced by several researchers in order to achieve glass and glass-ceramics (Figure I.2) endowed with antibacterial properties, resulting either in intrinsic and/or enhanced antibacterial activity. Those biomaterials can be applied through a diversity of final forms depending on their application in the body. As shown in Figure I.2a, glasses can either be designed with inorganic species into the bulk glass network or surface modified after glass formation. Moreover, different heating and cooling rates can be used to induce a phase separation, which can create groups of specific ionic components to be released at different rates, tuning biological response. On the other hand, glasses can be submitted to controlled thermal treatments, resulting in to a glass-ceramic (Figure I.2b). Different properties can be obtained either by inducing the formation of crystalline phases in a glass matrix or by the formation of a residual glass in to the glass-ceramic matrix providing different releasing profiles.

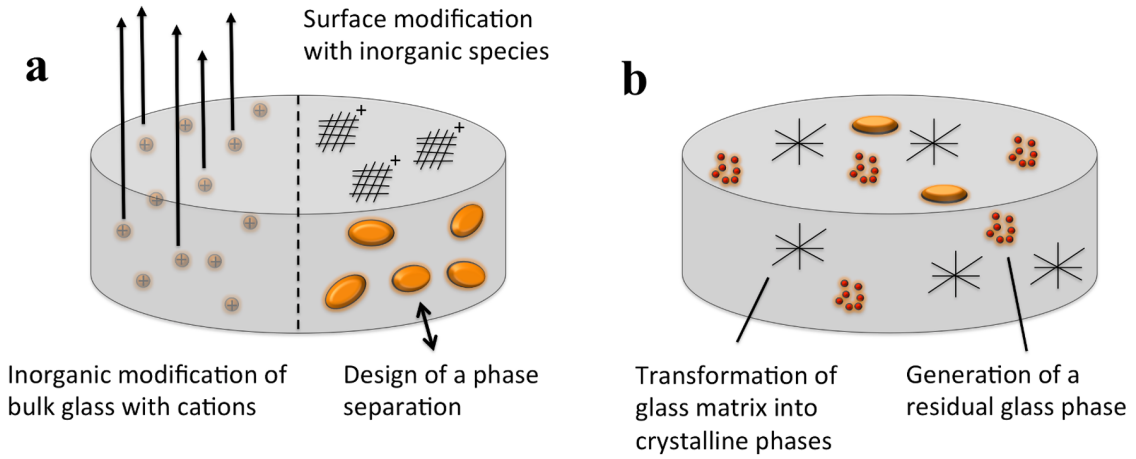

Figure I.2 - Potential routes to enhance the antimicrobial properties of a) BGs and b) glass-ceramics via crystallisation of the glass phase.

The following section will review the different glass and glass-ceramics currently proposed to reduce the risk of infection in bone and joint surgery, as well as the potential for these materials to be used to treat deep bone infections themselves.

3. Antimicrobial glass compositions and modifications

While there is undoubtedly a growing clinical need for antimicrobial devices, the regulatory environment makes it increasingly difficult to bring simple drug-device combinations to the market. Major pharmaceutical companies with the potential to make progress are also struggling to justify the development of antibiotics of last resort from an economic standpoint. The Food and Drug Administration (FDA) is approving increasingly fewer antibiotics. Statistical analysis performed by the Center for Disease Dynamics, Economics & Policy (CDDEP) highlighted that only six antibiotics were approved in the period between 2010 and 2014, 10 fewer than in the four-year period between 1983 and 1987. Actually, many of the drugs approved by FDA in the 1980s and 1990s have since been taken off the market for a variety of reasons, including: safety, efficacy or reduced of profitability [62]. Additionally, antibiotics are not an ideal solution due to challenges in reaching the target organisms, especially when these become associated with a medical device [10, 63, 64]. Local and/or preventive treatments may therefore be a superior approach to deal with bacterial infections. Different methods of

loading antibiotic into medical devices are been used for local application of antibiotic although manufactures are focusing their efforts to improve existing active ingredients instead of developing new compounds. Rahaman *et al.* have summarised part of the field, but they limited their review to a narrow range of papers and did not consider more detailed or complex aspects of glass design and structure properties relationships [65].

Glass and glass-ceramic biomaterials have been studied for more than 50 years resulting in the development of hundreds of different formulations. The controlled design or/and modification of the glass and glass-ceramics is the key factor to impart a suitable multifunctionality to the medical device [21, 28, 59, 66-68]. They are design to have suitable osteointegration and have been demonstrating antibacterial activity when specifically assessed [59, 69-72]. Allan *et al.* [69] tested with success the use of 45S5 bioglass® to inhibit several oral bacteria (including *Streptococcus sanguis*, *Streptococcus mutans* and *Actinomyces viscosus*) while repairing periodontal defects. This antibacterial activity has been generally attributed to the release of ions to the reaction media and their effect in the local physiological environment (e.g. pH, osmolarity). Zhang *et al*. [70] have demonstrated that BGs without any special bactericidal components exhibited antibacterial activity towards a large selection of bacteria in a concentration-dependent manner. The authors correlated this activity with the increase of pH and the concentration of alkali ions. In this study the glass S53P4 inhibited the proliferation of all the tested bacteria, e.g. *Escherichia coli*, *Pseudomonas aeruginosa*, *Moraxella catarrhalis*, *Enterococcus faecalis*, *Staphylococcus epidermidis*. Moya *et al.* [73, 74] studied borosilicate glasses (SiO_2–Na_2O–CaO–B_2O_3 system) with a high content of calcium oxide and found that Ca^{2+} concentration is related with the biocidal activity against Gram-positive, and Gram-negative bacteria. Several other authors also related the antibacterial effect of glass biomaterials with pH and ion concentrations [71, 75, 76]. This type of activity (based on intrinsic antibacterial properties) mainly relies on the degradation of the network and the leaching of species of the surrounding environment. Therefore, it is of most importance to fully understand the mechanisms of glass structure formation and their effect on degradation (Figure I.2) to specifically design glasses towards the final application.

Another important issue to consider while designing glass and glass-ceramic formulation are the external local environment generated by the degradation of the biomaterials that might be too harsh for the host tissue. Often, glasses are associated to a certain degree of

cytotoxicity, which can potentially affect host cell viability in areas surrounding the medical device [16, 38]. For instance, large increases of pH can induce adverse tissue responses, while the high local osmolarity variations can produce an unbalanced cellular response. Bakry *et al.* [77] showed that some the reported cytotoxic effects of 45S5 bioglass® were associated with the initially acidity of the local environment. In these cases it might be beneficial to use heat treatments in order to induce crystallisation of the glass phase forming a more-stable glass-ceramic, with a better controlled degradation rate [16, 36, 39, 40]. Hurrell-Gillingham *et al.* [40] investigated the effects of devitrification of glass-ionomer cements from SiO_2-Al_2O_3-P_2O_5-CaO-CaF_2 system onto a glass-ceramic improving its *in vitro* biocompatibility. More recently, we [16] also demonstrated that a controlled crystallisation of BBGs might be used to improve the biocompatibility of these glass-ceramic systems.

Several pathogenic microorganisms (predominantly *Staphylococcus aureus*, *S. epidermidis*, *E. coli* and *P. aeruginosa*) have been identified at the site of approximately 90% of all implants, and many of these microorganisms present resistance to antibiotics [9, 78, 79]. The critical complications of bacterial contamination are mostly related with the adhesion of bacteria to the medical device, which produce an hydrated extracellular matrix (ECM) generating biofilms [80-82]. These multifaceted structure made from microorganisms and ECM is capable of resisting antibiotics and antibacterial agents, and are at the root of many persistent and chronic bacterial infections [83]. Intrinsic glasses and glass-ceramics have been found to be effective against bacteria sessile communities that are at the root of many persistent and chronic infections. Allan *et al.* [84] showed that 45S5 bioglass® significantly lowered the viability of biofilms of *S. sanguis* when compared with an inert glass control. While, Batalu *et al.* [76] reported that although MgB_2 nano or micropowders did not affected the *S. aureus* biofilm formation, it strongly inhibited *E. coli* adhesion and viability. Once again, the authors related the activity mainly with pH and the release of boron derivatives.

The intrinsic activity of glass and glass-ceramics is rarely highly specific and uniquely oriented towards prokaryotic cells. However, antibacterial glass and glass-ceramics can be developed by the simple incorporation of specific ions (e.g. Ag^+, Ce^{3+}, Cu^+, Zn^{2+}, Sr^{2+}) with known antibacterial activity. These ions can either be incorporated into the bulk network of the glasses or at the surface (Figure I.2). Within the last few years, a number

of glasses and glass-ceramics have been studied specially for their antibacterial properties [58, 75, 85, 86]. The majority of the studies were carried out with silver doped glasses. For instance, Bellantone *et al*. [85] and Ahmed *et al*. [75] demonstrated that silver doped glasses present not only bacteriostatic, but they also caused a rapid bactericidal action against *E. coli*, *P. aeruginosa*, and *S. aureus*. Bellantone *et al*. [85] prepared their silica-based silver containing glass via an acid-catalysed sol-gel route and observed that the dissolution profiles of Ag^+ from the glasses were consistent with silver accumulation by the bacteria. While, Ahmed *et al*. [75] prepared phosphate-based silver containing glasses by melt-quenching and verified that the increase on antibacterial activity matched the increase in silver content in the glass formulation.

Several ions referred as antibacterial agents were also studied. Brauer *et al.* [87] developed a strontium-releasing injectable bone cement with antibacterial activity against *S. aureus* and *S. faecalis* for the treatment of osteoporosis-related vertebral compression fracture. Whereas, Mulligan *et al*. [86] used cooper doped glasses to eliminate *S. sanguis* biofilm found in the oral cavity. They prepared phosphate-based glasses doped with increasing amounts of copper by melt-quenching with the capacity to decrease the viability of *S. sanguis* biofilm. However, after a time period it returned to levels similar to those of the controls. Neel *et al*. [88] also prepared phosphate-based glasses containing copper in the final form of fibres. Those fibres were capable to reduce the number of viable *S. epidermidis* attached to the fibres and in the surrounding environment. Another well know metal, Zinc, was incorporated into silica-nanoparticles prepared by sol-gel showing well defined antimicrobial activity. Halevas *et al*. [89] tested different concentration of incorporated zinc against *S. aureus, Bacillus subtilis, Bacillus cereus, E. coli, P. aeruginosa, Xanthomonas campestris* exhibiting higher activity for higher concentrations. There are other ions, such as cerium and galium that were also tested for antibacterial properties. Goh *et al*. [58] have tested cerium doped glasses for their antibacterial properties. They reported significant improvements regarding the antibacterial activity against *E. coli* of silica-based glasses with 5 mol% of Ce or higher. Valappil *et al*. [90] tested phosphate-based glasses doped with gallium and silver to study their combined action. They showed that the simultaneous release of Ag^+ and Ga^{3+} from the glass reduced *Porphyromonas gingivalis* biofilm growth with a maximum effect after 168 h.

The composition of the glass is the essence of the antibacterial properties discussed in the paper. Modulating the release rate of ions and, consequently, the osmolarity and pH at the reaction site are at the centre of the reported activity. However, there are other features such as particle size and morphology that can alter the potency of these biomaterials. Mortazavi *et al*. [91] assessed the antibacterial effect of BG nanoparticles obtained by sol-gel reporting that the antibacterial activity was caused by a synergetic effect of a high calcium concentration and an alkaline pH, which might have been modulated by the reduction of particle size (20 to 90 nm). Glass composition 58S showed antibacterial activity against *E. coli*, *P. aeruginosa*, and *S. aureus* while 63S exhibit activity only against *E. coli*, *S. aureus* and 72S didn't show any activity. Some other studies reported the influence of particle size and morphology of glass and glass-ceramics [70, 92]. For instance, Waltimo *et al*. [92] studied SiO_2-Na_2O-CaO-P_2O_5 nano BGs and the influence of their specific surface area in the release of ions and antibacterial activity. They reported that the increase of surface area induces a faster dissolution of alkaline species to the medium, increasing the pH of the medium, and therefor the antibacterial activity.

In general, the bulk materials that exert an antibacterial action in the absence of modifications can generally be described as intrinsically antibacterial. They are designed specifically to present bone integration properties, however, while not being designed as antibacterial materials they can present such activity. Whereas, enhanced glass and glass-ceramics differ from the intrinsic ones because they either have one or more ionic species intentionally incorporated as antibacterial agents, or are loaded with bactericidal substances or coated with active functional molecules to impart a functional antibacterial activity. Table I.1 summarises substituted BGs or glass-ceramics that present antibacterial activity correlating them with their active components.

Table I.1 - Examples of BGs or glass-ceramic biomaterials that present antibacterial activity and the correlation with the factors and components responsible for that activity

Active factor	Glass system	Organisms		Ref
		Gram (-)	Gram (+)	
Ag^+	SiO_2-CaO-P_2O_5-Ag_2O	*E. coli*	-	32
		P. aeruginosa	*S. aureus*	85
		E. coli	*S. aureus*	93
	P_2O_5-CaO-Na_2O-Ag_2O	*E. coli, P. aeruginosa*	*S. aureus*	75
	B_2O_3-Na_2O-P2O_5-Ag_2O	-	*Listeria monocytogenes*	94
	SiO_2-Ag (ceramic)	*E. coli*	*S. aureus*	95
	Ag_2O-B_2O_3-SiO_2-CaO	*E. coli*	*S. aureus*	96
	SiO_2-CaO-P_2O_5-Al_2O_3-Na_2O-K_2O-Ag_2O	*E. coli*	*E. faecalis*	57
Ag^+; pH	CaO-SiO_2-Ag_2O	*E. coli*	*S. aureus*	97
Ag; Ga^{3+}	CaO-Na_2O-P_2O_5-Ga_2O-Ag_2O	biofilm (*Streptococcus gordonii* and *P. gingivalis*)		90
Ag^+; Zn^{2+}	Ceramic doped with Ag-Zn	*E. coli*	-	98
Ce^+; pH	SiO_2-CaO-P_2O_5-Ce	*E. coli*	-	58
Cu^+	Na_2O-CaO-P_2O_5-Cu	-	biofilm (*S. sanguis*)	86
	Na_2O-CaO-P_2O_5-Cu	-	*S. epidermidis*	88
Si^{4+}; pH	S53P4	*E. coli*	-	99

Zn^{2+}	SiO_2-Zn NPs	*E. coli*	*S. aureus*	100
	SiO_2-Zn NPs	*E. coli, P. aeruginosa, X. campestris*	*S. aureus, B. subtilis, B. cereus*	89
[ions]; pH	45S5 bioglass®	*E. coli, P. aeruginosa, Actinobacillus actinomycetemcomitans, P. gingivalis, Fusobacterium nucleatum*	*S. sanguis, S. mutans, A. viscosus* and *E. faecalis*	69, 92, 101
		biofilms (*S. sanguis*)		84
	58S and 63S bioglass®	*E. coli, P. aeruginosa, Salmonella typhi*	*S. aureus*	91
	S53P4	*Acinetobacter spp, Haemophilus influenza, Enterobacter aerogenes, M. catarrhalis, E. coli, P. aeruginosa*	*S. epidermidis, E. faecalis*	70, 71, 102
	MgB_2	*E. coli*	*S. aureus*	76
	Na_2O-MgO-CaO-B_2O_3-P_2O_3-SiO_2/K_2O/Al_2O_3	*Acinetobacter spp, H.*	*E. faecalis*	70

		influenza, E. coli, P. aeruginosa		
	Na_2O-K_2O-MgO-CaO-P_2O_3-SiO_2	*Acinetobacter spp, H. influenza, E. aerogenes, E. coli, P. aeruginosa*	*S. epidermidis, E. faecalis*	70
	Na_2O-K_2O-MgO-CaO-B_2O_3-P_2O_3-SiO_2	-	*S. epidermidis*	71
	P_2O_5-CaO-Na_2O	*E. coli, P. aeruginosa*	*S. aureus*	75
	SiO_2-B_2O_3-Na_2O-MgO/SrO	*P. aeruginosa*	*S. epidermidis*	59
	SiO_2-P_2O_5-CaO-Na_2O-SrO	*Aggregatibacter actinomycetemcomitans, Porphyromonas gingivalis*	-	25
$[Ca^{2+}]$	SiO_2-B_2O_3-Na_2O-CaO-K_2O-Al_2O_3	*E. coli, P. aeruginosa*	*S. aureus, S. epidermidis and Micrococcus luteus*	103
	SiO_2-Na_2O-CaO-P_2O_5-Al_2O_3-Fe_2O/B_2O_3/K_2O/MgO	*E. coli*	*M. luteus, Candida kruse*	74
	SiO_2-Na_2O-CaO-B_2O_3/K_2O-Al_2O_3	*E. coli*	-	73

$[Ca^{2+}]$; pH	SiO_2-CaO-Na_2O-K_2O-P_2O_5/MgO	-	*S. aureus*	72
$[Sr^{2+}]$	SiO-SrO-CaF_2-MgO	-	*S. aureus, E. faecalis*	87
pH	CaO-SiO_2	*E. coli*	*S. aureus*	97

4. Mechanisms of antimicrobial activity

Composition is the basis of the properties of glasses and glass-ceramics. It can modulate the rate of ions release and consequently the local osmolarity and pH, influencing the physiological conditions at the surrounding of the medical devices. Therefore, the antibacterial glasses and glass-ceramics is often engaged by their composition and dissolution properties [59, 69, 73, 84].

Recently, Echezarreta-López *et al*. [104] compiled from literature a large database on the production of glass biomaterials, bacterial properties and experiments using an artificial intelligence tool, named: neurofuzzy logic technology. They verified that the antibacterial properties of glass and glass-ceramics can be induced by the release of alkaline ions, particularly Ca^{2+} ions, and the increase of the pH of the medium. Briefly, the mechanisms of action are described in three steps: (i) release of ions that increases their (ii) osmolarity and (iii) pH at the reaction site, unbalancing the bacterial intracellular Ca^{2+}, which results in cell membrane depolarisation and their subsequent death. Cabal *et al*. [103] reported that borosilicate glass-ceramics were able to inhibit bacterial growth, minimise bacterial adhesion and prevent biofilm formation by the perturbation of intracellular Ca^{2+} compartmentalisation, causing cytotoxicity and resulting in either apoptotic or necrotic bacteria cell death. This work tested the borosilicate glasses against five ATCC strains (*S. aureus, S. epidermidis, P. aeruginosa, E. coli and M. lutea*) showing a reduction of the viability of bacteria.

However, there are several enhanced glass and glass-ceramics that have their antibacterial activity based in the use of stable metals, such as silver (between many other: Ce^{3+}, Cu^{+}, Zn^{2+}, Sr^{2+}), which are reported to present antibacterial activity [105]. In these cases, the antibacterial activity is oriented towards prokaryotic cells and it is usually specific. However, occasionally, they are associated to a certain degree of cytotoxicity towards animal cells [106]. Regarding the use of antibacterial metals, which is frequently active due to their corrosion in the physiological environment, or their leaching to surrounding medium, the high concentration of those ions might also cause local toxicity.

Even though the exact mechanism of the activity of the metal ions regarding antibacterial action is still unknown it is recognised that it relies on a combination of actions. Silver has been one of the most studied materials, and have been intentionally used in surgeries for its bactericidal properties. It acts by inactivating critical enzymes of the respiratory chain by biding to thiol groups and inducing the formation of hydroxyl radicals promoting oxidative stress [107]. However, other chemical activity, e.g. hydrogen, bonding may also be involved. In this case it inhibits the synthesis of the bacterial cell wall proteins and bacterial RNA and DNA. It has been also reported that it inhibits the metabolic pathway [107, 108]. Therefore, the activity is generally associated to the ionic form of the metal. Moreover, Jung *el al.* [107] demonstrated a higher antibacterial activity against Gram-negative (*E. coli*) than against Gram-positive (*S. aureus*) bacteria. This suggests that the antibacterial activity of the metal ions might be related to the thickness of the peptidoglycan layer of Gram-positive bacteria, which may difficult the action of the silver ions at the bacterial cell membrane. An overview of the hypothesised mechanisms associated with the antibacterial activity of metal particles is presented in Figure I.3

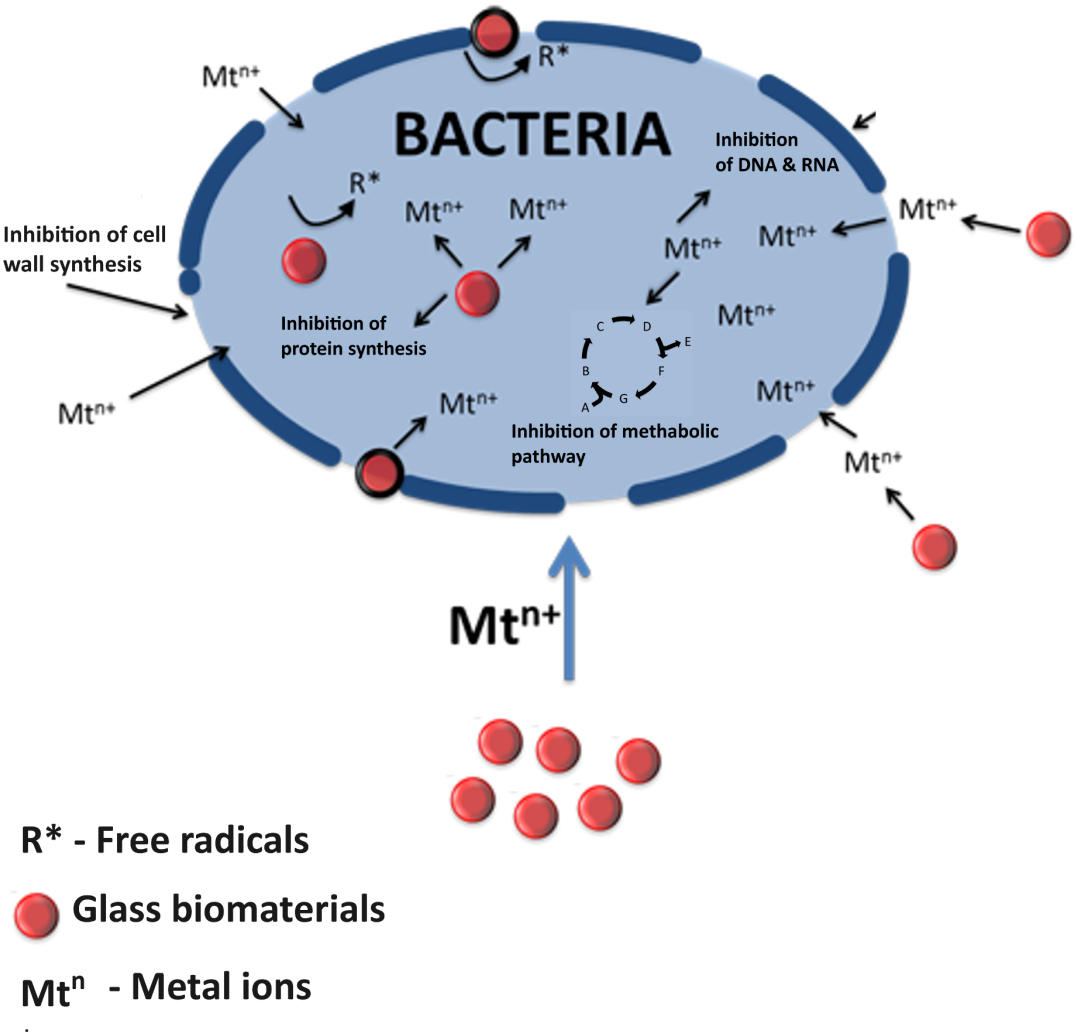

Figure I.3 - Overview of the hypothesised mechanisms associated with the antibacterial activity of metal ions. In the use of silver ions the most pronounced effects is related with cellular metabolic activity (inhibition of respiratory chain and cell pathways), as well as the generation of ROS (oxygen reactive species) and DNA and RNA damage. Diagram was modified from [109].

5. Conclusions and future outlook

This review clearly demonstrates that it is possible to use inorganic modification to generate BGs and glass-ceramics into biomaterials that are capable of supressing the growth of pathogenic organisms while at the same time increasing bone tissue regeneration. This strategy offers an alternative (or at least a potent adjuvant) to antibiotics. While a number of classical glass compositions such as S53P4 and 45S5 bioglass® appear to have some antimicrobial activity, there is no doubt that enhanced compositions are far more potent. For example, the addition of Ag^{+}, Zn^{2+}, Cu^{+}, Ce^{3+} and Sr^{2+} all increased the antimicrobial activity of the glasses. While the presence of these specific ions has a direct effect on bacteria, it is important to note that the disruption of the glass is also influenced by small compositional changes (i.e. pH, osmolarity, particle size), which affects the degradation rate of the glass phase. It was noted that these effects were frequently neglected by authors who instead focused solely on the effects of specific ions. Therefore there is a clear need to invest in the structural design of glass and glass-ceramics if truly innovative multifunctional systems are to be developed. These will then provide a predictable, local delivery of antimicrobial ions to the site of infection while promoting bone tissue regeneration.

References

(1) Navarro, M.; Michiardi, A.; Castaño, O.; Planell, J. A., Biomaterials in orthopaedics. *Journal of The Royal Society Interface* **2008,** 5, (27), 1137-1158.

(2) Gomes, F. O.; Pires, R. A.; Reis, R. L., Aluminum-free glass-ionomer bone cements with enhanced bioactivity and biodegradability. *Materials Science and Engineering: C* **2013,** 33, (3), 1361-1370.

(3) Harris, A. M.; Althausen, P. L.; Kellam, J.; Bosse, M. J.; Castillo, R.; Group, T. L. E. A. P. L. S., Complications Following Limb-Threatening Lower Extremity Trauma. *Journal of Orthopaedic Trauma* **2009,** 23, (1), 1-6.

(4) Anglen, J. O., Comparison of Soap and Antibiotic Solutions for Irrigation of Lower-Limb Open Fracture Wounds. *A Prospective, Randomized Study* **2005,** 87, (7), 1415-1422.

(5) Yin, J.-M.; Liu, Z.-T.; Zhao, S.-C.; Guo, Y.-J., Diagnosis, management, and prevention of prosthetic joint infections. In *Front Biosci (Landmark Ed)*, ed.; 2013; Vol. 18, pp 1349-1357.

(6) Ribeiro, M.; Monteiro, F. J.; Ferraz, M. P., Infection of orthopedic implants with emphasis on bacterial adhesion process and techniques used in studying bacterial-material interactions. *Biomatter* **2012,** 2, (4), 176-194.

(7) Miola, M.; Bistolfi, A.; Valsania, M. C.; Bianco, C.; Fucale, G.; Verné, E., Antibiotic-loaded acrylic bone cements: An in vitro study on the release mechanism and its efficacy. *Materials Science and Engineering: C* **2013,** 33, (5), 3025-3032.

(8) Axford, J. S., Joint and bone infections. *Medicine* **2010,** 38, (4), 194-201.

(9) Vassena, C.; Fenu, S.; Giuliani, F.; Fantetti, L.; Roncucci, G.; Simonutti, G.; Romanò, C. L.; De Francesco, R.; Drago, L., Photodynamic antibacterial and antibiofilm activity of RLP068/Cl against Staphylococcus aureus and Pseudomonas aeruginosa

forming biofilms on prosthetic material. *International Journal of Antimicrobial Agents* **2014,** 44, (1), 47-55.

(10) Bistolfi, A.; Massazza, G.; Verné, E.; Massè, A.; Deledda, D.; Ferraris, S.; Miola, M.; Galetto, F.; Crova, M., Antibiotic-Loaded Cement in Orthopedic Surgery: A Review. *ISRN orthopedics* **2011,** 2011, (290851), 8.

(11) Sia, I. G.; Berbari, E. F.; Karchmer, A. W., Prosthetic Joint Infections. *Infectious Disease Clinics of North America* **2005,** 19, (4), 885-914.

(12) Darouiche, R. O., Treatment of Infections Associated with Surgical Implants. *New England Journal of Medicine* **2004,** 350, (14), 1422-1429.

(13) Barros, A. A. A.; Alves, A.; Nunes, C.; Coimbra, M. A.; Pires, R. A.; Reis, R. L., Carboxymethylation of ulvan and chitosan and their use as polymeric components of bone cements. *Acta Biomaterialia* **2013,** 9, (11), 9086-9097.

(14) Pires, R. A.; Abrahams, I.; Nunes, T. G.; Hawkes, G. E., Multinuclear magnetic resonance studies of borosilicate glasses for use in glass ionomer cements: incorporation of CaO and Al2O3. *Journal of Materials Chemistry* **2006,** 16, (24), 2364-2373.

(15) Pires, R. A.; Abrahams, I.; Nunes, T. G.; Hawkes, G. E., The role of alumina in aluminoborosilicate glasses for use in glass-ionomer cements. *Journal of Materials Chemistry* **2009,** 19, (22), 3652-3660.

(16) Fernandes, J. S.; Gentile, P.; Moorehead, R.; Crawford, A.; Miller, C. A.; Pires, R. A.; Hatton, P. V.; Reis, R. L., Design and Properties of Novel Substituted Borosilicate Bioactive Glasses and Their Glass-Ceramic Derivatives. *Crystal Growth Design* **2016**.

(17) Boesel, L. F.; Azevedo, H. S.; Reis, R. L., Incorporation of alpha-amylase enzyme and a bioactive filler into hydrophilic, partially degradable, and bioactive cements (HDBCs) as a new approach to tailor simultaneously their degradation and bioactive behavior. *Biomacromolecules* **2006,** 7, (9), 2600-2609.

(18) Boesel, L. F.; Cachinho, S. C. P.; Fernandes, M. H. V.; Reis, R. L., The in vitro bioactivity of two novel hydrophilic, partially degradable bone cements. *Acta Biomaterialia* **2007,** 3, (2), 175-182.

(19) Boesel, L. F.; Mano, J. F.; Reis, R. L., Optimization of the formulation and mechanical properties of starch based partially degradable bone cements. *Journal of Materials Science –Materials in Medicine* **2004,** 15, (1), 73-83.

(20) Leonor, I. B.; Ito, A.; Onuma, K.; Kanzaki, N.; Zhong, Z. P.; Greenspan, D.; Reis, R. L., In situ study of partially crystallized Bioglas® and hydroxylapatite in vitro bioactivity using atomic force microscopy. *Journal of Biomedical Materials Research* **2002,** 62, (1), 82-88.

(21) Hench, L., The story of Bioglass. *Journal of Materials Science: Materials in Medicine* **2006,** 17, (11), 967-978.

(22) Rawlings, R. D., Bioactive glasses and glass-ceramics. *Clinical Materials* **1993,** 14, (2), 155-179.

(23) Hench, L. L., Bioceramics: From Concept to Clinic. *Journal of the American Ceramic Society* **1991,** 74, (7), 1487-1510.

(24) Gentleman, E.; Fredholm, Y. C.; Jell, G.; Lotfibakhshaiesh, N.; O'Donnell, M. D.; Hill, R. G.; Stevens, M. M., The effects of strontium-substituted bioactive glasses on osteoblasts and osteoclasts in vitro. *Biomaterials* **2010,** 31, (14), 3949-3956.

(25) Liu, J.; Rawlinson, S. C. F.; Hill, R. G.; Fortune, F., Strontium-substituted bioactive glasses in vitro osteogenic and antibacterial effects. *Dental Materials* **2016,** 32, (3), 412-422.

(26) Chen, Q. Z.; Thompson, I. D.; Boccaccini, A. R., 45S5 Bioglass®-derived glass–ceramic scaffolds for bone tissue engineering. *Biomaterials* **2006,** 27, (11), 2414-2425.

(27) Fu, H.; Fu, Q.; Zhou, N.; Huang, W.; Rahaman, M. N.; Wang, D.; Liu, X., In vitro evaluation of borate-based bioactive glass scaffolds prepared by a polymer foam replication method. *Materials Science and Engineering: C* **2009,** 29, (7), 2275-2281.

(28) Livingston, T.; Ducheyne, P.; Garino, J., *In vivo* evaluation of a bioactive scaffold for bone tissue engineering. *Journal of Biomedical Materials Research* **2002,** 62, (1), 1-13.

(29) Jones, J. R., Review of bioactive glass: From Hench to hybrids. *Acta Biomaterialia* **2013,** 9, (1), 4457-4486.

(30) Brauer, D. S., Bioactive Glasses—Structure and Properties. *Angewandte Chemie International Edition* **2015,** 54, (14), 4160-4181.

(31) Kaur, G.; Pandey, O. P.; Singh, K.; Homa, D.; Scott, B.; Pickrell, G., A review of bioactive glasses: Their structure, properties, fabrication and apatite formation. *Journal of Biomedical Materials Research A* **2014,** 102, (1), 254-274.

(32) Balamurugan, A.; Balossier, G.; Laurent-Maquin, D.; Pina, S.; Rebelo, A. H. S.; Faure, J.; Ferreira, J. M. F., An *in vitro* biological and anti-bacterial study on a sol–gel derived silver-incorporated bioglass system. *Dental Materials* **2008,** 24, (10), 1343-1351.

(33) Murphy, S.; Wren, A.; Towler, M.; Boyd, D., The effect of ionic dissolution products of Ca–Sr–Na–Zn–Si bioactive glass on *in vitro* cytocompatibility. *Journal of Materials Science: Materials in Medicine* **2010,** 21, (10), 2827-2834.

(34) Goel, A.; Kapoor, S.; Rajagopal, R. R.; Pascual, M. J.; Kim, H.-W.; Ferreira, J. M. F., Alkali-free bioactive glasses for bone tissue engineering: A preliminary investigation. *Acta Biomaterialia* **2012,** 8, (1), 361-372.

(35) Chen, Q. Z.; Xu, J. L.; Yu, L. G.; Fang, X. Y.; Khor, K. A., Spark plasma sintering of sol–gel derived 45S5 Bioglass®-ceramics: Mechanical properties and biocompatibility evaluation. *Materials Science and Engineering: C* **2012,** 32, (3), 494-502.

(36) Daguano, J. K. M. F.; Strecker, K.; Ziemath, E. C.; Rogero, S. O.; Fernandes, M. H. V.; Santos, C., Effect of partial crystallization on the mechanical properties and cytotoxicity of bioactive glass from the 3CaO.P2O5–SiO2–MgO system. *Journal of the Mechanical Behavior of Biomedical Materials* **2012,** 14, (0), 78-88.

(37) Kanchanarat, N.; Miller, C. A.; Hatton, P. V.; James, P. F.; Reaney, I. M., Early Stages of Crystallization in Canasite-Based Glass Ceramics. *Journal of the American Ceramic Society* **2005,** 88, (11), 3198-3204.

(38) Wallace, K. E.; Hill, R. G.; Pembroke, J. T.; Brown, C. J.; Hatton, P. V., Influence of sodium oxide content on bioactive glass properties. *Journal of Materials Science: Materials in Medicine* **1999,** 10, (12), 697-701.

(39) Freeman, C. O.; Brook, I. M.; Johnson, A.; Hatton, P. V.; Hill, R. G.; Stanton, K. T., Crystallization modifies osteoconductivity in an apatite–mullite glass–ceramic. *Journal of Materials Science: Materials in Medicine* **2003,** 14, (11), 985-990.

(40) Hurrell-Gillingham, K.; Reaney, I. M.; Miller, C. A.; Crawford, A.; Hatton, P. V., Devitrification of ionomer glass and its effect on the *in vitro* biocompatibility of glass-ionomer cements. *Biomaterials* **2003,** 24, (18), 3153-3160.

(41) Boccaccini, A. R.; Chen, Q.; Lefebvre, L.; Gremillard, L.; Chevalier, J., Sintering, crystallisation and biodegradation behaviour of Bioglass®-derived glass–ceramics. *Faraday Discussions* **2006,** 136, 27-44.

(42) Filho, O. P.; La Torre, G. P.; Hench, L. L., Effect of crystallization on apatite-layer formation of bioactive glass 45S5. *Journal of Biomedical Materials Research* **1996,** 30, (4), 509-514.

(43) Hench, L. L., Bioceramics. *Journal of the American Ceramic Society* **1998,** 81, (7), 1705-1728.

(44) Rahaman, M. N.; Day, D. E.; Sonny Bal, B.; Fu, Q.; Jung, S. B.; Bonewald, L. F.; Tomsia, A. P., Bioactive glass in tissue engineering. *Acta Biomaterialia* **2011,** 7, (6), 2355-2373.

(45) Fu, H.; Rahaman, M.; Day, D.; Huang, W., Long-term conversion of 45S5 bioactive glass–ceramic microspheres in aqueous phosphate solution. *Journal of Materials Science: Materials in Medicine* **2012,** 23, (5), 1181-1191.

(46) Xu, S.; Yang, X.; Chen, X.; Shao, H.; He, Y.; Zhang, L.; Yang, G.; Gou, Z., Effect of borosilicate glass on the mechanical and biodegradation properties of 45S5-derived bioactive glass-ceramics. *Journal of Non-Crystalline Solids* **2014,** 405, 91-99.

(47) Huang, W.; Day, D.; Kittiratanapiboon, K.; Rahaman, M., Kinetics and mechanisms of the conversion of silicate (45S5), borate, and borosilicate glasses to hydroxyapatite in dilute phosphate solutions. *Journal of Materials Science: Materials in Medicine* **2006,** 17, (7), 583-596.

(48) Rahaman, M. N.; Liang, W.; Day, D. E., Preparation and Bioactive Characteristics of Porous Borate Glass Substrates. In *Advances in Bioceramics and Biocomposites: Ceramic Engineering and Science Proceedings*, John Wiley & Sons, Inc.: 2008; pp 1-10.

(49) Pan, H. B.; Zhao, X. L.; Zhang, X.; Zhang, K. B.; Li, L. C.; Li, Z. Y.; Lam, W. M.; Lu, W. W.; Wang, D. P.; Huang, W. H.; Lin, K. L.; Chang, J., Strontium borate glass: potential biomaterial for bone regeneration. *Journal of The Royal Society Interface* **2010,** 7, (48), 1025-1031.

(50) Yang, X.; Zhang, L.; Chen, X.; Sun, X.; Yang, G.; Guo, X.; Yang, H.; Gao, C.; Gou, Z., Incorporation of B2O3 in CaO-SiO2-P2O5 bioactive glass system for improving strength of low-temperature co-fired porous glass ceramics. *Journal of Non-Crystalline Solids* **2012,** 358, (9), 1171-1179.

(51) Lakhkar, N. J.; Lee, I.-H.; Kim, H.-W.; Salih, V.; Wall, I. B.; Knowles, J. C., Bone formation controlled by biologically relevant inorganic ions: Role and controlled delivery from phosphate-based glasses. *Advanced Drug Delivery Reviews* **2013,** 65, (4), 405-420.

(52) Shen, Y.; Liu, W.; Wen, C.; Pan, H.; Wang, T.; Darvell, B. W.; Lu, W. W.; Huang, W., Bone regeneration: importance of local pH-strontium-doped borosilicate scaffold. *Journal of Materials Chemistry* **2012,** 22, (17), 8662-8670.

(53) Chapin, R.; Ku, W.; Kenney, M.; McCoy, H., The effects of dietary boric acid on bone strength in rats. *Biological Trace Element Research* **1998,** 66, (1-3), 395-399.

(54) Hoppe, A.; Güldal, N. S.; Boccaccini, A. R., A review of the biological response to ionic dissolution products from bioactive glasses and glass-ceramics. *Biomaterials* **2011,** 32, (11), 2757-2774.

(55) Maeno, S.; Niki, Y.; Matsumoto, H.; Morioka, H.; Yatabe, T.; Funayama, A.; Toyama, Y.; Taguchi, T.; Tanaka, J., The effect of calcium ion concentration on osteoblast viability, proliferation and differentiation in monolayer and 3D culture. *Biomaterials* **2005,** 26, (23), 4847-4855.

(56) Santocildes-Romero, M. E.; Crawford, A.; Hatton, P. V.; Goodchild, R. L.; Reaney, I. M.; Miller, C. A., The osteogenic response of mesenchymal stromal cells to strontium-substituted bioactive glasses. *Journal of Tissue Engineering and Regenerative Medicine* **2015,** 9, (5), 619-631.

(57) Chatzistavrou, X.; Fenno, J. C.; Faulk, D.; Badylak, S.; Kasuga, T.; Boccaccini, A. R.; Papagerakis, P., Fabrication and characterization of bioactive and antibacterial composites for dental applications. *Acta Biomaterialia* **2014,** 10, (8), 3723-3732.

(58) Goh, Y.-F.; Alshemary, A. Z.; Akram, M.; Abdul Kadir, M. R.; Hussain, R., In-vitro characterization of antibacterial bioactive glass containing ceria. *Ceramics International* **2014,** 40, (1, Part A), 729-737.

(59) Fernandes, J. S.; Martins, M.; Neves, N. M.; Fernandes, M. H. F. V.; Reis, R. L.; Pires, R. A., Intrinsic Antibacterial Borosilicate Glasses for Bone Tissue Engineering Applications. *ACS Biomaterials Science & Engineering* **2016**.

(60) Rahaman, M. N., 3 - Bioactive ceramics and glasses for tissue engineering. In *Tissue Engineering Using Ceramics and Polymers (Second Edition)*, Boccaccini, A. R.; Ma, P. X., Eds. Woodhead Publishing: 2014; pp 67-114.

(61) Bohner, M., Resorbable biomaterials as bone graft substitutes. *Materials Today* **2010,** 13, (1–2), 24-30.

(62) Society, R. A. P. US Lauches New Antibiotics Strategy, Calls for New Regulatory Efforts and Incentives. http://www.raps.org/Regulatory-Focus/News/2014/09/19/20376/US-Launches-New-Antibiotics-Strategy-Calls-for-New-Regulatory-Efforts-and-Incentives/ (3 Nov),

(63) Leprêtre, S.; Chai, F.; Hornez, J.-C.; Vermet, G.; Neut, C.; Descamps, M.; Hildebrand, H. F.; Martel, B., Prolonged local antibiotics delivery from hydroxyapatite functionalised with cyclodextrin polymers. *Biomaterials* **2009,** 30, (30), 6086-6093.

(64) Jiranek, W. A.; Hanssen, A. D.; Greenwald, A. S., Antibiotic-Loaded Bone Cement for Infection Prophylaxis in Total Joint Replacement. *The Journal of Bone & Joint Surgery* **2006,** 88, (11), 2487-2500.

(65) Rahaman, M. N.; Bal, B. S.; Huang, W., Review: Emerging developments in the use of bioactive glasses for treating infected prosthetic joints. *Materials Science and Engineering: C* **2014,** 41, 224-231.

(66) Gu, Y.; Wang, G.; Zhang, X.; Zhang, Y.; Zhang, C.; Liu, X.; Rahaman, M. N.; Huang, W.; Pan, H., Biodegradable borosilicate bioactive glass scaffolds with a trabecular microstructure for bone repair. *Materials Science and Engineering: C* **2014,** 36, 294-300.

(67) Bandyopadhyay-Ghosh, S.; Reaney, I. M.; Brook, I. M.; Hurrell-Gillingham, K.; Johnson, A.; Hatton, P. V., *In vitro* biocompatibility of fluorcanasite glass-ceramics for bone tissue repair. *Journal of Biomedical Materials Research A* **2007,** 80A, (1), 175-183.

(68) Bandyopadhyay-Ghosh, S.; Faria, P. E. P.; Johnson, A.; Felipucci, D. N. B.; Reaney, I. M.; Salata, L. A.; Brook, I. M.; Hatton, P. V., Osteoconductivity of modified

fluorcanasite glass–ceramics for bone tissue augmentation and repair. *Journal of Biomedical Materials Research A* **2010,** 94A, (3), 760-768.

(69) Allan, I.; Newman, H.; Wilson, M., Antibacterial activity of particulate Bioglass® against supra- and subgingival bacteria. *Biomaterials* **2001,** 22, (12), 1683-1687.

(70) Zhang, D.; Leppäranta, O.; Munukka, E.; Ylänen, H.; Viljanen, M. K.; Eerola, E.; Hupa, M.; Hupa, L., Antibacterial effects and dissolution behavior of six bioactive glasses. *Journals of Biomedical Materials Research A* **2010,** 93A, (2), 475-483.

(71) M. Vaahtio; E. Munukka; O. Leppäranta; D. Zhang; E. Eerola; H. O. Ylänen; T. Peltola, "Effect of Ion Release on Antibacterial Activity of Melt-Derived and Sol-Gel-Derived Reactive Ceramics". *Key Engineering Materials* **2006,** 309-311, (May), 349-354.

(72) Echezarreta-López, M. M.; De Miguel, T.; Quintero, F.; Pou, J.; Landin, M., Antibacterial properties of laser spinning glass nanofibers. *International Journal of Pharmaceutics* **2014,** 477, (1–2), 113-121.

(73) Moya, J. S.; Cabal, B.; Sanz, J.; da Silva, A. C.; Mello-Castanho, S.; Torrecillas, R.; Rojo, F., Mechanism of calcium lixiviation in soda-lime glasses with a strong biocide activity. *Materials Letters* **2012,** 70, (0), 113-115.

(74) Moya, J. S.; Esteban-Tejeda, L.; Pecharromán, C.; Mello-Castanho, S. R. H.; da Silva, A. C.; Malpartida, F., Glass Powders with a High Content of Calcium Oxide: A Step Towards a “Green” Universal Biocide. *Advanced Engineering Materials* **2011,** 13, (6), B256-B260.

(75) Ahmed, A. A.; Ali, A. A.; Mahmoud, D. A. R.; El-Fiqi, A. M., Preparation and characterization of antibacterial P2O5–CaO–Na2O–Ag2O glasses. *Journal of Biomedical Materials Research Part A* **2011,** 98A, (1), 132-142.

(76) Batalu, D.; Stanciuc, A. M.; Moldovan, L.; Aldica, G.; Badica, P., Evaluation of pristine and Eu2O3-added MgB2 ceramics for medical applications: hardness, corrosion resistance, cytotoxicity and antibacterial activity. *Materials Science and Engineering: C* **2014,** 42, 350-361.

(77) Bakry, A. S.; Tamura, Y.; Otsuki, M.; Kasugai, S.; Ohya, K.; Tagami, J., Cytotoxicity of 45S5 bioglass® paste used for dentine hypersensitivity treatment. *Journal of Dentistry* **2011,** 39, (9), 599-603.

(78) Simchi, A.; Tamjid, E.; Pishbin, F.; Boccaccini, A. R., Recent progress in inorganic and composite coatings with bactericidal capability for orthopaedic applications. *Nanomedicine: Nanotechnology, Biology and Medicine* **2011,** 7, (1), 22-39.

(79) Paladini, F.; Pollini, M.; Sannino, A.; Ambrosio, L., Metal-Based Antibacterial Substrates for Biomedical Applications. *Biomacromolecules* **2015,** 16, (7), 1873-1885.

(80) Rohde, H.; Frankenberger, S.; Zähringer, U.; Mack, D., Structure, function and contribution of polysaccharide intercellular adhesin (PIA) to Staphylococcus epidermidis biofilm formation and pathogenesis of biomaterial-associated infections. *European Journal of Cell Biology* **2010,** 89, (1), 103-111.

(81) Olson, M. E.; Garvin, K. L.; Fey, P. D.; Rupp, M. E., Adherence of Staphylococcus epidermidis to Biomaterials Is Augmented by PIA. *Clinical Orthopaedics and Related Research* **2006,** 451, 21-24.

(82) Costerton, J. W.; Stewart, P. S.; Greenberg, E. P., Bacterial Biofilms: A Common Cause of Persistent Infections. *Science* **1999,** 284, (5418), 1318-1322.

(83) Donlan, R. M.; Costerton, J. W., Biofilms: Survival Mechanisms of Clinically Relevant Microorganisms. *Clinical Microbiology Reviews* **2002,** 15, (2), 167-193.

(84) Allan, I.; Wilson, M.; Newman, H., Particulate Bioglass® reduces the viability of bacterial biofilms formed on its surface in an *in vitro* model. *Clinical Oral Implants Research* **2002,** 13, (1), 53-58.

(85) Bellantone, M.; Williams, H. D.; Hench, L. L., Broad-Spectrum Bactericidal Activity of Ag(2)O-Doped Bioactive Glass. *Antimicrobial Agents and Chemotherapy* **2002,** 46, (6), 1940-1945.

(86) Mulligan, A. M.; Wilson, M.; Knowles, J. C., The effect of increasing copper content in phosphate-based glasses on biofilms of Streptococcus sanguis. *Biomaterials* **2003,** 24, (10), 1797-1807.

(87) Brauer, D. S.; Karpukhina, N.; Kedia, G.; Bhat, A.; Law, R. V.; Radecka, I.; Hill, R. G., Bactericidal strontium-releasing injectable bone cements based on bioactive glasses. *Journal of the Royal Society Interface* **2013,** 10, (78).

(88) Abou Neel, E. A.; Ahmed, I.; Pratten, J.; Nazhat, S. N.; Knowles, J. C., Characterisation of antibacterial copper releasing degradable phosphate glass fibres. *Biomaterials* **2005,** 26, (15), 2247-2254.

(89) Halevas, E.; Nday, C. M.; Kaprara, E.; Psycharis, V.; Raptopoulou, C. P.; Jackson, G. E.; Litsardakis, G.; Salifoglou, A., Sol–gel encapsulation of binary Zn(II) compounds in silica nanoparticles. Structure–activity correlations in hybrid materials targeting Zn(II) antibacterial use. *Journal of Inorganic Biochemistry* **2015**.

(90) Valappil, S. P.; Coombes, M.; Wright, L.; Owens, G. J.; Lynch, R. J. M.; Hope, C. K.; Higham, S. M., Role of gallium and silver from phosphate-based glasses on *in vitro* dual species oral biofilm models of Porphyromonas gingivalis and Streptococcus gordonii. *Acta Biomaterialia* **2012,** 8, (5), 1957-1965.

(91) Mortazavi, V.; Nahrkhalaji, M. M.; Fathi, M. H.; Mousavi, S. B.; Esfahani, B. N., Antibacterial effects of sol-gel-derived bioactive glass nanoparticle on aerobic bacteria. *Journal of Biomedical Materials Research Part A* **2010,** 94A, (1), 160-168.

(92) Waltimo, T.; Brunner, T. J.; Vollenweider, M.; Stark, W. J.; Zehnder, M., Antimicrobial Effect of Nanometric Bioactive Glass 45S5. *Journal of Dental Research* **2007,** 86, (8), 754-757.

(93) El-Kady, A. M.; Ali, A. F.; Rizk, R. A.; Ahmed, M. M., Synthesis, characterization and microbiological response of silver doped bioactive glass nanoparticles. *Ceramics International* **2012,** 38, (1), 177-188.

(94) Magyari, K.; Stefan, R.; Vodnar, D. C.; Vulpoi, A.; Baia, L., The silver influence on the structure and antibacterial properties of the bioactive $10B_2O_3{-}30Na_2O{-}60P_2O_2$ glass. *Journal of Non-Crystalline Solids* **2014,** 402, (0), 182-186.

(95) Baheiraei, N.; Moztarzadeh, F.; Hedayati, M., Preparation and antibacterial activity of Ag/SiO2 thin film on glazed ceramic tiles by sol–gel method. *Ceramics International* **2012,** 38, (4), 2921-2925.

(96) Ciceo Lucacel, R.; Radu, T.; Tătar, A. S.; Lupan, I.; Ponta, O.; Simon, V., The influence of local structure and surface morphology on the antibacterial activity of silver-containing calcium borosilicate glasses. *Journal of Non-Crystalline Solids* **2014,** 404, (0), 98-103.

(97) Ni, S.; Li, X.; Yang, P.; Ni, S.; Hong, F.; Webster, T. J., Enhanced apatite-forming ability and antibacterial activity of porous anodic alumina embedded with CaO–SiO2–Ag2O bioactive materials. *Materials Science and Engineering: C* **2016,** 58, 700-708.

(98) Yang, S.; Zhang, Y.; Yu, J.; Zhen, Z.; Huang, T.; Tang, Q.; Chu, P. K.; Qi, L.; Lv, H., Antibacterial and mechanical properties of honeycomb ceramic materials incorporated with silver and zinc. *Materials & Design* **2014,** 59, 461-465.

(99) Zehnder, M.; Waltimo, T.; Sener, B.; Söderling, E., Dentin enhances the effectiveness of bioactive glass S53P4 against a strain of Enterococcus faecalis. *Oral Surgery, Oral Medicine, Oral Pathology, Oral Radiology, and Endodontology* **2006,** 101, (4), 530-535.

(100) Choi, H.-J.; Choi, J.-S.; Park, B.-J.; Eom, J.-H.; Heo, S.-Y.; Jung, M.-W.; An, K.-S.; Yoon, S.-G., Enhanced transparency, mechanical durability, and antibacterial activity of zinc nanoparticles on glass substrate. *Scientific Reports* **2014,** 4.

(101) Hu, S.; Chang, J.; Liu, M.; Ning, C., Study on antibacterial effect of 45S5 Bioglass®. *Journal of Materials Science: Materials in Medicine* **2009,** 20, (1), 281-286.

(102) Stoor, P.; Söderling, E.; Grenman, R., Interactions between the bioactive glass S53P4 and the atrophic rhinitis-associated microorganism Klebsiella ozaenae. *Journal of Biomedical Materials Research* **1999,** 48, (6), 869-874.

(103) Cabal, B.; Alou, L.; Cafini, F.; Couceiro, R.; Sevillano, D.; Esteban-Tejeda, L.; Guitian, F.; Torrecillas, R.; Moya, J. S., A New Biocompatible and Antibacterial Phosphate Free Glass-Ceramic for Medical Applications. *Scientifi. Reports* **2014,** 4.

(104) Echezarreta-López, M. M.; Landin, M., Using machine learning for improving knowledge on antibacterial effect of bioactive glass. *International Journal of Pharmaceutics* **2013,** 453, (2), 641-647.

(105) Top, A.; Ülkü, S., Silver, zinc, and copper exchange in a Na-clinoptilolite and resulting effect on antibacterial activity. *Applied Clay Science* **2004,** 27, (1–2), 13-19.

(106) Campoccia, D.; Montanaro, L.; Arciola, C. R., A review of the biomaterials technologies for infection-resistant surfaces. *Biomaterials* **2013,** 34, (34), 8533-8554.

(107) Jung, W. K.; Koo, H. C.; Kim, K. W.; Shin, S.; Kim, S. H.; Park, Y. H., Antibacterial Activity and Mechanism of Action of the Silver Ion in Staphylococcus aureus and Escherichia coli. *Applied and Environmental Microbiology* **2008,** 74, (7), 2171-2178.

(108) Furr, J. R.; Russell, A. D.; Turner, T. D.; Andrews, A., 3rd International Conference of the Hospital Infection SocietyAntibacterial activity of Actisorb Plus, Actisorb and silver nitrate. *Journal of Hospital Infection* **1994,** 27, (3), 201-208.

(109) Palza, H., Antimicrobial Polymers with Metal Nanoparticles. *International Journal of Molecular Sciences* **2015,** 16, (1), 2099.

2. SECTION

II. CHAPTER

Materials and Methods

II. CHAPTER

Materials and Methods

The aim of this chapter is to describe in detail, the experimental methods used within the scope of this thesis. Although each part of the work is provided with its specific materials and methods section, this chapter aims to be a guideline of this research. Chapter II is design to provide a more comprehensive view of the experimental and analytical techniques used, as well as to facilitate an overview by the readers.

1. Materials

1.1. Borosilicate bioactive glasses (BBGs)

Bioactive glasses (BGs) are widely reported to form a bone-like HA layer on their surface when placed in a simulated biological environment, which is extremely important for the osteointegration of the biomedical device [1, 2]. Although, the most widely used BGs are silica-based, they often present slow degradation and conversion to HA rates, which makes it difficult to match the degradation rate of the device remaining for long periods in the human body [3-5]. The addition of borate to the glass network is one approach that has the potential to overcome the limitations identified above, due to their ability to tune dissolution rates, as well as other properties, such as bone bonding [5-7]. Moreover, borosilicate bioactive glasses (BBGs) compositions can be used to achieve a more controlled release of specific ions in order to trigger a range of biological responses [8]. Therefore, different glass modifier cations such as magnesium (Mg^{2+}), calcium (Ca^{2+}) or strontium (Sr^{2+}) were incorporated. These modifications can stimulate several bone cell functions, such as: proliferation, differentiation and ECM mineralisation, as well as increase the rate of HA formation and new bone growth [9-12]. Furthermore, those glass modifier cations can provide antibacterial properties to BGs, as previously reported [32-34]. In this context, the incorporation of different cations can impart a series of therapeutic features into BGs, and their properties can be suited to meet the clinical needs.

Three BBGs incorporating different cations: BBG-Mg ($0.05Na_2O \cdot 0.35MgO \cdot 0.20B_2O_3 \cdot 0.40SiO_2$), BBG-Ca ($0.05Na_2O \cdot 0.35CaO \cdot 0.20B_2O_3 \cdot 0.40SiO_2$) and BBG-Sr ($0.05Na_2O \cdot 0.35SrO \cdot 0.20B_2O_3 \cdot 0.40SiO_2$) were synthesised by melt quenching. All chemicals used for the glass synthesis were reagent grade: boron oxide (B_2O_3, Alfa Aesar, Germany), calcium carbonate ($CaCO_3$, Sigma-Aldrich, UK), sodium bicarbonate ($NaHCO_3$, Sigma-Aldrich, Australia), silica gel 60M (SiO_2, Macherey-Nagel, Germany), magnesium oxide (MgO, Sigma-Aldrich, UK) and strontium carbonate ($SrCO_3$, Sigma-Aldrich, Australia).

1.2. Poly (L lactic) acid (PLLA)

Polylactic acid, also known as polylactide (PLA) is biodegradable aliphatic polyester that is produced by microbial fermentation of renewable resources (i.e. corn starch, tapioca roots or sugarcane). PLA can exist in three stereochemical forms: poly (L-lactide) (PLLA), poly (D-lactide) and poly (DL-lactide), however the L form is considered to be more biocompatible [13]. Poly L-lactic acid (PLLA) has been considered as one of the most promising biodegradable medical materials for tissue engineering purposes [14-17]. It is widely used in surgical and medical devices due to its important properties such as: nontoxicity, biodegradability and biocompatibility. In addition, the US Federal FDA have approved several medical devices produced with PLLA for clinical purposes. Some of its main advantages are its: flexibility and deformation capacity. It can also be efficiently processed by an enormous variety of techniques. For the purposes of this thesis it was used PLLA (with a L-lactide content of 99.6% and a M_w of 69 000 Da, from Cargill Dow LLC, USA) to produce the desired fibre scaffolds.

1.3. Poly L-lactic acid – borosilicate bioactive glasses (PLLA-BBGs) scaffolds

PLLA degradation yields the corresponding hydroxy acid, a natural metabolite of the body. The acidity of lactic acid may cause some inflammatory adverse response in the body[14]. Moreover, PLLA is not commonly considered osteoinductive [18, 19]. Therefore, the addition of an inorganic phase that produce an alkaline medium during degradation neutralise the degradation products, reducing the inflammation of the surrounding tissue and releasing inorganic species that can trigger a range of biological responses. It will also allow a better control of the degradation rate of the final PLLA-glass composite,

which can be used to manufacture scaffolds with a suitable degradation rate while progressively being substituted by the body's natural tissues [20, 21].

2. Glass synthesis and scaffolds fabrication

2.1. Glass syntheses by melt quenching

The melt quenching method is the oldest procedure used to produce bulk glasses and is still widely used. This process is based in the production of a glass melt in suitable crucibles and consequent pouring it into a cold water bath or metal plate, followed by annealing to reduce the internal stress of the glass [22]. The novel BBGs of general formula $0.05Na_2O \cdot xMgO \cdot yCaO \cdot (0.35\text{-}x\text{-}y)SrO \cdot 0.20B_2O_3 \cdot 0.40SiO_2$ (molar ratio, where x, y = 0.35 or 0.00, and $x \neq y$) were synthesised by melt quenching. The appropriate amounts of SiO_2, B_2O_3, $NaHCO_3$, and $CaCO_3$ or MgO or $SrCO_3$ were accurately mixed with ethanol (Sigma, Portugal) in a porcelain mortar and with the help of a pestle, fully dried overnight and transfer to a platinum crucible. The batch was heated to 1450 ºC in air for 1 h and subsequently the melt was quickly poured into a water bath at 4 ºC to form a glass frit. Afterwards, the as-quenched glasses were ground in an Agate mortar (RETSCH, Germany) and sieved to a particle size <63 μm (Chapters III to VI) or <45 μm (Chapter VII). In accordance with differential thermal (DTA) data (Figure III.1), crystallised glass was prepared from each BBG. Briefly, fast-quenched particles of the glass samples were heat-treated at a heating rate of 10 ºC · min^{-1} and maintained for 120 min at each temperature (T_g, T_{c1}, T_{c2} and T_{c3}) before cooling the samples to room temperature (RT). Before the *in vitro* tests BBG-Mg ($0.05Na_2O \cdot 0.35MgO \cdot 0.20B_2O_3 \cdot 0.40SiO_2$), BBG-Ca ($0.05Na_2O \cdot 0.35CaO \cdot 0.20B_2O_3 \cdot 0.40SiO_2$) or BBG-Sr ($0.05Na_2O \cdot 0.35SrO \cdot 0.20B_2O_3 \cdot 0.40SiO_2$) glass and glass-ceramics were weighted, dried and sterilised either at 160 ºC for at least 2 h (Chapter III and V) or by ethylene oxide (Chapter IV).

2.2. Fabrication of the fibre mesh scaffolds

2.2.1. Wet spun fibre mesh scaffolds

The wet spinning technique consists of a solution of a polymer in a suitable solvent extruded as a fibre into a coagulation bath containing a nonsolvent. The polymer concentration in the spinning solvent depends on factors such as: polymer solubility and solution spinning pressure. This technique offers excellent conditions to the design of random and porous micro-fibre structures with appropriate interface for biomedical applications [17]. PLLA-BBG fibres were fabricated through the wet spinning of a homogeneous mixture of PLLA with BBG particles. These fibres were transformed into circular shape fibre mesh scaffolds by fibre bonding. Three different PLLA-BBG scaffolds were fabricated (PLLA-Mg-BBG, PLLA-Ca-BBG and PLLA-Sr-BBG) using three different BBGs (Mg-BBG, Ca-BBG and Sr-BBG, that presented, respectively, Mg, Ca and Sr as divalent modifier cations). Unfilled PLLA scaffolds were used as control. After preparing a homogenised PLLA solution in chloroform (30% w/v), BBGs (30% BBG/PLLA w/w) were added under constant stirring to avoid particles agglomeration. Subsequently, the PLLA-BBG solution was wet spun thought a syringe equipped with a 25 G needle with the tip cut horizontally and perpendicular to the flow. The fibres were extruded at a rate of 15 $ml \cdot h^{-1}$ into a coagulation bath of methanol. Finally, fibres were collected and fully dried overnight on a fume hood at RT. To fabricate PLLA-BBG fibre mesh scaffolds, fibres (≈ 80 mg) were first pre-moulded into a 20 mm diameter metal mould and after bonded at 147 °C under a pressure of 1.56 KPa for 6 min. The fibre bonding temperature was optimised with the help of differential scanning calorimetry (DSC) analysis of PLLA (T_g of 56.7 °C and a T_m of 165.4 °C). Finally, a 6 mm puncture was used to obtain specimens of 6 mm diameter and 0.5 mm height. Before the *in vitro* tests the scaffolds were dried and sterilised by ethylene oxide.

2.2.2. Electrospun fibre mesh membranes

Electrospinning is another attractive technique for spinning polymers. It is a simple method of producing random nano-fibre structures by the control of the polymer concentration and/or surface tension of the solution. The major advantage of this

technique is the ability of spun thin nano-fibre structures of high surface area. Furthermore, electrospun membranes can mimic the ECM structure benefiting the cell attachment and proliferation [17]. PLLA-BBG-Sr membranes were fabricated inside a fume hood for safe solvent evaporation and prevent that the turbulent air interferes in the formation of the fibres. The PLLA concentration, the ratio of PLLA/ BBG-Sr and the process parameters (e.g. applied voltage, flow rate and distance from the collector) were optimised in order to obtain uniform membrane of fibres. The final electrospun membranes were fabricated using PLLA dissolved in dichloromethane (16% w/v) where the BBGs microparticles were suspended (10% w/w BBGs/PLLA). Docusate sodium salt (1.2% w/w relative to PLLA) was used to help the homogenisation of the solution avoiding the formation of agglomerates. The PLLA and PLLA-BBG-Sr solutions were stirred overnight and sonicated 5 min before use to remove air bubbles. The set up was mounted using a high voltage supplier, a syringe pump (Baxter AS50, UK) with a 20 G metal needle (Fisnar, New Jersey, USA) and a conductive collector. The PLLA and PLLA-BBG-Sr solutions were drawn up into a 1 ml syringe (BD Plastipak, New Jersey, USA). The solutions were electrospun using 17 kV and a flow rate of 3 $ml \cdot h^{-1}$ at a 19 cm distance between the collector and needle. The electrospun membranes were dried in a fume hood, for 24 h, collected and stored in a desiccator at RT. Before *in vitro* testing the scaffolds (i.e. PLLA, PLLA-BBG-Mg, PLLA-BBG-Ca and PLLA-BBG-Sr) were dried and sterilised by ethylene oxide.

3. Physicochemical characterisation techniques

3.1. Glass and glass-ceramics characterisation

3.1.1. X-ray fluorescence (XRF)

X-ray fluorescence spectroscopy (XRF) was used to confirm the glass composition (Philips PW2400 X-ray fluorescence spectrometer, Netherlands). Samples were prepared by fusing powdered glass with a known quantity of boron and a lithium tetraborate flux producing a glass-like bead. After which, they were irradiated with high-energy primary

X-ray photons. All the samples were run in triplicate and the percentage (w/w) of the oxides present were quantified.

3.1.2. Inductively coupled plasma atomic emission spectrometry (ICP-AES)

Inductively coupled plasma atomic emission spectrometry (ICP-AES, Horiba, Japan) was also used to confirm the elemental composition of the glasses (B, Si, Na, Ca, Sr and Mg) after total dissolution of 1 g of each BBG into hydrochloric acid. The sample absorption was measured at specific wavelengths (λ=588.995 for Na, λ=279.553 nm for Mg, λ= 393.366 nm for Ca, λ=588.995 nm for Sr, λ=249.773 nm for B and λ=251.611 nm for Si) and their concentration was determined using calibration curves obtained with standard solutions (VWR, Portugal) in the range between 5×10^3 and 10 ppm.

3.1.3. Scanning electron microscopy with energy dispersive X-ray spectroscopy (SEM/EDS)

The chemical composition at the surface of the synthesised glasses was also analysed by Scanning electron microscopy with energy dispersive X-ray spectroscopy (SEM/EDS, Leica Cambridge, UK). BBG samples were sputter-coated with gold (sputter coater model SC502, Fisons Instruments, UK) before analysis SEM was used to observe the morphology of the glass particles using a beam energy of 5.0 kV and a working distance of ≈ 5.2 mm.

3.1.4. Glass density

The glass density of the synthesised formulations was determined using a multi pycnometer (Quantachrome Instruments, USA). Measurements were performed with helium at 110 °C using ≈ 5 g of sample.

3.1.5. Differential thermal analysis (DTA)

The mid-point of glass transition (T_g), and crystallisation (T_c) temperatures were determined by differential thermal analysis (DTA, Perkin-Elmar DTA7, UK) running Pyris thermal analysis software in Unix at a heating rate of 10 ºC · min^{-1} between 50 and 1300 ºC.

3.1.6. X-ray diffraction analysis (XRD)

The glasses were analysed before and after each heat treatment by X-ray diffraction analysis (XRD, A STOE STADI P, UK). The glass samples were place in aluminium holders and analysed using Cu radiation of wavelength 1.5406 Å, a voltage of 40 kV and a current of 40 mA with a step size of 0.2° in a range of 2θ values between 10° and 80° and a scanning speed of 10 s/step. The crystalline patterns were identified by the use of the cards listed in the Joint Commission on Powder Diffraction Standards (JCPDS).

3.1.7. Attenuated total reflection Fourier transform infrared (ATR-FTIR) spectroscopy

The glasses were analysed before and after each heat treatment by and ATR-FTIR (Perkin-Elmer GX, UK). The ATR-FTIR spectra were acquired in the range of 4000-550 cm^{-1} (resolution 4 cm^{-1}) for the identification of the chemical moieties present in the glass and glass-ceramics.

3.2. Glass-polymer scaffolds characterisation

3.2.1. Differential scanning calorimetry (DSC) analysis

The glass transition (T_g) and melting (T_m) temperatures were determined by differential scanning calorimetry (DSC, TA Instrument Q100 calorimeter, USA), using a double run between -40 and 200 °C (first run to determine T_g and remove thermal history, and

second run to determine T_m), at a heating and cooling rates of 10 °C · min^{-1} under nitrogen atmosphere, using ~8 mg of sample.

3.2.2. Scanning electron microscopy (SEM)

SEM/EDS (Leica Cambridge, UK) was used to assess the surface morphology of the PLLA-BBG scaffolds, as well as to monitor the deposition of calcium phosphate structures on the fibre surfaces after 7 and 14 days of immersion in simulated body fluid (SBF) [23]. All the PLLA-BBG scaffolds were sputter-coated with gold before the analysis. All the micrographs were acquired using a beam energy of 5.0 kV and a working distance (WD) of ≈ 5.2 mm.

3.2.3. X-ray diffraction analysis (XRD)

The PLLA-BBG scaffolds were analysed before and after 7 and 14 days of immersion in SBF by XRD (Bruker D8 Discover, Germany) using a Cu radiation with a wavelength of 1.5406 Å, a voltage of 40 kV and a current of 40 mA, with a step size of 0.02 ° in a 2θ range between 5 ° and 50 °, using a scanning speed of 1 s/step. The crystalline patterns were identified by comparison with the data listed in the JCPDS.

3.2.4. Micro-computed tomography (μCT)

Wetspun PLLA-BBG and PLLA scaffolds were analysed by micro-computed tomography (μCT) using a high-resolution μ-CT scanner (Skyscan 1072, Belgium), a pixel size of 6 μm and integration time of 1.7 ms. The X-ray source was set at a voltage of 43 kV of energy and a current of 234 μA. Approximately 400 projections were acquired over a rotation range of 180° with a rotation of 0.45° per step. Data sets were reconstructed using standardised cone-beam reconstruction software (NRecon v1.4.3, SkyScan). The output format for each sample was 400 serial 1024 × 1024 bitmap images. Representative data sets were segmented into binary images using a dynamic threshold of 40-150 for the polymer (blue images, Figure VI.2) and 150-255 for the BBGs (red images, Figure VI.2). These representative data sets were used for morphometric three-dimensional (3D) analysis (CT Analyser, v1.5.1.5, SkyScan) and to build the 3D models

(ANT 3D creator, v2.4, SkyScan). The morphometric analysis included porosity, mean wall thickness, mean pore diameter and pore interconnectivity. 3D virtual models of representative regions in the bulk of the scaffolds were created, visualised, and registered using an image processing software (CT Analyser and ANT 3D creator).

Electrospun PLLA-BBG and PLLA membranes were analysed by μCT using the same equipment, with a pixel size of 9.8 μm and integration time of 160 ms. The X-ray source was set at a voltage of 50 kV of energy and a current of 200 μA. Approximately 400 projections were acquired over a rotation range of 180° with a rotation of 0.60° per step. Data sets were reconstructed using standardised cone-beam reconstruction software (NRecon v1.6.10.2, SkyScan). The output format for each sample was a series of 601 bitmap images (1224 × 1224 pixels). 3D virtual models of representative regions in the bulk of the scaffolds were created applying colour channel thresholds and visualised using an image processing software (CTvox).

3.2.5. Mechanical tests

Tensile strength and modulus of the PLLA and PLLA-BBG-Sr membranes were measured using an uniaxial universal testing machine (Instron 4505, USA) according to the standard Test Method for Tensile Properties of Plastics (ASTM D 638). The membranes were cut into strips with 50 mm length, 10 mm width and 0.1 mm thickness. The tests were conducted using a 1 kN load cell, with a G length of 20 mm and a crosshead speed of 5 mm · min^{-1} until rupture. The tensile strength was taken from the stress-strain curves as the maximum stress hold by the samples. Tensile modulus was estimated from the initial slope of the stress–strain curve (between 0.5% and 1% strain) using the linear regression method. The average and standard deviations (SD) were determined from the result of 5 specimens per composition.

3.2.6. Thermogravimetric analysis (TGA)

Thermogravimetric analysis (TGA) was used to determine changes in the weight (mass) of PLLA-BBG scaffolds as a function of degradation process. It was also used to determine the amount of BBGs in the PLLA-BBG composite materials. TGA

thermograms were obtained using a TGA Q500 series (TA Instruments, USA). Experiments were performed in platinum pans, at a heating rate of 40 °C · min^{-1} between 50 °C and 700 °C under oxygen atmosphere.

4. *In vitro* chemical evaluation

4.1. Glass and glass-ceramics

4.1.1. Bioactivity assay

SBF was produced in accordance with the procedure described by Kokubo *et al.* [23]. Triplicate samples of the prepared BBGs, with a particle size lower than 63 μm, were immersed in SBF at a ratio of 10:15 [BBG (mg): SBF (ml)] and incubated for 1, 3 and 7 days in an oven maintained at 37 °C. After each time point BBGs were recovered and dried at 37 ºC. The gold or carbon sputter coated samples were analysed by SEM (model S360, Leica Cambridge, UK) equipped with SEM/EDS link-eXL-II) for morphological and chemical analysis.

4.1.2. Degradation assay

Samples of the prepared BBGs were immersed in the bacterial growth medium Muller Hinton (MH) (at least in triplicate) at concentrations of 9, 18, 36 and 72 mg·ml^{-1} for 1, 3 and 7 days and maintained at 37 ºC in a water-shaking bath at 60 rpm. At each time point, the solutions were filtered and the pH was determined. The ICP-AES analyses were performed as described in Chapter II.3.1.2. to determine the concentrations of Si, B, Mg, Ca and Sr released by the BBGs into the MH medium.

4.2. Glass-polymer scaffolds

4.2.1. Bioactivity assay

The assay was performed as previously described for the glass particles. In this case the incubation was for 7 and 14 days in an oven and maintained at 37 °C. After each time point samples of PLLA-BBG scaffold were collected and dried at 37 ºC in order to obtain the XRD patterns and SEM micrographs. Each immersion solution was filtered and analysed by the inductive coupled plasma (ICP, Horiba, Japan) to determine the corresponding Ca and P concentrations present in the solution at each time point. The absorption was measured at specific wavelengths (λ= 393.366 nm for Ca; λ=213.62 nm for P) and the Ca and P concentrations were determined using calibration curves previously obtained with standard solutions (Alfa Aesar, UK).

4.2.2. Degradation assay

The PLLA-BBG scaffolds (n=3 per time point) were immersed in distilled water at a ratio of 10:10 [PLLA-BBG scaffolds (mg): distilled water (ml)] for 7, 14, 21, and 30 days in a water-shaking bath at 60 rpm and 37 °C. Each immersion solution was filtered and their respective pH was measured. ICP analysis was performed to determine the Si, B, Ca, Mg and Sr concentrations in the immersion solutions. The absorption was measured at specific wavelengths (λ= 251.611 nm for Si, λ= 249.773 nm for B, λ= 393.366 nm for Ca, λ= 407.771 nm for Sr and λ= 279.553 nm for Mg) and their concentrations were determined using calibration curves previously obtained with standard solutions (Alfa Aesar, UK).

The PLLA-BBG scaffolds were removed from water solution, the excess surface water was removed and the samples were immediately weighed. Afterwards, the samples were dried in the oven at 37 °C, to constant weight, recording the final mass of each specimen. The water uptake (WU) was calculated according to Eq. (1):

$$WU(\%) = \left(m_{tp} - m_f\right)/m_f \times 100 \qquad \text{Eq. (1)}$$

Where m_{tp} is the wet mass of the specimen at the specific time (days), and m_f is the final mass after immersion and drying. The weight loss (WL) was calculated according to Eq. (2):

$$WL(\%) = \left(m_f - m_i\right)/m_i \times 100 \qquad \text{Eq. (2)}$$

Where m_f is the mass of the dried specimen after its immersion in water, and m_i is the mass of the dried specimen before immersion in distilled water.

TGA was used to determine changes in the weight (mass) of PLLA-BBG scaffolds as a function of degradation process, as described previously under section II.3.2.6.

5. *In vitro* biological evaluation

5.1. Cell isolation and expansion

5.1.1. Expansion of immortalised mouse fibroblast-like cell line (L929)

Cells of the immortalised mouse fibroblast-like cell line (L929, Rockville, MD, UK) were expanded in dulbecco's modified eagle medium (DMEM, Sigma-Aldrich, UK) supplemented with 10% (v/v) fetal calf serum (Sigma-Aldrich, UK), penicillin (100 $U \cdot ml^{-1}$, Sigma-Aldrich, UK) and streptomycin (100 $\mu g \cdot ml^{-1}$, Sigma-Aldrich, UK), and non-essential amino acids (NEAA, Sigma-Aldrich, UK). The L929 cells were cultured and expanded at 37 °C in an atmosphere of 5% CO_2.

5.1.2. Expansion of human osteosarcoma cell line (SaOs-2)

Cells of the human osteosarcoma cell line (SaOs-2) were expanded in DMEM (Sigma, Portugal) supplemented with 10% heat-inactivated fetal bovine serum (FBS, Alfagene, Portugal) and 1% antibiotic/antimitotic solution (100 $U \cdot ml^{-1}$ penicillin and 100 $\mu g \cdot ml^{-1}$ streptomycin; Alfagene, Portugal). Cells were cultured at 37 °C in an atmosphere of 5% CO_2.

5.1.3. Isolation and expansion of rat bone marrow mesenchymal stem cells (BM-MSCs)

Bone marrow mesenchymal stem cells (BM-MSCs) were isolated from bone marrow of 4-5 week-old male Wistar rats according to the method established by Maniatopoulos *et al.* [15] and recently proposed by Santocildes-Romero [25]. BM-MSCs were expanded in basal medium consisting of DMEM (Sigma-Aldrich, UK), supplemented with 100 $U \cdot ml^{-1}$ penicillin (Sigma-Aldrich, UK) and 1 $mg \cdot ml^{-1}$ streptomycin (Sigma-Aldrich, UK). Cells were cultured and expanded at 37 ºC in an atmosphere of 5% CO_2.

5.1.4. Isolation and expansion of human adipose-derived stem cells (hASCs)

Human adipose-derived stem cells (hASCs) were isolated from human subcutaneous adipose tissue samples obtained from lipoaspiration procedures performed on women with ages between 35 and 50 years old under a protocol previously established with the Department of Plastic Surgery of Hospital da Prelada in Porto, Portugal and frozen at -80 °C. The cells were cultured and expanded in a culture medium consisting of α-medium, 10% FBS and 1% mixture of antibiotic-antimycotic.

5.2. Glass and glass-ceramic

5.2.1. Antibacterial properties of BBGs

The standard disc diffusion (DD) and the broth dilution (BD) assays [26, 27] were adapted to test the ability of the BBGs to act against the Gram-negative bacteria *P. aeruginosa* (American Type Culture Collection, ATCC 27853) and *E. coli* (Colección Española de Cultivos Tipo, CECT 434); and the Gram-positive *S. aureus* (ATCC 25913) and *S. epidermidis* (strain 9142, [28]). These bacterial strains were chosen to represent a spectrum of organisms associated with joint and bone infections [29]. For these experiments different concentrations [9, 18, 36, 72 $mg \cdot disc^{-1}$ (DD) or $mg \cdot ml^{-1}$ (BD)] of each BBGs were used. Additionally, 45S5 Bioglass® was used as commercial control; and culture medium without BBGs were used as a negative control. The antibacterial properties of BBGs as a

function of the culture time were investigated by BD assays for those glasses that exhibited antibacterial activity on DD. All experiments were performed at least in triplicate and repeated three times independently.

5.2.1.1 Disc diffusion assay

For the DD assay [26], agar discs (17 g·l^{-1} (Liofilchem, Portugal), Ø ≈ 9.5 mm) were loaded with different concentrations of BBGs and used on the same day. The direct colony suspension method was used to prepare a saline suspension of each microbial species previously grown in tryptone soya agar (TSA, Liofilchem, Portugal) at 37 ºC for 18 h. The density of the suspensions was adjusted to that of a McFarland 0.5 turbidity standard, corresponding to approximately 1-2×10^{8} CFU·ml^{-1}. The inoculum concentration was confirmed by enumeration of CFU after culture of serial dilutions onto TSA and incubation at 37 °C, 18–24 h in air. The test was performed by applying the bacterial inoculum with a sterile cotton swab onto the surface of a MH agar (Liofilchem, Portugal) plate containing 25 ml of medium. The glasses on agar discs were applied in the plates within 15 min of inoculation. The plates were incubated at 37 °C in air for 18h for all the bacteria. The diameter (in millimetres) of the inhibition zone around each disc was measured using a ruler. The presence of an inhibition halo was interpreted as bacterial susceptibility to the BBG.

5.2.1.2. Broth dilution assay

For the BD assay [27], the BBGs were immersed in 0.5 ml of MH (Fluka, Portugal) medium and incubated at 37 ºC in air for 0, 2 or 6 days. For each bacterium, the inoculum was prepared as described for the DD test. It was diluted to approximately 1×10^{6} CFU in 0.5 ml of culture medium, added to the different tubes containing known amounts of BBGs during the specific time frames and incubated at 37 ºC in air for 24 h. Overall, the bacteria were tested for a fixed period after 1, 3 and 7 days of BBGs dissolution in MH medium. One sample was removed from each tube, serially diluted in saline and inoculated onto TSA. After 24 h incubation at 37 ºC in air, the number of colonies was counted. The results are presented as log10 CFU·ml^{-1}. Bacteriostatic and bactericidal activities were defined as a reduction of bacteria less and more than 3 log10 CFU·ml^{-1},

respectively, expressed as the proportion of the inoculum (number of living CFUs introduced in culture) that is rendered incapable of reproduction on subculture [30]. Eradication was defined as the elimination of culturable bacteria upon subculture.

5.2.2. Cytotoxicity of BBGs by indirect contact (L929)

The indirect contact cytotoxicity study was designed adapting the international guidelines ISO 10993-5:2009 [31], using L929 in indirect contact with glass powders for 3 days. The samples were sterilised in an oven (Gallenkamp Hot Box, UK) at 160 °C for 120 min. After sterilisation, the glasses were added to DMEM (sigma, UK) solution at a concentration of 0.2 $g \cdot ml^{-1}$ and incubated for 24 h at 37 °C. After incubation, the glass-conditioned medium was removed and filtered through a 0.2 µm membrane. Confluent L929 cells at passages between 15 and 19 were harvested and seeded into 48-well culture plates (growth area 0.95 cm^2) at a density of 2×10^4 cells/well. After a 24 h culture period the culture media was discarded and replaced with 0.5 cm^3 of serially diluted, glass-conditioned medium (at a final concentrations of 100, 50, 25, 10, and 5%). L929 cells cultured in the absence of glass particles, was used as negative control and 45S5 bioglass®- conditioned medium as positive control. After 1 and 3 days time of culturing, the culture medium was removed and the morphology, viability and DNA content of the cultures were analysed using DAPI and phalloidin; PrestoBlue® and Picogreen® assays respectively.

5.2.2.1. Cell viability assessment (PrestoBlue®)

The PrestoBlue® reagent (Fisher Scientific, UK) is a resazurin-based non-fluorescent solution that is reduced to fluorescent resorufin by viable cells. The cells viability assays were performed according to the manufacturer's instructions. In brief, the PrestoBlue® reagent was added to a final concentration of 10% to the cell cultures and incubated for 1 h at 37 ºC. 200 µl of samples of the culture medium were removed and placed in 96-well plates and the resorufin fluorescence quantified spectrophotometrically using a plate reader (Tecan Infinite M200, UK). The fluorescence was determined at an excitation wavelength of 560 nm and emission wavelength of 590 nm. The cell viabilities are normalised as % of the metabolic activity of the control cell cultures.

5.2.2.2. DNA measurement (PicoGreen® assay)

The PicoGreen® dsDNA reagent (Invitrogen, USA) is an ultrasensitive fluorescent nucleic acid dye for quantification of double-stranded DNA (dsDNA) in solution. This assay enables measurement of cell proliferation. After each culturing period, the cell monolayers were washed with PBS and then incubated at 37 ºC for 3 h followed by freezing step at -80 ºC over night in ultra-pure water (1 ml) to ensure cell lysis. The assays were performed according to the manufacturer's protocol. The fluorescence was determined at an excitation wavelength of 485 nm and emission wavelength of 528 nm. The DNA values were normalised to those of the control cell cultures.

5.2.2.3. Morphological evaluation of L929 cells

After each culturing period the cell monolayers were washed with PBS and fixed with 4% formalin solution (0.5 ml) for 15 min at RT. The cell layers were then washed with PBS, containing 0.2% Triton X, for 2 min. After the fixation and permeation steps, the cell monolayers were washed again with PBS and stained with 4,6-diamidino-2-phenyindole dilactate (1:1000 DAPI, Sigma, UK) for 2 min at RT, and phalloidin-tetramethylrhodamine B isothiocyanate (Sigma, UK) for 1 h at RT. Finally, the cells were washed and observed using an Axioplan 2 imaging fluorescent microscope with a digital camera QIC AM 12-bit (Zeiss, UK).

5.2.3. Cytotoxicity of BBGs on SaOs-2 (direct contact)

The direct contact cytotoxicity assessment was performed by culture of the SaOs-2 in the presence of BBGs at concentrations of 9, 18, 36, 72 $mg \cdot ml^{-1}$ during 7 days. The SaOs-2 cells cultured in the absence of glass particles, were used as negative control and 45S5 Bioglass® as positive control. Confluent SaOs-2 cells between passages 15 and 19 were harvested and seeded onto the bottom of 24-well plates at a density of 2.3×10^5 cells/well. The BBGs at the desired concentrations and 45S5 Bioglass® were deposited, in cell culture inserts with porous membranes (0.4 μm ThinCerts™ Cell Culture Inserts; Greiner, Germany). After 1, 3 and 7 days of culture, the culture medium was removed and the

viability and DNA content of the cultures were determined using MTS and Picogreen® (as in Chapter II.5.2.2.1. and 5.2.2.2.) respectively.

5.2.3.1. Cell viability assessment (MTS)

The MTS reagent (3-(4,5-dimethylthiazol-2-yl)-5-(3-carboxymethoxyphenyl)-2-(4-sulfophenyl)-2 H-tetrazolium – Promega, UK) is based on the reduction of MTS tetrazolium compound by viable cells to generate a colored formazan product that is soluble in cell culture media. The assay was performed according to the manufacturer's instructions. In brief, the MTS reagent was added to a final concentration of 16.7% to the cell cultures and the cultures incubated for 3 h at 37 ºC. 200 µl samples of the culture medium were removed and placed in 96-well plates and the formazan absorbance quantified spectrophotometrically using a plate reader (Tecan Infinite M200, UK). The absorbance was determined at a wavelength of 490 nm. The cell viabilities are normalised as % of the metabolic activity of the control cell cultures.

5.2.4. Cytotoxicity of BBGs on BM-MSCs

Prior to the *in vitro* studies, BM-MSCs, at passage 2, were harvested and seeded into 24 well plates, at a density of 2×10^4 cells/well. Cells were cultured in the presence of the BBGs at concentrations of 20 and 50 $mg\cdot ml^{-1}$, for 7, 14 and 21 days under static conditions. The BM-MSCs cultured in the absence of BBGs were used as negative control and cultured in the presence of 45S5 bioglass® as positive control. The BBGs at the desired concentrations and 45S5 bioglass® were deposited, in cell culture inserts with porous membranes (0.4 µm ThinCerts™ Cell Culture Inserts; Greiner, Germany). All conditions were cultured in basal and osteogenic differentiation media (basal medium supplemented with 50 $mg\cdot ml^{-1}$ ascorbic acid, 10 mM β-glycerophosphate and 10^{-7} M dexamethasone). After 7, 14 and 21 days culture, the cell were evaluated for viability, DNA content and morphology as described in Chapter II.5.2.2.1., 5.2.2.2. and 5.2.2.3. respectively.

5.2.5. Osteogenic activity of BBGs on BM-MSCs

All conditions were cultured in basal and osteogenic differentiation media (basal medium supplemented with 50 mg·ml^{-1} ascorbic acid, 10 mM β-glycerophosphate and 10^{-7} M dexamethasone). After different specific times of culture, the cell were evaluated for the alkaline phosphatase (ALP) content, alizarin red staining and immunodetection of bone-specific proteins (i.e. osteopontin and osteocalcin).

5.2.5.1. Alkaline phosphatase (ALP) quantification

The concentration of ALP was determined for all the culture time periods, using the lysates used for DNA quantification. Briefly, the ALP quantity was assessed using the Alkaline Phosphatase, Diethanolamine Detection kit (Sigma-Aldrich, UK) in which p-nitrophenyl phosphatase (pNPP) solution is hydrolysed by ALP to yield a yellow free p-nitrophenol. In brief, a buffered pNPP solution was prepared and equilibrated at 37 ºC. Afterwards, 2% (v/v) of sample or control were added. Immediately after mixing the absorbance was read at 405 nm in a microplate reader (Tecan Infinite M200, UK) for ≈ 5 min. An ALP standard solution was used as control and a buffer as blank. The activity units·mg^{-1} solid were calculated according to the following equation: $\frac{(\frac{\Delta A_{405nm}}{min\ Test}-\frac{\Delta A_{405nm}}{min\ Blank})\times d_f\times V_F}{18.5\times V_E}$. Where d_f = dilution factor; V_F = Volume of final solution; 18.5 = millimolar extinction coefficient of pNPP at 405 nm and V_E = Volume of samples/ALP standard solution. ALP activity was calculated by normalising the ALP concentration per DNA concentration for each condition and time point.

5.2.5.2. Alizarin red staining

After 21 days of culture, the cells grown in tissue culture coverslips were fixed in 70% ice-cold methanol at -20 °C at least for 30 min. The cell layers were then washed with PBS and dried overnight. Afterwards, cells were stained with alizarin red solution (342 mg of alizarin red (Sigma-Aldrich, UK) in 25 ml of distilled water) and the pH was adjusted to 4.1 with 10% ammonium hydroxide (Sigma-Aldrich, UK) for 10 min. Then, washed in distilled water, dehydrated in an acetone/xylene (Sigma-Aldrich, UK) mixture

and mounted using an aqueous solution. The stained constructs were observed under an optical microscope (BX51, Olympus Corporation, UK) and images captured by a digital camera (DP70, Olympus Corporation, UK). The BM-MSCs morphology and mineral deposition was also observed using SEM/EDS (Leica Cambridge, UK) for the determination of the surface chemical composition.

5.2.5.3. Immunodetection of bone-specific proteins

Osteopontin (OP) and osteocalcin (OC) protein expression of BM-MSCs was assessed by immunoassay technique to evaluate their osteoblastic differentiation. The procedures were executed according to the manufacturer's instructions. The concentrations of OP and OC were determined for all the culture time periods, using the lysates used for DNA quantification. The OP quantitative determination was performed using Mouse/Rat Osteopontin Quantikine ELISA Kit (R&D Systems, UK). In brief, 50 µl of assay diluent RD1W and 50 µl of standard (2500 to 39 $pg \cdot ml^{-1}$), control and samples were added and the plate incubated for 2 h at RT. After 4 washing steps and drying, 100 µl of Mouse/Rat OP conjugated were added and incubated for 2 h at RT. The sandwich complex was washed 4 times and allowed to react with 100 µl of substrate solution before adding 100 µl of stop solution. Finally, the optical density was determined at 450 nm and the concentration of OP obtained from a standard curve plot. OC quantitative determination was performed by the use of Rat Gla-Osteocalcin High Sensitive EIA kit (Takara Clontech, Japan). In brief, 100 µl of samples and standard solution (16 to 0.25 $ng \cdot ml^{-1}$) were incubated for 1 h at 37 ºC with the capture-antibody, rat osteocalcin C-terminus-specific antibody. After OC capture and 3 washing steps, 100 µl of the enzyme-labelled antibody (GlaOC4-30) specific to Gla-OC was incubated for 1 h at RT. The sandwich complex was washed 4 times and allowed to react with 100 µl of substrate solution for 10-15 min. Finally, after adding the stop solution the optical density was determined at 450 nm and the concentration of OC obtained from a standard curve plot. OP and OC content was calculated by normalising OP or OC concentration per DNA concentration for each condition and time point.

5.3. Glass-polymer scaffolds

5.3.1. Cytotoxicity of wet spun scaffolds (direct contact) on SaOs-2

The cytotoxicity assessment was performed by culture of the SaOs-2 cells in the presence of the PLLA-BBG scaffolds. To this purpose, confluent SaOs-2 cells between passages 13 and 17 were harvested and seeded onto the bottom of 24-well plates at a density of 2×10^4 cells/well and allowed to make contact with the scaffolds. The SaOs-2 cells cultured in the presence of PLLA absent of glass particles was used as negative control and latex (6 mm discs) as positive control. The metabolic activity and cellular proliferation were monitored at 1, 3 and 7 days by MTS and PicoGreen®, respectively, using the protocols previously described in Chapter II.5.2.2.1 and II.5.2.2.1.

5.3.2. hASCs adhesion on wet spun scaffolds

The cell adhesion study was performed with hASCs. When an adequate cell number was obtained (passage 3), cells were detached with trypsin/EDTA and seeded at a density of 3×10^4 cells/scaffold. After 24 h of cell attachment, cell-constructs were placed in new 24-well plates and 1 ml of basal medium was added to each well. The basal culture medium consisted of α-minimum essential medium (αMEM, Gibco, UK) supplemented with 10% heat-inactivated foetal bovine serum (FBS; Biochrom AG, Germany) and 1% antibiotic/antimycotic solution (final concentration of penicillin 100 units·ml^{-1} and streptomycin 100 mg·ml^{-1}; Gibco, UK). The cell-constructs were cultured for 7 and 21 days in a humidified atmosphere at 37 °C, containing 5% CO_2 and analysed. The culture medium was changed every 2–3 days until the end of the experiment. The metabolic activity and cellular proliferation were monitored at 7 and 21 days by MTS and PicoGreen®, respectively, as detailed before. Cell morphology was also evaluated at day 7 and 21, cells were washed twice with PBS and then fixed with formalin for 15 min at RT. Previous to the analysis by SEM (model S360, Leica Cambridge, UK) equipped with an EDS link-eXL-II), the samples were gold or carbon sputter coated (Fisons Instruments SC502, UK).

5.3.3. Cytotoxicity of electrospun scaffolds on BM-MSCs

Prior to the *in vitro* studies, rat BM-MSCs, at passage 2, were harvested and seeded at a density of 3×10^4 cells/membrane of Ø = 6.5 mm held by the inserts (CellCrown™24, Scaffdex, UK). Cells were cultured for 7, 14 and 21 days under static conditions. All conditions were cultured in basal and osteogenic differentiation media (basal medium supplemented with 50 $mg\cdot ml^{-1}$ ascorbic acid, 10 mM β-glycerophosphate and 10^{-7} M dexamethasone). After 7, 14 and 21 days time of culture, the cells were evaluated for viability, DNA content and morphology as detailed in Chapter II.5.2.2.1., 5.2.2.2. and 5.2.2.3. respectively.

5.3.4. Osteogenic activity of electrospun scaffolds on BM-MSCs

All conditions were culture in basal and osteogenic differentiation media (basal medium supplemented with 50 $mg\cdot ml^{-1}$ ascorbic acid, 10 mM β-glycerophosphate and 10^{-7} M dexamethasone). Cell culture conditions were the same used for ALP quantification as detailed in section II.5.2.5.1. For the quantification of the osteogenic markers (i.e. *Bglap*. *Spp1*, *Sp7*, *Alpl*) the cell's RNA was extracted with Tri-reagent (Sigma-Aldrich, UK) according to manufacturer's instructions. The RNA concentration was determined by microspectrophotometry (NanoDrop 1000, Germany). The complementary DNA (cDNA) synthesis was performed using the qScript cDNA synthesis kit (Quanta BioSciences, VWR, Germany) with 100 ng of RNA template in a final volume of 20 µl. Cycling was as follows: 1 cycle at 22 °C, 5 min; 1 cycle at 42 °C, 30 min; 1 cycle at 85 °C, 5 min. The amplification of the target cDNA was performed using the PerfeCTa SYBR Green FastMix (Quanta BioSciences, Germany) with 1 µl of cDNA, 200 nM of each primer (Table II.1) in a final volume of 20 µl. Real time-PCR cycling was as follows: 1 cycle at 95 °C, 2 min; 44 cycles at 95 °C; 10 s/gene annealing temperature (Table II.1); 30 s/72 °C; followed by dissociation curve analysis. All the reactions were carried out on a PCR cycler Mastercycler Realplex (Eppendorf, Germany). The transcripts expression data were normalised to the housekeeping gene glyceraldehyde-3-phosphate dehydrogenase (*Gapdh*) in each sample. The quantification was performed according to the Livak method ($2^{-\Delta\Delta Ct}$ method), considering as calibrator at each time point the PLLA - basal

medium for PLLA- osteogenic medium and PLLA-BBG-Sr basal medium for PLLA-BBG-Sr osteogenic medium (threshold = 1).

Table II.1 - Primers used for rtPCR

Gene	Primer sequence 5'-3' Forward/ reverse	T_m (ºC)
Osteocalcin (*Bglap*)	CATCTATGGCACCACCGTTT	60.0
	AGAGAGAGGGAACAGGGAGG	
Osteopontin (*Spp1*)	ATCTCACCATTCCGATGAATCT	60.0
	CAGTCCATAAGCCAAGCTATCA	
Osterix (*Sp7*)	CACTGGCTCCTGGTTCTCTC	60.0
	CCACTCCTCCTCTTCGTGAG	
Alkaline phosphatase (*Alpl*)	TGCCTTACCAACTCATTTGTG	57.4
	ACGCGATGCAACACCACTC	

References

(1) Hench, L., The story of Bioglass. *Journal of Materials Science: Materials in Medicine* **2006,** 17, (11), 967-978.

(2) Hench, L. L., Bioceramics: From Concept to Clinic. *Journal of the American Ceramic Society* **1991,** 74, (7), 1487-1510.

(3) Xu, S.; Yang, X.; Chen, X.; Shao, H.; He, Y.; Zhang, L.; Yang, G.; Gou, Z., Effect of borosilicate glass on the mechanical and biodegradation properties of 45S5-derived bioactive glass-ceramics. *Journal of Non-Crystalline Solids* **2014,** 405, 91-99.

(4) Rahaman, M. N.; Day, D. E.; Sonny Bal, B.; Fu, Q.; Jung, S. B.; Bonewald, L. F.; Tomsia, A. P., Bioactive glass in tissue engineering. *Acta Biomaterialia* **2011,** 7, (6), 2355-2373.

(5) Huang, W.; Day, D.; Kittiratanapiboon, K.; Rahaman, M., Kinetics and mechanisms of the conversion of silicate (45S5), borate, and borosilicate glasses to hydroxyapatite in dilute phosphate solutions. *Journal of Materials Science: Materials in Medicine* **2006,** 17, (7), 583-596.

(6) Pan, H. B.; Zhao, X. L.; Zhang, X.; Zhang, K. B.; Li, L. C.; Li, Z. Y.; Lam, W. M.; Lu, W. W.; Wang, D. P.; Huang, W. H.; Lin, K. L.; Chang, J., Strontium borate glass: potential biomaterial for bone regeneration. *Journal of The Royal Society Interface* **2010,** 7, (48), 1025-1031.

(7) Rahaman, M. N.; Liang, W.; Day, D. E., Preparation and Bioactive Characteristics of Porous Borate Glass Substrates. In *Advances in Bioceramics and Biocomposites: Ceramic Engineering and Science Proceedings*, John Wiley & Sons, Inc.: 2008; pp 1-10.

(8) Yang, X.; Zhang, L.; Chen, X.; Sun, X.; Yang, G.; Guo, X.; Yang, H.; Gao, C.; Gou, Z., Incorporation of B_2O_3 in CaO-SiO_2-P_2O_5 bioactive glass system for improving strength of low-temperature co-fired porous glass ceramics. *Journal of Non-Crystalline Solids* **2012,** 358, (9), 1171-1179.

(9) Wu, C.; Fan, W.; Gelinsky, M.; Xiao, Y.; Simon, P.; Schulze, R.; Doert, T.; Luo, Y.; Cuniberti, G., Bioactive $SrO–SiO_2$ glass with well-ordered mesopores: Characterization, physiochemistry and biological properties. *Acta Biomaterialia* **2011,** 7, (4), 1797-1806.

(10) Hoppe, A.; Güldal, N. S.; Boccaccini, A. R., A review of the biological response to ionic dissolution products from bioactive glasses and glass-ceramics. *Biomaterials* **2011,** 32, (11), 2757-2774.

(11) Yamasaki, Y.; Yoshida, Y.; Okazaki, M.; Shimazu, A.; Uchida, T.; Kubo, T.; Akagawa, Y.; Hamada, Y.; Takahashi, J.; Matsuura, N., Synthesis of functionally graded MgCO3 apatite accelerating osteoblast adhesion. *Journal of Biomedical Materials Research* **2002,** 62, (1), 99-105.

(12) Maeno, S.; Niki, Y.; Matsumoto, H.; Morioka, H.; Yatabe, T.; Funayama, A.; Toyama, Y.; Taguchi, T.; Tanaka, J., The effect of calcium ion concentration on osteoblast viability, proliferation and differentiation in monolayer and 3D culture. *Biomaterials* **2005,** 26, (23), 4847-4855.

(13) Madhavan Nampoothiri, K.; Nair, N. R.; John, R. P., An overview of the recent developments in polylactide (PLA) research. *Bioresource Technology* **2010,** 101, (22), 8493-8501.

(14) Almeida, C. R.; Serra, T.; Oliveira, M. I.; Planell, J. A.; Barbosa, M. A.; Navarro, M., Impact of 3-D printed PLA- and chitosan-based scaffolds on human monocyte/macrophage responses: Unraveling the effect of 3-D structures on inflammation. *Acta Biomaterialia* **2014,** 10, (2), 613-622.

(15) Bettahalli, N. M. S.; Steg, H.; Wessling, M.; Stamatialis, D., Development of poly(l-lactic acid) hollow fiber membranes for artificial vasculature in tissue engineering scaffolds. *Journal of Membrane Science* **2011,** 371, (1–2), 117-126.

(16) Lou, T.; Wang, X.; Song, G.; Gu, Z.; Yang, Z., Fabrication of PLLA/β-TCP nanocomposite scaffolds with hierarchical porosity for bone tissue engineering. *International Journal of Biological Macromolecules* **2014,** 69, 464-470.

(17) Gupta, B.; Revagade, N.; Hilborn, J., Poly(lactic acid) fiber: An overview. *Progress in Polymer Science* **2007,** 32, (4), 455-482.

(18) Sui, G.; Yang, X.; Mei, F.; Hu, X.; Chen, G.; Deng, X.; Ryu, S., Poly-L-lactic acid/hydroxyapatite hybrid membrane for bone tissue regeneration. *Journal of Biomedical Materials Research Part A* **2007,** 82A, (2), 445-454.

(19) Haimi, S.; Suuriniemi, N.; Haaparanta, A.-M.; Ellä, V.; Lindroos, B.; Huhtala, H.; Räty, S.; Kuokkanen, H.; Sándor, G. K.; Kellomäki, M.; Miettinen, S.; Suuronen, R., Growth and Osteogenic Differentiation of Adipose Stem Cells on PLA/Bioactive Glass and PLA/β-TCP Scaffolds. *Tissue Engineering Part A* **2008,** 15, (7), 1473-1480.

(20) Shakya, A. K.; Holmdahl, R.; Nandakumar, K. S.; Kumar, A., Polymeric cryogels are biocompatible, and their biodegradation is independent of oxidative radicals. *Journal of Biomedical Materials Research Part A* **2014,** 102, (10), 3409-3418.

(21) Niu, Y.; Guo, L.; Liu, J.; Shen, H.; Su, J.; An, X.; Yu, B.; Wei, J.; Shin, J.-W.; Guo, H.; Ji, F.; He, D., Bioactive and degradable scaffolds of the mesoporous bioglass and poly(l-lactide) composite for bone tissue regeneration. *Journal of Materials Chemistry B* **2015,** 3, (15), 2962-2970.

(22) Kothiyal, G. P.; Ananthanarayanan, A.; Dey, G. K., 9 - Glass and Glass-Ceramics. In *Functional Materials*, Tyagi, S. B. K., Ed. Elsevier: London, 2012; pp 323-386.

(23) Kokubo, T.; Takadama, H., How useful is SBF in predicting *in vivo* bone bioactivity? *Biomaterials* **2006,** 27, (15), 2907-2915.

(24) Maniatopoulos, C.; Sodek, J.; Melcher, A. H., Bone formation *in vitro* by stromal cells obtained from bone marrow of young adult rats. *Cell Tissue Research* **1988,** 254, (2), 317-330.

(25) Santocildes-Romero, M. E.; Crawford, A.; Hatton, P. V.; Goodchild, R. L.; Reaney, I. M.; Miller, C. A., The osteogenic response of mesenchymal stromal cells to strontium-substituted bioactive glasses. *Journal of Tissue Engineering and Regenerative Medicine* **2015,** 9, (5), 619-631.

(26) Matuschek, E.; Brown, D. F. J.; Kahlmeter, G., Development of the EUCAST disk diffusion antimicrobial susceptibility testing method and its implementation in routine microbiology laboratories. *Clinical Microbiology and Infection* **2014,** 20, (4), O255-O266.

(27) Chryssanthou, E.; Cuenca-Estrella, M., Comparison of the EUCAST-AFST broth dilution method with the CLSI reference broth dilution method (M38-A) for susceptibility testing of posaconazole and voriconazole against Aspergillus spp. *Clinical Microbiology and Infection* **2006,** 12, (9), 901-904.

(28) Tchouaffi-Nana, F.; Ballard, T. E.; Cary, C. H.; Macdonald, T. L.; Sifri, C. D.; Hoffman, P. S., Nitazoxanide Inhibits Biofilm Formation by Staphylococcus epidermidis by Blocking Accumulation on Surfaces. *Antimicrobial Agents and Chemotherapy* **2010,** 54, (7), 2767-2774.

(29) Axford, J. S., Joint and bone infections. *Medicine* **2010,** 38, (4), 194-201.

(30) European Committee for Antimicrobial Susceptibility Testing of the European Society of Clinical, M.; Infectious, D., Terminology relating to methods for the determination of susceptibility of bacteria to antimicrobial agents. *Clinical Microbiology and Infection* **2000,** 6, (9), 503-508.

(31) ISO/EN10993–5, Biological Evaluation of Medical Devices— Par 5: Tests for Cytotoxicity: *In Vitro* Methods. *Geneva, Switzerland: International Standards* **1992**.

(32) Ren, L.; Lin, X.; Tan, L.; Yang, K., Effect of surface coating on antibacterial behavior of magnesium based metals. *Materials Letters* **2011,** 65, (23–24), 3509-3511.

(33) Zhang, L.; Tan, P. Y.; Chow, C. L.; Lim, C. K.; Tan, O. K.; Tse, M. S.; Sze, C. C., Antibacterial activities of mechanochemically synthesized perovskite strontium titanate ferrite metal oxide. *Colloids and Surfaces A: Physicochemical and Engineering Aspects* **2014,** 456, (0), 169-175.

(34) Lin, Y.; Yang, Z.; Cheng, J.; Wang, L., Synthesis, characterization and antibacterial property of strontium half and totally substituted hydroxyapatite nanoparticles. *J. Wuhan University.of Technology-Materials Science Edit.* **2008,** 23, (4), 475-479.

3. SECTION

III. CHAPTER

Design and Properties of Novel Substituted Borosilicate Bioactive Glasses

CHAPTER III
DESIGN AND PROPERTIES OF NOVEL SUBSTITUTED BOROSILICATE BIOACTIVE GLASSES

III. CHAPTER

Design and Properties of Novel Substituted Borosilicate Bioactive Glasses[2]

Abstract

Three novel borosilicate bioactive glasses (BBGs) of general formula of $0.05Na_2O{\cdot}0.35x{\cdot}0.20B_2O_3{\cdot}0.40SiO_2$ (molar ratio, where x = MgO or CaO or SrO) were prepared and used to investigate the effect of crystallisation on their properties including cytotoxicity. The three post-melt compositions were determined using ARF and crystallisation events were studied using DTA and XRD. This information was used to determine heat treatments to prepare glass-ceramics by controlled crystallisation. XRD analysis and Fourier transform infrared spectroscopy showed that, after higher heat treatment temperatures (800-900 ºC), borosilicate bioactive glass-ceramics (BBGCs) contained mainly borate and silicate crystalline phases. Specifically, BBG-Mg, BBG-Ca and BBG-Sr glass-ceramics detected the presence of magnesium silicate-$Mg_2(SiO_3)_2$ and magnesium borate-$Mg_2B_2O_5$; wollastonite-2M-$CaSiO_3$ and calcium borate-$Ca(BO_2)_2$; and strontium silicate-$SrSiO_3$ and strontium borate-$Sr_2B_2O_5$, respectively. *In vitro* cytotoxicity tests were performed using the L929. Glass and glass ceramics at concentrations lower than 50 $mg{\cdot}ml^{-1}$ did not exhibit any level of cytotoxicity when compared with the control. However, quantitative evaluation indicated that greater cell growth occurred in the presence of materials with crystalline phases. Control of BBGs crystallisation may therefore be used to influence the biocompatibility of these glass-ceramic systems.

[2] This chapter is based on the following publication:

João S. Fernandes, Piergiorgio Gentile, Robert Moorehead, Aileen Crawford, Cheryl A. Miller, Ricardo A. Pires, Paul V. Hatton, Rui L. Reis; Design and Properties of Novel Borosilicate Bioactive Glasses for Bone Tissue Applications, Crystal Growth and Design 2016, 16 (7), pp 3731–3740

1. Introduction

BGs and bioactive glass-ceramics (BGCs) have been evaluated for a wide range of clinical applications related to bone tissue repair and regeneration [1]. BGs and BGCs are widely reported to form a bone-like HA layer on their surface when placed in a simulated biological environment [2]. This has also been demonstrated to occur *in vivo* [3]. Formation of a bone-like HA layer is a fundamental requirement for the establishment of a strong interfacial bond between implants and bone [4]. Since Hench *et al.* [2] proposed the CaO: SiO_2: Na_2O: P_2O_5 system in 1969, 45S5 bioglass® (or Bioglass®) has become the gold standard for this type of material. However, slow degradation rate is a major disadvantage of the silicate based BG, which makes it difficult to match the degradation rate of the BG scaffolds with the rate of new tissue formation [5, 6]. Moreover, some studies with silicate glasses report slow conversion rate to a bone-like HA and often this conversion remains incomplete. Therefore unconverted glass containing SiO_2 could remain in human body long after its implantation, raising uncertainty regarding the long-term effects of SiO_2 *in vivo* [7, 8].

The addition of boron oxide to the glass network is one approach that has the potential to overcome the limitations identified above by modifying dissolution rates, as well as other properties including tissue bonding [9]. The incorporation of boron in a silicate glass matrix involves lower melting temperatures, with an increased bio-degradation and increased conversion to HA [8, 10, 11]. Furthermore, boron is reported to be beneficial for bone healing and its controlled release stimulates bone formation and maintenance. Frequently, it has been associated with the increase in bone resistance to fractures [12-14]. Thereby, BBGs composition may be used to achieve a more controlled release of specific component ions in order to trigger a range of biological responses [15]. Control of the surface reactions and therefore of the biodegradation and bioactivity of implanted materials can be achieved by varying the chemical nature and/or concentration of the BBGs constituents. For instance, Ciceo Lucacel *et al.* [16] have used the calcium BBGs doped with silver (Ag^+) to better control Ag^+ antibacterial properties. Xu *et al.* [6] have also proposed a sol–gel-derived calcium BBG system for reinforcing glass-ceramic porous biomaterials and accurately control their biodegradability. In another study, Wang *et al.* [17] evaluated the of osteogenic properties of BBGs doped with Zinc (Zn^{2+}); these BBGs significantly enhanced bone

regeneration in bone defects when implanted into rats *in vivo*. Baiano *et al.* [18] used BGs-based trabecular coating for the development of a novel prosthetic acetabular cup with an improved *in vivo* interfacial bond with bone.

While studies have been demonstrating the ability of BBGs to better control degradation, thus increasing the beneficial properties of ions release, there are still concerns regarding toxicity when those glasses are implanted [19, 20]. There are several metal ions that at higher concentrations are extremely toxic. In particular, boron release has been associated with cell growth inhibition for concentrations greater then 2.5 mM, and also causes cytotoxicity due to the release of $(BO_3)^{3-}$ into the medium [12, 19, 20]. Several cellular studies investigated the cytotoxicity of BGs and reported the inhibition of cell viability and proliferation for high doses of ions in culture [21, 22]. For instance, Santocildes-Romero *et al.* [23] have showed an increase on the cytotoxicity of BGs dissolution by increasing the amount of glass powders used, and the level of strontium substitution in the glass composition. Moreover, specific component ions released in a controlled rate may stimulate differently cells. Metallic ions such as magnesium (Mg^{2+}), calcium (Ca^{2+}) or strontium (Sr^{2+}) can stimulate bone cell proliferation, differentiation and ECM mineralisation, as well as increase the production rate of HA and bone [21, 22, 24-26]. For instance, Mg^{2+} is commonly related with cells' adhesion and stability [24], while Ca^{2+} [25] and Sr^{2+} [26] are generally associated to the apatite formation process and cells differentiation and mineralisation. Moreover, Sr^{2+} has been successfully studied for the treatment of osteoporosis[21].

Various studies have been reported concerning the use of heat treatments in order to induce crystallisation in BGs to promote changes in their physico-chemical properties [27-31]. For instance, Rao *et al.* [32] have observed improvements in the dielectric constant and less dielectric loss of sodium borosilicate glasses (SiO_2–B_2O_3–Na_2O system) with the increase in the duration of the heat treatment. Daguano *et al.* [27] developed and characterised BGs and BGCs from the CaO-P_2O_5-SiO_2-MgO system, using different degrees of crystallinity. They showed that partial crystallisation improved the mechanical properties by phase transformation, which modified the microstructure of the base glassy material. Therefore, after studying the thermal profile of BGs, appropriate heat treatment cycle with a controlled temperature increase could be applied to promote the re-arrangement of the glass structures generating a well-ordered and crystalline structure.

The properties of the formed glass-ceramics are mostly influenced by the characteristics of the finely dispersed crystalline and the residual glassy phases, which can be controlled by the composition of the base glass. However, few authors have reported that the formation of new crystalline phases provoked the modification of the toxic effects induced by the glasses in cells [27, 30]. Specially, Hurrell-Gillingham *et al.* [30] investigated the effects of devitrification of glass-ionomer cements (GICs) from SiO_2-Al_2O_3-P_2O_5-CaO-CaF_2 system on glass-ceramic formation and *in vitro* biocompatibility. They demonstrated that crystallisation might be used to improve the *in vitro* biocompatibility of GICs. Also Freeman *et al.* [33] studied the response to implantation of apatite glass-ceramics. They demonstrated that crystallisation significantly improved the bone tissue response.

It seems likely that devitrification of glasses represents a route to modify and study their properties including biocompatibility. However, few attempts to modify the biocompatibility of medical grade glasses using this approach have been reported [30, 33]. This study aimed to firstly synthesise and characterise the thermal and chemical properties of three novel substituted BBGs. The incorporation of different ions (i.e. Mg^{2+}, Ca^{2+} and Sr^{2+}) in BBGs lies on the fact that specific effects can be used to achieve different human cell behaviour by the release of ionic dissolution products. Secondly, we aimed to investigate the effect of BBGs crystallisation on their cytotoxic effects, providing a method for the improvement of bioactive borosilicate glass-ceramics cellular properties.

2. Materials and Methods

2.1. Materials

All chemical compounds used for melt-quenched synthesis were reagent grade: di-boron trioxide (Alfa Aesar, Germany), calcium carbonate (Sigma-Aldrich, Portugal), sodium bicarbonate (Sigma-Aldrich, Australia), silica gel 60M (Macherey-Nagel, Germany), magnesium oxide (Sigma-Aldrich, Portugal) and strontium carbonate (Sigma-Aldrich, Australia).

2.2. Glass synthesis and preparation

The novel BBGs of general formula $0.05Na_2O \cdot xMgO \cdot yCaO \cdot (0.35\text{-}x\text{-}y)SrO \cdot 0.20B_2O_3 \cdot 0.40SiO_2$ (molar ratio, where x, y = 0.35 or 0.00, and $x \neq y$) were synthesised by melt quenching. The appropriate amounts of SiO_2, B_2O_3, $NaHCO_3$, and $CaCO_3$ or MgO or $SrCO_3$ were accurately mixed with ethanol (Sigma, Portugal) in a porcelain mortar and with the help of a pestle, fully dried overnight and transferred to a platinum crucible. The batch was heated to 1450 ˚C in air for 1 h and subsequently the melt was quickly poured into a water bath at 4 ˚C to form a glass frit. The glass frit was ground into an Agate mortar (RETSCH, Germany) to obtain microparticles and then, sieved for a size smaller than 63 μm.

2.3. Characterisation

2.3.1. X-ray fluorescence (XRF)

The XRF was used to confirm the glass composition (Philips PW2400 X-ray fluorescence spectrometer, UK). Samples were prepared by fusing powdered glass with a known quantity of boron and a flux producing a glass-like bead. After which, they were irradiated with high-energy primary X-ray photons. All the samples were run in triplicate and the percentage (w/w) of the oxides present were determined. Afterwards, molar percentage was calculated for all the samples.

2.3.2. Differential thermal analysis (DTA) and heat treatment

The mid point of glass transition (T_g), and crystallisation (T_c) temperatures were determined by DTA analysis (Perkin-Elmar DTA7 running Pyris thermal analysis software in Unix, UK) at a heating rate of 10 ºC min^{-1} from 50 to 1300 ºC.

In accordance with DTA data, crystallised glasses were prepared for each sample. Briefly, fast-quenched particles of the glass samples were heat-treated with a heating rate of 10 ºC min^{-1} and held for 120 min at each temperature (T_g, T_{c1}, T_{c2} and T_{c3}) before cooling to RT.

2.3.3. X- ray diffraction analysis (XRD) and attenuated total reflection Fourier transform infrared (ATR-FTIR) spectroscopy

The glasses were analysed before and after each heat treatment by XRD and ATR-FTIR. A STOE STADI P X-ray diffractometer was used to identify the crystalline phases. The glass samples were place in aluminium holders and analysed by Cu radiation of wavelength 1.5406 Å at a voltage of 40 kV and a current of 40 mA with a step size of 0.2° in a range of 2θ values from 10° to 80° at a scanning speed of 10 s/step. The crystalline patterns were identified by the use of the cards listed in the JCPDS. The ATR-FTIR spectra were aquired using a Perkin-Elmer GX, UK instrument in the range of 4000-550 cm^{-1} (resolution 4 cm^{-1}) for the identification of the chemical bonds present in the glass or glass-ceramic structures.

2.4. *In vitro* cytotoxicity

The *in vitro* cytotoxicity study was design following the international guidelines ISO 10993-5:2009 [34], using immortalised L929 (Rockville, MD) in indirect contact with glass particles for 3 days. The samples were sterilised in an oven (Gallenkamp Hot Box, UK) at 160 °C for 120 min. After sterilisation, the glasses were added to DMEM (Sigma-Aldrich, UK) solution at a concentration of 0.2 $g \cdot ml^{-1}$ and incubated for 24 h at 37 °C. After incubation, the glass-conditioned medium was removed and filtered through a 0.2 μm membrane.

The L929 cells were expanded in DMEM supplemented with 10 % (v/v) fetal calf serum (Sigma-Aldrich, UK), penicillin (100 U·ml, Sigma-Aldrich, UK) and streptomycin (100 μg·ml, Sigma-Aldrich, UK), and NEAA (Sigma-Aldrich, UK). The L929 cells were cultured at 37 °C in an atmosphere of 5 % CO_2. Confluent L929 cells at passages between 15 and 19 were harvested and seeded into 48-well culture plates (growth area 0.95 cm^2) at a density of 2×10^4 cells/well. After a 24 h culture period the culture media was discarded and replaced with 0.5 cm^3 of serially diluted, glass-conditioned medium (at a final concentrations of 100, 50, 25, 10, and 5%). L929 cells cultured in the absence of glass particles, was used as negative control and 45S5 bioglass®- conditioned medium as positive control. After 1 and 3 days time of culturing, the culture medium was removed

and the viability and DNA content of the cultures were analysed using PrestoBlue® and Picogreen® assays respectively.

2.4.1. Cell viability assessment

The PrestoBlue® reagent (Fisher Scientific, UK) is a resazurin-based non-fluorescent solution that is reduced to fluorescent resorufin by viable cells. The assay was performed according to the manufacturer's instructions. In brief, the PrestoBlue® reagent was added to a final concentration of 10% to the cell cultures and the cultures incubated for 1 h at 37°C. 200 µl samples of the culture medium were removed and placed in 96-well plates and the resorufin fluorescence quantified spectrophotometrically using a plate reader (Tecan Infinite M200, UK). The fluorescence was determined at an excitation wavelength of 560 nm and emission wavelength of 590 nm. The cell viabilities were normalised as % of the metabolic activity of the control cell cultures.

2.4.2. DNA measurement

The PicoGreen® dsDNA reagent (Invitrogen, USA) is an ultrasensitive fluorescent nucleic acid dye for quantification of dsDNA in solution. This assay enables the measurement of cell proliferation. After each culturing period, the cell monolayers were washed with PBS and then incubated at 37 ºC for 3 h followed by freezing step at -80 ºC for at least over night in ultra-pure water (1 ml) to ensure cell lysis. The assay was performed according to the manufacturer's protocol. And the fluorescence was determined at an excitation wavelength of 485 nm and emission wavelength of 528 nm. The DNA values were normalised to those of the control cultures.

2.4.3. Morphological evaluation of cell cultures

After each culturing period the cell monolayers were washed with PBS and fixed with 4% formalin solution (0.5 ml) for 15 min at RT. The cell layers were then washed with PBS, containing 0.2% Triton X, for 2 min. After the fixation and permeation steps, the cell monolayers were washed again with PBS and stained with DAPI (1:1000, Sigma, UK) for 2 min at RT, and phalloidin-tetramethylrhodamine B isothiocyanate (Sigma, UK) for 1 h

at RT. Finally, the cells were washed and observed using an Axioplan 2 imaging fluorescent microscope with a digital camera QIC AM 12-bit (Zeiss, UK).

2.5. Statistical analysis

Experiments were run at least in triplicate for each sample. All data were expressed as mean ± SD. Statistical analysis was determined using Graphpad Prism® software, version 6.0. The normality of the data distribution was monitored by Shapiro-Wilk test ($p < 0.05$). Some of the datasets were not considered to have a normal distribution, requiring a non-parametric statistical evaluation. In this context, Kruskal-Wallis test ($p < 0.05$) was applied to all dataset, followed by a Dunn's Multiple Comparison test.

3. Results and Discussion

3.1. Glass characterisation

3.1.1. X-ray fluorescence

The XRF data, presented in Table III.1, confirmed that the experimental compositions of BBGs obtained by melt-quench method were close to the expected theoretical composition, indicating that the glass network structure was formed as aimed. The slight differences between theoretical and XRF data may have been caused by the high volatility of alkali-borate compounds during the melting process [35].

Table III.1 - XRF estimation of elemental concentration (mol %) of BBGs. BBG-Mg, -Ca and -Sr glasses (* varies with the specific ion for each glass). All analysis were performed in triplicate and SD < 0.05.

Samples / composition	Si (mol %)	B (mol %)	Na (mol %)	Ions* (mol %)
BBG-Mg	37.6 (40)	34.8 (40)	10.4 (10)	39.7 (35)
BBG-Ca	36.9 (40)	43.8 (40)	10.4 (10)	36.0 (35)
BBG-Sr	37.5 (40)	41.4 (40)	10.4 (10)	36.7 (35)

3.1.2. Differential thermal analysis

The DTA was used to study the phase transformation temperatures of the BBGs in order to determine the heat treatment schedule. DTA patterns from all BBGs are presented in Figure III.1a. For BBG-Mg and BBG-Sr along with the mid point of glass transition temperature (T_g - endothermic peak), two crystallisation temperatures (T_c - exothermic peaks) were found; while BBG-Ca glasses presented a T_g and one exothermic (T_{c1}) peak followed by a doublet exothermic peak (T_{c2} and T_{c3}). The T_g and T_c used for the different glass compositions are listed in Figure III.1b. The BBGs revealed crystallisation temperatures within the range of temperatures of 700 to 900 °C with two phases frequently related with borate and silicate crystal phases [15]. The endothermic peaks are related to the molecular re-arrangement in glass structure preceding and during glass crystallisation, a process known for crystal nucleation and growth [15, 29]. In order to induce crystal nucleus formation in the glass structure, BBGs were kept for 2 h at T_g and subsequently for 2 h at each T_c. Each well-defined exothermic peak may result in the formation of a different crystalline phase [28]. For each BBGs different heat treatment schedules were applied according to the endo- and exothermic peak temperatures reported in Figure III.1b.

a b

Temp (°C) / Samples	T_g	T_{c1}	T_{c2}	T_{c3}
BBG-Mg	623	726	856	-
BBG-Ca	622	716	827	897
BBG-Sr	606	697	862	-

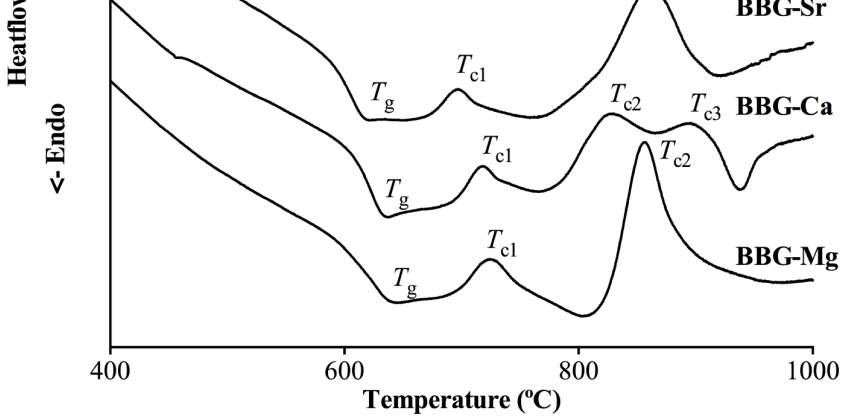

Figure III.1 - (a) DTA patterns of BBG-Mg, BBG-Ca and BBG-Sr glasses. T_g – mid point of glass transition temperature and T_c – crystallisation temperature. (b) The mid point of glass transition temperature and crystallisation temperatures for the BBGs (BBG-Mg, -Ca and -Sr glasses) determined by DTA analysis (T_g – mid point of glass transition temperature and T_c – crystallisation temperature).

3.1.3. X- ray diffraction and attenuated total reflection Fourier transform infrared

The XRD analysis was performed in order to study the crystallinity of the glasses before and after heat treatments and the respective phases formed (Table III.2). Figure III.2a, 2b and 2c shows the phase evolution XRD patterns of BBG-Mg, -Ca and -Sr glasses, respectively, from amorphous to crystalline phase after the different heat treatment schedules. Heat treatment schedule at T_g were performed and exhibit no significant difference in respect with the as quenched XRD patterns.

The XRD patterns of BBG-Mg glass after the first crystallisation heat treatment (BBG-Mg_T_{c1}) showed a predominantly amorphous phase with weak diffraction peaks, which

can be assigned to silicon oxide (SiO_2, JCPDS Card No. 11-252). After T_{c2} heat treatment (BBG-Mg_T_{c2}) two predominant crystalline phases of magnesium silicate ($Mg_2(SiO_3)_2$, JCPDS Card No. 86-433) and magnesium borate ($Mg_2B_2O_5$, JCPDS Card No. 73-2232) were observed.

In the case of XRD patterns of BBG-Ca glass after the first crystallisation heat treatment (BBG-Ca_T_{c1}) it was observed a predominantly amorphous phase with some weak diffraction peaks, which can be attributed either to calcium silicate ($CaSiO_3$, JCPDS Card No. 76-186) and/or calcium borate ($Ca(BO_2)_2$, JCPDS Card No. 31-155), indicating that after T_{c1} crystallisation started to occur. After the second heat treatment (BBG-Ca_T_{c2}) there is the formation of two predominant crystalline phases, calcium silicate, commonly referred as wollastonite-2M and calcium borate. After the T_{c3} heat treatment (BBG-Ca_T_{c3}) the diffraction patterns are comparable to the previous heat treatment patterns (T_{c2}), which indicates that no detectable amount of different crystalline phase is forming.

For the BBG-Sr glass, after the first crystallisation heat treatment (BBG-Sr_T_{c1}) it was observed a predominant amorphous phase of the glass and a weak diffraction peak, in which the weak peaks can be attributed either to strontium silicate ($SrSiO_3$, JCPDS Card No. 87-474) and/or strontium borate ($Sr_2B_2O_5$, JCPDS Card No. 19-1268), suggesting that the formation of crystalline phases starts after the first crystallisation heat treatment. After the second heat treatment (BBG-Sr_T_{c2}) two crystalline phases of strontium silicate and strontium borate were formed.

Finally, XRD data showed that for all BBGs after heat treatment with lower crystallisation temperatures (T_{c1}), there was a predominantly amorphous phase with only a small amount of crystals' formation. However, after the latter heat treatments (T_{c2} and T_{c3}) occurred the formation of crystalline phases resulting in new silicate and borate glass-ceramics.

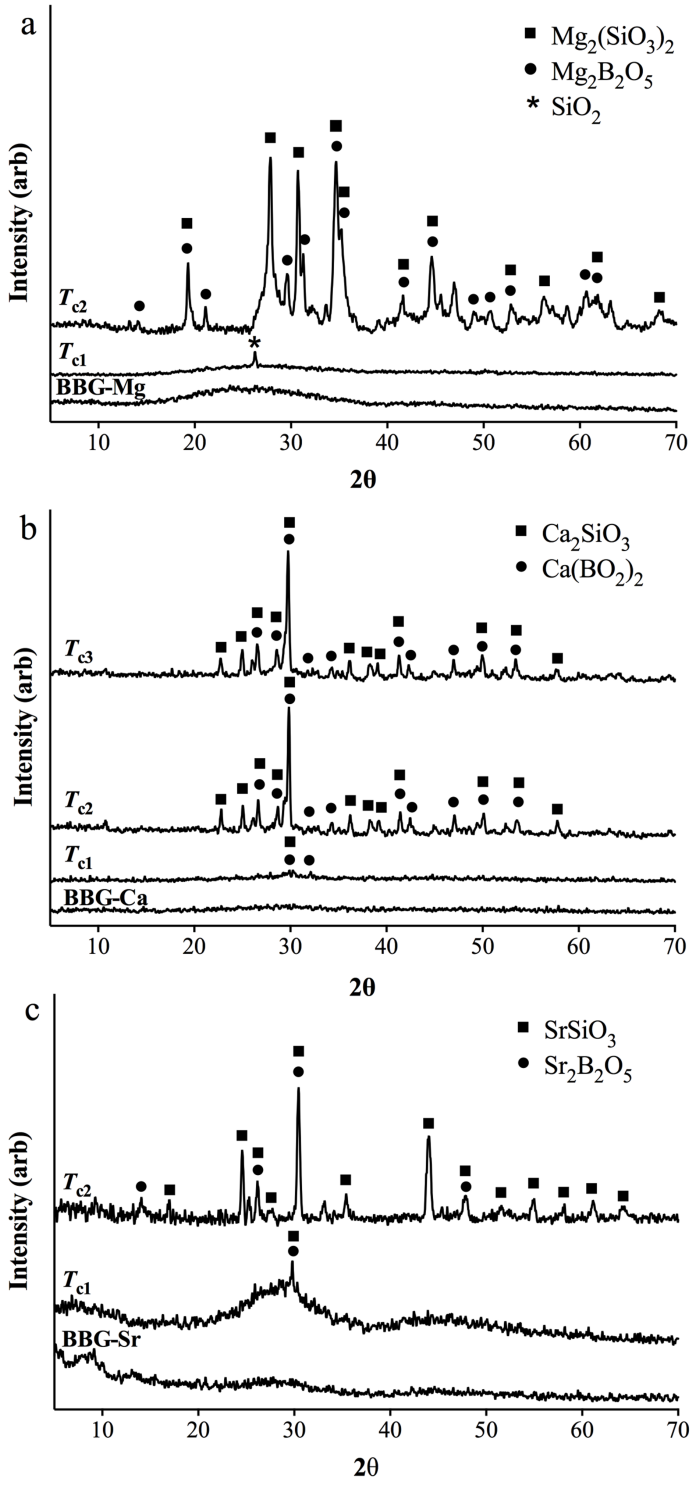

Figure III.2 - XRD patterns of phase evolution over increasing crystallisation temperatures for BBG-Mg (a), -Ca (b), -Sr (c) glasses (BBG-ion - before heat treatment, T_{c1} - after first heat treatment, T_{c2} - after second heat treatment, T_{c3} - after third heat treatment).

Table III.2 - Crystalline phases of BBG-Mg, -Ca and -Sr glasses obtained after heat treatments

Heat treatment	Heat temperature conditions	Crystalline phases
BBG-Mg_T_{c1}	623 °C / 2h + 726 °C / 2 h	Glass and SiO_2
BBG-Mg_T_{c2}	623 °C / 2 h + 856 °C / 2 h	$Mg_2(SiO_3)_2$; $Mg_2B_2O_5$
BBG-Ca_T_{c1}	622 °C / 2 h + 716 °C / 2 h	Glass and $Ca(BO_2)_2$
BBG-Ca_T_{c2}	622 °C / 2 h + 827 °C / 2 h	$CaSiO_3$; $Ca(BO_2)_2$
BBG-Ca_T_{c3}	622 °C / 2 h + 897 °C / 2 h	$CaSiO_3$; $Ca(BO_2)_2$
BBG-Sr_T_{c1}	606 °C / 2 h + 697 °C / 2 h	Glass and $SrSiO_3$; $Sr_2B_2O_5$
BBG-Sr_T_{c2}	606 °C / 2 h + 862 °C / 2 h	$SrSiO_3$; $Sr_2B_2O_5$

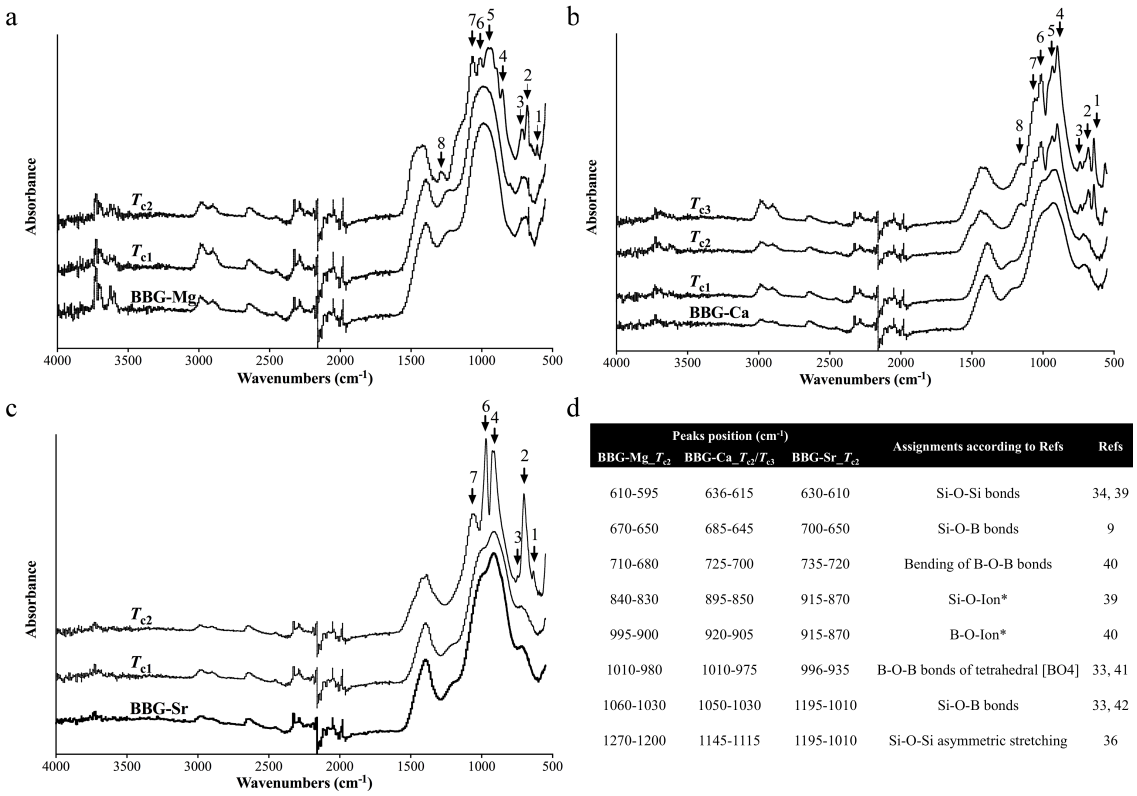

Peaks position (cm^{-1})			Assignments according to Refs	Refs
BBG-Mg_T_{c2}	BBG-Ca_T_{c2}/T_{c3}	BBG-Sr_T_{c2}		
610-595	636-615	630-610	Si-O-Si bonds	34, 39
670-650	685-645	700-650	Si-O-B bonds	9
710-680	725-700	735-720	Bending of B-O-B bonds	40
840-830	895-850	915-870	Si-O-Ion*	39
995-900	920-905	915-870	B-O-Ion*	40
1010-980	1010-975	996-935	B-O-B bonds of tetrahedral [BO4]	33, 41
1060-1030	1050-1030	1195-1010	Si-O-B bonds	33, 42
1270-1200	1145-1115	1195-1010	Si-O-Si asymmetric stretching	36

Figure III.3 - ATR-FTIR spectra of BBG-Mg (a), -Ca (b) and -Sr (c) glasses (BBG-ion - before heat treatment, T_{c1} - after first heat treatment, T_{c2} - after second heat treatment, T_{c3} - after third heat treatment). The numbers are referred to the type of bond found: 1 and 8 – Si-O-Si; 2 and 7 – Si-O-B; 3 and 6 – B-O-B; 4 – Si-O-Ion; 5 – B-O-Ion. (d) ATR-FTIR band assignments.

The ATR-FTIR analysis was performed to evaluate the possible changes on the vibrational spectra after the heat treatments, because they can induce a process of structural grouping re-arrangements, implying important modifications in the properties of the glasses [30, 36]. ATR-FTIR spectra of BBG-Mg, -Ca, -Sr glasses and glass-ceramics are presented in Figure III.3a, 3b and 3c, respectively. ATR-FTIR spectra of all BBGs consist of dominant broad bands from 740-585 and 1210-740 cm^{-1} generally attributed to B-O stretching of tetrahedral [BO_4] units, and 1550-1260 cm^{-1}, which are attributed to B-O stretching of trigonal [BO_3] unit [10, 36]. On the other hand the same broad bands from 740-585 and 1240-740 cm^{-1} can be also assigned to Si-O-Si symmetric and asymmetric stretching, respectively [37, 39]. The presence of these intense bands indicates the coexistence of silicate and borate bonds, which supports the presence of borosilicate network structure in the amorphous phase. There are two additional less intense bands

ranging from 3000 to 2800 and 3750 to 3500 cm^{-1} in all spectra before and after heat treatment, which can be associated with water content. The bands in the range 3000 to 2800 cm^{-1} have origin in hydrogen bonds and peaks from 3750 to 3500 cm^{-1} are due to OH- groups [36, 40, 41]. Furthermore, there are no significant differences comparing ATR-FTIR spectra of BBGs before and after T_{c1} heat treatment (comparing BBG-ion with T_{c1} of Figure III.3a, 3b and 3c). This fact suggests that there was no formation of detectable crystalline phases. However, for the latter heat treatments (T_{c2} and T_{c3}) all BBGs showed a splitting of the intense broad bands in several sharp peaks. The splitting of the broad bands might indicate structural grouping re-arrangements (e.g. 1210-740 cm^{-1} broad band is splitting into 4 different peaks for BBG-Mg glass-ceramic; Figure III.3a). Thus, temperatures higher than 800 °C indeed affected the glass network by rearranging the borosilicate structure. Moreover ATR-FTIR spectra of BBG-Ca glass-ceramics (after T_{c2} and T_{c3} heat treatment - Figure III.3b) did not show significant differences. This analysis agrees with XRD data, indicating that the crystallisation temperatures of the double exothermic peak found by DTA (Figure III.1) did not introduce an evident different molecular re-arrangement in glass structure and thereby theirs ATR-FTIR spectra will be analysed as one. The correspondent assignments for sharp peaks formed after the latter heat treatments (T_{c2} and T_{c3}) are presented in Figure III.3d, from where vibrational peaks ranging from 636-595 and 1270-1010 cm^{-1} can be attributed to the formation of Si-O-Si bonds and Si-O-Si asymmetric stretching, respectively [37, 39, 42]. On the other hand peaks ranging from 735-680 and 1010-935 cm^{-1} can be assigned to bending of B_2-O bonds in the borate glassy network and B_2-O bond of tetrahedral [BO_4] [36, 43, 44]. Finally, peaks ranging from 680-645 and 1195-1010 cm^{-1} can be attributed to the formation of Si-O-B bonds [10, 36, 45]. These assigned peaks confirmed the existence of new silicon and boron units at the structure network as shown by XRD data. Of highlighting are the peaks found from 915-830 and 955-870 cm^{-1} that can be assigned to the formation of Si–O–Ion and B-O-Ion bonds. That indicates the presence of silicate and borate structures bonding to metallic ions, which is in agreement with the formation of metal silicates and borates found by XRD analysis [10, 42, 43].

The ATR-FTIR analysis showed that for the latter heat treatments there are peaks that can be attributed to B-O-B and Si-O-Si bonds formation. The presence of those bonds supports the formation of silicate and borate crystalline phases previously indicated by XRD data. Also, peaks in the region of 950 to 850 cm^{-1} that are related with the formation

either of ion-O-Si and ion-O-B, strongly supports the presence of crystalline phases metal silicate and borate.

3.2. *In vitro* cytotoxicity

The cytotoxicity studies were designed to evaluate whether the degradation or dissolution of glasses and glass-ceramics affected the viability and proliferation of L929. The experimental design was based on the international guidelines of ISO 10993-5:2009 with some adjustments as described in the methods section [34]. Each glass and glass-ceramic sample was pre-incubated in DMEM to give a glass-conditioned media that were added to the cell cultures for 1 and 3 days.

The PrestoBlue® viability data (Figure III.4) showed that L929 cells in the presence either of glass- or glass-ceramic-conditioned medium exhibited a metabolic activity higher than 50% for concentrations lower than 50 mg·ml^{-1}. In the case of BBG-Mg glass and glass-ceramics even after 3 days of culture, the cells displayed good metabolic activity for media conditioned by concentrations of 50 mg·ml^{-1} (e.g.: for BBG-Mg_ T_{c2} at 50 mg·ml^{-1} concentration, cells present 74% of metabolic activity). However, all BBGs before and after heat treatment showed far higher metabolic activity than the commercial 45S5 bioglass (e.g.: after 3 days of culture with 45S5 bioglass®-conditioned media, L929 cells showed only 1% of the metabolic activity observed in the control cultures).

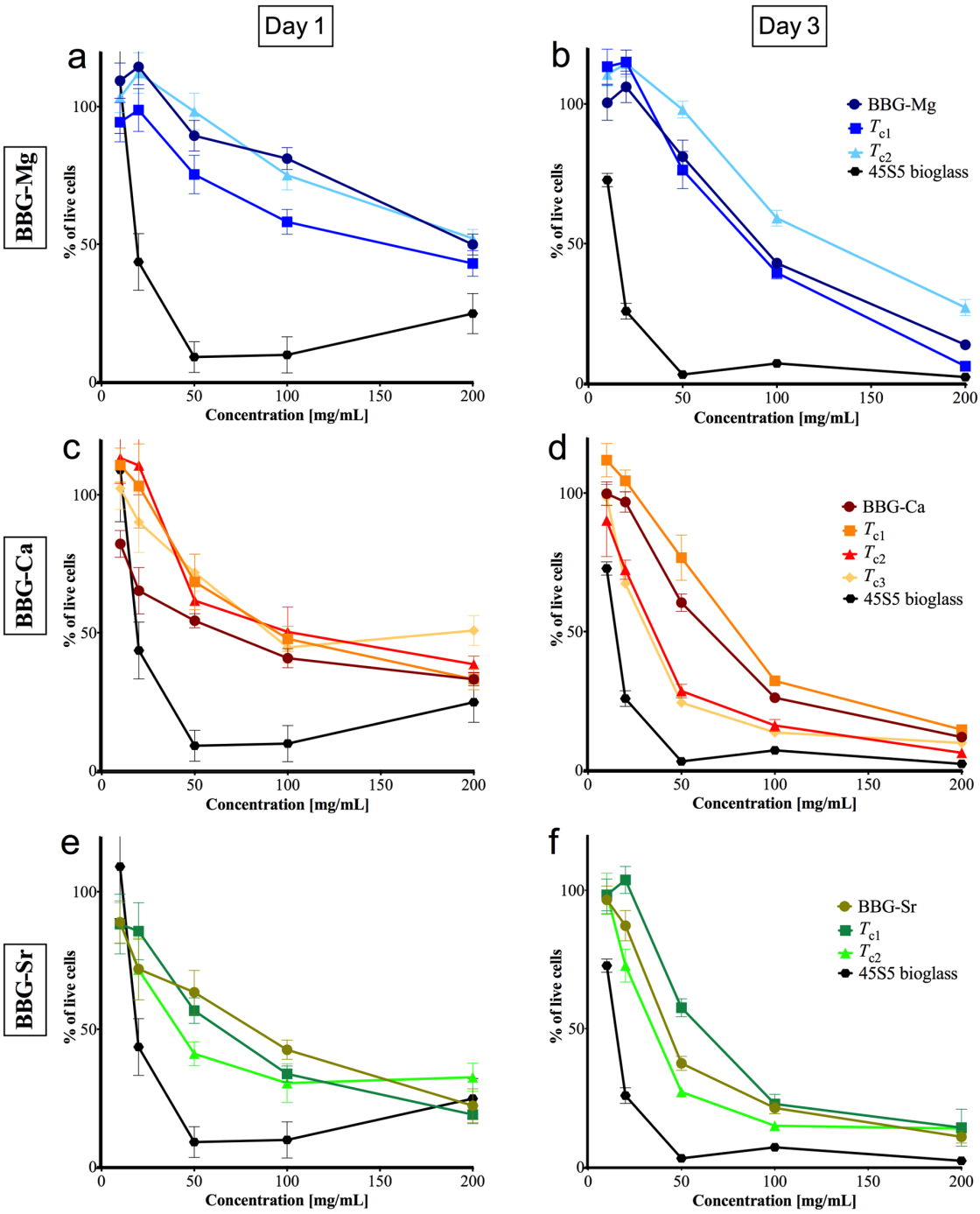

Figure III.4 - The cell viability of L929 cells after 1 and 3 days of culture with conditioned medium from BBG-Mg, -Ca and -Sr glass and glass-ceramics. (Figure a, c and e – 1 day of culture, Figure b, d and f - 3 days of culture).

Figure III.5 exhibits the DNA measurements of L929 culture normalised to the control cultures incubated in culture medium only. For all BBGs, before and after heat treatment, concentrations below 50 $mg \cdot ml^{-1}$ showed DNA levels indicating cell proliferation rates close to 100%, meaning that the conditioned medium was not affecting cell proliferation. Similarly to the results observed in the cell viability assays, BBG-Mg glass or glass-ceramics exhibited less cytotoxic effects than BBG-Ca and -Sr glasses and glass-ceramics. Higher proliferation rates were observed with the media conditioned with BBG-Mg than for the BBG-Ca or BBG-Sr-conditioned media (Figure III.5). Furthermore, culture medium conditioned by 45S5 bioglass® was found to be significantly more cytotoxic than culture medium conditioned with BBG glasses and glass-ceramics. Crystallisation of the glasses was found to have no significant effect on cellular behaviour at day 1; however at day 3, different cellular behaviour profiles were observed at all the concentrations tested. Specifically, for the BBG-Mg glasses, an increase in cytotoxicity was detected for the first heat-treated glass-ceramics (T_{c1}), which could be related to the formation of SiO_2 during the heat treatment. The formation of SiO_2 molecules reduces the amount of silicate in the dominant amorphous phase, which may increase the ratio of borate in the amorphous glass matrix. The borate-rich amorphous phase has a faster degradation rate [15], increasing the quantity of ions in solution as well as the pH (~ 8.0-9.0) [46]. On the other hand, the BBG-Mg glass-ceramics formed after the second heat treatment (T_{c2}) showed a reduction in cytotoxic, which may have been due to the formation of two different crystalline phases (magnesium silicate and magnesium borate) so reducing the availability of ions contained largely within the stable crystalline phases [27, 30].

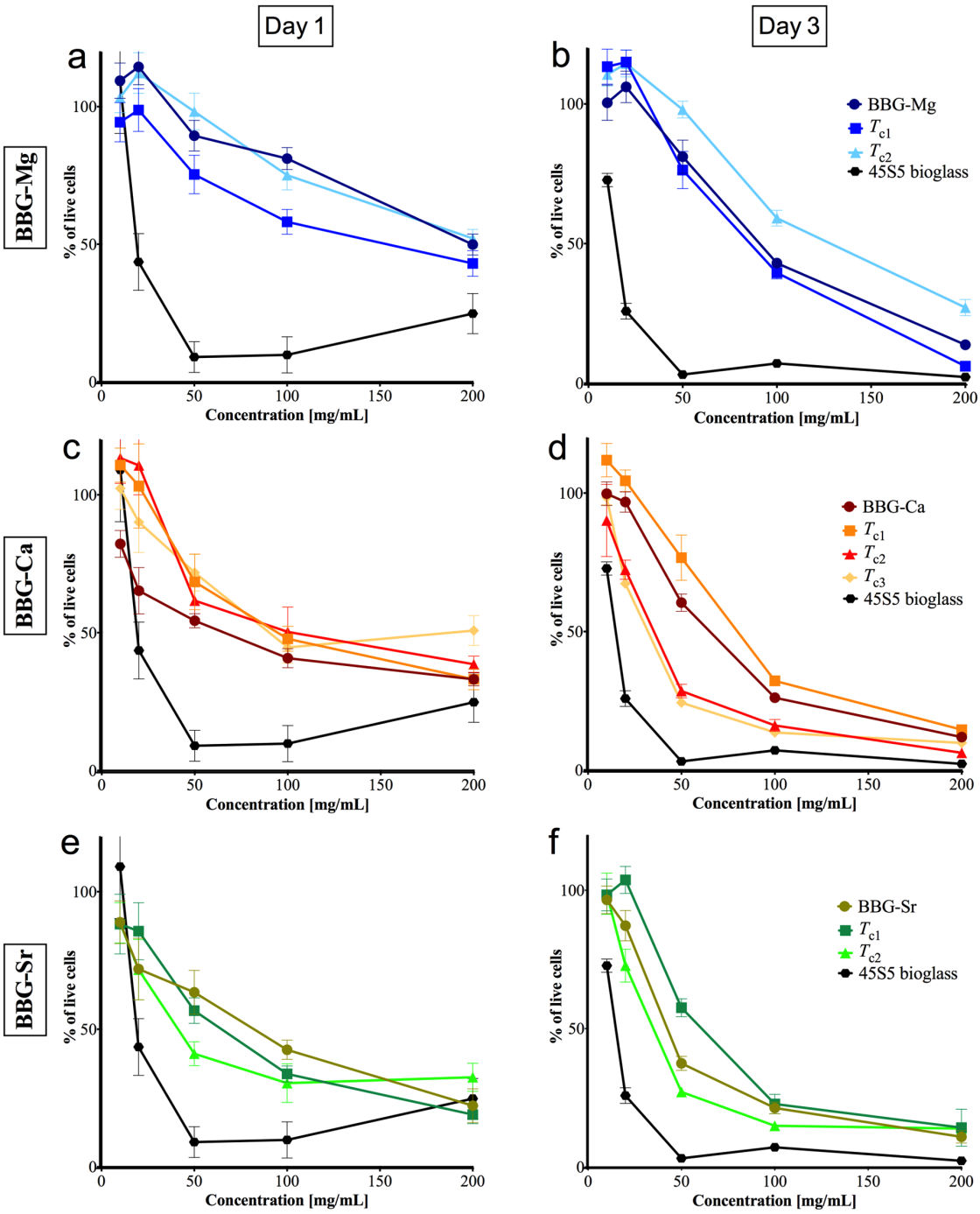

Figure III.5 - The proliferation of L929 cells in contact with BBG-Mg, -Ca and -Sr glass and glass-ceramic-conditioned media after 1 and 3 days of culture (a, c and 3 - after 1 day of culture, b, d and f - after 3 days of culture).

The glass-ceramics produced from heat-treated BBG-Ca and -Sr glasses also showed different cellular behaviour from the parent glasses. A reduction in cytotoxicity was found for glass-ceramics formed after the first heat treatment (T_{c1}) and an increase in cytotoxicity with further heat treatments (T_{c2} and T_{c3}). These results may be explained by the formation of different crystalline phases with higher availability for ion release, which may have increased the pH and can be directly observed by colour changes in medium culture [30]. The pH of the non-conditioned and conditioned media was measured and found to range from 8.0 to 8.5 for all BBG glasses and glass ceramics. The pH of conditioned media from 45S5 bioglass® ranged between 8.5 and 9. While the addition of boron to glass matrix is associated with bone healing and formation as well higher conversion rates to HA [6, 12]; the cytotoxic evaluation demonstrated that it is possible to modify the cytotoxic effects of BBGs by a controlled crystallisation of the constituent glasses. Together, these features make BBGs suitable candidates for BTE applications.

After 3 days of culture, morphologic assessment of L929 cells (Figure III.6) revealed a concentration dependent behaviour of the BBG-Mg-, BBG-Ca- and BBGCs-conditioned media. Where of 10 mg·ml^{-1} of BBG-Mg, BBG-Ca, BBG-Sr or BBGCs were used to prepare the conditioned media, the cells, showed characteristic fibroblast morphology with the formation of actin filaments that was similar to that of the control cultures in the absence of glass-conditioned media. The use of 50 mg·ml^{-1} of BBG-Mg, BBG-Ca and BBG-Sr and BBGCs to prepare the conditioned media, resulted in fewer cells with a classical elongated fibroblastic and a greater proportion exhibiting a more rounded morphology. The use of BBG-Mg, BBG-Ca, BBG-Sr or BBGCs concentrations of 200 mg·ml^{-1} gave conditioned media in which only a few rounded L929 cells could be observed after 3 days. These results are in agreement with cell viability and cell proliferation data (Figure III.4 and Figure III.5) supporting a concentration dependence cytotoxic effect. In the case of the commercial 45S5 bioglass® cultures, for concentrations higher than 10 mg·ml^{-1} in the conditioned media, no live cells were observed after 3 days of culture. At lower 45S5 bioglass® concentrations (10 mg·ml^{-1}), culture of L929 cells in the 45S5 bioglass®-conditioned media resulted in cells having a fibroblastic morphology similar to the control cell cultures. As showed by the viability and the DNA assays, crystallisation of the glasses was found to have a positive or negative effect on cellular

morphology at day 3 of culture. Especially for a concentration of 50 mg·ml^{-1}, it was observed that the less toxic samples (i.e. BBG-Mg_T_{c2}, BBG-Ca_T_{c1} and BBG-Sr_$_{Tc1}$) presented a higher number of cells with a classical elongated fibroblastic morphology. This is consistent with the typical lower solubility of the ceramic phases when compared to the glassy ones, limiting the release of ionic components from the BBGCs and maintaining them at non-cytotoxic concentrations in the culture medium.

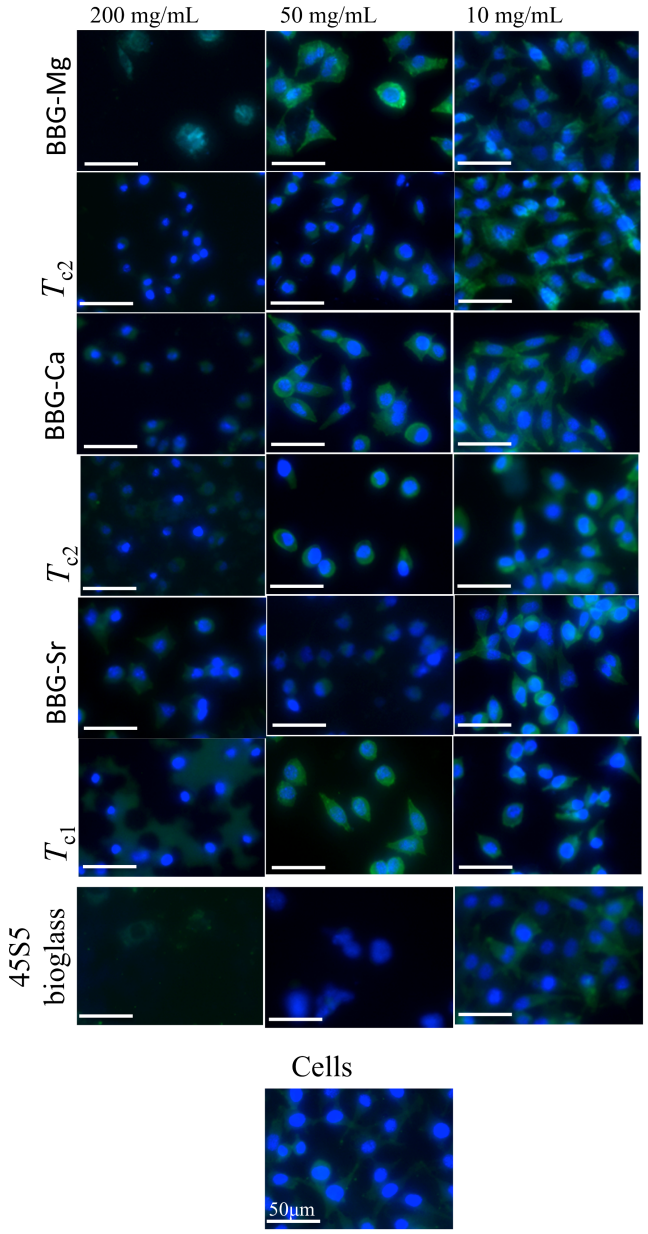

Figure III.6 - Fluorescence microscopy of L929 cells morphology after 3 days incubation with BBGs or BBGCs -conditioned media. Conditioned media were prepared with 10

$mg \cdot ml^{-1}$, 50 $mg \cdot ml^{-1}$ or 200 $mg \cdot ml^{-1}$ BBG glass or BBGCs. Cells cultured with non-conditioned medium was used as negative control and 45S5 bioglass® conditioned media was used as positive control (the blue colour (DAPI staining) shows the nucleus of cells; green colour (phalloidin staining) shows the actin filaments).

Specifically, for the BBG-Mg glasses, an increase in cytotoxicity was detected for the first heat-treated glass-ceramics (T_{c1}), which could be related to the formation of SiO_2 during the heat treatment. The formation of SiO_2 molecules reduces the amount of silicate in the dominant amorphous phase, which may increase the ratio of borate in the amorphous glass matrix. The borate-rich amorphous phase has a faster degradation rate [15], increasing the quantity of ions in solution, as well as the pH (~ 8.0-9.0) [46]. On the other hand, the BBG-Mg glass-ceramics formed after the second heat treatment (T_{c2}) showed a reduction in cytotoxic, which may have been due to the formation of two different crystalline phases (magnesium silicate and magnesium borate) so reducing the availability of ions contained largely within the stable crystalline phases [27, 30].

The glass-ceramics produced from heat-treated BBG-Ca and -Sr glasses also showed different cellular behaviour from the parent glasses. A reduction in cytotoxicity was found for glass-ceramics formed after the first heat treatment (T_{c1}) and an increase in cytotoxicity with further heat treatments (T_{c2} and T_{c3}). These results may be explained by the formation of different crystalline phases with higher availability for ion release, which may have increased the pH and can be directly observed by colour changes in the culture medium [30]. The pH of the non-conditioned and conditioned media was measured and found to range from 8.0 to 8.5 for all BBG glasses and glass ceramics. The pH of conditioned media from 45S5 bioglass® ranged between 8.5 and 9.0.

4. Conclusions

Three novel amorphous BBGs with different glass modifiers have been successfully synthesised by the melt quench technique. The DTA analysis allowed the identification of two or more exothermic peaks indicative of crystallisation. However, after a controlled heat treatment at these temperatures, XRD and ATR-FTIR data indicated that only the samples that were treated at the higher crystallisation temperatures produced significant crystalline phase(s). Also, different crystalline phases were formed for the different substituted BBGs. Specifically for, BBG-Mg, BBG-Ca and BBG-Sr glass-ceramics was detected the presence of magnesium silicate-$Mg_2(SiO_3)_2$ and magnesium borate-$Mg_2B_2O_5$; wollastonite-2M-$CaSiO_3$ and calcium borate-$Ca(BO_2)_2$; and strontium silicate-$SrSiO_3$ and strontium borate-$Sr_2B_2O_5$, respectively. To our knowledge, this is the first time it is demonstrated that controlled crystallisation of BBGs might produce glass-ceramics with less cytotoxic effects on cells. Moreover, neither BBGs nor BBGCs induced a cytotoxic effect on cells at concentrations lower than 50 $mg \cdot ml^{-1}$ and they exhibited less cytotoxicity compared to 45S5 bioglass® at all concentrations used. Finally, interaction of BBGs with cells in a biological environment is a complex process that is continuously under study from the scientific and medical device communities. However, the great biodegradable properties of BBGs combined with the fact that partial or total crystallisation permits cytotoxicity reduction. The BBGs can be used to achieve medical-grade materials for the development of a new generation of BTE medical devices.

References

(1) El-Meliegy, E.; Van Noort, R., In Glasses and Glass Ceramics for Medical Applications. *Springer* **2012**.

(2) Hench, L., The story of Bioglass. *Journal of. Materials Science: Materials.in Medicine* **2006,** 17, 967-978.

(3) Bhakta, S.; Faira, P.; Salata, L.; de Oliveira Neto, P.; Miller, C.; van Noort, R.; Reaney, I.; Brook, I.; Hatton, P., Determination of relative *in vivo* osteoconductivity of modified potassium fluorrichterite glass–ceramics compared with 45S5 bioglass. *Journal of. Materials Science: Materials.in Medicine* **2012,** 23, 2521-2529.

(4) Hench, L. L., Bioceramics: From Concept to Clinic. *Journal of The American Ceramic Society*. **1991,** 74, 1487-1510.

(5) Fu, H.; Rahaman, M.; Day, D.; Huang, W., Long-term conversion of 45S5 bioactive glass–ceramic microspheres in aqueous phosphate solution. *Journal of. Materials Science: Materials.in Medicine* **2012,** 23, 1181-1191.

(6) Xu, S.; Yang, X.; Chen, X.; Shao, H.; He, Y.; Zhang, L.; Yang, G.; Gou, Z., Effect of borosilicate glass on the mechanical and biodegradation properties of 45S5-derived bioactive glass-ceramics. *Journal of Non-Crystalline Solids* **2014,** 405, 91-99.

(7) Rahaman, M. N.; Day, D. E.; Sonny Bal, B.; Fu, Q.; Jung, S. B.; Bonewald, L. F.; Tomsia, A. P., Bioactive glass in tissue engineering. *Acta Biomaterialia* **2011,** 7, 2355-2373.

(8) Huang, W.; Day, D.; Kittiratanapiboon, K.; Rahaman, M., Kinetics and mechanisms of the conversion of silicate (45S5), borate, and borosilicate glasses to hydroxyapatite in dilute phosphate solutions. *Journal of. Materials Science: Materials.in Medicine* **2006,** 17, 583-596.

(9) Brink, M.; Turunen, T.; Happonen, R.-P.; Yli-Urpo, A., Compositional dependence of bioactivity of glasses in the system Na_2O-K_2O-MgO-CaO-B_2O_3-P_2O_5-SiO_2. *Journal of Biomedical Materials Research.* **1997,** 37, 114-121.

(10) Pan, H. B.; Zhao, X. L.; Zhang, X.; Zhang, K. B.; Li, L. C.; Li, Z. Y.; Lam, W. M.; Lu, W. W.; Wang, D. P.; Huang, W. H.; Lin, K. L.; Chang, J., Strontium borate glass: potential biomaterial for bone regeneration. *Journal of The Royal Society Interface* **2010,** 7, 1025-1031.

(11) Rahaman, M. N.; Liang, W.; Day, D. E., Preparation and Bioactive Characteristics of Porous Borate Glass Substrates. In *Advances in Bioceramics and Biocomposites: Ceramic Engineering and Science Proceedings*, John Wiley & Sons, Inc.: 2008; 1-10.

(12) Lakhkar, N. J.; Lee, I.-H.; Kim, H.-W.; Salih, V.; Wall, I. B.; Knowles, J. C., Bone formation controlled by biologically relevant inorganic ions: Role and controlled delivery from phosphate-based glasses. *Advanced Drug Delivery Reviews* **2013,** 65, 405-420.

(13) Shen, Y.; Liu, W.; Wen, C.; Pan, H.; Wang, T.; Darvell, B. W.; Lu, W. W.; Huang, W., Bone regeneration: importance of local pH-strontium-doped borosilicate scaffold. *Journal of Materials Chemistry.* **2012,** 22, 8662-8670.

(14) Chapin, R.; Ku, W.; Kenney, M.; McCoy, H., The effects of dietary boric acid on bone strength in rats. *Biological Trace Elements. Res.* **1998,** 66, 395-399.

(15) Yang, X.; Zhang, L.; Chen, X.; Sun, X.; Yang, G.; Guo, X.; Yang, H.; Gao, C.; Gou, Z., Incorporation of B2O3 in CaO-SiO2-P2O5 bioactive glass system for improving strength of low-temperature co-fired porous glass ceramics. *Jounal of Non-Crystalline. Solids* **2012,** 358, 1171-1179.

(16) Ciceo Lucacel, R.; Radu, T.; Tătar, A. S.; Lupan, I.; Ponta, O.; Simon, V., The influence of local structure and surface morphology on the antibacterial activity of silver-containing calcium borosilicate glasses. *Journal of Non-Crystalline Solids* **2014,** 404, 98-103.

(17) Wang, H.; Zhao, S.; Xiao, W.; Cui, X.; Huang, W.; Rahaman, M. N.; Zhang, C.; Wang, D., Three-dimensional zinc incorporated borosilicate bioactive glass scaffolds for rodent critical-sized calvarial defects repair and regeneration. *Colloids Surface, B* **2015,** Jun 1, 149-56.

(18) Baino, F.; Minguella, J.; Kirk, N.; Montealegre, M. A.; Fiaschi, C.; Korkusuz, F.; Orlygsson, G.; Chiara, V.-B., Novel full-ceramic monoblock acetabular cup with a bioactive trabecular coating: design, fabrication and characterization. *Ceramics International* **2016,** 42, 6833-6845.

(19) Fu, Q.; Rahaman, M. N.; Bal, B. S.; Bonewald, L. F.; Kuroki, K.; Brown, R. F., Silicate, borosilicate, and borate bioactive glass scaffolds with controllable degradation rate for bone tissue engineering applications. II. *In vitro* and *in vivo* biological evaluation. *Journal of Biomedical Materials Research, Part A | Oct 2010* **2010,** 95A.

(20) Rahaman, M. N., In *Tissue Engineering Using Ceramics and Polymers (Second Edition)*, Boccaccini, A. R.; Ma, P. X., Eds. Woodhead Publishing, 2014; Chapter 3, 67-114.

(21) Wu, C.; Fan, W.; Gelinsky, M.; Xiao, Y.; Simon, P.; Schulze, R.; Doert, T.; Luo, Y.; Cuniberti, G., Bioactive SrO–SiO2 glass with well-ordered mesopores: Characterization, physiochemistry and biological properties. *Acta Biomaterialia* **2011,** 7, 1797-1806.

(22) Hoppe, A.; Güldal, N. S.; Boccaccini, A. R., A review of the biological response to ionic dissolution products from bioactive glasses and glass-ceramics. *Biomaterials* **2011,** 32, 2757-2774.

(23) Santocildes-Romero, M. E.; Crawford, A.; Hatton, P. V.; Goodchild, R. L.; Reaney, I. M.; Miller, C. A., The osteogenic response of mesenchymal stromal cells to strontium-substituted bioactive glasses. *Journal of Tissue Engineering and Regenerative Medicine* **2015,** 9, 619-631.

(24) Yamasaki, Y.; Yoshida, Y.; Okazaki, M.; Shimazu, A.; Uchida, T.; Kubo, T.; Akagawa, Y.; Hamada, Y.; Takahashi, J.; Matsuura, N., Synthesis of functionally graded MgCO3 apatite accelerating osteoblast adhesion. *Journal of Biomedical Material Research* **2002,** 62, 99-105.

(25) Maeno, S.; Niki, Y.; Matsumoto, H.; Morioka, H.; Yatabe, T.; Funayama, A.; Toyama, Y.; Taguchi, T.; Tanaka, J., The effect of calcium ion concentration on osteoblast viability, proliferation and differentiation in monolayer and 3D culture. *Biomaterials* **2005,** 26, 4847-4855.

(26) Marie, P. J.; Ammann, P.; Boivin, G.; Rey, C., Mechanisms of Action and Therapeutic Potential of Strontium in Bone. *Calcified Tissue International* **2001,** 69, 121-129.

(27) Daguano, J. K. M. F.; Strecker, K.; Ziemath, E. C.; Rogero, S. O.; Fernandes, M. H. V.; Santos, C., Effect of partial crystallization on the mechanical properties and cytotoxicity of bioactive glass from the $3CaO.P_2O_5$–SiO_2–MgO system. *Journal of Mechanical Behaviour of Biomedical Materials* **2012,** 14, 78-88.

(28) Cao, J.; Wang, Z., Effect of Na2O and heat-treatment on crystallization of glass–ceramics from phosphorus slag. *Journal of Alloys Compounds.* **2013,** 557, 190-195.

(29) Wu, L.; Li, Y.; Teng, Y.; Meng, G., Preparation and characterization of borosilicate glass-ceramics containing zirconolite and titanite crystalline phases. *J. Non-Crystalline Solids* **2013,** 380, 123-127.

(30) Hurrell-Gillingham, K.; Reaney, I. M.; Miller, C. A.; Crawford, A.; Hatton, P. V., Devitrification of ionomer glass and its effect on the *in vitro* biocompatibility of glass-ionomer cements. *Biomaterials* **2003,** 24, 3153-3160.

(31) Baino, F.; Marshall, M.; Kirk, N.; Vitale-Brovarone, C., Design, selection and characterization of novel glasses and glass-ceramics for use in prosthetic applications. *Ceramics International* **2016,** 42, 1482-1491.

(32) Venkateswara Rao, G.; Shashikala, H. D., Effect of heat treatment on optical, dielectric and mechanical properties of silver nanoparticle embedded $CaOCaF_2P_2O_5$ glass. *Journal of Alloys Compounds.* **2015,** 622, 108-114.

(33) Freeman, C. O.; Brook, I. M.; Johnson, A.; Hatton, P. V.; Hill, R. G.; Stanton, K. T., Crystallization modifies osteoconductivity in an apatite–mullite glass–ceramic. *Journal of Material Science: Materials in Medicine* **2003,** 14, 985-990.

(34) ISO/EN10993–5, Biological Evaluation of Medical Devices— Par 5: Tests for Cytotoxicity: *In Vitro* Methods. *Geneva, Switzerland: International Standards* **1992**.

(35) Schaut, R. A., The Effect of Boron Oxide on the Composition, Structure, and Adsorptivity of Glass Surfaces. *Ph.D. Thesis, The Pennsylvania State University, U.S.A.* **2008**.

(36) Gautam, C. R.; Kumar, D.; Parkash, O.; Singh, P., Synthesis, IR, crystallization and dielectric study of (Pb, Sr)TiO 3 borosilicate glass–ceramics. *Bulletin of Material Science* **2013,** 36, 461-469.

(37) Echezarreta-López, M. M.; De Miguel, T.; Quintero, F.; Pou, J.; Landin, M., Antibacterial properties of laser spinning glass nanofibers. *Internationl Journal of Pharmacology* **2014,** 477, 113-121.

(38) Efimov, A. M.; Pogareva, V. G., IR absorption spectra of vitreous silica and silicate glasses: The nature of bands in the 1300 to 5000 cm−1 region. *Chemical Geology* **2006,** 229, 198-217.

(39) Serra, J.; González, P.; Liste, S.; Serra, C.; Chiussi, S.; León, B.; Pérez-Amor, M.; Ylänen, H. O.; Hupa, M., FTIR and XPS studies of bioactive silica based glasses. *J. Non-Crystalline Solids* **2003,** 332, 20-27.

(40) Husung, R. D.; Doremus, R. H., The infrared transmission spectra of four silicate glasses before and after exposure to water. *Journal of Materials Research.* **1990,** 5, 2209-2217.

(41) Dunken, H.; Doremus, R. H., Short time reactions of a na2o-cao-sio2 glass with water and salt solutions. *J. Non-Crystalline Solids* **1987,** 92, 61-72.

(42) Goh, Y.-F.; Alshemary, A. Z.; Akram, M.; Abdul Kadir, M. R.; Hussain, R., In-vitro characterization of antibacterial bioactive glass containing ceria. *Ceramics International* **2014,** 40, 729-737.

(43) Doweidar, H.; Zeid, M. A. A.; El-Damrawy, G. M., Effect of gamma radiation and thermal treatment on some physical properties of ZnO-PbO-B 2 O 3 glasses. *Journal of Physics D: Applied Physics* **1991,** 24, 2222.

(44) Singh, S.; Singh, A.; Bhatti, S. S., Elastic moduli of some mixed alkali borate glasses. *Journal of Materials Science* **1989,** 24, 1539-1542.

(45) Tenney, A. S.; Wong, J., Vibrational Spectra of Vapor‐Deposited Binary Borosilicate Glasses. *The Journal of Chemical Physics.* **1972,** 56, 5516-5523.

(46) Teo, A.; Mantalaris, A.; Lim, M., Influence of culture pH on proliferation and cardiac differentiation of murine embryonic stem cells. Journal of *Biochemical Engineering* **2014,** 90, 8-15.

IV. CHAPTER

Intrinsic Antibacterial Borosilicate Glasses for Bone Tissue Engineering Applications

CHAPTER IV
INTRINSIC ANTIBACTERIAL BOROSILICATE GLASSES FOR BONE TISSUE ENGINEERING APPLICATIONS

IV. CHAPTER

Intrinsic Antibacterial Borosilicate Glasses for Bone Tissue Engineering Applications[3]

Abstract

Three novel BBGs were prepared and used to investigate their bioactive and antibacterial properties. The BBGs were prepared by melt quenching using different glass modifiers, i.e. Mg^{2+}, Ca^{2+} and Sr^{2+}, and their amorphous nature was confirmed by XRD. SEM/EDS allowed the visualisation of apatite-like structures upon 7 days of immersion in SBF. BBG-Ca generated surface structures with a Ca/P ratio ≈ 1.67, while the surface of the BBG-Sr was populated with structures with a Sr/P ratio ≈ 1.7. Moreover, bacterial tests showed that the BBG-Mg and BBG-Sr glasses (at concentrations of 9, 18, 36 and 72 $mg \cdot ml^{-1}$) present antibacterial characteristics. In particular, BBG-Sr, at concentrations of 9 $mg \cdot ml^{-1}$, exhibited bacteriostatic activity against *P. aeruginosa*, and at concentrations ≥ 18 $mg \cdot ml^{-1}$ it was able to eradicate this bacterium. These results evidence an antibacterial activity dependent on the BBGs composition, concentration and bacterial species. Cellular studies showed that the developed BBGs do not present statistically significant cytotoxic effect against SaOs-2 cells after 3 days of culture showing better performance (in the cases of BBG-Ca and BBG-Sr) than commercial 45S5 bioglass® up to 7 days of culture. Overall, this study demonstrates that BBGs can be effectively designed to combine bioactivity and intrinsic antibacterial activity targeting BTE applications.

---

[3] This chapter is based on the following publiation:

João S. Fernandes, Margarida Martins, Nuno M. Neves, Maria H. Fernandes, Rui Reis, Ricardo A. Pires; Intrinsic Antibacterial Borosilicate Glasses for Bone Tissue Engineering Applications, ACS Biomaterials Science & Engineering 2016, 2 (7), pp 1143–1150

1. Introduction

In recent years, tissue engineering has shown great promise for the repair, replacement and even regeneration of bone defects. A large diversity of bioactive glasses (BGs) has been reported. Usually they present enhanced capacity to interact with bone due to their capability to form a HA layer under simulated physiological conditions [1]. The $CaO:SiO_2:Na_2O:P_2O_5$ system (45S5 bioglass®) [1] has been the gold standard for BGs, but it has limitations, namely related with its degradation rates. When transformed into glass ceramics, these silica based BGs have slow degradation rates, after being implanted, which makes it difficult to match with the rate of new tissue formation [2, 3]. The conversion of the BGs to a bone-like HA is slow and often incomplete [2]. Moreover, the huge increase in joint and bone surgeries is usually accompanied by an increase in the incidence of medical device-related bacterial infections. This can lead to the failure of the medical device - a growing public health concern in developed countries [4, 5].

A broad spectrum of bacterial species can be found at surgery sites, including *P. aeruginosa, E. coli, S. aureus* and *S. epidermidis.* These species have been associated with joint and bone infections [4, 6]. As an example, *P. aeruginosa* and *S. aureus* were reported by Malizos *et al*. [7] to be related with ankle and foot osteomyelitis after surgical treatment. Consequently, it is becoming urgent to develop double-edged materials capable of perfectly bond to bone and exhibit intrinsic antibacterial activity.

The BBGs have been gaining interest due to the possibility to easily control their degradation rates and due to their strong bioactivity [8, 9]. The compositional flexibility of these glasses is high and can be tailored to improve BBGs osteogenic and angiogenic properties by the addition of specific glass modifiers [10, 11]. On one hand, network formers such as silicon and boron are well known to stimulate bone formation and precipitation of HA. Silicon is known to be essential for different processes, such as, bone formation and calcification [12, 13]. In addition, boron is related with the improved adhesion of bone cells and bone resistance to fracture [14]. On the other hand, the therapeutic cations, such as Mg^{2+} [15, 16], Ca^{2+} [17] and Sr^{2+} [18, 19] are involved in cells adhesion and stability; apatite formation process and cell differentiation; and bone formation and mineralisation, respectively. In fact, Sr^{2+} has been reported for the treatment of osteoporosis [20].

Furthermore, several cations can provide antibacterial properties to BGs. Specifically, silver [21], copper [22], and cerium [23] present bacteriostatic and/or bactericidal properties. Remarkably, other cations may also provide antibacterial properties to BGs, as previously shown for Mg^{2+} [24], Ca^{2+} and Sr^{2+} [25, 26]. In this context, the incorporation of different cations can impart a series of therapeutic features into BGs, and their properties can be suited to meet the clinical needs.

Therefore, the main objective of this work is twofold: 1) to develop three novel melt-quench BBGs, prepared with the glass modifiers Ca^{2+}, Sr^{2+} or Mg^{2+}, that are able to present enhanced bioactivity; 2) to investigate their intrinsic antibacterial properties. We aimed to contribute to the development of BBGs that couples bone regenerative properties with intrinsic antibacterial activity relevant in the BTE context.

2. Materials and Methods

2.1. Glass' fabrication

BBGs of general formula $0.05Na_2O \cdot xMgO \cdot yCaO \cdot (0.35\text{-}x\text{-}y)SrO \cdot 0.20B_2O_3 \cdot 0.40SiO_2$ (molar ratio, where x, y = 0.35 or 0.00, and $x \neq y$) were fabricated by melt-quenching. The appropriate amounts of di-boron trioxide (B_2O_3, Alfa Aesar, Germany), sodium bicarbonate ($NaHCO_3$, Sigma-Aldrich, Australia), silica gel 60 M (SiO_2, Macherey-Nagel, Germany) and magnesium oxide (MgO, Sigma-Aldrich, Portugal) or calcium carbonate ($CaCO_3$, Sigma-Aldrich, Portugal), or strontium carbonate ($SrCO_3$, Sigma-Aldrich, Portugal) were thoroughly mixed with the addition of ethanol in a porcelain mortar with the help of a pestle, dried overnight and transferred to a platinum crucible. Afterwards, the batch was heated to 1450 ˚C in air for 1 h and subsequently the melt was quickly poured into cold water for a fast cooling step forming a glass frit with no crystalline phases. Afterwards, pieces of the as-quenched glass were quickly removed from water, dried to remove all the non-structural water and ground in an Agate mortar (RETSCH, Germany). After overnight vacuum drying, the glasses were sieved to a particle size lower than 63 μm. Before the *in vitro* tests the BBG-Mg, BBG-Ca, BBG-Sr were weighted and sterilised by ethylene oxide (the sterilising gas was composed by 88%

CO_2 and 12% ethylene oxide using the following physical parameters: temperature of 45 ºC ± 3 ºC; pressure of 180 + 3 kPa; humidity of 55 ± 10% HR and exposure time of 10 h).

2.2. Glasses characterisation

2.2.1. Morphology and density

Scanning electron microscope (SEM) was used to observe the morphology of the BBGs particles. Prior to the analysis all BBG samples were sputter-coated with gold (sputter coater model SC502, Fisons Instruments, UK). All the micrographs were acquired on a Leica Cambridge S360 microscope (Leica Cambridge, UK) using beam energy of 5.0 kV and working distance of ≈ 5.2 mm. The BBGs density was determined using a multi pycnometer (Quantachrome Instruments, USA). Measurements were performed with helium at 110 °C using ≈ 5 g of each sample.

2.2.2. Crystallinity

X-ray powder diffraction (XRD) was used to confirm the amorphous state of BBGs. The BBGs diffractograms were collected on a Bruker D8 Discover (Germany), operating with a CuKα radiation θ/2θ mode between 10° and 60°, with a step increment of 0.04° and an acquisition time of 1s/step.

2.2.3. Elemental composition

The ICP-AES (Horiba, Japan) was used to determine the elemental composition of the glasses (B, Si, Na, Ca, Sr and Mg) after total dissolution of 1 g of each BBG into hydrofluoric acid. The sample absorption was measured at specific wavelengths (λ=588.995 nm for Na, λ=279.553 nm for Mg, λ= 393.366 nm for Ca, λ=588.995 nm for Sr, λ=249.773 nm for B and λ=251.611 nm for Si) and their concentration was determined using calibration curves obtained with standard solutions (VWR, Portugal) in the range from 5×10^3 to 10 ppm.

2.3. Bioactivity of the glasses

SBF was produced in accordance with the procedure described by Kokubo *et al*. [27]. Triplicate samples of the prepared BBGs, with a particle size lower than 63 μm, were immersed in SBF at a ratio of 10:15 [BBG (mg): SBF (ml)] and incubated for 1, 3 and 7 days in an oven maintained at 37 °C. After each time point BBGs were recovered and dried at 37 ºC. The gold or carbon sputter coated samples were analysed by SEM (model S360, Leica Cambridge, UK) equipped with SEM/EDS link-eXL-II for morphological and chemical analysis.

2.4. Degradation of the glass

Samples of the fabricated BBGs were immersed in the bacterial growth medium MH (at least in triplicate) at concentrations of 9, 18, 36 and 72 $mg \cdot ml^{-1}$ for 1, 3 and 7 days and maintained at 37 ºC in water-shaking bath at 60 rpm. At each time point, the solutions were filtered and the pH was assessed. The ICP-AES analyses were performed as described in section IV.2.2.3 to determine the concentrations of Si, B, Mg, Ca and Sr released by the BBGs in MH.

2.5. Antibacterial properties

The standard DD (2.5.1) and the BD (2.5.2) assays [28, 29] were adapted to test the ability of the BBGs to act against the Gram-negative bacteria *P. aeruginosa* (ATCC 27853) and *E. coli* (CECT 434); and the Gram-positive *S. aureus* (ATCC 25913) and *S. epidermidis* (strain 9142 [30]). These bacterial strains were chosen to represent a spectrum of organisms associated with joint and bone infections [4]. For these experiments different concentrations [9, 18, 36, 72 $mg \cdot disc^{-1}$ (DD) or $\cdot ml^{-1}$ (BD)] of each BBGs were used. Additionally, 45S5 bioglass® (NOVABONE, USA) was used as commercial control; and culture medium without BBGs were used as a negative control. The antibacterial properties of BBGs as a function of the culture time were investigated by BD assays for those glasses that exhibited antibacterial activity on DD. All experiments were performed at least in triplicate and repeated three times independently.

2.5.1. Disc diffusion assay

For the DD assay [28], agar discs (17 $g \cdot l^{-1}$ (Liofilchem, Portugal), Ø ≈ 9.5 mm) were charged with different concentrations of BBGs and used on the same day.

The direct colony suspension method was used to prepare a saline suspension of each microbial species previously grown in TSA (Liofilchem, Portugal) at 37 ºC for 18 h. The density of the suspensions was adjusted to that of a McFarland 0.5 turbidity standard, corresponding to, approximately, $1\text{-}2\times10^{8}$ CFU $\cdot ml^{-1}$. The inoculum concentration was confirmed by enumeration of CFU after culture of serial dilutions onto TSA and incubation at 37 °C, 18–24 h in air. The test was performed by applying the bacterial inoculum with a sterile cotton swab onto the surface of a MH agar (Liofilchem, Portugal) plate containing 25 ml of medium. The glasses on agar discs were applied in the plates within 15 min of inoculation. The plates were incubated at 37 °C in air for 18 h for all the bacteria. The diameter (in millimeters) of the inhibition zone around each disc was measured using a ruler. The presence of an inhibition halo was interpreted as bacterial susceptibility to the BBG.

2.5.2. Broth dilution assay

For the BD assay [29], the BBGs were immersed in 0.5 ml of MH (Fluka, Portugal) medium and incubated at 37 ºC in air for 0, 2 or 6 days.

For each bacterium, the inoculum was prepared as described for the DD test. It was diluted to approximately 1×10^{6} CFU in 0.5 ml of culture medium, added to the different tubes containing known amounts of BBGs dissolved during the specific time frames and incubated at 37 ºC in air for 24 h. Overall, the bacteria were tested for a fixed period after 1, 3 and 7 days of BBGs dissolution in MH medium. One sample was removed from each tube, serially diluted in saline and inoculated onto TSA. After 24 h incubation at 37 ºC in air, the number of colonies were counted. The results are presented as $\log_{10}$ $CFU \cdot ml^{-1}$. Bacteriostatic and bactericidal activities were defined as a reduction of bacteria less and more than 3 $\log_{10}$ $CFU \cdot ml^{-1}$, respectively, expressed as the proportion of the inoculum (number of living CFUs introduced in culture) that is rendered incapable of reproduction

on subculture [31]. Eradication was defined as the elimination of culturable bacteria upon subculture.

2.6. Cytotoxicity assay

The cytotoxicity assessment was performed by adapting the ISO 10993 5:2009 to the targeted BTE application. The SaOs-2 cells derived from human bone were cultured with BBGs at concentrations of 9, 18, 36, 72 $mg \cdot ml^{-1}$ during 7 days. The cells cultured in the absence of glass particles were used as negative control, and in the presence of 45S5 bioglass® as positive control. Cells were expanded in DMEM (Sigma, Portugal) supplemented with 10% heat-inactivated FBS (Alfagene, Portugal) and 1% antibiotic/antimitotic solution (100 $U \cdot ml^{-1}$ penicillin and 100 $\mu g \cdot ml^{-1}$ streptomycin; Alfagene, Portugal). Cells were cultured at 37 °C in an atmosphere of 5% CO_2. Confluent SaOs-2 cells between passages 15 and 19 were harvested and seeded onto the bottom of 24-well plates at a density of 2.3×10^5 cells/well. The BBGs at the desired concentrations and 45S5 bioglass® were put on top, in cell culture inserts with porous membranes (0.4 μm ThinCerts™ Cell Culture Inserts; Greiner, Germany). The fabricated BBGs presented great biological performance without the common washing step before contact with cells. Therefore cytotoxicity assay of samples and control (45S5 bioglass®) was performed without the common pre-washing step.

The metabolic activity and cellular proliferation were monitored at 1, 3 and 7 days by MTS (Promega, UK) and PicoGreen® (Quant-iT™ PicoGreen® dsDNA Assay Kit – Invitrogen, USA), respectively, according to the supplier's instructions.

2.7. Statistical analysis

Experiments were run at least in triplicate for each sample. All the data were expressed as mean ± SD. Statistical analysis was performed using Graphpad Prism® software, version 6.0. The normality of the data distribution was monitored by Shapiro-Wilk test. Some of the datasets were not considered to have a normal distribution, requiring a non-parametric statistical evaluation. In this context, Kruskal-Wallis test was applied to all dataset, followed by a Dunn's multiple comparison test. Values of $p<0.001$ were considered

extremely significant, of $0.001<p<0.01$ were considered very significant and of $0.01<p<0.05$ were considered significant.

3. Results and discussion

3.1. BBGs fabrication and characterisation

The BBGs network was designed to be a borosilicate (i.e. $0.2B_2O_3{:}0.4SiO_2$) containing different network modifiers following the general formula $0.05Na_2O{\cdot}x\text{MgO}{\cdot}y\text{CaO}{\cdot}(0.35\text{-}x\text{-}y)\text{SrO}{\cdot}0.20B_2O_3{\cdot}0.40SiO_2$ (molar ratio, where x, y = 0.35 or 0.00, and $x \neq y$). The BBGs were successfully obtained by melt-quench and ground in a controlled manner. All the compositions presented a density ranging from 2.5 to 3.0 $g{\cdot}cm^{-3}$. The increase on density was associated with the higher molecular weight of the glass modifier used to prepare the BBG, i.e. $Mg^{2+} < Ca^{2+} < Sr^{2+}$. Figure IV.1 presents the XRD data obtained for the three compositions, which confirm that the melting procedure and the fast quenching in water was adequate strategy to obtain amorphous BBGs. In Figure IV.2 (column t0) are presented the SEM images of BBGs after the grinding process. The BBGs exhibited an angular shape with low sphericity. The ICP-AES analysis (Table IV.1) confirmed the elemental composition of the BBGs, showing values close to the nominal theoretical composition.

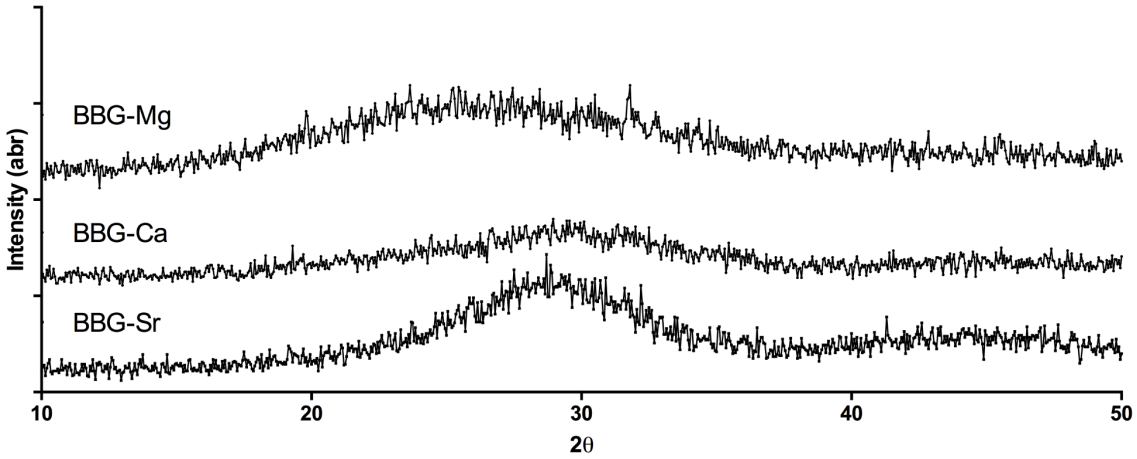

Figure IV.1 - XRD patterns of the as-quenched glass frits, i.e. BBG-Mg, BBG-Ca and BBG-Sr. Three replicates were performed for each sample and representative diffractograms are presented.

3.2. BBGs *in vitro* bioactivity and degradation

The formation of bone-like apatite structures was assessed after the immersion of BBGs into the SBF buffer. Figure IV.2 presents the SEM images and Ca/P ratios before and after 1, 3 and 7 days of immersion into SBF. The *in vitro* bioactivity assay revealed the presence of bone-like apatite structures onto the surface of all the BBGs, even though they are at different stages of crystallisation.

The BBG-Mg particles exhibited the formation of bone-like apatite structures on their surface for days 1 and 3. However, there was a decrease of those structures at day 7. In fact, Salimi *et al*. [32] showed that the Mg^{2+} has a marked inhibiting effect on HA growth due to its adsorption onto active growth sites. The BBG-Ca and 45S5 bioglass® presented a constant increase in the formation of bone-like apatite structures over time. Additionally, the structures observed at days 1, 3 and 7 of immersion presented the cauliflower-like morphology, typical of HA. Moreover, at day 7 BBG-Ca reached Ca/P ≈ 1.67, which is commonly associated with HA [33]. Finally, at day 7 the BBG-Sr glass also presented the formation of bone-like apatite structures onto the particles' surface with a cauliflower-like morphology. These structures were formed during a longer time period and also they did not present the Ca/P ratio expected for HA. However, the Sr/P ratio of

BBG-Sr decreased over time, reaching ≈ 1.7 at day 7. This suggests the formation of strontium-substituted bone-like apatite (Sr-HA) [34]. Indeed, Ravi *et al*. [35] supported the use of Sr^{2+} in the place of Ca^{2+} in HA structure forming synthetic Sr-HA. In fact, in the mechanism for the formation of apatite-like structures, proposed by Hench *et al*. [36], Sr^{2+} can replace Ca^{2+} and migrate to the surface of SiO_2–rich layer precipitated on the surface of BBGs, forming a $SrO\text{-}P_2O_5$-rich film.

The BBG-Ca and BBG-Sr glasses have shown high capacity to form bone-like apatite structures at their surface with cation/P ratio ≈ 1.67 upon immersion in SBF, which might enable the glasses to establish direct contact with living bone cells [37].

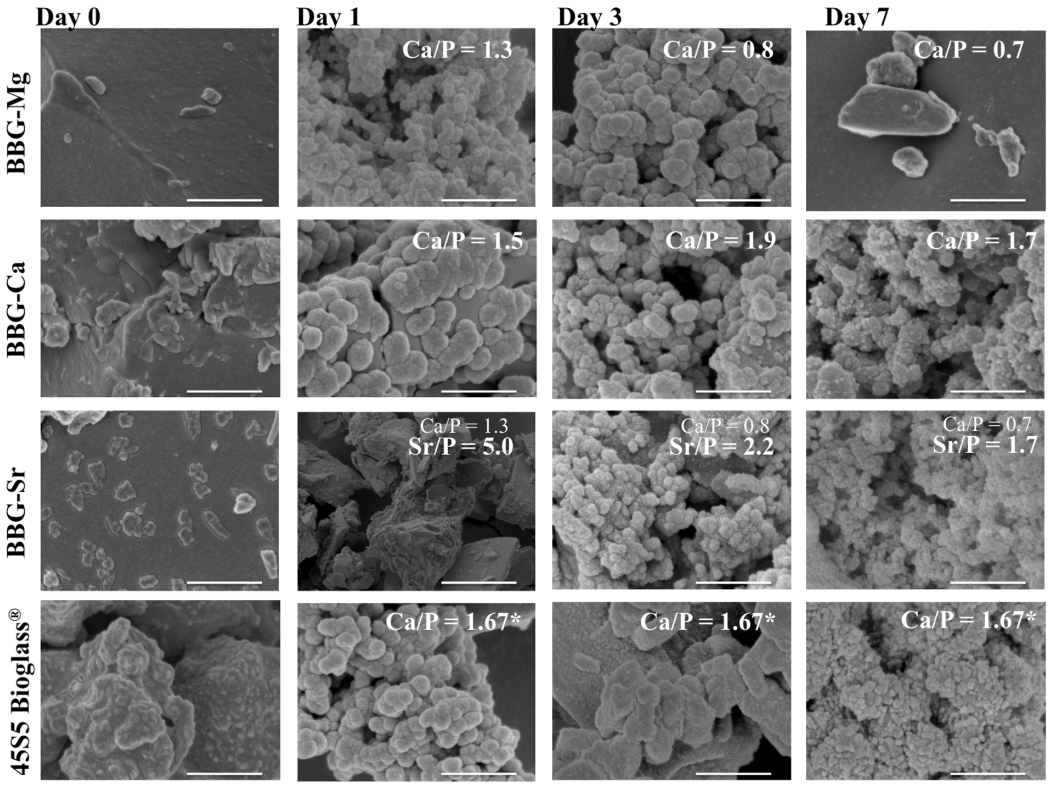

Figure IV.2 - SEM micrographs of BBGs (BBG-Mg, BBG-Ca and BBG-Sr) before and after 1, 3 and 7 days of immersion in SBF. The 45S5 bioglass® was used as a control. The Ca/P or Sr/P ratios on the surface of the BBGs were determined by EDS and presented on the right corner from day 1 to 7. The asterisk (45S5 bioglass®) represents the theoretical value of 45S5 bioglass® Ca/P ratio. Scale bar = 0.25 μm.

Table IV.1 - Elemental composition of BBGs (BBG-Mg, BBG-Ca and BBG-Sr) as determined by ICP-AES. The data was obtained from three replicates and is presented as the mean of % molar composition in 1 g of sample (± SD). Theoretical values are presented in parenthesis

Sample	Si (mol %)	B (mol %)	Divalent cation* (mol %)	Na (mol %)
BBG-Mg	37.2 ± 0.2 (40)	17.0 ± 0.1 (20)	40.6 ± 0.1 (35)	4.9 ± 0.1 (5)
BBG-Ca	33.7 ± 0.3 (40)	21.0 ± 0.1 (20)	37.9 ± 0.3 (35)	7.3 ± 0.1 (5)
BBG-Sr	34.8 ± 0.3 (40)	21.0 ± 0.1 (20)	38.9 ± 0.3 (35)	5.1 ± 0.1 (5)

*Varies with the modifier cation present in each composition, i.e. Mg^{2+}, Ca^{2+} and Sr^{2+}, from top to bottom.

In order to better understand the kinetics of BBGs dissolution, a glass solubilisation study was performed in MH medium (Figure IV.3). For BBG-Mg and BBG-Sr there was a fast initial glass dissolution up to day 3 and a subsequent slower increase over time. In contrast, the BBG-Ca presented a faster dissolution at day 1 followed by an increasing release over time. However, the amount of Mg^{2+} in BBG-Mg and Sr^{2+} in BBG-Sr derived-solutions, were ≈ 3 times higher than Ca^{2+} in the BBG-Ca derived-solution (Figure IV.3c). This data shows that the nature of the substituted cations influences differently their release rate from the BBG network, which might induce distinctive activities to cells. In fact, studies by Mestres *et al.* [38] showed that the high Mg^{2+} concentrations in the extracts of Mg-containing cements contribute to their activity against *E. coli* and *P. aeruginosa* by hyperosmotic stress. On the other hand, the burst release of cations after 1 day, led to an increase of pH (≈ 1 unit of pH, Figure IV.3d), which might be related with the observed BBGs antibacterial properties. Indeed, Zhang *et al.* [25], while studying BGs correlated mainly the pH increase in the solution with antibacterial activity. The lower release of Ca^{2+} into the BBG-Ca solution observed in the present work (Figure IV.3c) might explain the lower increase in the solution pH (Figure IV.3d), when compared with the dissolution solutions of BBG-Mg and BBG-Sr (e.g. average of all concentrations for BBG-Mg at day 1 is 8.76, for BBG-Ca is 8.35 and for BBG-Sr is 8.90). These results are also consistent with the observed release profile of Mg^{2+} and Sr^{2+} from the respective BBG compositions over time (generating similar pH

values ~8.8-8.9 in the degradation solutions). These variations in the release kinetics of the divalent cations might influence differently the final BBGs properties, namely their bioactivity and antibacterial activity. In fact, Allan *et al.* [39] reported that degradation of 45S5 bioglass® increases the pH having an antibacterial effect on specific oral bacteria (e.g.: *S. sanguis* and *P. gingivalis*).

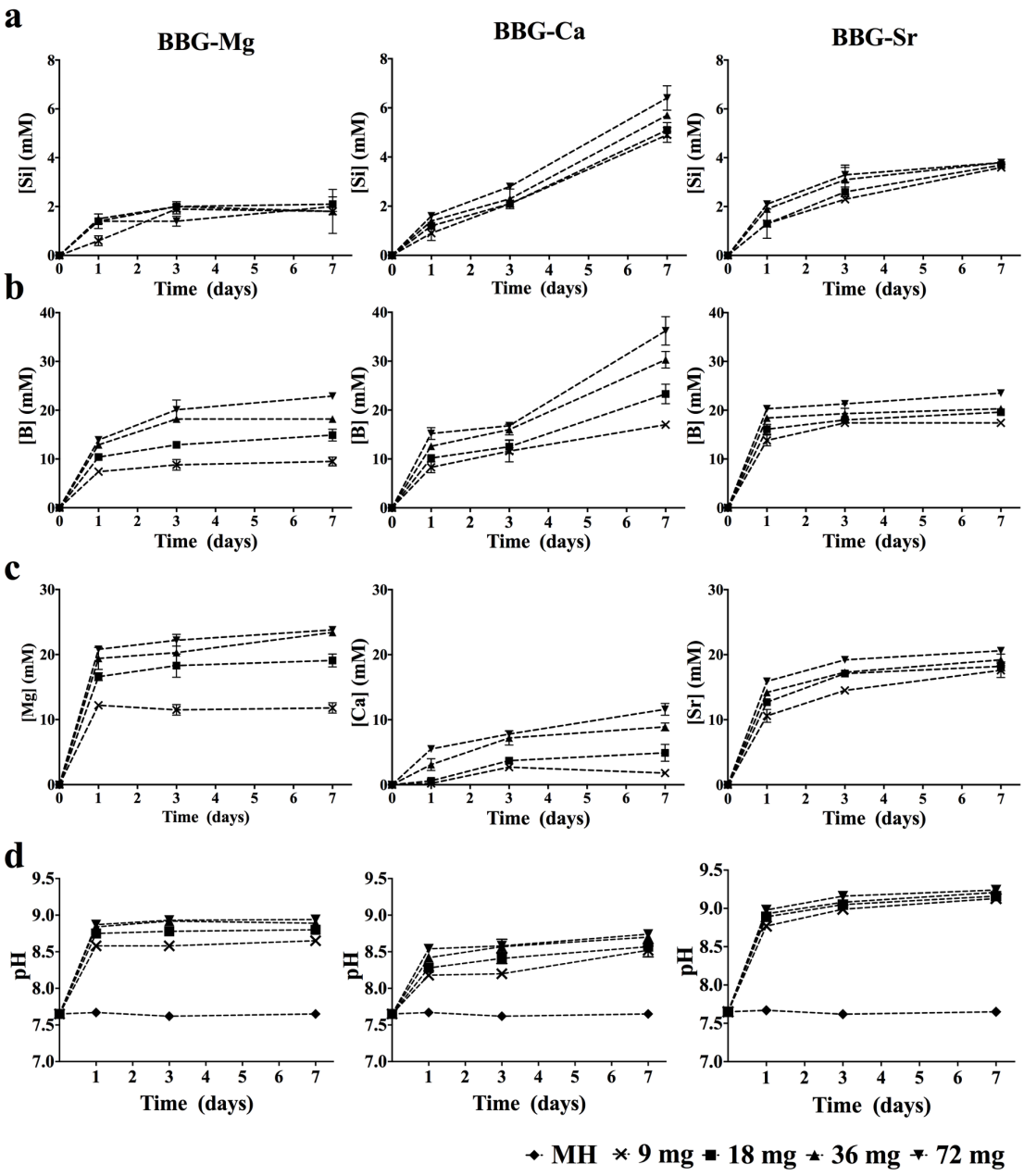

Figure IV.3 - Release of chemical species from the BBGs (BBG-Mg, BBG-Ca and BBG-Sr) into the MH medium (a-c) and the corresponding pH of the solution (d) loaded with different BBG concentrations (9-72 mg·ml^{-1}) after 1, 3 and 7 days of incubation at 37 ºC

under agitation. The concentrations were assessed by ICP-AES. The data was obtained from at least three independent samples and is expressed as mean ± SD.

3.3. BBGs antibacterial properties

The susceptibility of the Gram-negative (*P. aeruginosa* and *E. coli*) and Gram-positive (*S. aureus* and *S. epidermidis*) bacterial species against variable concentrations of BBGs was initially tested using the DD assay. Table IV.2 shows the values of the zones of growth inhibition around each BBG containing disc. The results indicate that 45S5 bioglass® exhibited antibacterial activity against *S. epidermidis* and *P. aeruginosa*, although a high concentration was required to impair the growth of the latest species. Regarding BBGs glasses, BBG-Mg showed antibacterial activity against *S. epidermidis* and BBG-Sr against *P. aeruginosa*, independently of the BBG's concentration. In contrast, the BBG-Ca did not present any detrimental effect on the growth of the studied bacterial species.

Table IV.2 - BBGs (BBG-Mg, BBG-Ca, BBG-Sr) and 45S5 bioglass® as control antibacterial activity against *P. aeruginosa, E. coli, S. aureus* and *S. epidermidis* as assessed by the DD assay at BBGs concentration (9 – 72 mg·disc^{-1}) during 18 h. Data from at least three independent experiments and is expressed as the median [min – max] values of the zones of growth inhibition around each glass agar disc measured in mm

Sample	Concen-tration (mg·disc^{-1})	Ø zone [min-max] (mm)			
		P. aeruginosa	*E. coli*	*S. aureus*	*S. epidermidis*
BBG-Mg	9	0	0	0	11 [0-15]
	18	0	0	0	12 [11-17]
	36	0	0	0	11 [11-18]
	72	0	0	0	12 [10-20]
BBG-Ca	9	0	0	0	0
	18	0	0	0	0
	36	0	0	0	0
	72	0	0	0	0
BBG-Sr	9	17 [12-20]	0	0	0
	18	17 [13-21]	0	0	0
	36	16 [14-20]	0	0	0
	72	18 [15-21]	0	0	0
45S5 Bioglass®	9	0	0	0	11 [0-11]
	18	0	0	0	14 [0-15]
	36	0	0	0	16 [14-19]
	72	11 [0-22]	0	0	20 [18-22]

These promising results lead us to further characterise the antibacterial properties of the developed BBG-Mg and BBG-Sr, including the effect of their dissolution over time by the BD assay. The BD assay data indicates that BBG-Mg (Figure IV.4a) prevented the

growth of *S. epidermidis*, having a bacteriostatic effect, regardless of the BBG-Mg concentration used and the time of dissolution (activity also observed for the control sample, *i.e.* 45S5 bioglass®). Surprisingly, the BBG-Sr (Figure IV.4b), presented bactericidal activity against *P. aeruginosa* for all the tested concentrations, although, at 9 $mg \cdot ml^{-1}$, for the first day, it was only observed a bacteriostatic effect with 2.6 log_{10} reduction in the initial inoculum. BBG-Sr was able to eradicate *P. aeruginosa* at concentrations $\geq$ 18 $mg \cdot ml^{-1}$ even at the first day of contact. This outperforms, 45S5 bioglass® that only showed bacteriostatic or bactericidal activity at higher concentrations and/or dissolution times against *S. epidermidis* (Figure IV.4c) and *P. aeruginosa* (Figure IV.4d) [e.g. at the first day of dissolution, BBG-Sr at 18 $mg \cdot ml^{-1}$ eradicated *P. aeruginosa* (Figure IV.4c) while at the same concentration 45S5 bioglass® had a bacteriostatic effect (Figure IV.4d)]. Other authors also reported bactericidal activity of 45S5 bioglass®: Brown *et al.* [40] could eradicate *P. aeruginosa* using a concentration of 50 $mg \cdot ml^{-1}$ for a period of 24 h incubation under 200 rpm shaking; *Hu et al.* [41] also showed 99% bactericidal activity for concentrations higher than 50 $mg \cdot ml^{-1}$ against *S. epidermidis*, among other bacteria. However, to our knowledge, this work describes for the first time BBGs that are able to eradicate bacteria with such a low concentrations of glass particles (i.e. 18 $mg \cdot ml^{-1}$).

Therefore, the BD assay allowed evaluating the concentration dependence, as well as the ability of BBG-Sr to eradicate *P. aeruginosa*, as a complement to DD assay. Thus, BBG-Sr glasses presented relevant antibacterial properties, some of them higher than the ones observed for commercial glasses (e.g. Figure IV.4c and 4d). Several authors [38, 42] suggested the influence of increased pH in the antibacterial activity. As an example, Mestres *et al.* [31], showed that magnesium phosphate cements presented antibacterial activity against *S. Sanguinis*, which was attributed to the alkaline pH. Also, findings from Allan *et al.* [39] revealed that supernates from 45S5 bioglass® rapidly increase their pH to, approximately, 10. Therefore, the authors suggested that the high pH alone could be responsible for the observed antibacterial activity. In our case, the pH variation between BBG-Sr 9 $mg \cdot ml^{-1}$ and BBG-Sr 18 $mg \cdot ml^{-1}$ at day 1 was not significant (Figure IV.3d, BBG-Sr), while variations in the antibacterial activity was observed (from bacteriostatic to bactericidal). Furthermore, the same pH value was recorded for BBG-Mg 72 $mg \cdot ml^{-1}$ at day 1 (Figure IV.3d, BBG-Mg) and it only exhibited bactericidal activity against a different bacterial species (Figure IV.4). While a high pH has been associated with the

inhibition of bacterial growth, it is noteworthy that pH might not be the only parameter influencing the antibacterial properties. Indeed, the release of specific cations has also been shown to elicit an antibacterial effect. For example, Ohtsu *et al.* [43] demonstrated that Sr^{2+} present an antibacterial activity against *P. aeruginosa*, through the contact of the bacterium with a strontium borate pigment. In fact, both the release of Sr^{2+} from the BBG-Sr glass particles and its antibacterial activity towards *P. aeruginosa*, are dose dependent (Figure IV.3c and Figure IV.4c). This observation is consistent with the contribution of the released Sr^{2+} to the antibacterial activity of BBG-Sr [25, 35] suggesting that the BBG-Sr's activity towards *P. aeruginosa* may result from a synergist effect of several independent factors (e.g. Sr^{2+} release, pH increase, among others).

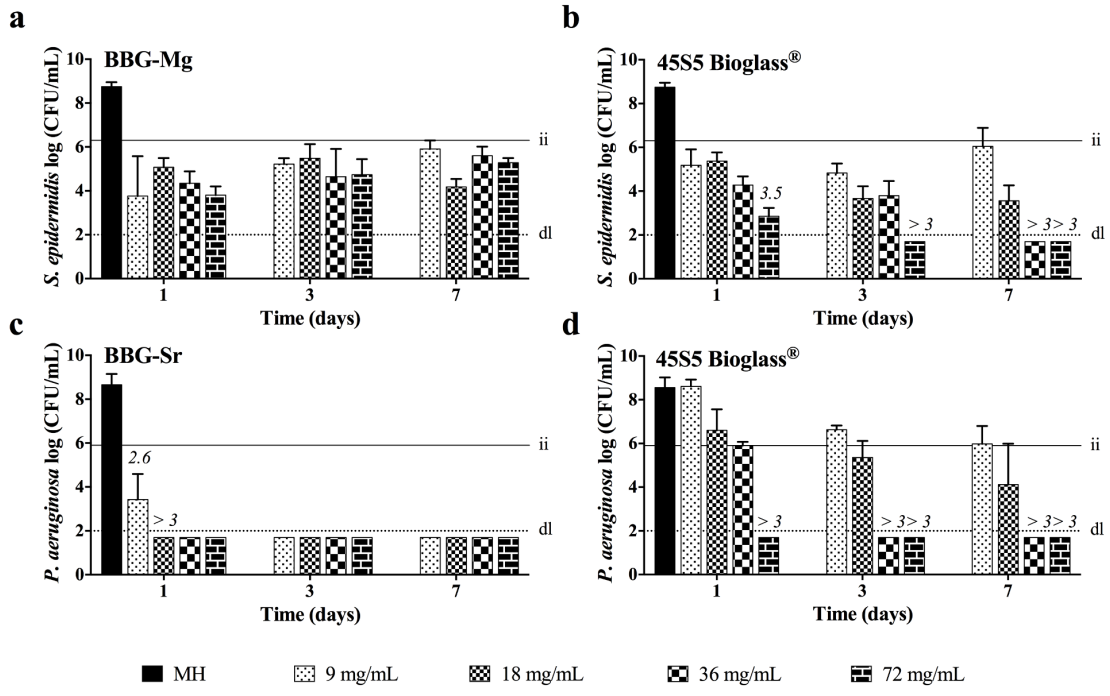

Figure IV.4 - BBG-Mg antibacterial activity against *S. epidermidis* (a) and of, BBG-Sr against *P. aeruginosa* (c). Activity of 45S5 bioglass® against *S. epidermidis* (b) and *P. aeruginosa* (d) used as control, while MH without BBG was included as a bacterial positive growth control. Bacterial cultures were assessed by the BD assay after 1, 3 and 7 days of variable concentrations of BBGs (9 – 72 $mg \cdot ml^{-1}$) dissolution in MH medium. Each bacterium was diluted to, approximately, 1 x 10^6 CFU in 0.5 ml of culture medium, added to the different tubes containing known amounts of BBGs dissolved during the specific time frames and incubated at 37 ºC in air for 24 h. The data was obtained from at least three independent samples and is expressed as mean ± SD. Whenever appropriate,

the proportion of the initial inoculum that is rendered incapable of reproduction on subculture is indicated on the top of the bar as the mean $\log_{10}$ reduction. The initial inoculum concentration (ii) and the detection limit (dl) are represented. For bacteria viable counts below the detection limit, one half of the detection limit is presented (2 log $CFU \cdot ml^{-1}$).

It is remarkable that in the case of BBG-Sr there is a concentration dependence of the antibacterial activity. Although, the interactions between BBGs and bacteria in *in vitro* conditions are complex, these data suggest that the incorporation of different substituted cations in the BBGs might be used to tune the antibacterial properties of the glasses.

3.4. *In vitro* cytotoxic evaluation

In order to be applied as a biomaterial it is of extreme relevance to study the potential cytotoxic effects of the developed BBGs. A screening of *in vitro* BBGs cytotoxicity was performed in SaOs-2 cultures.

The MTS assay was used to assess the cell viability of SaOs-2 cultured in the presence of BBGs for 7 days (Figure IV.5). Based on previous works using the 45S5 bioglass® (the control in the present work) the threshold for metabolic activity was set at 50% [44]. The BBGs and the commercial control (45S5 bioglass®) showed high cell viability for 3 days of culture. However, after 7 days of culture a significant reduction in cells' viability was observed for BBG-Mg and 45S5 bioglass® for all concentration. This might be related with the faster release rate of the alkali cation, sodium, from the BBGs, when compared with calcium and strontium. In fact, 45S5 bioglass® is composed by a high sodium percentage (24.5%). On the other hand, Kansal *et al.* showed that the increase of Na^+/Mg^{2+} ratio causes a decrease in the chemical durability of the glasses, which might result in higher release of sodium [45]. While for BBG-Ca and –Sr glasses only at concentrations higher than 36 $mg \cdot ml^{-1}$ a decay of viability was noticed. In general, the three novel BBGs exhibited similar or greater viability than 45S5 bioglass® (e.g. for the concentration of 18 $mg \cdot ml^{-1}$, after 3 days of culture, Saos-2 viabilities were of 90, 74, 60, and 66% for BBG-Mg, -Ca, -Sr and 45S5 bioglass®, respectively).

Additionally, the cell proliferation profile was assessed by PicoGreen® assay for 7 days of culture (Figure IV.6). The data showed that cell proliferation decreases only after 7 days of culture, reducing the Saos-2 population to half or less than half the control cell population, corroborating with cell viability data (Figure IV.5). The reduction of cell viability and proliferation over time can be related with the release of cations (e.g. Mg^{2+}, Ca^{2+}, Sr^{2+}) to the culture medium and the resulting increase of pH, which can be deleterious to cells by affecting essential biochemical reactions [46]. Nevertheless, for a wide range of concentrations, the BBGs showed higher number of cells in respect to the 45S5 bioglass®. Notwithstanding the reduction of cell number and viability over time there are a wide variety of BBGs concentrations that do not present significant cytotoxicity to cells (taken as 50% of metabolic activity from previous studies with 45S5 bioglass® [44]). Moreover, BBGs presented lower cytotoxicity than the commercially available 45S5 bioglass® [47]. Therefore, BBGs can be used to achieve medical-grade materials that couple bone regeneration properties with intrinsic antibacterial activity for the development of biomaterials for BTE applications.

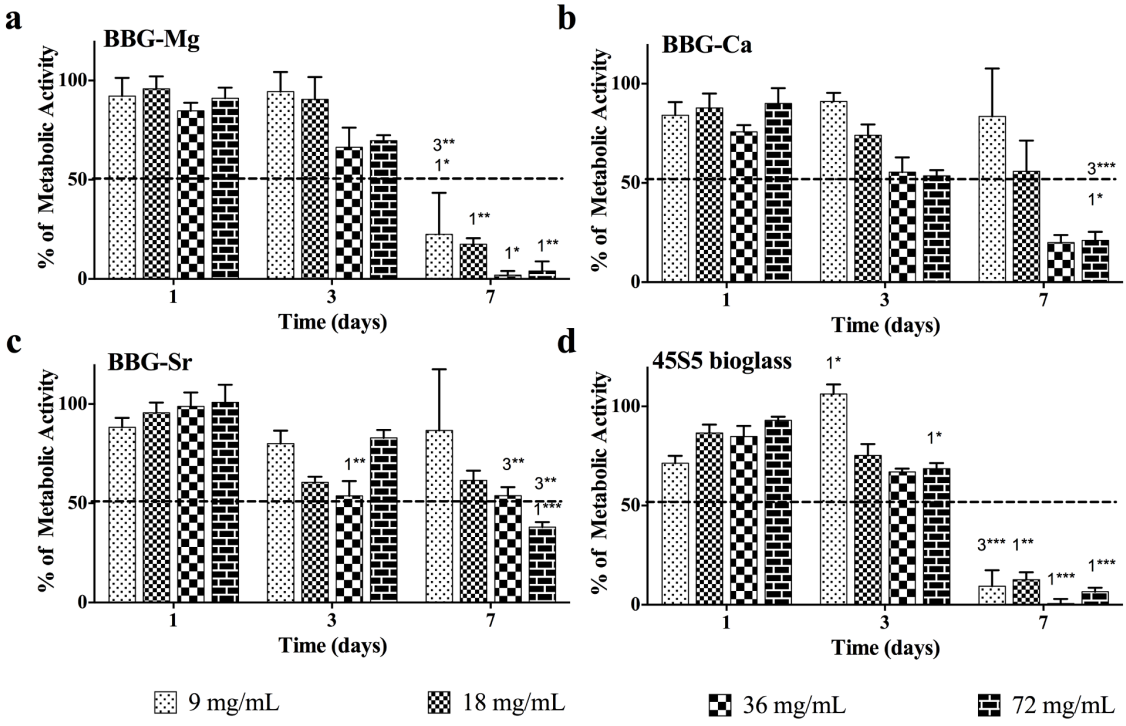

Figure IV.5 - Metabolic activity of SaOs-2 in the presence of BBG-Mg (a), BBG-Ca (b), BBG-Sr (c) assessed by MTS after 1, 3 and 7 days of variable concentrations of BBGs (9 - 72 $mg \cdot ml^{-1}$) in the media. The 45S5 bioglass® (d) was used as control. Standard culture

medium was used as negative control. The data represents the relative metabolic activity (expressed as percentage of the control). The data was obtained from at least three independent samples and is expressed as mean ± SD. Error bars represent SD. The data was analysed by non-parametric statistics: Kruskal-Wallis test (p<0.001), followed by a Dunn's Multiple Comparison test. *** Extremely significant (p<0.001); ** Very significant (0.001<p<0.01); * Significant (0.01<p<0.05). 1 in respect to day 1; 3 in respect to day 3.

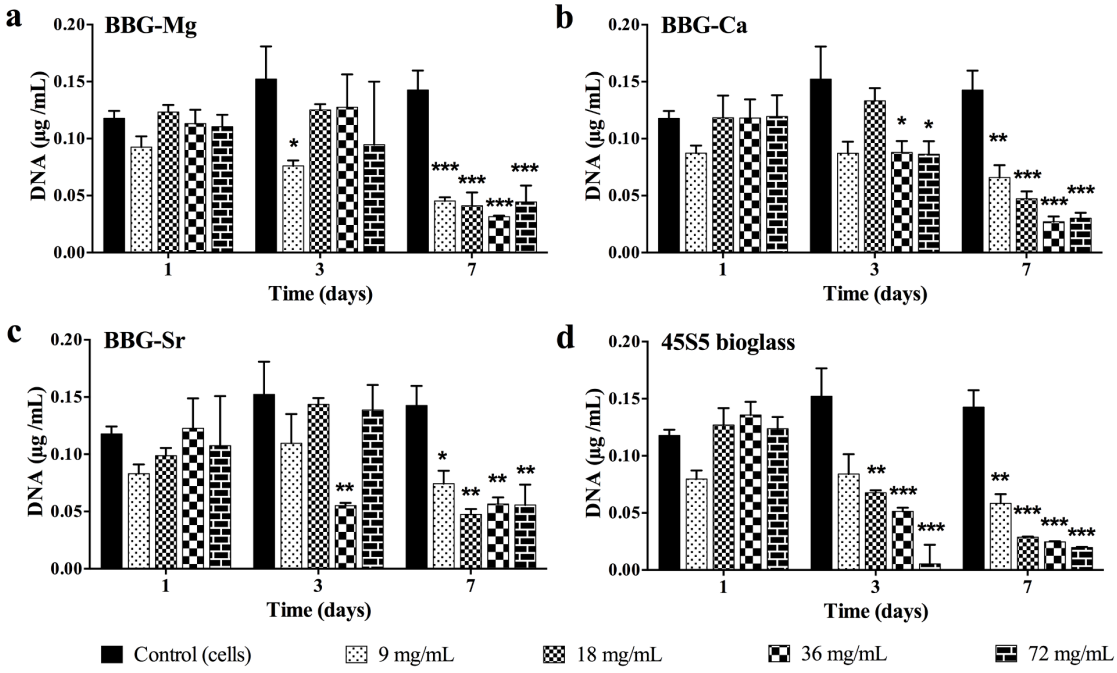

Figure IV.6 - Cell proliferation of SaOs-2 in the presence of BBG-Mg (a), BBG-Ca (b), BBG-Sr (c) assessed by PicoGreen® after 1, 3 and 7 days of variable concentrations of BBGs (9 - 72 mg·ml^{-1}) in the media. The 45S5 bioglass® (d) was used as control. Standard culture medium was used as negative control. The data was obtained from at least three independent samples and is expressed as mean ± SD. Error bars represent SD. The data was analysed by non-parametric statistics: Kruskal-Wallis test (p<0.001), followed by a Dunn's Multiple Comparison test. *** Extremely significant (p<0.001); ** Very significant (0.001<p<0.01); * Significant (0.01<p<0.05). The statistical significance of each condition was calculated in relation to the negative control at the respective time point.

The BGs provided a considerable set of new solutions for bone implantation, however the increase of surgical interventions contributed to the escalation on the incidence of bacterial bone infections. A large number of bone infections cause the failure of the medical device and require revision surgery that causes prolonged hospitalisation and occasionally leads to failure of the medical devices [48]. Moreover, nowadays, physicians are having difficulties to manage bacterial infections due to the upsurge of drug-resistance bacteria [49]. Building on the promising results from *in vitro* tests, BBGs can be used in the development of medical-grade materials with intrinsic antibacterial properties relevant for BTE applications.

4. Conclusions

BBGs with different substituted cations (Ca^{2+}, Sr^{2+} or Mg^{2+}) were successfully fabricated by melt-quenching technique. *In vitro* studies revealed that the novel BBGs exhibit bioactive and antibacterial properties relevant for BTE applications, with no cytotoxic effects for most of the active concentrations. Specially, BBG-Ca (≈ 1.67 Ca/P ratio) and BBG-Sr (≈ 1.67 Sr/P ratio) produced bone-like apatite structures onto the surface. BBG-Mg exhibited bacteriostatic activity against *S. epidermidis*, although, it did not reach the activity observed for the control sample 45S5 bioglass®. However, BBG-Sr presented bacteriostatic activity against *P. aeruginosa* at a concentration of 9 $mg \cdot ml^{-1}$ and was able to eradicate this bacterium at higher concentrations (≥ 18 $mg \cdot ml^{-1}$). Finally, this study demonstrated that BBGs can be used as relevant biomaterials that present different characteristics appropriate for BTE applications: providing bone integration properties (BBG-Ca); antibacterial capacity (BBG-Mg); or even coupled properties (BBG-Sr).

References

(1) Hench, L., The story of Bioglass. *Journal of Materials Science: Materials in Medicine* **2006,** 17, (11), 967-978.

(2) Fu, H.; Rahaman, M.; Day, D.; Huang, W., Long-term conversion of 45S5 bioactive glass–ceramic microspheres in aqueous phosphate solution. *Journal of Materials Science: Materials in Medicine* **2012,** 23, (5), 1181-1191.

(3) Xu, S.; Yang, X.; Chen, X.; Shao, H.; He, Y.; Zhang, L.; Yang, G.; Gou, Z., Effect of borosilicate glass on the mechanical and biodegradation properties of 45S5-derived bioactive glass-ceramics. *Journal of Non-Crystalline Solids* **2014,** 405, 91-99.

(4) Axford, J. S., Joint and bone infections. *Medicine* **2010,** 38, (4), 194-201.

(5) Vassena, C.; Fenu, S.; Giuliani, F.; Fantetti, L.; Roncucci, G.; Simonutti, G.; Romanò, C. L.; De Francesco, R.; Drago, L., Photodynamic antibacterial and antibiofilm activity of RLP068/Cl against Staphylococcus aureus and Pseudomonas aeruginosa forming biofilms on prosthetic material. *International Journal of Antimicrobial Agents* **2014,** 44, (1), 47-55.

(6) Simchi, A.; Tamjid, E.; Pishbin, F.; Boccaccini, A. R., Recent progress in inorganic and composite coatings with bactericidal capability for orthopaedic applications. *Nanomedicine: Nanotechnology, Biology and Medicine* **2011,** 7, (1), 22-39.

(7) Malizos, K. N.; Gougoulias, N. E.; Dailiana, Z. H.; Varitimidis, S.; Bargiotas, K. A.; Paridis, D., Ankle and foot osteomyelitis: Treatment protocol and clinical results. *Injury* **2010,** 41, (3), 285-293.

(8) Rahaman, M. N.; Liang, W.; Day, D. E., Preparation and Bioactive Characteristics of Porous Borate Glass Substrates. In *Advances in Bioceramics and Biocomposites: Ceramic Engineering and Science Proceedings*, John Wiley & Sons, Inc.: 2008; pp 1-10.

(9) Pan, H. B.; Zhao, X. L.; Zhang, X.; Zhang, K. B.; Li, L. C.; Li, Z. Y.; Lam, W. M.; Lu, W. W.; Wang, D. P.; Huang, W. H.; Lin, K. L.; Chang, J., Strontium borate glass: potential biomaterial for bone regeneration. *Journal of The Royal Society Interface* **2010,** 7, (48), 1025-1031.

(10) Lakhkar, N. J.; Lee, I.-H.; Kim, H.-W.; Salih, V.; Wall, I. B.; Knowles, J. C., Bone formation controlled by biologically relevant inorganic ions: Role and controlled delivery from phosphate-based glasses. *Advanced Drug Delivery Reviews* **2013,** 65, (4), 405-420.

(11) Hoppe, A.; Güldal, N. S.; Boccaccini, A. R., A review of the biological response to ionic dissolution products from bioactive glasses and glass-ceramics. *Biomaterials* **2011,** 32, (11), 2757-2774.

(12) Jones, J. R., Review of bioactive glass: From Hench to hybrids. *Acta Biomaterialia* **2013,** 9, (1), 4457-4486.

(13) Rahaman, M. N., 3 - Bioactive ceramics and glasses for tissue engineering. In *Tissue Engineering Using Ceramics and Polymers (Second Edition)*, Boccaccini, A. R.; Ma, P. X., Eds. Woodhead Publishing: 2014; pp 67-114.

(14) Chapin, R.; Ku, W.; Kenney, M.; McCoy, H., The effects of dietary boric acid on bone strength in rats. *Biological Trace Elemental Research* **1998,** 66, (1-3), 395-399.

(15) Yamasaki, Y.; Yoshida, Y.; Okazaki, M.; Shimazu, A.; Uchida, T.; Kubo, T.; Akagawa, Y.; Hamada, Y.; Takahashi, J.; Matsuura, N., Synthesis of functionally graded MgCO3 apatite accelerating osteoblast adhesion. *Journal of Biomedical Materials Research* **2002,** 62, (1), 99-105.

(16) Zreiqat, H.; Howlett, C. R.; Zannettino, A.; Evans, P.; Schulze-Tanzil, G.; Knabe, C.; Shakibaei, M., Mechanisms of magnesium-stimulated adhesion of osteoblastic cells to commonly used orthopaedic implants. *Journal of Biomedical Materials Research* **2002,** 62, (2), 175-184.

(17) Maeno, S.; Niki, Y.; Matsumoto, H.; Morioka, H.; Yatabe, T.; Funayama, A.; Toyama, Y.; Taguchi, T.; Tanaka, J., The effect of calcium ion concentration on osteoblast viability, proliferation and differentiation in monolayer and 3D culture. *Biomaterials* **2005,** 26, (23), 4847-4855.

(18) Marie, P. J.; Ammann, P.; Boivin, G.; Rey, C., Mechanisms of Action and Therapeutic Potential of Strontium in Bone. *CalcifiedTissue International* **2001,** 69, (3), 121-129.

(19) Marie, P. J., Strontium ranelate: A physiological approach for optimizing bone formation and resorption. *Bone* **2006,** 38, (2, Supplement 1), 10-14.

(20) Wu, C.; Fan, W.; Gelinsky, M.; Xiao, Y.; Simon, P.; Schulze, R.; Doert, T.; Luo, Y.; Cuniberti, G., Bioactive SrO–SiO2 glass with well-ordered mesopores: Characterization, physiochemistry and biological properties. *Acta Biomaterialia* **2011,** 7, (4), 1797-1806.

(21) Jones, J.; Ehrenfried, L.; Saravanapavan, P.; Hench, L., Controlling ion release from bioactive glass foam scaffolds with antibacterial properties. *Journal of Materials Science: Materials in Medicine* **2006,** 17, (11), 989-996.

(22) Palza, H.; Escobar, B.; Bejarano, J.; Bravo, D.; Diaz-Dosque, M.; Perez, J., Designing antimicrobial bioactive glass materials with embedded metal ions synthesized by the sol–gel method. *Materials Science and Engineering: C* **2013,** 33, (7), 3795-3801.

(23) Goh, Y.-F.; Alshemary, A. Z.; Akram, M.; Abdul Kadir, M. R.; Hussain, R., In-vitro characterization of antibacterial bioactive glass containing ceria. *Ceramics International* **2014,** 40, (1, Part A), 729-737.

(24) Ren, L.; Lin, X.; Tan, L.; Yang, K., Effect of surface coating on antibacterial behavior of magnesium based metals. *Materials Letters* **2011,** 65, (23–24), 3509-3511.

(25) Zhang, L.; Tan, P. Y.; Chow, C. L.; Lim, C. K.; Tan, O. K.; Tse, M. S.; Sze, C. C., Antibacterial activities of mechanochemically synthesized perovskite strontium titanate

ferrite metal oxide. *Colloids and Surfaces A: Physicochemical and Engineering Aspects* **2014,** 456, (0), 169-175.

(26) Lin, Y.; Yang, Z.; Cheng, J.; Wang, L., Synthesis, characterization and antibacterial property of strontium half and totally substituted hydroxyapatite nanoparticles. *Journal of Wuhan University of Technology-Mataterials Science Edition* **2008,** 23, (4), 475-479.

(27) Kokubo, T.; Takadama, H., How useful is SBF in predicting *in vivo* bone bioactivity? *Biomaterials* **2006,** 27, (15), 2907-2915.

(28) Matuschek, E.; Brown, D. F. J.; Kahlmeter, G., Development of the EUCAST disk diffusion antimicrobial susceptibility testing method and its implementation in routine microbiology laboratories. *Clinical Microbiology and Infection* **2014,** 20, (4), O255-O266.

(29) European Committee for Antimicrobial Susceptibility Testing of the European Society of Clinical, M.; Infectious, D., Determination of minimum inhibitory concentrations (MICs) of antibacterial agents by broth dilution. *Clinical Microbiology and Infection* **2003,** 9, (8), ix-xv.

(30) Tchouaffi-Nana, F.; Ballard, T. E.; Cary, C. H.; Macdonald, T. L.; Sifri, C. D.; Hoffman, P. S., Nitazoxanide Inhibits Biofilm Formation by Staphylococcus epidermidis by Blocking Accumulation on Surfaces. *Antimicrobial Agents and Chemotherapy* **2010,** 54, (7), 2767-2774.

(31) European Committee for Antimicrobial Susceptibility Testing of the European Society of Clinical, M.; Infectious, D., Terminology relating to methods for the determination of susceptibility of bacteria to antimicrobial agents. *Clinical Microbiology and Infection* **2000,** 6, (9), 503-508.

(32) Salimi, M. H.; Heughebaert, J. C.; Nancollas, G. H., Crystal growth of calcium phosphates in the presence of magnesium ions. *Langmuir* **1985,** 1, (1), 119-122.

(33) Wang, H.; Lee, J.-K.; Moursi, A.; Lannutti, J. J., Ca/P ratio effects on the degradation of hydroxyapatite *in vitro*. *Journal of Biomedical Materials Research A* **2003,** 67A, (2), 599-608.

(34) Fredholm, Y. C.; Karpukhina, N.; Brauer, D. S.; Jones, J. R.; Law, R. V.; Hill, R. G., Influence of strontium for calcium substitution in bioactive glasses on degradation, ion release and apatite formation. *Journal of The Royal Society Interface* **2012,** 9, (70), 880-889.

(35) Ravi, N. D.; Balu, R.; Sampath Kumar, T. S., Strontium-Substituted Calcium Deficient Hydroxyapatite Nanoparticles: Synthesis, Characterization, and Antibacterial Properties. *Journal of the American Ceramic Society* **2012,** 95, (9), 2700-2708.

(36) Hench, L. L., Bioceramics. *Journal of the American Ceramic Society* **1998,** 81, (7), 1705-1728.

(37) Ohtsuki, C.; Kushitani, H.; Kokubo, T.; Kotani, S.; Yamamuro, T., Apatite formation on the surface of ceravital-type glass-ceramic in the body. *Journal of Biomedical Materials Research* **1991,** 25, (11), 1363-1370.

(38) Mestres, G.; Abdolhosseini, M.; Bowles, W.; Huang, S. H.; Aparicio, C.; Gorr, S. U.; Ginebra, M. P., Antimicrobial properties and dentin bonding strength of magnesium phosphate cements. *Acta Biomaterialia* **2013,** 9, (9), 8384-8393.

(39) Allan, I.; Newman, H.; Wilson, M., Antibacterial activity of particulate Bioglass® against supra- and subgingival bacteria. *Biomaterials* **2001,** 22, (12), 1683-1687.

(40) Brown, L.; Darmoc, M.; Havener, M.; Clineff, T.; Ins., O.; Malven, P., Antibacterial Effects od 45S5 Bioactive Glass against Four Clnicaly Relevant Bacterial Species. In ed.; 55'" Annual Meeting of the Orthopedic Research Society, Las Vegas, NV. (2009), 2009.

(41) Hu, S.; Chang, J.; Liu, M.; Ning, C., Study on antibacterial effect of 45S5 Bioglass®. *Journal of Materials Science: Materials in Medicine* **2009,** 20, (1), 281-286.

(42) Leung, Y. H.; Ng, A. M. C.; Xu, X.; Shen, Z.; Gethings, L. A.; Wong, M. T.; Chan, C. M. N.; Guo, M. Y.; Ng, Y. H.; Djurišić, A. B.; Lee, P. K. H.; Chan, W. K.; Yu, L. H.; Phillips, D. L.; Ma, A. P. Y.; Leung, F. C. C., Mechanisms of Antibacterial Activity of MgO: Non-ROS Mediated Toxicity of MgO Nanoparticles Towards Escherichia coli. *Small* **2013.**

(43) Ohtsu, K.; Yoshida, H.; Akamatsu, N., Strontium borate pigment composition, method of making same, and processes for imparting anti-corrosive, anti-bacterial and/or anti-fungal, and non-flammable properties to materials by using same. In ed.; Google Patents: 1995.

(44) Rismanchian, M.; Khodaeian, N.; Bahramian, L.; Fathi, M.; Sadeghi-Aliabadi, H., In-vitro Comparison of Cytotoxicity of Two Bioactive Glasses in Micropowder and Nanopowder forms. *Iranian Journal of Pharmaceutical Research : IJPR* **2013,** 12, (3), 437-443.

(45) Kansal, I.; Reddy, A.; Muñoz, F.; Choi, S.-J.; Kim, H.-W.; Tulyaganov, D. U.; Ferreira, J. M. F., Structure, biodegradation behavior and cytotoxicity of alkali-containing alkaline-earth phosphosilicate glasses. *Materials Science and Engineering: C* **2014,** 44, 159-165.

(46) Teo, A.; Mantalaris, A.; Lim, M., Influence of culture pH on proliferation and cardiac differentiation of murine embryonic stem cells. *Biochemical Engineering Journal* **2014,** 90, (0), 8-15.

(47) Krishnan, V.; Lakshmi, T., Bioglass: A novel biocompatible innovation. *Journal of Advanced Pharmaceutical Technology & Research* **2013,** Apr-Jun, (4(2)), 78-83.

(48) Miola, M.; Bruno, M.; Maina, G.; Fucale, G.; Lucchetta, G.; Vernè, E., Antibiotic-free composite bone cements with antibacterial and bioactive properties. A preliminary study. *Materials Science and Engineering: C* **2014,** 43, (0), 65-75.

(49) Zhao, X., 5 - Antibacterial bioactive materials. In *Bioactive Materials in Medicine*, Zhao, X.; Courtney, J. M.; Qian, H., Eds. Woodhead Publishing: 2011; pp 97-123.

V. CHAPTER

Substituted Borosilicate Glasses with Improved Osteogenic Capacity for Bone Tissue Engineering

CHAPTER V - SUBSTITUTED BOROSILICATE GLASSES WITH IMPROVED OSTEOGENIC CAPACITY FOR BONE TISSE ENGINEERING

V. CHAPTER

Substituted Borosilicate Glasses with Improved Osteogenic Capacity for Bone Tissue Engineering[4]

Abstract

BBGs have shown capacity to improve the new bone formation when compared to silicate BGs. Herein, we assessed the capacity of BBGs to induce the osteogenic differentiation of BM-MSCs, as a function of their substituted divalent cations (Mg^{2+}, Ca^{2+}, Sr^{2+}). To this purpose, we synthesised BBG particles by melt quench. The cell viability, proliferation and morphology, (i.e. PrestoBlue®, PicroGreen®, and DAPI and Phalloidin stainings, respectively), as well as protein expression (of ALP, osteopontin and osteocalcin) of BM-MSCs in contact with the BBGs were evaluated for 21 days. We observed an enhanced expression of bone-specific proteins (ALP, osteopontin and osteocalcin) and high mineralisation of BM-MSCs under BBG-Mg and BBG–Sr conditioned osteogenic media for concentrations of 20 and 50 $mg{\cdot}ml^{-1}$ with low cytotoxic effects. Moreover, BBG-Sr at a concentration of 50 $mg{\cdot}ml^{-1}$ was able to increase the mineralisation and expression of bone-specific proteins even under basal media conditions. These results indicated that the proposed BBGs improved the osteogenic differentiation of BM-MSCs, showing therefore have great potential for the regeneration of bone tissue.

[4] This chapter is based on the following publication:

João S. Fernandes, Piergiorgio Gentile, Aileen Crawford, Ricardo A. Pires, Paul V. Hatton, Rui L. Reis; Substituted Borosilicate Glasses with Improved Osteogenic Properties for Bone Tissue Engineering (2016); under peer revision.

1. Introduction

The properties of BGs support their key relevance of in clinical applications associated to bone tissue repair and regeneration [1, 2]. They are part of a tissue engineering-based strategy that can overcome the drawbacks of the traditionally used autologous bone grafts (e.g. lack of adequate amount and quality of bone, donor site morbidity). BGs are considered relevant for bone tissue repair since they: (i) promote osteointegration (forming a bone-like HA layer on their surface); (ii) are biocompatible; and (iii) their degradation shows positive biological effects after implantation [2-5]. There are however drawbacks associated with conventional BGs including *in vitro* cytotoxicity related to the release of Na^+ ions, and interest in modified compositions has increased in recent years.[6]

Recently, BBGs have attracted interest in BTE [1, 7, 8]. BBGs have shown capability to improve the new bone formation when compared to silicate-based BGs [9, 10]. They present controllable degradation rates and have a high compositional flexibility that potentially allows BBGs to be tailored with enhanced osteogenic properties, as well as with antibacterial activity [11, 12]. On one hand, as shown by Huang *et al.*, a glass network composed of borosilicates have more controllable conversion rates to HA [13]. This has also been demonstrated to occur *in vivo* [14]. As a matter of fact, the addition of borate to the glass network can also be beneficial for bone healing, as well as formation and maintenance of new bone, while supporting cell osteogenic differentiation [15]. Frequently, it has been associated with the increase in bone resistance to fracture [16, 17]. On the other hand, by exploiting the compositional flexibility of BBGs, inorganic divalent cations, such as Mg^{2+}, Ca^{2+} and Sr^{2+} can be incorporated and play a key role in bone metabolism. For instance, Mg^{2+} increases bone formation rate as well as stimulates bone cell adhesion, increasing their stability [18, 19]. The Ca^{2+} is known to be essential during the apatite formation process, being also favourable to osteoblast proliferation, differentiation and the mineralisation of the ECM [20]. Sr^{2+} also has bone therapeutic potential. Different studies evidenced its beneficial effects on bone cells and bone formation *in vivo* [21, 22] being even used for the treatment of osteoporosis [23].

BGs are known to be osteoinductive materials, capable of stimulating the function and osteogenic differentiation of bone and stem cells without any additional supplementation. Findings from Fu *et al.* suggested that the borosilicate 13-93B1 scaffolds supported the

proliferation and function of osteogenic murine osteocyte-like cell line (MLO-A5) [15], while Gentleman *et al.* demonstrated that Sr^{2+}-substituted BGs stimulated osteoblast metabolic activity promoting cell proliferation and ALP activity [24]. More significantly, Santocildes *et al.* demonstrated that Sr-containing BGs appeared to be capable of promoting osteoblastic differentiation of BM-MSCs that were in some way pre-committed to this lineage [25]. Liang *et al.* showed that borate glasses support the attachment and differentiation of human bone marrow derived mesenchymal stem cells and human mesenchymal stem cell derived osteoblasts [26].

The present study aims to fabricate three substituted BBGs to be used in bone tissue repair and regeneration. The incorporation of different divalent cations (i.e. Mg^{2+}, Ca^{2+}, Sr^{2+}) into the BBGs was tested due to the fact that the release of these cations might induce specific effects on BM-MSCs, such as: in their proliferation, differentiation and the mineralisation of the ECM, as well as stimulating bone cells and promoting bone formation [11]. BM-MSCs are a cell type of especial interest for bone tissue research and therapy because of their ease and reproducibility of isolation, as well as their ability to differentiate into mesodermal lineage cells such as osteoblasts, osteoclasts and osteocytes [27]. Therefore, we aimed to investigate the effects of BBGs biological activity over viability, proliferation, and differentiation of BM-MSCs, providing novel biocompatible BBGs that promote osteointegration and cell differentiation for BTE.

2. Materials and Methods

2.1. Preparation of BBGs

The BBGs of general formula $0.05Na_2O \cdot xMgO \cdot yCaO \cdot (0.35\text{-}x\text{-}y)SrO \cdot 0.20B_2O_3 \cdot 0.40SiO_2$ (molar ratio, where x, y = 0.35 or 0.00, and $x \neq y$) were synthesised by melt-quenching. The suitable amounts of, silica (SiO_2, Macherey-Nagel, Germany), boron oxide (B_2O_3, Alfa Aesar, Germany), sodium bicarbonate ($NaHCO_3$, Sigma-Aldrich, Australia), and magnesium oxide (MgO, Sigma-Aldrich, Portugal), or calcium carbonate ($CaCO_3$, Sigma-Aldrich, Portugal), or strontium carbonate ($SrCO_3$, Sigma-Aldrich, Portugal) were thoroughly mixed with the addition of ethanol in a porcelain mortar with the help of a pestle, vacuum dried overnight and transferred to a platinum crucible. After

entirely dried, each batch was heated to 1450 ˚C in air for 1 h and subsequently the melt was quickly poured into cold water to form the glass frit. Afterwards, the as-quenched glasses were ground in an Agate mortar (RETSCH, Germany) and sieved to a particle size <63 μm. Before the *in vitro* tests BBG-Mg ($0.05Na_2O \cdot 0.35MgO \cdot 0.20B_2O_3 \cdot 0.40SiO_2$), BBG-Ca ($0.05Na_2O \cdot 0.35CaO \cdot 0.20B_2O_3 \cdot 0.40SiO_2$) or BBG-Sr ($0.05Na_2O \cdot 0.35SrO \cdot 0.20B_2O_3 \cdot 0.40SiO_2$) were weighted, dried and sterilised at 160 ºC for at least 2 h.

2.2. Morphology and chemical composition of BBGs

The morphology of the synthesised BBGs was observed by SEM/EDS (Leica Cambridge, UK) for the determination of the surface chemical composition.

2.3. Isolation and expansion of mesenchymal stem cells

BM-MSCs were isolated from bone marrow of 4-5 week-old male Wistar rats according to the method established by Maniatopoulos *et al.* [28] and recently proposed by Santocildes-Romero [25]. BM-MSCs were expanded in basal medium consisting of DMEM (Sigma-Aldrich, UK), supplemented with 100 $U \cdot ml^{-1}$ penicillin (Sigma,-Aldrich, UK) and 1 $mg \cdot ml^{-1}$ streptomycin (Sigma-Aldrich, UK). Cells were cultured at 37 ºC in an atmosphere of 5% CO_2.

Prior to the *in vitro* studies, BM-MSCs, at passage 2, were harvested and seeded into 24 well plates, at a density of 2×10^4 cells/well. Cells were cultured in the presence of the BBGs at concentrations of 20 and 50 $mg \cdot ml^{-1}$, for 7, 14 and 21 days under static conditions. The BM-MSCs cultured in the absence of BBGs were used as negative control and in the presence of 45S5 bioglass® as positive control. The BBGs at the desired concentrations and 45S5 bioglass® were deposited on top of the cells, in cell culture inserts with porous membranes (0.4 μm ThinCerts™ Cell Culture Inserts; Greiner, Germany). All conditions were cultured in basal and osteogenic differentiation media (basal medium supplemented with 50 $\mu g \cdot ml^{-1}$ ascorbic acid, 10 mM β-glycerophosphate and 10^{-8} M dexamethasone).

2.4. Potential cytotoxic effects of BBGs dissolution and BM-MSCs

2.4.1. Cell viability and proliferation (PrestoBlue® and PicoGreen® assays).

The PrestoBlue® reagent (Fisher Scientific, UK) is a resazurin-based solution that is reduced to resorufin by viable cells which can be detected fluorimetrically. The cell viability assay was executed according to the manufacturer's instructions. In brief, the PrestoBlue® reagent was added to a final concentration of 10% to the wells and the cells were incubated for 1 h at 37 ^{o}C. Afterwards, 200 µL samples of the culture medium were removed and placed in 96-well plates and the resorufin fluorescence was quantified spectrophotometrically using a plate reader (Tecan Infinite M200, UK). The fluorescence was determined at an excitation wavelength of 560 nm and emission wavelength of 590 nm. The metabolic activity was presented in fluorescence values and compared with the control (cell cultured in the absence of glass particles under basal medium conditions).

The PicoGreen® dsDNA reagent (Invitrogen, USA) is an ultrasensitive fluorescent nucleic acid dye for quantification of dsDNA in solution. This assay enables the measurement of cell proliferation. After each culturing period, the cell monolayers were washed with PBS and then incubated at 37 ºC for 3 h followed by a freezing step at -80 ºC for at least overnight in ultra-pure water (1 ml) to ensure cell lysis. The assay was performed according to the manufacturer's protocol. And the fluorescence was determined at an excitation wavelength of 485 nm and emission wavelength of 528 nm. The DNA concentration was presented in $\mu g \cdot ml^{-1}$ and compared with the control (cell cultured in the absence of glass particles under basal medium conditions).

2.4.2. Cell morphology and distribution.

After each culturing period the cell grown in tissue culture coverslips were washed with PBS and fixed with 4% formalin solution (0.5 ml) for 15 min at RT. The cell layers were then washed with PBS, containing 0.2% Triton X, for 2 min. After the fixation and permeation steps, the cell monolayers were washed again with PBS and stained with 4,6-DAPI (1:1000, Sigma, UK) for 2 min at RT, and phalloidin-tetramethylrhodamine B isothiocyanate (Sigma, UK) for 1 h at RT. Finally, the cells were washed and observed

using an Axioplan 2 imaging fluorescent microscope with a digital camera QIC AM 12-bit (Zeiss, UK).

2.5. Osteogenic capacity of BBGs and BM-MSCs

2.5.1. Alkaline phosphatase (ALP) quantification.

The concentration of ALP was determined for all the culture time periods, using the lysates used for DNA quantification. Briefly, the ALP quantity was assessed using the Alkaline Phosphatase, Diethanolamine Detection kit (Sigma-Aldrich, UK) in which pNPP solution is hydrolysed by ALP to yellow free p-nitrophenol. In brief, a buffered pNPP solution was prepared and equilibrated at 37 ºC. Afterwards, 2% (v/v) of sample or control were added. Immediately after mixing the absorbance was read at 405 nm in a plate reader (Tecan Infinite M200, UK) for ≈ 5 min. An ALP standard solution was used as control and buffer as blank. The units were calculated according to the following equation: $\frac{(\Delta A_{405nm}/\min\ Test - \Delta A_{405nm}/\min\ Blank)\times df \times V_F}{18.5 \times V_E}$. Where df = dilution factor; V_F = Volume of final solution; 18.5 = millimolar extinction coefficient of pNPP at 405 nm and V_E = Volume of samples/ALP standard solution. ALP activity was calculated by normalising ALP concentration per DNA concentration for each condition and time point.

2.5.2. Alizarin red staining

After 21 days culture, the cells grown in tissue culture coverslips were fixed in 70% ice-cold methanol at -20 °C at least for 30 min. The cell layers were then washed with PBS and dried overnight. Afterwards, cells were stained with alizarin red solution for 10 min [342 mg of alizarin red, (Sigma-Aldrich, UK) in 25 ml of distilled water and the pH was adjusted to 4.1 with 10% ammonium hydroxide (Sigma-Aldrich, UK)] for 10 min. The coverslips were then, washed in distilled water, dehydrated in acetone/xylene (Sigma-Aldrich, UK) solution, and mounted using an aqueous mountant. The stained constructs were observed under an optical microscope (BX51, Olympus Corporation, UK) and images captured by a digital camera (DP70, Olympus Corporation, UK). The BM-MSCs morphology and mineral deposition was also observed using SEM/EDS (Leica Cambridge, UK) for the determination of the surface chemical composition.

2.5.3. Immunodetection of bone-specific proteins

OP and OC protein expression of BM-MSCs was assessed by immunoassay technique to evaluate their osteoblastic differentiation. The procedures were executed according to the manufacturer's instructions. The concentrations of OP and OC were determined for all the culture time periods, using the lysates used for DNA quantification. The OP quantitative determination was performed using Mouse/Rat Osteopontin Quantikine ELISA Kit (R&D Systems, UK). In brief, 50 µl of assay diluent RD1W and 50 µl of standard (2500 to 39 $pg \cdot ml^{-1}$), control and samples were added and the plate incubated for 2 h at RT. After 4 washing steps and drying, 100 µl of Mouse/Rat OP Conjugated were added and incubated for 2 h at RT. The sandwich complex was washed 4 times and allowed to react with 100 µl of substrate solution before adding 100 µl of stop solution. Finally, the optical density was determined at 450 nm and the concentration of OP obtained from a standard curve plot. OC quantitative determination was performed by the use of Rat Gla-Osteocalcin High Sensitive EIA kit (Takara Clontech, Japan). In brief, 100 µL of samples and standard solution (16 to 0.25 $ng \cdot ml^{-1}$) were incubated for 1 h at 37 ºC with the capture-antibody, rat osteocalcin C-terminus-specific antibody. After OC capture and 3 washing steps, 100 µl of the enzyme-labelled antibody (GlaOC4-30) specific to Gla-OC was incubated for 1 h at RT. The sandwich complex was washed 4 times and allowed to react with 100 µl of substrate solution for 10-15 min. Finally, after adding the stop solution the optical density was determined at 450 nm and the concentration of OC obtained from a standard curve plot. OP and OC content was calculated by normalising OP or OC concentration per DNA concentration for each condition and time point.

2.6. Statistical analysis

Results are expressed as mean ± SD with n = 3 for each sample. Error bars represent SD. The data was analysed by non-parametric statistics: Kruskal-Wallis test ($p<0.0001$), followed by a Dunn's multiple comparison test. *** $p<0.001$; ** $p<0.01$; * $p<0.05$ in respect to the control.

3. Results and discussion

3.1. Morphology of BBGs and their chemical composition

BBGs' frits were successfully obtained by melt quenching and ground in a controlled manner. Figure V.1a, 1b and 1c show the SEM/EDS analysis of BBGs, which exhibited an angular shape with low sphericity and confirmed the successful incorporation of the different modifier divalent cations (i.e. Mg^{2+}, Ca^{2+} and Sr^{2+}). The composition of BBGs was confirmed in a prior work[42] by the use of XRF and follows the general formula $0.05Na_2O{\cdot}x MgO{\cdot}y CaO{\cdot}(0.35\text{-}x\text{-}y)SrO{\cdot}0.20B_2O_3{\cdot}0.40SiO_2$ (molar ratio, where x, y = 0.35 or 0.00, and $x \neq y$).

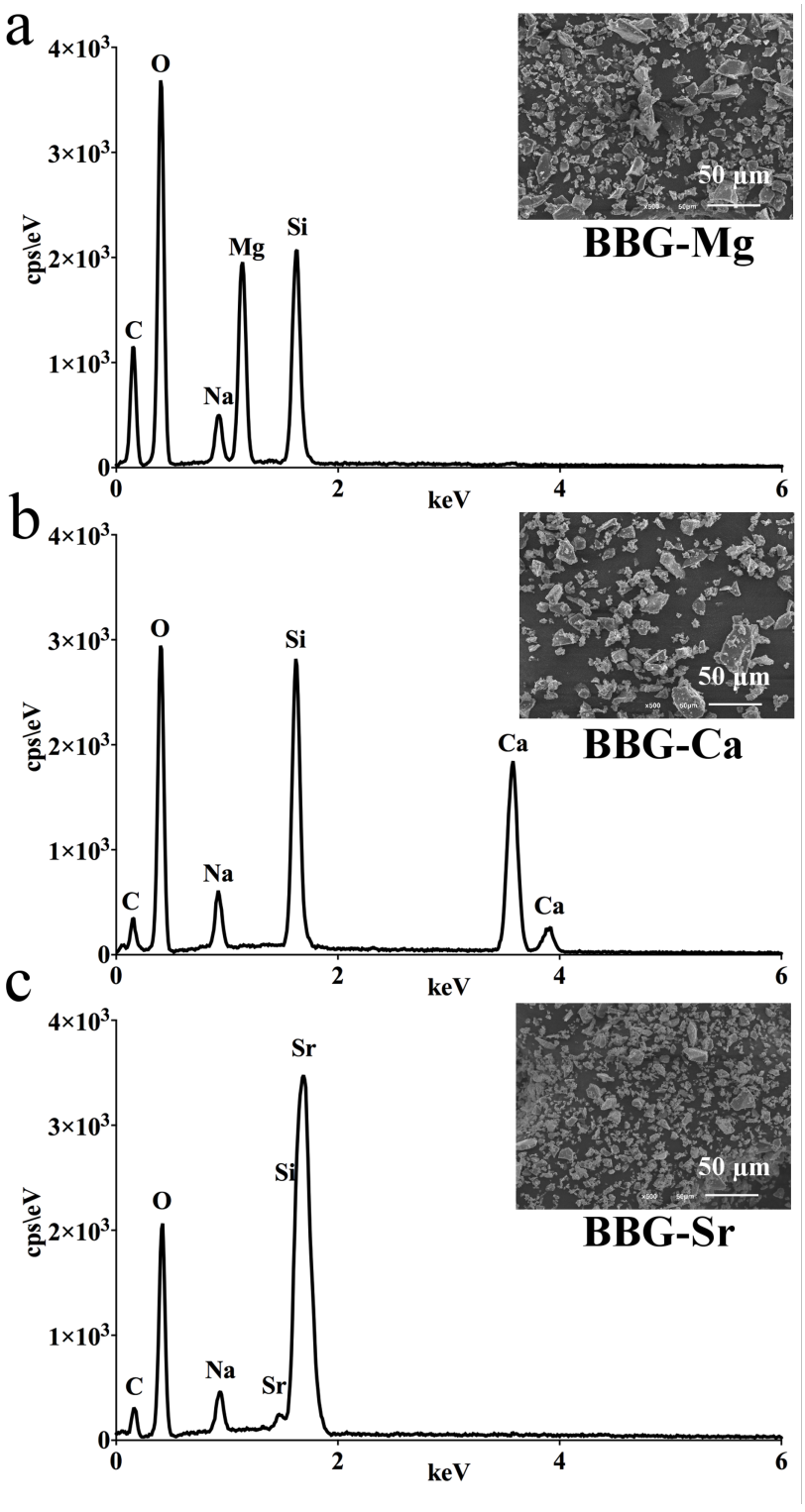

Figure V.1 - SEM/EDS micrographs of BBGs, a) BBG-Mg, b) BBG-Ca and c) BBG-Sr. SEM images are shown as insets, displaying the morphology of the glass particles. The specific modifier divalent cation is highlighted in yellow for each BBG.

3.2. *In vitro* biological evaluation

Osteoblast differentiation can be divided into three stages: cell proliferation, ECM synthesis and maturation, and ECM mineralisation, each with a cellular characteristic behaviour [29].

3.2.1. Potential cytotoxicity effect of BBGs leachable on BM-MSCs

The effect of BBGs concentration on cell viability and proliferation was studied on a previous work. It showed that a concentration between 20 and 50 $mg \cdot ml^{-1}$ did not significantly affect cell viability and proliferation. On the other hand, Romero *et al.* [30] studied the osteogenic response of BM-MSCs to strontium-substituted bioactive glasses (SrBG) and observed that 20 mg of Sr50BG promoted the osteoblastic differentiation of BM-MSCs. Based on these results, we set the BBGs concentrations on the culture medium to 20 and 50 $mg \cdot ml^{-1}$.

Herein, we cultured BM-MSCs in basal and osteogenic differentiation media for 7, 14 and 21 days under static conditions, in the presence and absence of BBGs, in order to evaluate their biological activity and capacity to maintain their structural integrity. The cellular metabolism and proliferation was evaluated by quantifying the conversion of resazurin-to resorufin by viable cells; the amount of double stranded DNA (live cells) in the culture wells; and their morphology. The data was analysed in comparison with the BM-MSCs (without any BBGs, i.e. control experiment) to evaluate the impact of BBGs in the cell behaviour.

Fluorescence microscopy images showed the morphology of BM-MSCs in culture containing BBGs or 45S5 bioglass® (Figure V.2). The adhered BM-MSCs exhibited a well-spread morphology, exhibiting cell-to-cell contacts in a comparable manner on the BBGs conditioned cultures as in the control experiment. While BM-MSCs cultured with 45S5 bioglass® presented a round shape for the last time point (21 days), suggesting cell death. At the same timepoint, especially for cultures under osteogenic differentiation media (e.g. BBG-Sr), there was distinguishable well-spread polygonal shape cells, suggesting osteoblast-like morphology.

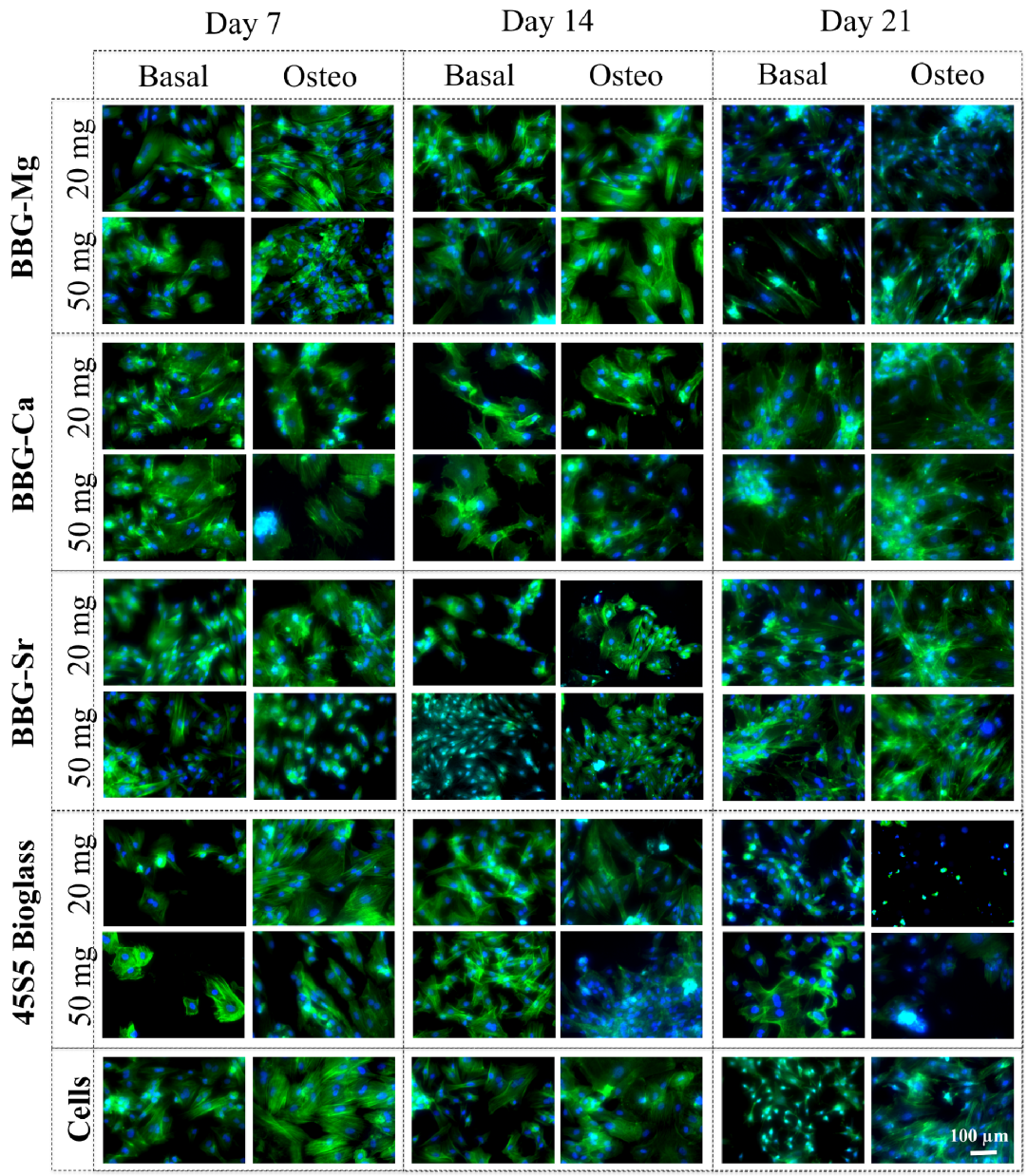

Figure V.2 - BM-MSCs morphology observed by fluorescence microscopy, after 7, 14 and 21 days culture with BBGs either under basal or osteogenic culture medium. Each sample was incubated at two different concentrations (20 and 50 mg·ml^{-1}). Cells cultured with basal and osteo medium were used as negative control and 45S5 bioglass® incubated with medium was used as positive control. Nuclei stained blue by DAPI; Actin stained green by Phalloidin.

From the PrestoBlue® data (Figure V.3a, 3c, 3e and 3g) it is possible to observe that the metabolic activity of BM-MSCs increased over the time. However, until the day 7, the BM-MSCs viability reduced in respect to the cells culture under basal condition,

especially for BBG-Ca culture conditions. In contrast, from day 14, BM-MSC cultures under osteogenic media displayed a reduction of metabolic activity with respect to the control (absence of glass particles and cell cultured under basal medium). It is noteworthy that BM-MSC cultures at day 21 with 45S5 bioglass® under osteogenic media showed very low metabolic activity when compared with the control experiment (osteogenic media), being consistent with the cell death observed by fluorescent microscopy (Figure V.2). Complementary to the viability analysis, the cellular proliferation was also assessed by measuring the total cell DNA (Figure V.3b, 3d, 3f, 3h). The Picogreen® data showed an increase on the number of BM-MSCs over time. However, under osteogenic media, the cells presented lower proliferation rates than cultures under basal media from day 14. Noteworthy, is the prominent reduction of BM-MSCs for cultures with BBG-Mg (osteogenic and basal media) and 45S5 bioglass® (osteogenic media) at day 21. To emphasise, BBG-Sr and 45S5 bioglass® under osteogenic media showed a significant reduction on the cell proliferation at day 14 when compared with the cells cultured under basal media, suggesting an alteration of biological behaviour [31]. Regarding the effect of concentration, there was no potential toxic effects with time except in the case of BM-MSCs cultured in the presence of BBG-Mg (osteogenic and basal media) and 45S5 bioglass® (osteogenic media) at day 21, where a large reduction in cell number was observed in relation to the control (basal media).

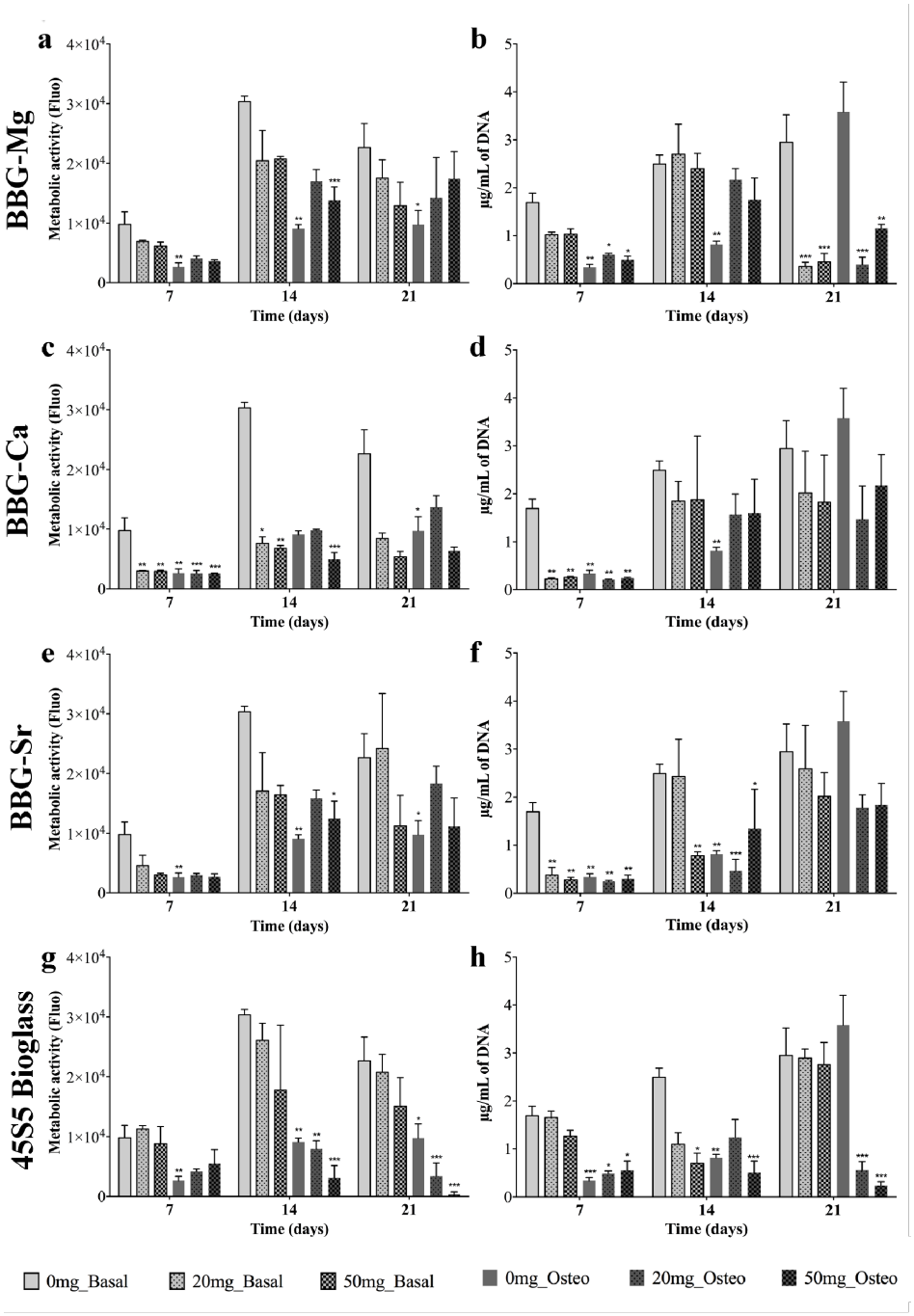

Figure V.3 - Metabolic activity (PrestoBlue® assay) and proliferation (PicoGreen® assay) of BM-MSCs cultured either in basal or osteogenic media in the presence of different concentrations (20 and 50 mg·ml^{-1}) of BBG-Mg (a, b), BBG-Ca (c, d) and BBG-Sr (e, f). The 45S5 bioglass® (g, h) was used as control. Standard culture medium was used as negative control. The statistical significance is represented relative to the control, i.e. BM-MSCs culture in basal media.

3.2.2. Alkaline phosphate quantification

It is commonly accepted that changes of the specific activity of ALP in bone cells are associated with a shift of their differentiated state [32]. In general, an increase of the ALP activity is correlated with osteogenesis, increasing during the bone formation stage [33]. Not surprisingly, the ALP quantification data (Figure V.4) showed a significantly higher ALP activity when cells were cultured under osteogenic media rather than basal media [34]. However, at day 21 the levels of ALP activity on BBG-Mg, -Sr and 45S5 bioglass® cultured under osteogenic media are significantly higher than the cultures without glass addition (e.g. at day 21, under osteogenic media, the addition of 20 mg of BBG-Sr (c) induced a highly significantly (p<0.001) enhanced ALP activity in relation to the cells cultured in the absence of glass particles). BBG-Mg, -Sr and 45S5 bioglass® were not capable of inducing the ALP protein expression alone, however, they were capable to increase the ALP expression during the differentiation process of BM-MSCs into osteoblasts under osteogenic media (for 21 days of cell culture). It is also relevant to highlight the fact that along with the increase of ALP activity for the case of BBG-Mg and -Sr glasses there was observed an increase of cell proliferation. In contrast, the viability and proliferation data, presented a reduction of viable and live cells for the BM-MSCs cultured in the presence of these BBG-Ca and 45S5 bioglass®. Remarkably, BBG-Sr promoted the increase of ALP activity for both concentrations of glass particles, i.e. 20 and 50 $mg \cdot ml^{-1}$.

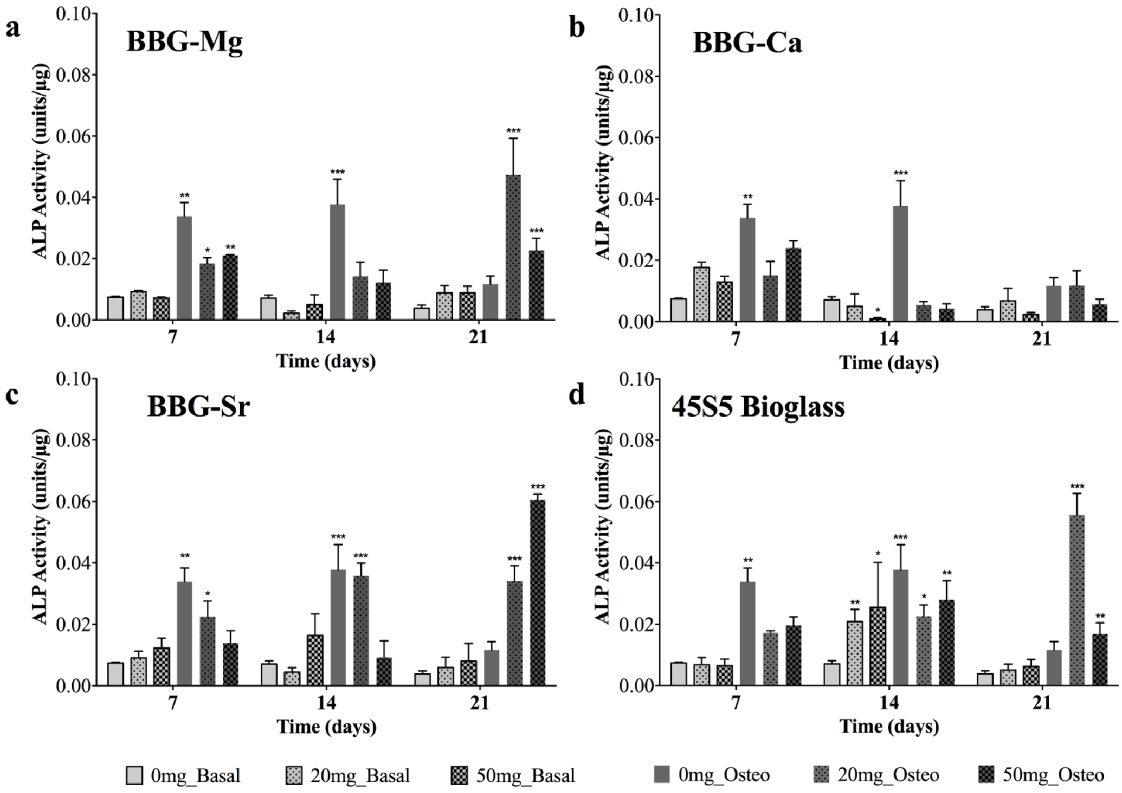

Figure V.4 - ALP activity of BM-MSCs (cultured either in basal or osteogenic media in the presence of different concentrations (0, 20 and 50 mg·ml^{-1}) of BBG-Mg (a), BBG-Ca (b) and BBG-Sr (c). The 45S5 bioglass® (d) was used as control. The statistical significance was calculated in relation to BM-MSC cultured in basal media.

3.2.3. Matrix mineralisation

Similar results were found at day 21 after alizarin red staining for mineral deposits (Figure V.5). In agreement with ALP activity data, cells cultured under osteogenic media yielded more bone-like nodules, resulting from ECM mineralisation [35]. The intense red spots dispersed in the cell culture correspond to the mineralised nodules. Of importance, and corroborating with ALP activity data, mineral deposits were more evident with BBG-Mg, -Sr and 45S5 bioglass® (Figure V.5a, 5c and 5d) and an increase of red nodules with the increase of concentrations can be observed in the case of the cells cultured in the presence of BBG-Sr (Figure V.5c, osteo 20 mg·ml^{-1} and 50 mg·ml^{-1}). Higher concentrations of BBG-Sr and 45S5 bioglass® show the presence of red nodules even in cells cultured in basal medium. However, ALP activity data, suggests that BBG-Sr and

45S5 bioglass® (Figure V.4c and d basal for a concentration of 50 mg·ml^{-1}) are capable to induce ECM mineralisation by themselves. Therefore, the combination of ALP activity and mineralisation results suggest the use of BBG-Sr to promote osteogenesis [36].

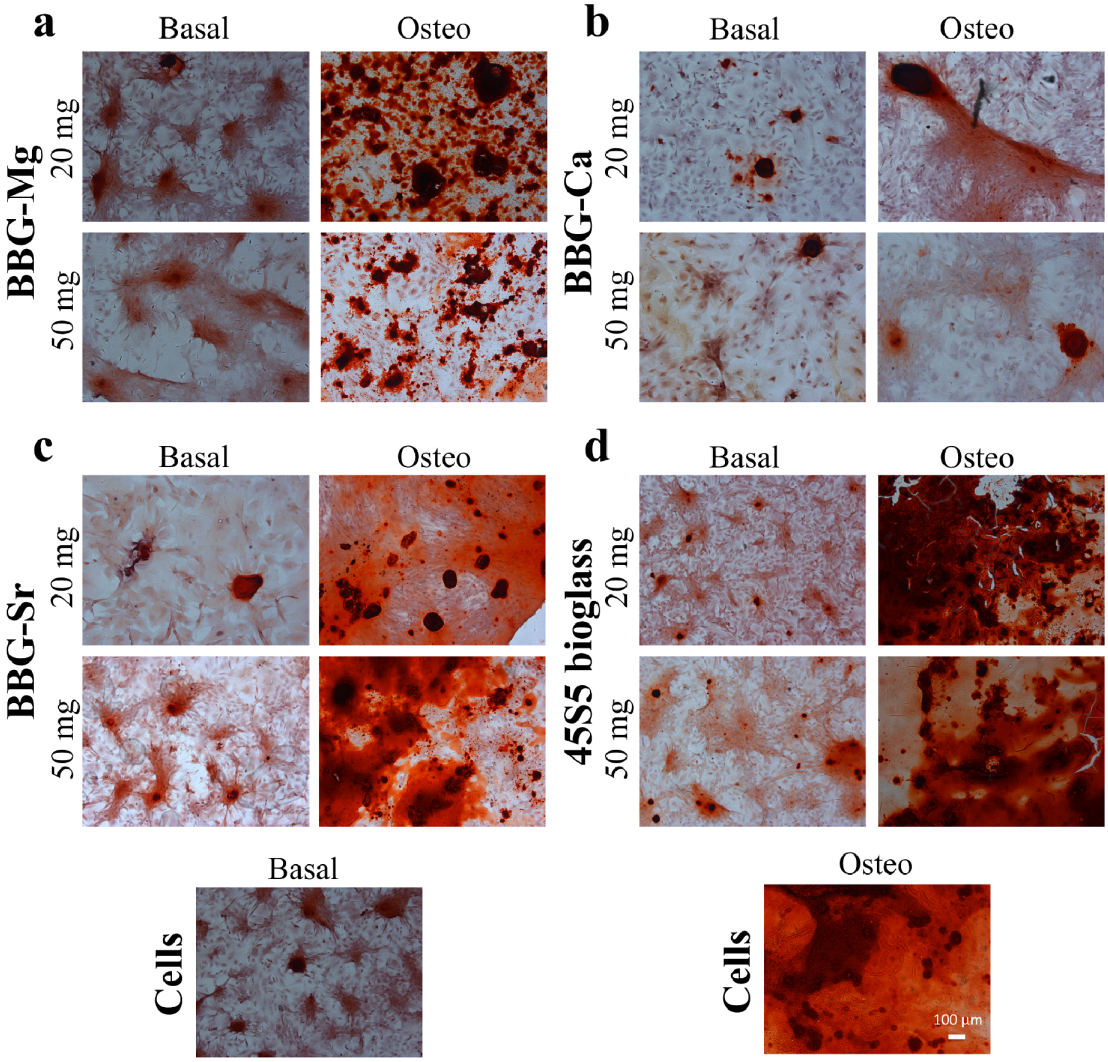

Figure V.5 - Alizarin red staining of BM-MSCs cultured during 21 days, either in basal or osteogenic media in the presence of different concentrations (20 and 50 mg·ml^{-1}) of BBG-Mg (a), BBG-Ca (b) and BBG-Sr (c). The 45S5 bioglass® (d) was used as control.

In Figure V.6 we show the SEM micrographs of BM-MSCs cultured for 21 days in the presence of BBGs and 45S5 bioglass®. In the images it is possible to observe the deposition of minerals over the dense layer of cells, when they were cultured in the presence of BBG-Mg, -Sr and 45S5 bioglass® (Figure V.6a, 6c and 6d). The presence of

these glass compositions in the culture medium promoted a mineralisation typical to occur while BM-MSCs differentiate into osteoblasts [34]. This mineralisation is in agreement with the alizarin red data where the mineral deposits were more evident in the cells cultured in the presence of BBG-Mg, -Sr and 45S5 bioglass® (Figure V.5a, 5c and 5d). In these culture conditions, it is observed in the SEM images calcium phosphate deposits over the dense cellular layer. Once more, higher concentrations of BBG-Sr and 45S5 bioglass® under basal culture conditions promoted the deposition of a higher amounts of calcium phosphate structures, suggesting that BBG-Sr and 45S5 bioglass® (Figure V.6c and 6d basal for a concentration of 50 $mg \cdot ml^{-1}$) are capable of inducing ECM mineralisation by itself, which could be beneficial for bone regeneration [36].

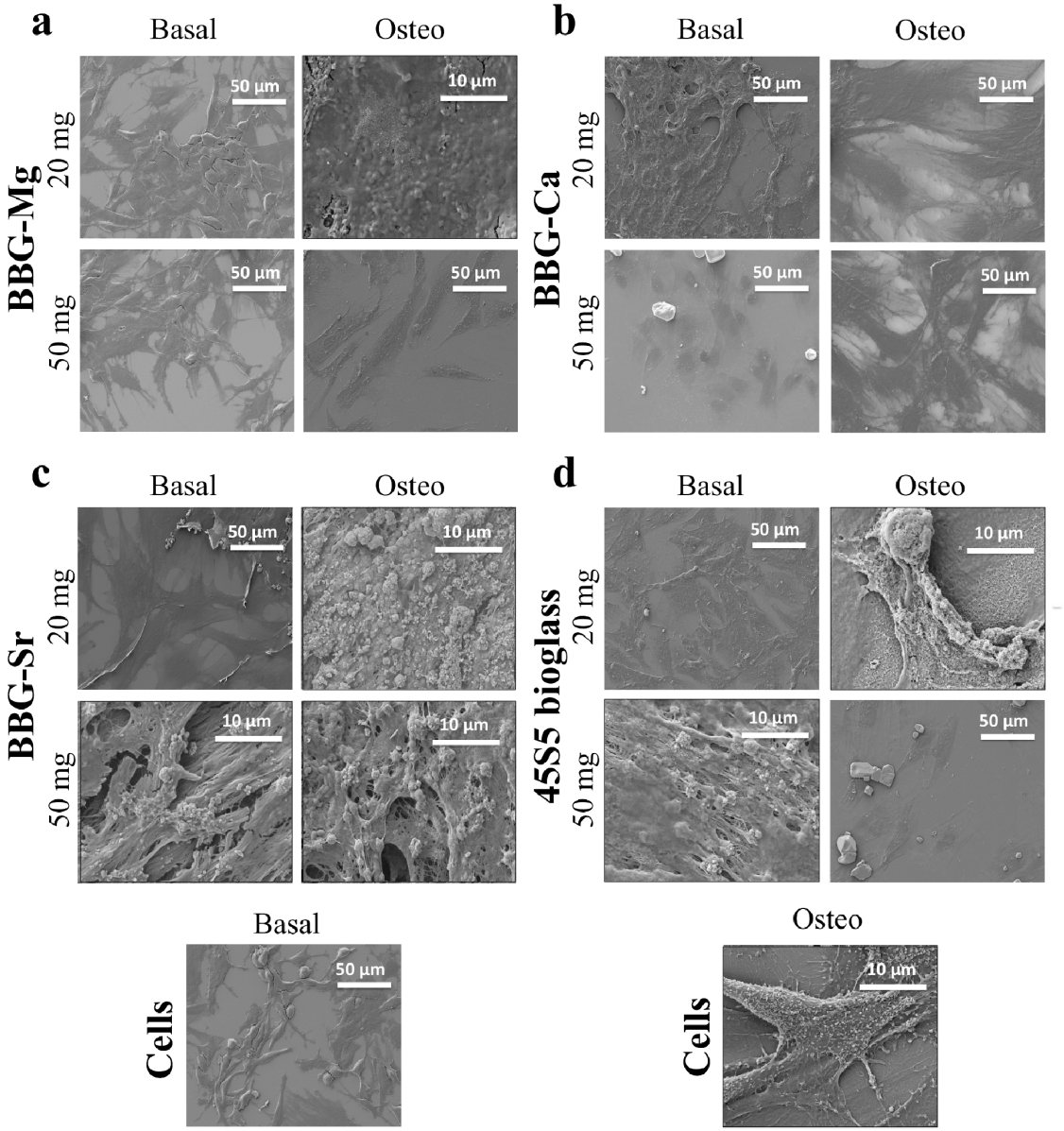

Figure V.6 - SEM micrographs of BM-MSCs in the presence of different concentrations (20 and 50 mg·ml^{-1}) of BBG-Mg (a), BBG-Ca (b) and BBG-Sr (c) after 21 days of cell culture either in basal or osteogenic media. The 45S5 bioglass® was used as a control.

3.2.4. Protein expression (OP and OC)

Complementary to the reported biological data, the differentiation level of BM-MSC, cultured in the presence (20 and 50 mg·ml^{-1}) and absence of BBG-Mg, -Ca, -Sr and 45S5 bioglass® (either in basal or osteogenic media) was assessed by the quantification of the

expression level of two major bone-specific proteins, i.e. OP and OC. The relative expression of these proteins was normalised in relation to the number of cells, i.e. amount of dsDNA. It is well known that osteoblasts are differentiated cells that mineralise the bone matrix. OP is a phosphoprotein synthesised by bone forming cells, which present calcium-binding domains and is responsible for cell attachment, proliferation, and ECM mineralisation [37]. In the case of OC, it is a bone-specific glycoprotein capable of binding to calcium, which promotes ECM calcification [37]. Not surprisingly, the OP and OC quantification data (Figure V.7 and Figure V.8) showed a significantly higher protein expression when BM-MCSs were cultured under osteogenic media rather than basal media [38]. In the case of OP, as expected, a delay in the protein synthesis is observed (Figure V.7). At day 7 there was no significant difference of OP expression in relation to the control (absence of glass particles and cell culture in basal medium). However, at day 14 there is a high expression peak by BM-MSCs cultured in osteogenic medium (in the presence of BBG-Mg, -Sr and 45S5 bioglass®), which determines the decay of the matrix deposition phase and the beginning of the mineralisation phase. Moreover, BBG-Sr and 45S5 bioglass® continue to induce a significant overexpression of OP over time (e.g. at day 21), supporting the mineralisation demonstrated by ALP and alizarin red analysis (Figure V.4 and Figure V.5, respectively). In the OC case there was a high protein expression up to day 14, indicating bone ECM maturation (Figure V.8) [39]. At day 7 there is a significant difference in OP expression in relation to the control (cell culture in basal medium and in the absence of glass particles). After day 7 there was a reduction of OC expression, consistent with matrix mineralisation. Noteworthy is the observation that BBG-Sr under basal medium induced the BM-MSCs to exhibit a peak of OC expression at day 14. This data suggested that the BBG-Sr glass particles (at a concentration of 50 $mg \cdot ml^{-1}$) induced the OC protein expression, which is also in agreement with the ALP and alizarin red data. Also, BBG-Sr and 45S5 bioglass® prolonged the OC overexpression over the 21 days of culture. In addition, the 45S5 bioglass® promoted a high deposition of OC at day 21 (Figure V.8d) compared with high BM-MSCs density in the case of BBG-Sr (Figure V.8c). However, it is important consider that in the case of the cultures in the presence of 45S5 bioglass® a very low BM-MSCs cell density was observed, which might be related with the cytotoxicity of 45S5 bioglass® [40]. Therefore, and overall, our data suggests that the BBG-Sr glass particles are able to induce the BM-MSCs to express higher levels of OP and OC, while maintaining the BM-MSCs cell density.

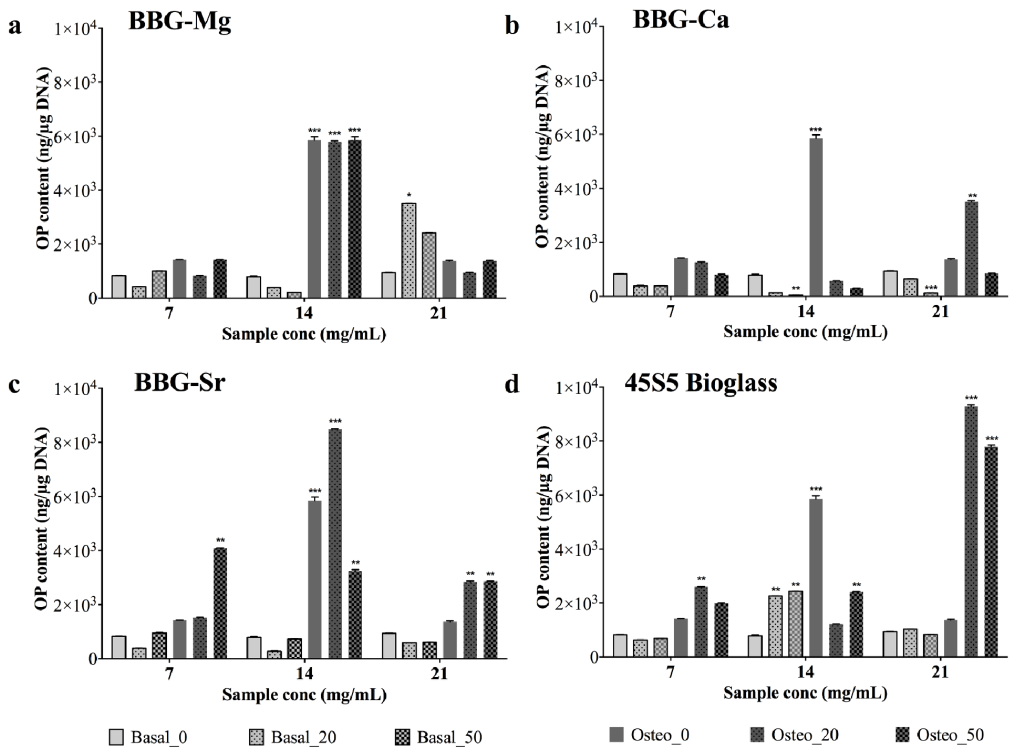

Figure V.7 - OP protein content of BM-MSCs cultured either with basal or osteogenic media in the presence of different concentrations (20 and 50 mg·ml^{-1}) of BBG-Mg (a), BBG-Ca (b) and BBG-Sr (c). The 45S5 bioglass® (d) was used as control. Results are expressed as mean ± SD with n = 3 for each bar. The statistical significance is calculated in relation to the control experiment, i.e. BM-MSCs cell cultures in basal media at each time point.

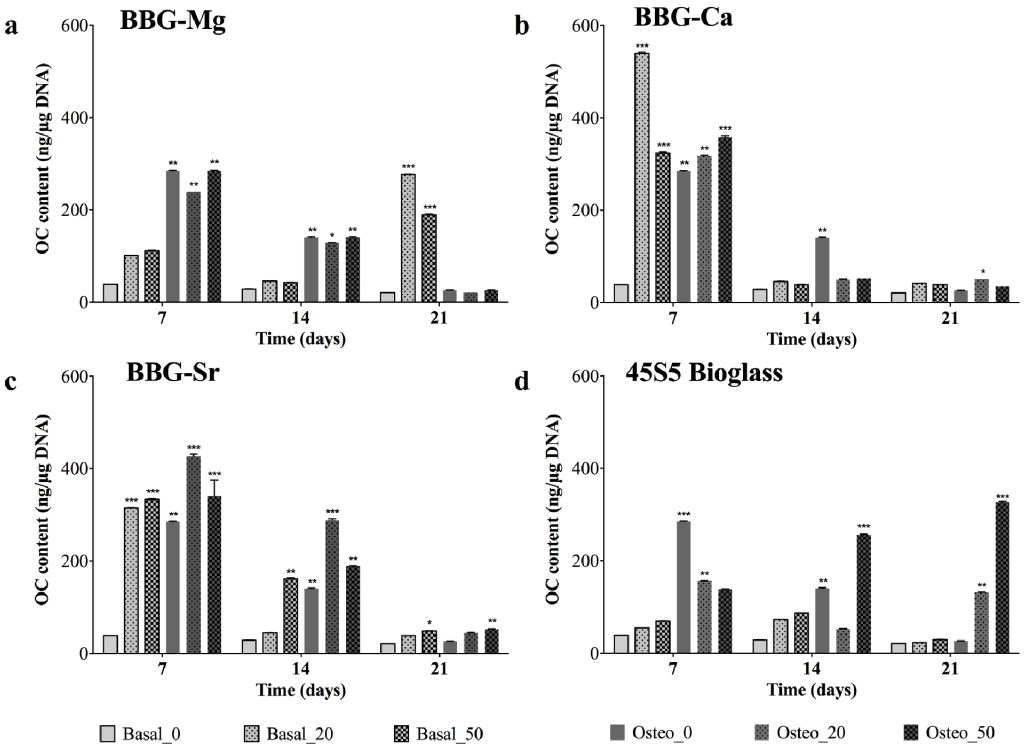

Figure V.8 - OC protein content of BM-MSCs cultured either with basal or osteogenic media in the presence of different concentrations (20 and 50 mg·ml^{-1}) of BBG-Mg (a), BBG-Ca (b) and BBG-Sr (c). The 45S5 bioglass® (d) was used as control. Results are expressed as mean ± SD with n = 3 for each bar. The statistical significance was calculated in relation to the control experiment, i.e. BM-MSCs cell cultures in basal media at each time point.

Hence, combining the obtained biological data, i.e. viability, proliferation, mineralisation and protein expression analysis (ALP, OC and OP), we were able to identify the BBG-Mg, -Sr (at concentrations of 20 to 50 mg·ml^{-1}) as relevant promoters of the osteogenic differentiation of BM-MSCs. Surprisingly, BBG-Sr (at a concentration of 50 mg·ml^{-1} and 21 days of culture) presented the capacity of induce osteogenic response in BM-MSCs in the absence of osteogenic medium. The ALP activity results showed the shift of BM-MSCs to a more differentiated state, while the alizarin red analysis demonstrated that the cells in the presence of BBG-Mg and BBG-Sr glass particles present intense and dispersed red spots in the cell culture, corresponding to the mineralisation promoted by the BM-MSCs. In agreement with this data, we also observed that they can also influence the ECM maturation and mineralisation, through the promotion of the OP and OC protein

overexpression suggesting that these glass compositions may be effective in inducing and sustaining the osteoblastic phenotype [41].

4. Conclusions

BBGs with different substituted divalent cations (Ca^{2+}, Sr^{2+} or Mg^{2+}) were successfully synthesised by melt quenching. *In vitro* studies demonstrated that the studied BBGs exhibit the capability to improve the osteogenic differentiation of BM-MSCs with no deleterious effects over cell viability and proliferation. Specially, BBG-Mg and BBG-Sr (at 20 and 50 $mg \cdot ml^{-1}$) provided favourable conditions for BM-MSCs to differentiate to osteoblast-like cells and induce the formation of a high amount of mineralised nodules. The phenotypic expression of two major bone-specific proteins, namely, OP and OC confirmed the osteogenic potential of the BBGs.

Finally, these findings demonstrated that BBG compositions possessed potential for applications in regenerative medicine. Based on these promising results we propose the incorporation of BBGs into medical devices for bone regeneration. The use of BBGs enhanced the biocompatibility of the medical devices and promoted the osteogenic differentiation of BM-MSCs. The proposed BBGs are relevant candidates for further *in vivo* evaluation.

References

(1) Rahaman, M. N., 3 - Bioactive ceramics and glasses for tissue engineering. In *Tissue Engineering Using Ceramics and Polymers (Second Edition)*, Boccaccini, A. R.; Ma, P. X., Eds. Woodhead Publishing: 2014; pp 67-114.

(2) Rabiee, S. M.; Nazparvar, N.; Azizian, M.; Vashaee, D.; Tayebi, L., Effect of ion substitution on properties of bioactive glasses: A review. *Ceramics International* **2015,** 41, (6), 7241-7251.

(3) Hench, L., The story of Bioglass. *Journal of Materials Science: Materials in Medicine* **2006,** 17, (11), 967-978.

(4) Bhakta, S.; Faira, P.; Salata, L.; de Oliveira Neto, P.; Miller, C.; van Noort, R.; Reaney, I.; Brook, I.; Hatton, P., Determination of relative *in vivo* osteoconductivity of modified potassium fluorrichterite glass–ceramics compared with 45S5 bioglass. *Journal of Materials Science: Materials in Medicine* **2012,** 23, (10), 2521-2529.

(5) Gomes, F. O.; Pires, R. A.; Reis, R. L., Aluminum-free glass-ionomer bone cements with enhanced bioactivity and biodegradability. *Materials Science and Engineering: C* **2013,** 33, (3), 1361-1370.

(6) Wallace, K. E.; Hill, R. G.; Pembroke, J. T.; Brown, C. J.; Hatton, P. V., Influence of sodium oxide content on bioactive glass properties. *Journal of Materials Science: Materials in Medicine* 10, (12), 697-701.

(7) Pires, R. A.; Abrahams, I.; Nunes, T. G.; Hawkes, G. E., Multinuclear magnetic resonance studies of borosilicate glasses for use in glass ionomer cements: incorporation of CaO and Al2O3. *Journal of Materials Chemistry* **2006,** 16, (24), 2364-2373.

(8) Pires, R. A.; Abrahams, I.; Nunes, T. G.; Hawkes, G. E., The role of alumina in aluminoborosilicate glasses for use in glass-ionomer cements. *Journal of Materials Chemistry* **2009,** 19, (22), 3652-3660.

(9) Pan, H. B.; Zhao, X. L.; Zhang, X.; Zhang, K. B.; Li, L. C.; Li, Z. Y.; Lam, W. M.; Lu, W. W.; Wang, D. P.; Huang, W. H.; Lin, K. L.; Chang, J., Strontium borate glass: potential biomaterial for bone regeneration. *Journal of The Royal Socieaty Interface* **2010,** 7, (48), 1025-1031.

(10) Rahaman, M. N.; Day, D. E.; Sonny Bal, B.; Fu, Q.; Jung, S. B.; Bonewald, L. F.; Tomsia, A. P., Bioactive glass in tissue engineering. *Acta Biomaterialia* **2011,** 7, (6), 2355-2373.

(11) Hoppe, A.; Güldal, N. S.; Boccaccini, A. R., A review of the biological response to ionic dissolution products from bioactive glasses and glass-ceramics. *Biomaterials* **2011,** 32, (11), 2757-2774.

(12) Lakhkar, N. J.; Lee, I.-H.; Kim, H.-W.; Salih, V.; Wall, I. B.; Knowles, J. C., Bone formation controlled by biologically relevant inorganic ions: Role and controlled delivery from phosphate-based glasses. *Advanced Drug Delivery Reviews* **2013,** 65, (4), 405-420.

(13) Huang, W.; Day, D.; Kittiratanapiboon, K.; Rahaman, M., Kinetics and mechanisms of the conversion of silicate (45S5), borate, and borosilicate glasses to hydroxyapatite in dilute phosphate solutions. *Journal of Materials Science: Materials in Medicine* **2006,** 17, (7), 583-596.

(14) Yao, A.; Deping Wang; Huang, W., *In Vitro* Bioactive Characteristics of Borate-Based Glasses with

Controllable Degradation Behavior. *Journal of American Ceramics Society* **2006,** 1, (90), 303–306.

(15) Fu, Q.; Rahaman, M. N.; Bal, B. S.; Bonewald, L. F.; Kuroki, K.; Brown, R. F., Silicate, borosilicate, and borate bioactive glass scaffolds with controllable degradation rate for bone tissue engineering applications. II. *In vitro* and *in vivo* biological evaluation. Journals of Biomedical Metraisl Research A, *Oct 2010* **2010,** 95A, (1).

(16) Shen, Y.; Liu, W.; Wen, C.; Pan, H.; Wang, T.; Darvell, B. W.; Lu, W. W.; Huang, W., Bone regeneration: importance of local pH-strontium-doped borosilicate scaffold. *Journal of Materials Chemistry* **2012,** 22, (17), 8662-8670.

(17) Chapin, R.; Ku, W.; Kenney, M.; McCoy, H., The effects of dietary boric acid on bone strength in rats. *Biol Trace Elem Res* **1998,** 66, (1-3), 395-399.

(18) Yamasaki, Y.; Yoshida, Y.; Okazaki, M.; Shimazu, A.; Uchida, T.; Kubo, T.; Akagawa, Y.; Hamada, Y.; Takahashi, J.; Matsuura, N., Synthesis of functionally graded MgCO3 apatite accelerating osteoblast adhesion. *Journal of Biomedical Materials Research* **2002,** 62, (1), 99-105.

(19) Zreiqat, H.; Howlett, C. R.; Zannettino, A.; Evans, P.; Schulze-Tanzil, G.; Knabe, C.; Shakibaei, M., Mechanisms of magnesium-stimulated adhesion of osteoblastic cells to commonly used orthopaedic implants. *Journal of Biomedical Materials Research* **2002,** 62, (2), 175-184.

(20) Maeno, S.; Niki, Y.; Matsumoto, H.; Morioka, H.; Yatabe, T.; Funayama, A.; Toyama, Y.; Taguchi, T.; Tanaka, J., The effect of calcium ion concentration on osteoblast viability, proliferation and differentiation in monolayer and 3D culture. *Biomaterials* **2005,** 26, (23), 4847-4855.

(21) Marie, P. J.; Ammann, P.; Boivin, G.; Rey, C., Mechanisms of Action and Therapeutic Potential of Strontium in Bone. *Calcified Tissue International* **2001,** 69, (3), 121-129.

(22) Marie, P. J., Strontium ranelate: A physiological approach for optimizing bone formation and resorption. *Bone* **2006,** 38, (2, Supplement 1), 10-14.

(23) Wu, C.; Fan, W.; Gelinsky, M.; Xiao, Y.; Simon, P.; Schulze, R.; Doert, T.; Luo, Y.; Cuniberti, G., Bioactive SrO–SiO2 glass with well-ordered mesopores: Characterization, physiochemistry and biological properties. *Acta Biomaterialia* **2011,** 7, (4), 1797-1806.

(24) Gentleman, E.; Fredholm, Y. C.; Jell, G.; Lotfibakhshaiesh, N.; O'Donnell, M. D.; Hill, R. G.; Stevens, M. M., The effects of strontium-substituted bioactive glasses on osteoblasts and osteoclasts *in vitro*. *Biomaterials* **2010,** 31, (14), 3949-3956.

(25) Santocildes-Romero, M. E.; Crawford, A.; Hatton, P. V.; Goodchild, R. L.; Reaney, I. M.; Miller, C. A., The osteogenic response of mesenchymal stromal cells to strontium-substituted bioactive glasses. *Journal of Tissue Engineering and Regenerative Medicine* **2015,** 9, (5), 619-631.

(26) Liang, W.; Rahaman, M. N.; Day, D. E.; Marion, N. W.; Riley, G. C.; Mao, J. J., Bioactive borate glass scaffold for bone tissue engineering. *Journal of Non-Crystalline Solids* **2008,** 354, (15-16), 1690-1696.

(27) Brooke, G.; Cook, M.; Blair, C.; Han, R.; Heazlewood, C.; Jones, B.; Kambouris, M.; Kollar, K.; McTaggart, S.; Pelekanos, R.; Rice, A.; Rossetti, T.; Atkinson, K., Therapeutic applications of mesenchymal stromal cells. *Seminars in Cell & Developmental Biology* **2007,** 18, (6), 846-858.

(28) Maniatopoulos, C.; Sodek, J.; Melcher, A. H., Bone formation *in vitro* by stromal cells obtained from bone marrow of young adult rats. *Cell Tissue Research.* **1988,** 254, (2), 317-330.

(29) Stein, G. S.; Lian, J. B., 2 – Molecular Mechanisms Mediating Developmental and Hormone-regulated Expression of Genes in Osteoblasts: An Integrated Relationship of Cell Growth and Differentiation. In *Cellular and Molecular Biology of Bone*, Noda, M., Ed. Academic Press: San Diego, 1993; pp 47-95.

(30) Romero, M., The osteogenic response of mesenchymal stromal cells to strontium-substituted bioactive glasses. *Journal of Tissue Engineering and Regenerative Medicine* **2015**.

(31) Lian, J. B.; Stein, G. S., Development of the osteoblast phenotype: molecular mechanisms mediating osteoblast growth and differentiation. *The Iowa Orthopaedic Journal* **1995,** 15, 118-140.

(32) Malaval, L.; Liu, F.; Roche, P.; Aubin, J. E., Kinetics of osteoprogenitor proliferation and osteoblast differentiation *in vitro*. *Journal of Cellular Biochemistry* **1999,** 74, (4), 616-627.

(33) Sabokbar, A.; Millett, P. J.; Myer, B.; Rushton, N., A rapid, quantitative assay for measuring alkaline phosphatase activity in osteoblastic cells *in vitro*. *Bone and Mineral* **1994,** 27, (1), 57-67.

(34) Martins, A.; Duarte, A. R. C.; Faria, S.; Marques, A. P.; Reis, R. L.; Neves, N. M., Osteogenic induction of hBMSCs by electrospun scaffolds with dexamethasone release functionality. *Biomaterials* **2010,** 31, (22), 5875-5885.

(35) Huang, S.-C.; Wu, B.-C.; Ding, S.-J., Stem cell differentiation-induced calcium silicate cement with bacteriostatic activity. *Journal of Materials Chemistry B* **2015,** 3, (4), 570-580.

(36) Bosetti, M.; Cannas, M., The effect of bioactive glasses on bone marrow stromal cells differentiation. *Biomaterials* **2005,** 26, (18), 3873-3879.

(37) Karsenty, G., The genetic transformation of bone biology. *Genes & Development* **1999,** 13, (23), 3037-3051.

(38) Amorim, S.; Martins, A.; Neves, N. M.; Reis, R. L.; Pires, R. A., Hyaluronic acid/poly-l-lysine bilayered silica nanoparticles enhance the osteogenic differentiation of human mesenchymal stem cells. *Journal of Materials Chemistry B* **2014,** 2, (40), 6939-6946.

(39) Mizuno, M.; Kuboki, Y., Osteoblast-Related Gene Expression of Bone Marrow Cells during the Osteoblastic Differentiation Induced by Type I Collagen. *Journal of Biochemistry* **2001,** 129, (1), 133-138.

(40) Chen, Q. Z.; Xu, J. L.; Yu, L. G.; Fang, X. Y.; Khor, K. A., Spark plasma sintering of sol–gel derived 45S5 Bioglass®-ceramics: Mechanical properties and biocompatibility evaluation. *Materials Science and Engineering: C* **2012,** 32, (3), 494-502.

(41) Habibovic, P.; de Groot, K., Osteoinductive biomaterials—properties and relevance in bone repair. *Journal of Tissue Engineering and Regenerative Medicine* **2007,** 1, (1), 25-32.

(42) Fernandes, J. S.; Gentile, P.; Moorehead, R.; Crawford, A.; Miller, C. A.; Pires, R. A.; Hatton, P. V.; Reis, R. L., Design and Properties of Novel Substituted Borosilicate Bioactive Glasses and Their Glass-Ceramic Derivatives. *Cryst Growth Des* **2016**.

VI. CHAPTER

Wetspun Poly-L-(Lactic Acid)-Borosilicate Bioactive Glass Scaffolds for Guided Bone Regeneration

CHAPTER VI - WETSPUN POLY-L-(LACTIC ACID)-BOROSILICATE BIOACTIVE GLASS SCAFFOLDS FOR GUIDED BONE REGENERATION

VI. CHAPTER

Wetspun Poly-L-(Lactic Acid)-Borosilicate Bioactive Glass Scaffolds for Guided Bone Regeneration[5]

Abstract

We developed a porous Poly-L-lactic acid (PLLA) scaffold compounded with BBGs endowing it with bioactive properties. Porous PLLA-BBGs fibre mesh scaffolds were successfully prepared by the combination of wet spinning and fibre bonding techniques. μCT confirmed that the PLLA-BBG scaffolds containing ≈ 25% of BBGs (w/w) exhibited randomly interconnected pores (58 to 62% of interconnectivity and 53 to 67% of porosity) with mean pore diameters higher that 100 μm. Bioactivity and degradation studies were performed by immersing the scaffolds in SBF and ultrapure water, respectively. The PLLA-BBG scaffolds presented a faster degradation rate with a constant release of inorganic species, which are capable to produce calcium phosphate structures at the surface of the material after 7 days of immersion in SBF (Ca/P ratio of ~1.7). Cellular *in vitro* studies with SaOs-2 and hASCs showed that PLLA-BBGs are not cytotoxic to cells, while demonstrating their capacity to promote cell adhesion and proliferation. Overall, we showed that the proposed scaffolds present a tailored kinetics on the release of inorganic species and controlled biological response under conditions that mimic the bone physiological environment.

[5] This chapter is based on the following publication:

João S. Fernandes, Rui Reis, Ricardo A. Pires; Wet spun poly L (lactic acid)-Borosilicate Bioactive Glass Scaffolds for Guided Bone Regeneration; Materials Science and Engineering C 2016, (http://dx.doi.org/10.1016/j.msec.2016.10.007).

1. Introduction

Bone has a remarkable auto-regenerative capacity; however, when a large defect is generated, by accident or disease, it cannot regenerate the lost tissue by itself. At present, both autogenic and allogenic transplants have been used for bone repair, but with different limitations, namely: the autogenic strategy is restricted in supply and limited by the size of the defect; while the allogenic one may present incompatibility and a high risk of infection and of transplant rejection [1, 2]. In this context, BTE is a promising approach that provides a strategy based on the use of biodegradable porous scaffolds that serves as a support and mimics of the bone ECM, which promotes cell attachment and proliferation. The matching of the scaffolds degradation kinetics with the timeframe of the cellular regenerative processes, allows the formation of new bone while the scaffolds are degraded [3-5].

Numerous biomaterials have been developed based on natural and synthetic biodegradable polymers or bioactive ceramics [6-12]. Synthetic materials present limited variability allowing the optimisation of the scaffold's properties (e.g. porosity and degradation) to promote cell adhesion and proliferation, as well as the capacity to induce the formation of new bone. PLLA is one of such polymers: it is biodegradable and has been accepted in different medical devices by the US Federal FDA, which makes it highly attractive for biomedical applications. Furthermore, PLLA is a biocompatible material, which can be manufactured through various techniques [13-17]. On the other hand, inorganic materials, e.g. silicate-based BG, HA and tricalcium phosphates, have been widely studied due to their reported bioactivity, osteoconductivity, and ability to directly bond to bone; as well as improving cell adhesion, proliferation and differentiation [18-22]. Moreover, some inorganic materials (e.g. composed by Si, B, Sr, Ca, Mg or Zn) are reported to have a part in bone metabolism, osteo- and angiogenesis, cell proliferation, as well as, presenting antibacterial properties [18, 23-26].

Hitherto no single material have all the essential attributes required for an ideal scaffold for BTE. Therefore, there is a rising interest in 3D scaffolds that can combine the bioresorbability of the polymer with the bioactivity of glass/ceramic phases, resulting in a material that combines all the properties that were previously described. Herein we propose a composite system of PLLA-borosilicate bioactive glass (PLLA-BBG) that

provides a structural support for cellular attachment and proliferation, leading to the engineering of bone tissue that combine its chemical, biochemical and biological properties. PLLA as a slow degradation rate that makes it a more suitable material for bone regeneration, in which the healing times are longer. Moreover, it degrades into lactic acid, which can be subsequently secreted as carbon dioxide by entering the Krebs cycle. While, the composite fillers (i.e. BBGs) might be able to improve its mechanical properties, they can control the acidity of the surrounding tissue (generated by the inflammatory process that precedes tissue regeneration) during its degradation. The release of glass modifier cations from the BBGs, can be used by the surrounding cellular environment to produce a phosphated mineral phase, which is essential to create a strong interfacial adhesion between the scaffold and bone [5].

Wet spinning methodology allows the fabrication of complex 3D structures with controlled properties such as, porosity, pore structure and interconnectivity, influencing: cell adhesion, proliferation and vascularisation through the scaffold [27, 28]. In wet spinning, the polymer dissolved in a suitable solvent is extruded into a liquid that is miscible with the spinning solvent but a non-solvent of the polymer. This results in to solvent removal and fibres precipitation. Unlike electrospinning, wet spinning is able to create macro to micro-scale fibres allowing cell penetration through the scaffold for bone regeneration and vascularisation. The required pore size might differ between cell types [29], however, numerous studies support that the optimal pore size for regeneration and mineralisation of bone ranges from 100 to 300 μm [30, 31]. Recent studies of the effect of porosity on the ingrowth of MC3T3-E1 pre-osteoblastic cells into 3D scaffolds reported a suitable cellular response within this range [32].

In this context, we compounded PLLA-BBG into fibrous scaffolds (25% w/w of BBGs), where the BBGs were formulated with different divalent modifier cations (i.e. Ca^{2+}, Mg^{2+} and Sr^{2+}), and tested them for their biodegradability, bioactivity and biological response using Saos-2 and hASCs.

2. Materials and Methods

2.1. Materials

All chemicals used for the glass synthesis were reagent grade: boron oxide (Alfa Aesar, Germany), calcium carbonate (Sigma-Aldrich, Portugal), sodium bicarbonate (Sigma-Aldrich, Australia), silica gel 60M (Macherey-Nagel, Germany), magnesium oxide (Sigma-Aldrich, Portugal) and strontium carbonate (Sigma-Aldrich, Australia). PLLA (with a L-lactide content of 99.6% and an average M_w of 69 000 $g.mol^{-1}$, from Cargill Dow LLC, USA) was used to produce the desired fibre meshes. BBGs were produced by mixing appropriate amounts of SiO_2, B_2O_3, $NaHCO_3$, and $CaCO_3$, or MgO, or $SrCO_3$ on an agate mortar with ethanol. Upon drying, the mixture was heated to 1450 ºC on air for 1 h. Afterwards, the melt was quickly poured into a water bath maintained at 4 ºC to form a glass frit. The glasses, of general formula $0.05Na_2O \cdot x$MgO $\cdot y$CaO $\cdot$ (0.35-x-y)SrO $\cdot$ $0.20B_2O_3 \cdot 0.40SiO_2$ (molar ratio, where x, y = 0.35 or 0.00, and $x \neq y$), were ground in an Agate mortar (RETSCH, Germany) to obtain microparticles and, afterwards, sieved to a size smaller than 63 μm. The density of the BBGs was measured using a Multi pycnometer (Quantachrome Instruments, USA) with helium at 110 °C using ≈ 5 g of each sample.

2.2. Preparation of wet spun fibre mesh scaffolds

PLLA-BBG fibres were fabricated through the wet spinning of a PLLA solution containing a homogeneous suspension of BBG particles. These fibres were transformed into circular shape fibre mesh scaffolds by fibre bonding. Three different PLLA-BBG scaffolds were fabricated (PLLA-BBG-Mg, PLLA-BBG-Ca and PLLA-BBG-Sr) using three different BBGs (BBG-Mg, BBG-Ca and BBG-Sr, that present, respectively, Mg, Ca and Sr as divalent modifier cations). Unfilled PLLA scaffolds were used as control.

2.2.1. Wet spinning

After preparing a PLLA solution in chloroform (30% w/v), BBGs (25% BBG/PLLA w/w) were added under constant stirring to avoid the agglomeration of BBG particles. Subsequently, the PLLA-BBG solution was wet spun thought a syringe equipped with a 25 G needle with the tip cut horizontally and perpendicular to the flow. The fibres were extruded at a rate of 15 $ml \cdot h^{-1}$ into a coagulation bath of methanol. Finally, fibres were collected and dried overnight on the fume hood at RT.

2.2.2. Fibre Bonding

To fabricate the PLLA-BBG fibre mesh scaffolds, fibres (≈ 80 mg) were first pre-moulded into a 20 mm diameter metal mould and bonded at 147 °C under a pressure of 1.56 kPa for 6 min. The fibre bonding temperature was optimised with the help of DSC analysis of PLLA (T_g of 56.7 °C and a T_m of 165.4 °C). Finally, a 6 mm puncture was used to obtain specimens of 6 mm diameter and 0.5 mm height.

2.3 *In vitro* characterisation of wet-spun fibre mesh scaffolds

2.3.1. Differential scanning calorimetry (DSC) analysis

The glass transition (T_g) and melting (T_m) temperatures of the PLLA were determined by DSC (TA Instrument Q100 calorimeter, USA), using a double run between -40 to 200 °C (first run to determine T_g and to remove thermal history, and second run to determine T_m), at a heating and cooling rates of 10 $°C \cdot min^{-1}$ under nitrogen atmosphere, using ~8 mg of sample.

2.3.2. Scanning electron microscopy (SEM)

SEM/EDS (Leica Cambridge, UK) was used to assess the surface morphology of the PLLA-BBG scaffolds, as well as to monitor the deposition of calcium phosphate structures on the surface of the fibres after 7 and 14 days of immersion in SBF [33]. All the

PLLA-BBG scaffolds were sputter-coated (Fisons Instruments SC502, UK) with gold before the analysis. All the micrographs were acquired using a beam energy of 5.0 kV and a working distance (WD) of ≈5.2 mm.

2.3.3. X-ray diffraction analysis (XRD)

The PLLA-BBG scaffolds were analysed before and after 7 and 14 days of immersion in SBF by XRD (Bruker D8 Discover, Germany), using Cu radiation at a wavelength of 1.5406 Å at a voltage of 40 kV and a current of 40 mA, with a step size of 0.02 ° in a 2θ range between 5 ° and 50 ° and a scanning speed of 1 $s \cdot step^{-1}$. The crystalline patterns were identified by comparison with the data listed in the JCPDS.

2.3.4. Micro-computed tomography (μCT)

Three samples from each PLLA-BBG and PLLA scaffolds were analysed by μCT using a high-resolution μ-CT scanner (Skyscan 1072, Kontich, Belgium), a pixel size of 6 μm and integration time of 1.7 ms. The X-ray source was set at a voltage of 43 kV and a current of 234 μA of current. Approximately 400 projections were acquired over a rotation range of 180°, with a rotation step of 0.45°. Data sets were reconstructed using standardised cone-beam reconstruction software (NRecon v1.4.3, SkyScan). The output format for each sample was 400 serial 1024 × 1024 bitmap images. Representative data sets were segmented into binary images using a dynamic threshold of 40-150 for the polymer (blue images, Figure VI.2) and 150-255 for BBGs (red images, Figure VI.2). These representative data sets were used for morphometric 3D analysis (CT Analyser, v1.5.1.5, SkyScan) and to build 3D models (ANT 3D creator, v2.4, SkyScan). The morphometric analysis included porosity, mean wall thickness, mean pore diameter and pore interconnectivity. 3D virtual models of representative regions in the bulk of the scaffolds were created, visualised, and registered using image processing software (CT Analyser and ANT 3D creator).

2.3.5. Bioactivity assay

SBF was prepared in accordance with the procedure of Kokubo *et al.* [33]. Triplicate samples of the PLLA-BBG scaffolds, were immersed in SBF at a ratio of 10:10 [PLLA-BBG scaffolds (mg): SBF (ml)] and incubated for 7 and 14 days in an oven maintained at 37 °C. After each time point the samples of PLLA-BBG scaffold were collected and dried at 37 ºC in order to obtain the XRD patterns and SEM micrographs. Each immersion solution was filtered and analysed by inductive coupled plasma (ICP, Horiba, Japan) to determine the corresponding Ca and P concentrations present in the solution at each time point. The ICP absorption was measure at specific wavelengths (λ= 393.366 nm for Ca; λ=213.62 nm for P) and the Ca and P concentrations were determined using calibration curves previously obtained with standard solutions (Alfa Aesar).

2.3.6. Degradation assay

The PLLA-BBG scaffolds (n=3 per time point) were immersed in ultrapure water at a ratio of 10:10 [PLLA-BBG scaffolds (mg): water (ml)] for 7, 14, 21, 28, 60 and 90 days in a water-shaking bath at 60 rpm and 37°C. Each immersion solution was filtered and their respective pH was measured. ICP analysis was performed to determine the Si, B, Ca, Mg and Sr concentrations in the immersion solutions. The absorption was measure at specific wavelengths (λ= 251.611 nm for Si, λ= 249.773 nm for B, λ= 393.366 nm for Ca, λ= 407.771 nm for Sr and λ= 279.553 nm for Mg) and their concentrations were determined using calibration curves previously obtained with standard solutions (Alfa Aesar, Portugal).

The PLLA-BBG scaffolds were removed from the immersion solution, the excess surface water was removed, and the samples were immediately weighed. Afterwards, the samples were dried in the oven at 37 °C, to constant weight, recording the final mass of each specimen. The water uptake (WU) was calculated according to Eq. (1):

$$WU(\%) = \left(m_{tp} - m_f\right)/m_f \times 100 \qquad \text{Eq. (1)}$$

Where m_{tp} is the wet mass of the specimen at the specific time (days), and m_f is the final mass after immersion and drying. The weight loss (WL) was calculated according to Eq. (2):

$$WL(\%) = \left(m_f - m_i\right)/m_i \times 100 \quad \text{Eq. (2)}$$

Where m_f is the mass of the dried specimen after its immersion in water, and m_i is the mass of the dried specimen before immersion in water.

TGA was used to determine the amount of BBGs incorporated in the PLLA-BBGs composites and to monitor changes in the weight (mass) of the inorganic BBGs present in the scaffolds as a function of degradation process. TGA thermograms were obtained using a TGA Q500 series (TA Instruments, USA). Experiments were performed in platinum pans, at a heating rate of 40 °C·min^{-1} from 50 °C to 700 °C under oxygen atmosphere.

2.4. Cytotoxicity evaluation

The cytotoxicity assessment was performed by culturing SaOs-2 cells in the presence of the PLLA-BBG scaffolds. Cells were expanded in DMEM (Sigma, USA) supplemented with 10% heat-inactivated foetal bovine serum (FBS, Alfagene, USA) and 1% antibiotic/antimycotic solution (100 U·ml^{-1} penicillin and 100 µg·ml^{-1} streptomycin; Alfagene, USA). Cells were cultured at 37 °C in an atmosphere of 5% CO_2. Confluent SaOs-2 cells between passages 13 and 17 were harvested and seeded onto the bottom of 24-well plates at a density of 2×10^4 cells/well before put in contact with scaffolds. The SaOs-2 cells cultured in the presence of PLLA and absence of glass particles were used as negative control and latex (6 mm discs) were used as positive control. The metabolic activity and cellular proliferation of the Saos-2 cells were monitored at 1, 3 and 7 days by MTS (Promega, UK) and PicoGreen® (Quant-iT™ PicoGreen® dsDNA Assay Kit – Invitrogen, USA), respectively, following the supplier's instructions.

2.5. Cell adhesion experiments

The cell adhesion study was performed with hASCs. The hASCs cells were isolated from human subcutaneous adipose tissue samples obtained from lipoaspiration procedures performed on women with ages between 35 and 50 years old (under a protocol previously established with the Department of Plastic Surgery of Hospital da Prelada in Porto, Portugal) and frozen at -80 °C. The cells were grown in a culture medium consisting of αMEM, 10% FBS and 1% of antibiotic-antimycotic mixture. When an adequate cell number was obtained (passage 3), cells were detached with trypsin/EDTA and seeded at a density of 3×10^4 cells onto the surface of each scaffold. After 24 h of cell attachment, cell-constructs were placed in new 24-well plates and 1 ml of basal medium was added to each well. The basal culture medium consisted of αMEM (Gibco, UK) supplemented with 10% FBS and 1% antibiotic/antimycotic solution (final concentration of penicillin 100 units·ml^{-1} and streptomycin 100 mg·ml^{-1}). The cell-constructs were cultured for 7 and 21 days in a humidified atmosphere at 37 °C, containing 5% CO_2. The culture medium was changed every 2–3 days until the end of the experiment. The metabolic activity and cellular proliferation were monitored at 7 and 21 days by MTS (Promega, UK) and PicoGreen® (Quant-iT™ PicoGreen® dsDNA Assay Kit – Invitrogen, USA), respectively, following the supplier's instructions. Cell morphology was also evaluated at 7 and 21 days; cells were washed twice with phosphate buffer saline (PBS) and then fixed with Formalin for 15 min at RT. Prior to the analysis by SEM (Leica Cambridge S360, UK) equipped with an EDS; link-eXL-II, the samples were sputter coated (Fisons Instruments SC502, UK) with gold or carbon.

3. Results and Discussion

Silicate-based BG particles have been reported to improve the bioactive performance of scaffolds for tissue engineering [34, 35], as well as, stimulating the proliferation and differentiation of cells [4, 18]. Herein, we evaluated the impact of borosilicate-based glasses (presenting different divalent modifier cations, i.e. Mg^{2+}, Ca^{2+} and Sr^{2+}) on the degradation and bioactivity of wet-spun PLLA-BBG composites, as well as, their cytotoxicity towards SaOs-2 and hASCs and the adhesion and proliferation of hASCs cultured onto the scaffolds.

3.1. Characterisation of wet-spun fibre mesh scaffolds

PLLA-BBG fibres were produced using a solution of PLLA in chloroform to which the synthesised BBGs (<63 μm and density of ~2.8 $g.cm^{-3}$) were suspended. Upon injection of this suspension into a methanolic coagulation bath the fibres were dried and moulded by fibre bonding. Scaffold specimens were prepared as 6 mm diameter discs (using a puncture), sterilised (88% CO_2 and 12% ethylene oxide at 45 °C with 180 kPa and 55% of humidity for 10 h) and preserved in a desiccator. Figure VI.1 presents the SEM images and XRD patterns of the PLLA-BBG scaffolds.

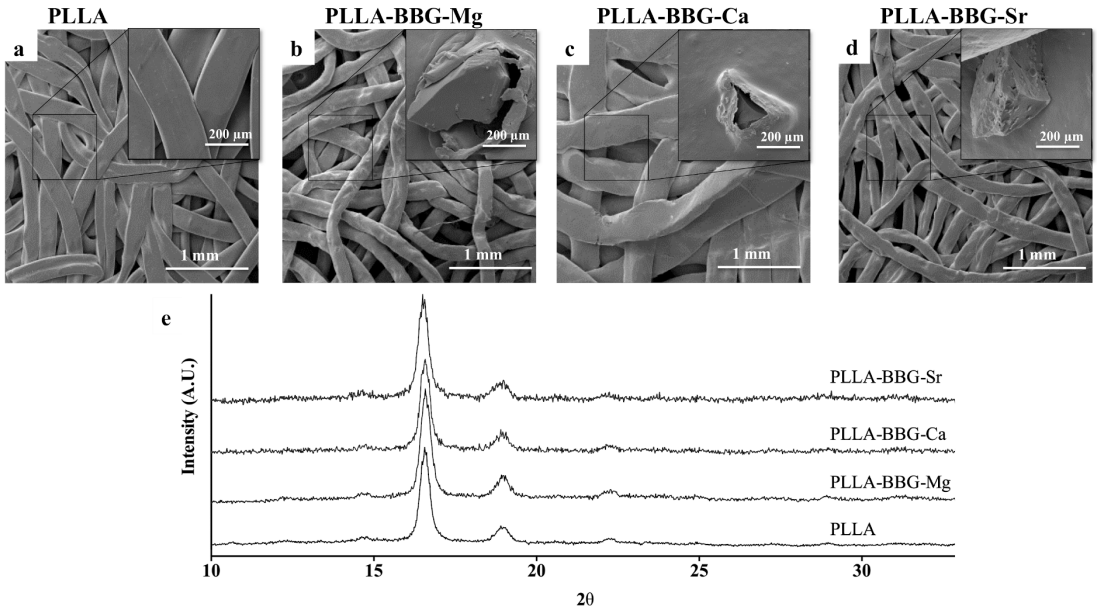

Figure VI.1 - SEM micrographs with insets of BBG particles incorporated into the fibres (a, b, c and d) and XRD patterns (e) of PLLA and PLLA-BBG scaffolds (PLLA-BBG-Mg, PLLA-BBG-Ca and PLLA-BBG-Sr).

The XRD patterns of the scaffolds exhibited the characteristic peaks of PLLA at 2θ = 12.5 °, 14.7 °, 16.6 °, 19.1° and 22.3°, while there are no detectable peaks of BBGs due to their amorphous state and low concentration at the scaffold surface [36].

The morphological analysis of the PLLA and PLLA-BBGs scaffolds was executed by μ-CT (Figure VI.2). We observed the typical fibre mesh structure with random porous distribution, which are vital for cell ingrowth [27, 37], as well as a homogenous dispersion of

BBGs all over the scaffolds. From the mathematical analysis of the data (performed by the CTAn software, Table VI.1) it is possible to determine the porosity, interconnectivity and thickness of the scaffolds. These properties were unchanged with the incorporation of BBGs. The whole set of scaffolds presented porosities ranging from 53 to 67% and interconnectivity between 58 and 62%. It is also relevant to point out that the mean pore diameters are >100 µm, within the range of optimal pore size for cell penetration, regeneration and mineralisation of bone [27, 38]. Therefore, combining wet spinning and fibre bonding we were able to prepare PLLA-BBGs scaffolds with morphological characteristics appropriate for cell colonisation.

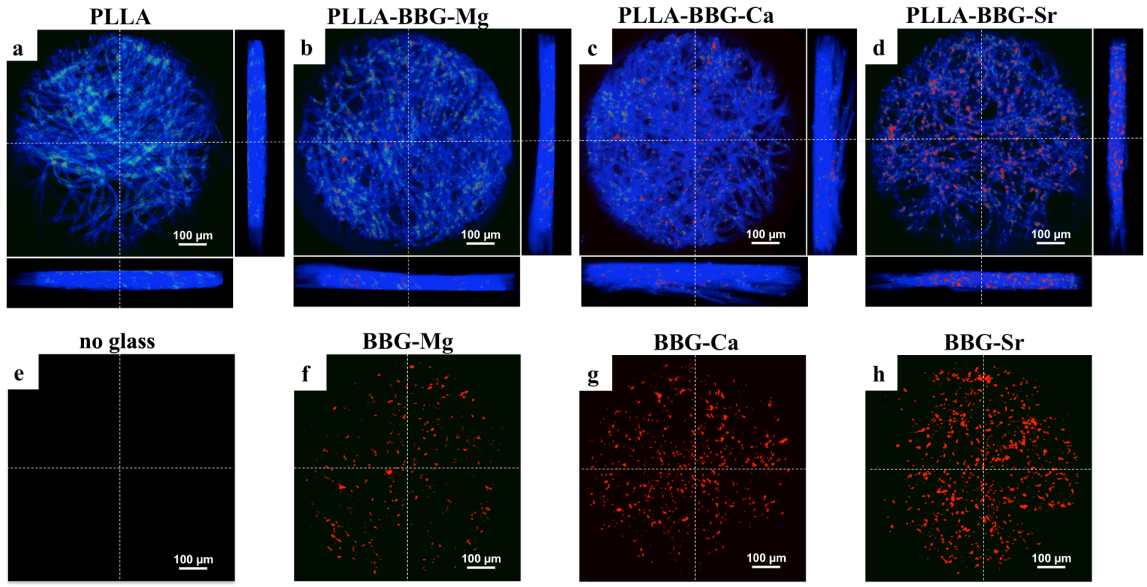

Figure VI.2 - Representative µCT cross-sections of the PLLA and PLLA-BBGs scaffolds. The upper images combine the PLLA fibres (blue) and the distribution of the BBGs (red), while the bottom images represent only the distribution of BBG particles (red) within the scaffold.

Table VI.1 - Porosity, mean pore diameter and interconnectivity of the scaffolds determined by μCT

Samples	Porosity (%)*	Mean pore diameter (μm)*	Interconnectivity (%)*
PLLA	64.57 ± 7	117.41 ± 7	57.53 ± 4
PLLA-BBG-Mg	53.39 ± 2	148.77 ± 6	57.80 ± 5
PLLA-BBG-Ca	66.75 ± 2	111.65 ± 6	61.55 ± 6
PLLA-BBG-Sr	63.53 ± 5	126.17 ± 6	58.91 ± 3

* No statistically significant differences were detected.

3.2. *In vitro* degradation and bioactivity

The WL and WU are strongly correlated with the water stability and biodegradability of the scaffolds. They are extremely relevant properties to determine their expected lifetime under the physiological environment [39]. The WL (Figure VI.3a) data shows a faster degradation rate for the PLLA-BBGs compared to PLLA over 30 days of immersion in ultrapure water (e.g. at day 30, the PLLA-BBGs' WL is ~15% higher than the PLLA's WL). This data clearly suggests that the addition of BBG particles to the scaffolds augments its biodegradability, reflected in the increase of the WL of the composites [6, 40].

In the case of the WU (Figure VI.3b), while the PLLA scaffolds uptake a constant amount of water throughout the tested time period (i.e. ~15%), the PLLA-BBGs scaffolds present a WU peak at day 7 (similar to the PLLA WU) followed by a subsequent reduction over the immersion time. This latter reduction is probably associated with the increase of the local concentrations of inorganic species leached from the glass that, subsequently, at the latter time point, deposit in the surface of the glass particles, limiting the exchange of water between the immersion solution and the inorganic portion of the composites.

The release profile of inorganic species (Figure VI.3c, data obtained by ICP) showed a continuous release of B, Si, Ca/Sr/Mg–related species over the tested timeframe. This was

accompanied with an increase of the solution pH (from ≈6 to ≈9.6 over 30 days), which might be critical to balance the pH decrease generated by the inflammatory process that precedes tissue regeneration of the implanted scaffold. There was a higher release rate in the case of PLLA-BBG-Mg scaffolds, which can be related with the relatively smaller size of Mg^{2+} (when compared with Ca^{2+} and Sr^{2+}) that enhance its diffusion from the glass particles to the surrounding medium. This was also confirmed by TGA where we detected a larger reduction of the glass percentage in the composites containing BBG-Mg after 30 days of immersion (from ~24% to ~18%).

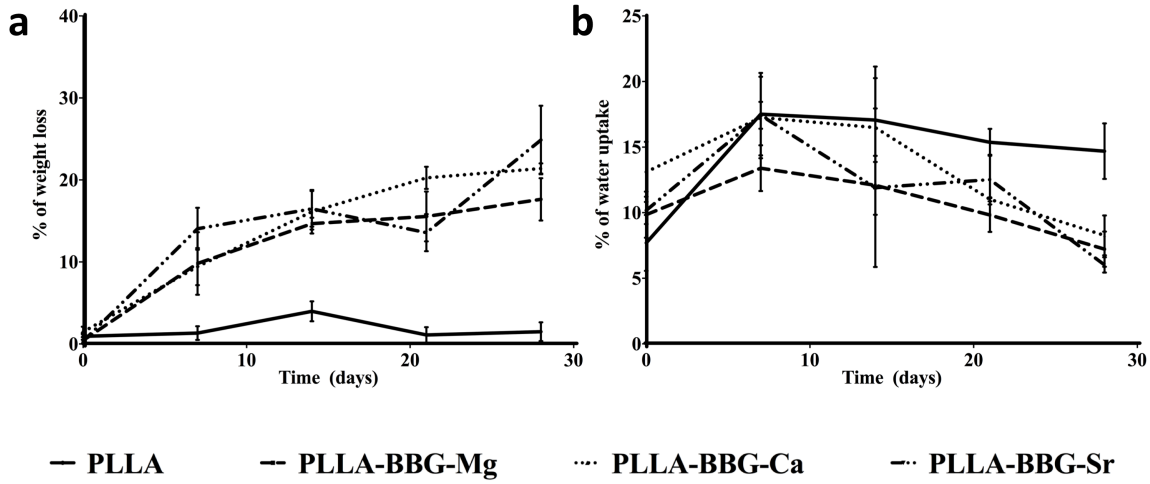

c

PLLA-BBG-Mg	Concentration (μM)		
Time (days)	Mg	Si	B
0	9	5	8
7	168	96	190
14	227	70	244
21	284	121	345
30	357	194	439

PLLA-BBG-Ca	Concentration (μM)		
Time (days)	Ca	Si	B
0	4	6	3
7	31	26	34
14	43	28	60
21	64	36	94
30	72	44	113

PLLA-BBG-Sr	Concentration (μM)		
Time (days)	Sr	Si	B
0	8	8	5
7	48	39	35
14	64	42	60
21	99	30	92
30	105	60	95

Figure VI.3 - WL (a), WU (b) and release profile of chemical species (c) of the PLLA and PLLA-BBG scaffolds over 30 day of immersion in ultrapure water at 37 ºC.

Typically, a bioactive material should promote the formation of a calcium phosphate layer on its surface upon immersion in SBF [41]. In Figure VI.4 we present the SEM images and the XRD patterns of the PLLA and PLLA-BBGs after immersion in SBF for 0, 7 and 14 days. The SEM images clearly demonstrate the deposition of an apatite-like layer in the surface of the composites, namely close to the glass particles, after 7 and 14 days of immersion in SBF. These layers present a cauliflower morphology, which is the characteristic shape of HA [42, 43]. Furthermore, the EDS analysis executed on the regions where the inorganic deposits were observed indicate Ca/P ratios of ~1.5 for day 7 and ~1.7 for day 14, which is close to the typical apatite Ca/P ratio of 1.67 [44]. In addition, the

ICP quantification of the Ca and P present in the SBF as a function of time corroborates this findings, revealing a fast deposition of phosphates onto the surface of the PLLA-BBG scaffolds which might be related with the initial formation of ACPs and, afterwards, to their evolution to a crystalline phase [45]. Nevertheless, in the case of the PLLA scaffolds (Figure VI.4a, used as controls), the SEM micrographs do not show any deposition of inorganic layers at the surface of the scaffolds.

The XRD patterns of the PLLA-BBG scaffolds after 7 and 14 days of immersion in SBF presented characteristic peaks of crystalline phosphate structures (2θ = 28.9 º and 2θ = 25.8 º), while there are no peaks observed for the PLLA scaffolds [46, 47]. The peak 2θ = 28.9 º, which appeared in all PLLA-BBG scaffolds (Figure VI.4b, 4c and 4d), is commonly attributed to HA structures [47]. To emphasise, PLLA-BBG-Ca scaffolds (Figure VI.4c) presented a ~5 times higher peak (2θ = 28.9 º) at day 14 of immersion comparing with other two scaffolds, PLLA-BBG-Mg and PLLA-BBG-Sr (Figure VI.4c in relation to Figure VI.4b and Figure VI.4d, respectively). This observation is indicates that the higher concentration of Ca^{2+} cations (from the SBF and leached from the BBG-Ca glass particles) promotes an increase on the formation of calcium phosphate crystalline structures on the surface of the scaffolds. The peak at 2θ = 28.9 º can also be attributed to tricalcium phosphate (i.e. $Ca_3(PO_4)_2$).[48] Regarding the PLLA-BBG-Mg scaffolds, the same peak (2θ = 28.9 º) is found, but with lower intensity, which can be also related with the formation of magnesium phosphate crystalline structures (i.e. $Mg_3(PO_4)_2$) [49]. The peaks at 2θ = 25.4 º and 2θ = 28.9 º are also present in the PLLA-BBG-Sr XRD pattern, however, they are with lower intensity than the ones recorded for the PLLA-BBG-Ca (Figure VI.4d and 4c, respectively). These two peaks are commonly associated with the formation of apatite structures [47, 50]. In the specific case of the peak at 2θ = 25.4 º, it is usually associated with apatite structures where calcium is substituted by strontium [46]. The lower intensity of the peaks may be due to the fact that the Sr^{2+} cations affect the adsorption of Ca^{2+} in the initial stages of apatite formation [51]. Those two peaks are also found in the strontium phosphate crystalline phases, such as $SrHPO_4$ [52]. Overall, the XRD data is consistent with the deposition of Ca/Mg/Sr phosphates on the surface of the PLLA-BBGs scaffolds, that subsequently evolve to form different crystalline phases until it forms an HA-like surface layer with their characteristic cauliflower morphology.

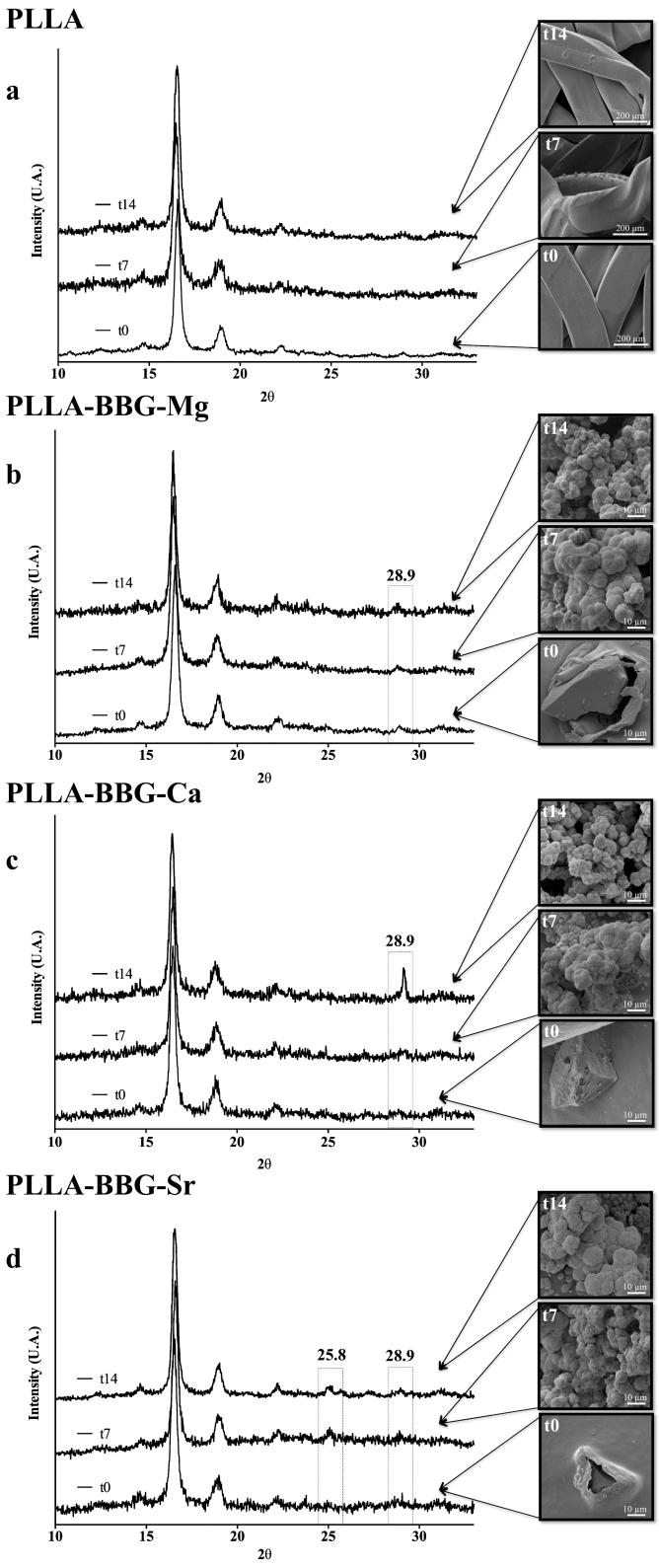

Figure VI.4 - XRD patterns and SEM micrographs of (a) PLLA, (b) PLLA-BBG-Mg, (c) PLLA-BBG-Ca, and (d) PLLA-BBG-Sr, after 7 and 14 days of immersion in SBF at 37 ºC.

3.3. *In vitro* cytotoxicity

The PLLA and PLLA-BBGs scaffolds were tested for their *in vitro* cytotoxicity. To this purpose, we evaluated the metabolic activity and cell proliferation of SaOs-2 cells cultured in direct contact with the scaffolds for 7 days (Figure VI.5a). Under these experimental conditions, neither PLLA nor PLLA-BBG scaffolds induced a significant reduction of the cellular metabolic activity. DNA quantification (Figure VI.5b) presents a similar profile, indicating that a similar amount of DNA was detected when the cells were in contact with PLLA and PLLA-BBG scaffolds. In conjunction the metabolic activity and DNA quantification data revealed that the presence of the BBGs particles did not induce any significant differences in cell proliferation, demonstrating that the incorporation of BBGs did not elicit any cytotoxic effects.

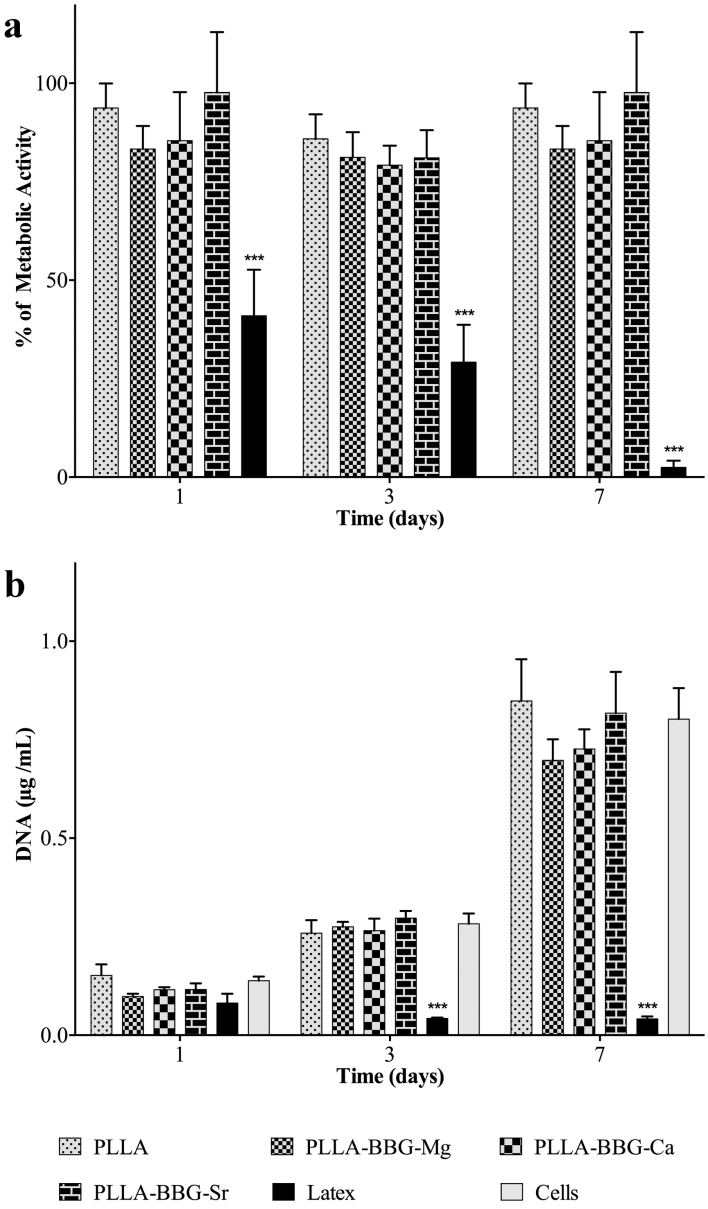

Figure VI.5 - MTS (a) and DNA (b) quantification data of SaOs-2 cells cultured in direct contact with PLLA and PLLA-BBG scaffolds during 1, 3 and 7 days. Latex discs were used as positive control and standard culture medium was used as negative control. The data was obtained from at least 3 independent experiments and is expressed as mean ± SD. The data was analysed by non-parametric statistics: Kruskal-Wallis test (p<0.001), followed by a Dunn's multiple comparison test. ***Extremely significant (p<0.001); **Very significant (0.001<p<0.01); *Significant (0.01<p<0.05).

3.4. Cell adhesion assay

The hASCs are widely studied for BTE due to their high abundance in fat tissue, ease to harvest and proliferate and, specially, because they present a high percentage of their population with an osteogenic potential [53, 54]. The cell adhesion assay was used to evaluate the suitability of the PLLA-BBG scaffolds for guided bone regeneration. hASCs were directly seeded on the top of the scaffolds (PLLA and PLLA-BBGs) and their morphology and ability to proliferate were assessed by SEM (Figure VI.6a through 6h), MTS and DNA quantification (Figure VI.6i and 6j, respectively).

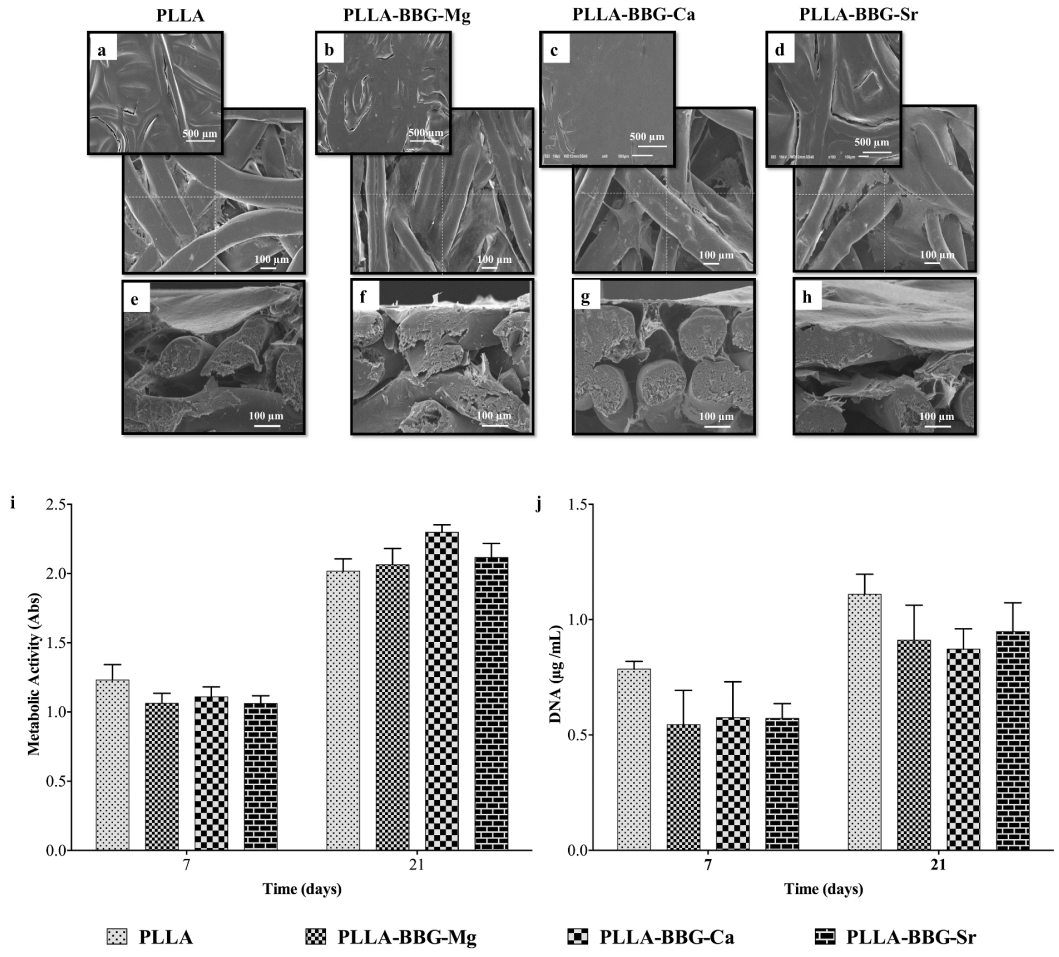

Figure VI.6 - Adhesion and proliferation study of the hASCs cultured on PLLA and PLLA-BBG scaffolds analysed by SEM after 21 days of cell culture: (a) PLLA, (b) PLLA-BBG-Mg, (c) PLLA-BBG-Ca and (d) PLLA-BBG-Sr. Cross-sections of (e) PLLA, (f) PLLA-BBG-Mg, (g) PLLA-BBG-Ca and (h) PLLA-BBG-Sr scaffolds are presented to

evaluate the capacity of the hASCs to colonise the interior of the scaffolds. Red dashed circles show cell that are driving from the top layer to the interior of the scaffolds. (i) MTS and (j) DNA quantification executed after 7 and 21 days of hASC cell culture. Standard culture medium was used as negative control. The metabolic activity and cell proliferation data is expressed as mean ± SD. The data was analysed by non-parametric statistics: Kruskal-Wallis test ($p<0.001$), followed by a Dunn's multiple comparison test. ***Extremely significant ($p<0.001$); **Very significant ($0.001<p<0.01$); *Significant ($0.01<p<0.05$).

The SEM micrographs show that cells were able to attach and spread on the surface of all the scaffolds, as well as to penetrate through their pores (Please see red dashed circles, Figure VI.6e through 6h). MTS and DNA quantification data showed no significant differences between the PLLA/PLLA-BBGs scaffolds and the control experiment. It is also relevant to emphasise that, after 21 days of cell culture a complete monolayer of cells were attached to the outer surface of the scaffolds in all the cases. However, this phenomenon was more pronounced for the PLLA-BBGs scaffolds, in particular for the composite that was formulated with the BBG-Ca microparticles, i.e. PLLA-BBG-Ca (Figure VI.6c). In combination with the bioactivity analysis (where the PLLA-BBG-Ca scaffold presented a higher deposition of calcium phosphate crystalline phases), the biological evaluation data supports the suitability of this composition to generate a 3D porous structure that is able to promote cell attachment, proliferation and colonisation of the bulk of the scaffold [54]. The great biodegradable and bioactive properties of PLLA-BBG composite scaffolds combined with their suitability for cell colonisation support that PLLA-BBG composite scaffolds can be used to achieve medical-grade material for development of BTE medical devices. Other *in vivo* mechanical and biocompatibility studies will be done in the near future.

4. Conclusions

PLLA-BBG scaffolds were successfully prepared through the incorporation of 25% (w/w) of BBGs (with different divalent glass modifier cations, i.e. Mg^{2+}, Ca^{2+} and Sr^{2+}) into the PLLA matrix. The μCT analysis demonstrated that our procedure generated 3D scaffolds with an interconnected structured with a high degree of porosity (58 to 62% of interconnectivity and 53 to 67% of porosity) and a mean pore diameter >100 μm - suitable for cell colonisation of the bulk of the scaffolds. Degradation studies confirmed that the incorporation of BBG particles enhance the degradability of the composites with a constant release of inorganic species to the surrounding media. Bioactivity studies demonstrated that PLLA-BBG scaffolds are capable to produce a calcium phosphate-rich surface layer (PLLA-BBG-Ca and PLLA-BBG-Sr) after 7 days of culture (Ca/P ratio ~1.7). *In vitro* cell studies revealed that the proposed PLLA-BBG scaffolds do not elicit any cytotoxicity over 7 days of culture, while hASC's were able to adhere and proliferate throughout the surface and inner sections of the porous scaffolds, being suitable candidates for BTE.

References

(1) Juhasz, J.; Best, S., Bioactive ceramics: processing, structures and properties. *Journal of Materials Science* **2012,** 47, (2), 610-624.

(2) Giannoudis, P. V.; Dinopoulos, H.; Tsiridis, E., Bone substitutes: An update. *Injury* **2005,** 36, (3, Supplement), S20-S27.

(3) Fu, Q.; Saiz, E.; Rahaman, M. N.; Tomsia, A. P., Bioactive glass scaffolds for bone tissue engineering: state of the art and future perspectives. *Materials Science and Engineering: C* **2011,** 31, (7), 1245-1256.

(4) Gantar, A.; da Silva, L. P.; Oliveira, J. M.; Marques, A. P.; Correlo, V. M.; Novak, S.; Reis, R. L., Nanoparticulate bioactive-glass-reinforced gellan-gum hydrogels for bone-tissue engineering. *Materials Science and Engineering: C* **2014,** 43, (0), 27-36.

(5) Rezwan, K.; Chen, Q. Z.; Blaker, J. J.; Boccaccini, A. R., Biodegradable and bioactive porous polymer/inorganic composite scaffolds for bone tissue engineering. *Biomaterials* **2006,** 27, (18), 3413-3431.

(6) Mota, J.; Yu, N.; Caridade, S. G.; Luz, G. M.; Gomes, M. E.; Reis, R. L.; Jansen, J. A.; Walboomers, X. F.; Mano, J. F., Chitosan/bioactive glass nanoparticle composite membranes for periodontal regeneration. *Acta Biomaterialia* **2012,** 8, (11), 4173-4180.

(7) Li, Y.; Wu, Z.-g.; Li, X.-k.; Guo, Z.; Wu, S.-h.; Zhang, Y.-q.; Shi, L.; Teoh, S.-h.; Liu, Y.-c.; Zhang, Z.-y., A polycaprolactone-tricalcium phosphate composite scaffold as an autograft-free spinal fusion cage in a sheep model. *Biomaterials* **2014,** 35, (22), 5647-5659.

(8) Hoppe, A.; Boccaccini, A. R., 7 - Bioactive glass foams for tissue engineering applications. In *Biomedical Foams for Tissue Engineering Applications*, Netti, P. A., Ed. Woodhead Publishing: 2014; pp 191-212.

(9) Boesel, L. F.; Azevedo, H. S.; Reis, R. L., Incorporation of α-Amylase Enzyme and a Bioactive Filler into Hydrophilic, Partially Degradable, and Bioactive Cements (HDBCs) as a New Approach To Tailor Simultaneously Their Degradation and Bioactive Behavior. *Biomacromolecules* **2006,** 7, (9), 2600-2609.

(10) Barros, A. A. A.; Alves, A.; Nunes, C.; Coimbra, M. A.; Pires, R. A.; Reis, R. L., Carboxymethylation of ulvan and chitosan and their use as polymeric components of bone cements. *Acta Biomaterialia* **2013,** 9, (11), 9086-9097.

(11) Gomes, F. O.; Pires, R. A.; Reis, R. L., Aluminum-free glass-ionomer bone cements with enhanced bioactivity and biodegradability. *Materials Science and Engineering: C* **2013,** 33, (3), 1361-1370.

(12) Amorim, S.; Martins, A.; Neves, N. M.; Reis, R. L.; Pires, R. A., Hyaluronic acid/poly-l-lysine bilayered silica nanoparticles enhance the osteogenic differentiation of human mesenchymal stem cells. *Journal of Materials Chemistry B* **2014,** 2, (40), 6939-6946.

(13) Madhavan Nampoothiri, K.; Nair, N. R.; John, R. P., An overview of the recent developments in polylactide (PLA) research. *Bioresource Technology* **2010,** 101, (22), 8493-8501.

(14) Liang, H.-Q.; Wu, Q.-Y.; Wan, L.-S.; Huang, X.-J.; Xu, Z.-K., Polar polymer membranes via thermally induced phase separation using a universal crystallizable diluent. *Journal of Membrane Science* **2013,** 446, (0), 482-491.

(15) Martins, M.; Craveiro, R.; Paiva, A.; Duarte, A. R. C.; Reis, R. L., Supercritical fluid processing of natural based polymers doped with ionic liquids. *Chemical Engineering Journal* **2014,** 241, (0), 122-130.

(16) Mikos, A. G.; Bao, Y.; Cima, L. G.; Ingber, D. E.; Vacanti, J. P.; Langer, R., Preparation of poly(glycolic acid) bonded fiber structures for cell attachment and transplantation. *Journal of Biomedical Materials Research* **1993,** 27, (2), 183-189.

(17) Veysi, M.; Daniel, G.-P.; Tyler, N.; John, J. L.; Derek, J. H., Controlled neuronal cell patterning and guided neurite growth on micropatterned nanofiber platforms. *Journal of Micromechanics and Microengineering* **2015,** 25, (12), 125001.

(18) Hoppe, A.; Güldal, N. S.; Boccaccini, A. R., A review of the biological response to ionic dissolution products from bioactive glasses and glass-ceramics. *Biomaterials* **2011,** 32, (11), 2757-2774.

(19) Chakraborty, J.; Sengupta, S.; Ray, S.; Ghosh, S.; Kapoor, R.; Gouri, S. P.; Pande, G.; Datta, S., Multifunctional gradient coatings of phosphate-free bioactive glass on SS316L biomedical implant materials for improved fixation. *Surface and Coatings Technology* **2014,** 240, (0), 437-443.

(20) Labbaf, S.; Tsigkou, O.; Müller, K. H.; Stevens, M. M.; Porter, A. E.; Jones, J. R., Spherical bioactive glass particles and their interaction with human mesenchymal stem cells *in vitro*. *Biomaterials* **2011,** 32, (4), 1010-1018.

(21) Okuda, T.; Ioku, K.; Yonezawa, I.; Minagi, H.; Kawachi, G.; Gonda, Y.; Murayama, H.; Shibata, Y.; Minami, S.; Kamihira, S.; Kurosawa, H.; Ikeda, T., The effect of the microstructure of β-tricalcium phosphate on the metabolism of subsequently formed bone tissue. *Biomaterials* **2007,** 28, (16), 2612-2621.

(22) Rouahi, M.; Champion, E.; Hardouin, P.; Anselme, K., Quantitative kinetic analysis of gene expression during human osteoblastic adhesion on orthopaedic materials. *Biomaterials* **2006,** 27, (14), 2829-2844.

(23) Lakhkar, N. J.; Lee, I.-H.; Kim, H.-W.; Salih, V.; Wall, I. B.; Knowles, J. C., Bone formation controlled by biologically relevant inorganic ions: Role and controlled delivery from phosphate-based glasses. *Advanced Drug Delivery Reviews* **2013,** 65, (4), 405-420.

(24) Uysal, T.; Ustdal, A.; Sonmez, M. F.; Ozturk, F., Stimulation of Bone Formation by Dietary Boron in an Orthopedically Expanded Suture in Rabbits. *The Angle Orthodontist* **2009,** 79, (5), 984-990.

(25) Fredholm, Y. C.; Karpukhina, N.; Brauer, D. S.; Jones, J. R.; Law, R. V.; Hill, R. G., Influence of strontium for calcium substitution in bioactive glasses on degradation, ion release and apatite formation. *Journals of The Royal Society Interface* **2012,** 9, (70), 880-889.

(26) Yang, F.; Yang, D.; Tu, J.; Zheng, Q.; Cai, L.; Wang, L., Strontium Enhances Osteogenic Differentiation of Mesenchymal Stem Cells and *In Vivo* Bone Formation by Activating Wnt/Catenin Signaling. *STEM CELLS* **2011,** 29, (6), 981-991.

(27) Karageorgiou, V.; Kaplan, D., Porosity of 3D biomaterial scaffolds and osteogenesis. *Biomaterials* **2005,** 26, (27), 5474-5491.

(28) Park, K., Vascularization in 3D bioprinted scaffolds. *Journal of Controlled Release* **2014,** 184, (0), 79.

(29) Zhang, K.; Zhang, Y.; Yan, S.; Gong, L.; Wang, J.; Chen, X.; Cui, L.; Yin, J., Repair of an articular cartilage defect using adipose-derived stem cells loaded on a polyelectrolyte complex scaffold based on poly(l-glutamic acid) and chitosan. *Acta Biomaterialia* **2013,** 9, (7), 7276-7288.

(30) Hulbert, S. F.; Young, F. A.; Mathews, R. S.; Klawitter, J. J.; Talbert, C. D.; Stelling, F. H., Potential of ceramic materials as permanently implantable skeletal prostheses. *Journal of Biomedical Materials Research* **1970,** 4, (3), 433-456.

(31) Sobral, J. M.; Caridade, S. G.; Sousa, R. A.; Mano, J. F.; Reis, R. L., Three-dimensional plotted scaffolds with controlled pore size gradients: Effect of scaffold geometry on mechanical performance and cell seeding efficiency. *Acta Biomaterialia* **2011,** 7, (3), 1009-1018.

(32) Danilevicius, P.; Georgiadi, L.; Pateman, C. J.; Claeyssens, F.; Chatzinikolaidou, M.; Farsari, M., The effect of porosity on cell ingrowth into accurately defined, laser-made, polylactide-based 3D scaffolds. *Applied Surface Science*, (0).

(33) Kokubo, T.; Takadama, H., How useful is SBF in predicting *in vivo* bone bioactivity? *Biomaterials* **2006,** 27, (15), 2907-2915.

(34) Hong, Z.; Reis, R. L.; Mano, J. F., Preparation and *in vitro* characterization of scaffolds of poly(l-lactic acid) containing bioactive glass ceramic nanoparticles. *Acta Biomaterialia* **2008,** 4, (5), 1297-1306.

(35) Xu, X.; Chen, X.; Liu, A.; Hong, Z.; Jing, X., Electrospun poly(l-lactide)-grafted hydroxyapatite/poly(l-lactide) nanocomposite fibers. *European Polymer Journal* **2007,** 43, (8), 3187-3196.

(36) Kaczmarek, H.; Nowicki, M.; Vuković-Kwiatkowska, I.; Nowakowska, S., Crosslinked blends of poly(lactic acid) and polyacrylates: AFM, DSC and XRD studies. *J Polymer Research* **2013,** 20, (3), 1-12.

(37) Boccaccini, A. R.; Erol, M.; Stark, W. J.; Mohn, D.; Hong, Z.; Mano, J. F., Polymer/bioactive glass nanocomposites for biomedical applications: A review. *Composites Science and Technology* **2010,** 70, (13), 1764-1776.

(38) Hutmacher, D. W., Scaffolds in tissue engineering bone and cartilage. *Biomaterials* **2000,** 21, (24), 2529-2543.

(39) Wren, A. W.; Cummins, N. M.; Coughlan, A.; Towler, M. R., The effect of adding organic polymers on the handling properties, strengths and bioactivity of a Ca–Sr–Zn–Si glass polyalkenoate cement. *Journal of Materials Science* **2010,** 45, (13), 3554-3562.

(40) Armentano, I.; Dottori, M.; Fortunati, E.; Mattioli, S.; Kenny, J. M., Biodegradable polymer matrix nanocomposites for tissue engineering: A review. *Polymer Degradation and Stability* **2010,** In Press, Corrected Proof.

(41) Hench, L. L., Bioceramics. *Journal of the American Ceramic Society* **1998,** 81, (7), 1705-1728.

(42) Pattanayak, D. K., Apatite wollastonite–poly methyl methacrylate bio-composites. *Materials Science and Engineering: C* **2009,** 29, (5), 1709-1714.

(43) Zhang, K.; Wang, Y.; Hillmyer, M. A.; Francis, L. F., Processing and properties of porous poly(l-lactide)/bioactive glass composites. *Biomaterials* **2004,** 25, (13), 2489-2500.

(44) Lu, H. H.; Tang, A.; Oh, S. C.; Spalazzi, J. P.; Dionisio, K., Compositional effects on the formation of a calcium phosphate layer and the response of osteoblast-like cells on polymer-bioactive glass composites. *Biomaterials* **2005,** 26, (32), 6323-6334.

(45) Huang, W.; Day, D.; Kittiratanapiboon, K.; Rahaman, M., Kinetics and mechanisms of the conversion of silicate (45S5), borate, and borosilicate glasses to hydroxyapatite in dilute phosphate solutions. *Journal of Materials Science: Materials in Medicine* **2006,** 17, (7), 583-596.

(46) Terra, J.; Dourado, E. R.; Eon, J.-G.; Ellis, D. E.; Gonzalez, G.; Rossi, A. M., The structure of strontium-doped hydroxyapatite: an experimental and theoretical study. *Physical Chemistry Chemical Physics* **2009,** 11, (3), 568-577.

(47) Rey, C.; Combes, C.; Drouet, C.; Grossin, D., 1.111 - Bioactive Ceramics: Physical Chemistry. In *Comprehensive Biomaterials*, Ducheyne, P., Ed. Elsevier: Oxford, 2011; pp 187-221.

(48) Granados-Correa, F.; Bonifacio-MartÍNez, J.; Serrano-GÓMez, J., Synthesis and characterization of calcium phosphate and its relation to Cr(VI) adsorption properties. *Revista internacional de contaminación ambiental* **2010,** 26, 129-134.

(49) Jia, J.; Zhou, H.; Wei, J.; Jiang, X.; Hua, H.; Chen, F.; Wei, S.; Shin, J.-W.; Liu, C., Development of magnesium calcium phosphate biocement for bone regeneration. *Journal of The Royal Society Interface* **2010,** 7, (49), 1171-1180.

(50) Tavares, D. d. S.; Resende, C. X.; Quitan, M. P.; Castro, L. d. O.; Granjeiro, J. M.; Soares, G. d. A., Incorporation of strontium up to 5 Mol. (%) to hydroxyapatite did not affect its cytocompatibility. *Materials Research* **2011,** 14, 456-460.

(51) Lindahl, C.; Engqvist, H.; Xia, W., Effect of strontium ions on the early formation of biomimetic apatite on single crystalline rutile. *Applied Surface Science* **2013,** 266, (0), 199-204.

(52) Liang, Y.; Li, H.; Xu, J.; Li, X. I. N.; Li, X.; Yan, Y.; Qi, M.; Hu, M. I. N., Strontium coating by electrochemical deposition improves implant osseointegration in osteopenic models. *Experimental and Therapeutic Medicine* **2015,** 9, (1), 172-176.

(53) Zuk, P. A.; Zhu, M.; Ashjian, P.; De Ugarte, D. A.; Huang, J. I.; Mizuno, H.; Alfonso, Z. C.; Fraser, J. K.; Benhaim, P.; Hedrick, M. H., Human Adipose Tissue Is a Source of Multipotent Stem Cells. *Molecular Biology of the Cell* **2002,** 13, (12), 4279-4295.

(54) Lee, J. H.; Rhie, J. W.; Oh, D. Y.; Ahn, S. T., Osteogenic differentiation of human adipose tissue-derived stromal cells (hASCs) in a porous three-dimensional scaffold. *Biochemical and Biophysical Research Communications* **2008,** 370, (3), 456-460.

VII. CHAPTER

Reinforcement of Poly-L-lactic acid Electrospun Membranes with Strontium Borosilicate Bioactive Glasses for Bone Tissue Engineering

CHAPTER VII - REINFORCEMENT OF POLY-L-LACTIC ACID ELECTROSPUN MEMBRANES WITH STRONTIUM BOROSILICATE BIOACTIVE GLASSES FOR BONE TISSUE ENGINEERING

VII. CHAPTER

Reinforcement of Poly-L-lactic acid Electrospun Membranes with Strontium Borosilicate Bioactive Glasses for Bone Tissue Engineering[6]

Abstract

Herein, for the first time, we combined PLLA with a strontium BBG (BBG-Sr) using electrospinning to fabricate a composite bioactive PLLA membrane loaded with 10 % (w/w) of BBG-Sr glass particles (PLLA-BBG-Sr). The composites were characterised by SEM and microcomputed tomography (μCT), and the results showed that we successfully fabricated smooth and uniform fibres (1 to 3 μm in width) with a homogeneous distribution of BBG-Sr microparticles (< 45μm). Degradation studies (in phosphate buffered saline) demonstrated that the incorporation of BBG-Sr glass particles into the PLLA membranes increased their degradability and water uptake with a continuous release of cations. The addition of BBG-Sr glass particles enhanced the membrane's mechanical properties (69% higher Young modulus and 36% higher tensile strength). Furthermore, cellular *in vitro* evaluation using BM-MSCs demonstrated that PLLA-BBG-Sr membranes promoted the osteogenic differentiation of the cells as demonstrated by increased ALP activity and up-regulated osteogenic gene expression (*Alpl, Sp7* and *Bglap*) in relation to PLLA alone. These results strongly suggest that the composite PLLA membranes reinforced with the BBG-Sr glass particles have potential as an effective biomaterial capable of promoting bone regeneration.

[6] This chapter is based on the following publication:

João S. Fernandes, Piergiorgio Gentile, Margarida Martins, Nuno M. Neves, Cheryl Miller, Aileen Crawford, Ricardo A. Pires, Paul Hatton, Rui L. Reis; Reinforcement of Poly L lactic acid Electrospun Membranes by Addition of Strontium Borosilicate Glasses for Bone Tissue Engineering, Acta Biomaterialia 2016 Oct 15;44:168-77

1. Introduction

The development of biomaterials for guided BTE has been a hot topic of research in recent years. Biomaterials can act as a short-term template in which cells proliferate and deposit ECM, helping bone ingrowth as a part of its regeneration process. A suitable biomaterial for BTE should present appropriate mechanical properties that is able to withstand the mechanical stress occurring at the lesion site and to support cell ingrowth as part of the bone formation process. The capacity to shape the biomaterial substrate to fit exactly in the bone lesion is of particular relevance, too [1, 2].

Electrospinning is a versatile technique that applies electrostatic forces to manufacture ultrathin fibre meshes from melted polymers or polymer solutions. This methodology has been used to obtain biomaterials composed by micro- or nano-fibres with high surface areas and mechanical properties suitable for BTE by playing with its different processing parameters [2, 3]. Furthermore, electrospun membranes closely mimic the ECM promoting cell attachment and proliferation [4].

PLLA is a biodegradable and biocompatible polymer, widely investigated for BTE, specially due to the approval of different PLLA medical devices for clinical use by the US Federal FDA [5]. Furthermore, PLLA has appropriate flexibility and deformation capacity, and can be processed by different techniques (e.g. melt, dry and wet spinning, as well as electrospinning) [6-9]. However, PLLA is not commonly considered osteoinductive [4, 10]. Thus, in order to improve the biological performance of PLLA fibres, the polymeric matrix can be combined with inorganic materials, such as BGs and glass-ceramics, improving its osteoinductive potential [11, 12]. Moreover, the PLLA degradation rate can be shaped by several different variables (e.g. chemical structure and crystallinity of the polymer, size and shape of the final material), although, the matching of the rate of degradation and the kinetics of the formation of new bone tissue is still difficult to achieve [13, 14]. The addition of an inorganic phase allows a better control of the degradation rate of the final PLLA-glass composite, which can be used to manufacture a composite with a suitable degradation rate while progressively being substituted by the new bone that is being formed [15].

BGs are a group of inorganic bioactive materials that are able to form a bone-like HA layer on their surface capable to strongly bond to hard and soft tissues [11, 16-18]. Immediately after the launch of the 45S5 Bioglass® in the market (chemical composition by mol: $0.45SiO_2 \cdot 0.06P_2O_5 \cdot 0.245Na_2O \cdot 0.245CaO$) it became the gold standard for BG materials [16]. Subsequently, a wide range of BGs based on the 45S5 composition have been developed and studied for BTE [19, 20]. The addition of borate glass forming units is one approach that has potential to lower melting temperatures while controlling bio-degradation and increasing conversion rates to HA [21, 22]. Borosilicate-based BGs (BBGs) have been previously studied as biomaterials and have shown relevant capacity as osteointegrative antibacterial materials to be used in BTE [23, 24]. BBGs have been also incorporated into scaffolds: Wang *et al*. [25] successfully incorporated copper doped borosilicate glasses (BBG-Cu) into a polymeric scaffold for tissue engineering purposes. They observed an improvement in the stability of the glass network and the BBG-Cu promoted the angiogenesis in rat calvarial defects.

Moreover, in our previous studies we tested a BBG glass composition (e.g. molar ratio: BBG-Sr: $0.05Na_2O \cdot 0.35SrO \cdot 0.20B_2O_3 \cdot 0.40SiO_2$) for their osteogenic capacity (Chapter V). We found that the presence of BBG-Sr glass particles improved the osteogenic differentiation of BM-MSCs and induced the formation of mineralised tissue. We also demonstrated that BBG-Sr, at concentrations $\geq$ 18 $mg \cdot ml^{-1}$ it was able to eradicate *P. aeruginosa* bacterium [26]. Numerous reports have already associated Sr^{2+} with bone therapeutic potential [19]. Depending on the concentration, Sr^{2+} can exerts different effects on bone metabolism at the tissue and cellular levels, as well as in bone formation of *in vivo* [27, 28]. For instance, Marie *et al*. [27] demonstrated strontium modulates bone cell function (e.g. cell proliferation and differentiation) *in vitro* stimulating bone formation and inhibiting bone resorption. Moreover, Hesaraki *et al*. showed that glasses doped with strontium promoted osteoblast proliferation and ALP activity when directly in culture with cells [29]. For instance, Wu *et al*. [30] developed a strontium silicate glass that promoted a high ALP activity in BM-MSC cell culture, which was associated with the release of Sr^{2+} and silica. Also, Santocildes-Romero *et al*. [31] demonstrated that strontium-substituted BGs promoted osteogenic differentiation of BM-MSCs cultures in the presence of strontium-containing BGs. They showed an increased expression of genes such as *Alpl* and *Bglap*. Moreover, Gentleman *et al*. [32] studied the effect of the release of Si- and Sr-

related chemical entities from PCL-SrBG scaffolds, and they detected that the SrBG particles stimulated osteoblast proliferation and ALP activity in relation to the SrBG-free PCL scaffold. Moreover, BM-MSCs are of special interest due to their capacity of differentiation into different lineages (including osteoblastic cells) with appropriate external stimuli, and the fact that it is relatively easy to isolate [33]. For that reason, BM-MSCs have received extensive attention as promoters of tissue regeneration.

To our knowledge, the PLLA-BBG-Sr composite membranes fabricated by electrospinning has not been achieved to-date. Therefore, we aimed to evaluate the potential of PLLA-BBG-Sr composite membranes for BTE and bone regeneration. Herein, we investigated the impact of the incorporation of BBG-Sr glass particles in PLLA fibre meshes on their tensile strength and degradation. Moreover, we evaluated the response of BM-MSCs in the presence of PLLA-BBG-Sr fibres, namely in what regards to their morphology, proliferation and ability to induce its differentiation.

2. Materials and methods

2.1. Materials

All chemicals used for the melt-quenched synthesis were reagent grade: boron oxide (B_2O_3, Alfa Aesar, Germany), calcium carbonate ($CaCO_3$, Sigma-Aldrich, UK), sodium bicarbonate ($NaHCO_3$, Sigma-Aldrich, Australia), silica gel 60M (SiO_2, Macherey-Nagel, Germany), magnesium oxide (MgO, Sigma-Aldrich, UK) and strontium carbonate ($SrCO_3$, Sigma-Aldrich, Australia). All the chemical reagents used for electrospinning were reagent grade: PLLA with a L-lactide content of 99.6% and an average M_w of 69,000 $g.mol^{-1}$ (Cargill Dow LLC, USA), dichloromethane (Sigma-Aldrich, UK), and the anionic surfactant docusate sodium salt (Sigma-Aldrich, UK). The BBGs were produced as described elsewhere (Chapter II.2.1.). Briefly, the appropriate amounts of SiO_2, B_2O_3, $NaHCO_3$, and $CaCO_3$ or MgO or $SrCO_3$, were accurately mixed with ethanol (Sigma, Portugal) in a porcelain pestle and mortar, fully dried overnight and transferred to a platinum crucible (ZGS platinum, Johnson Matthey, UK). Each batch (~ 50 g) was heated to 1450 ºC in air for 1 h and, subsequently, the melt was quickly poured into an ice-water bath at ~ 0 ˚C to form a glass frit. Afterwards, the glasses of general formula $0.05Na_2O \cdot$

xMgO · yCaO · (0.35-x-y)SrO · 0.20B_2O_3 · 0.40SiO_2 (molar ratio, where x, y = 0.35 or 0.00, and $x \neq y$) were ground into an Agate mortar (RETSCH, Germany) to obtain microparticles and sieved to a size <45 μm to be homogeneously incorporated in the polymeric matrix during the fabrication of the fibres. The density of the BBGs was measured by a Multi pycnometer (Quantachrome Instruments, USA) under helium at 110 °C using ~ 5 g of each sample.

2.2 Glass synthesis and membranes preparation

2.2.1. Electrospinning

PLLA-BBG-Sr membranes were fabricated inside a fume hood cabinet for safe solvent evaporation and in order to prevent that the turbulent air interferes in the formation of the fibres. The PLLA concentration, the ratio of PLLA/BBG-Sr and the process parameters (e.g. applied voltage, flow rate and distance from the collector) were optimised in order to obtain uniform membrane of fibres. The final electrospun membranes were fabricated using PLLA dissolved in dichloromethane (16% w/v) where the BBGs microparticles were suspended (10% w/w BBGs/PLLA). Docusate sodium salt (1.2% w/w relative to PLLA) was used to help the homogenisation of the solution avoiding the formation of agglomerates. The PLLA and PLLA-BBG-Sr solutions were stirred overnight and sonicated 5 min before use to remove air bubbles. The set up was mounted using a high voltage supplier, a syringe pump (Baxter AS50) with a 20 G metal needle (Fisnar, New Jersey, USA) and a conductive collector. The PLLA and PLLA-BBG-Sr solutions were drawn up into a 1 ml syringe (BD Plastipak, New Jersey, USA). The solutions were electrospun using a voltage of 17 kV and a flow rate of 3 ml·h^{-1} at a 19 cm distance between the collector and needle. The electrospun membranes were dried in a fume hood, at RT, for 24 h, collected and stored in a desiccator at RT.

2.3. Characterisation of electrospun membranes

2.3.1. Scanning electron microscopy (SEM)

The SEM/EDS (Leica Cambridge, UK) was used to assess the surface morphology of the fabricated PLLA and PLLA-BBG-Sr membranes. Prior to the analysis, all the scaffolds were sputter-coated with gold. The micrographs were acquired using a beam energy of 5.0kV and working distance (WD) of ~ 5.2 mm.

2.3.2. Micro-computed tomography (μCT)

μCT analysis was carried out on a high-resolution μCT scanner (SkyScan1272, Bruker, Kontich, Belgium), using a pixel size of 9.8 μm and integration time of 160 ms. The X-ray source was set at voltage of 50 kV and a current of 200 μA of current. Approximately 400 projections were acquired over a rotation range of 180 ° with a rotation step of 0.60 °. Data sets were reconstructed using standardised cone-beam reconstruction software (NRecon v1.6.10.2, SkyScan). The output format for each sample was a series of 601 bitmap images (1224 × 1224 pixels). 3D virtual models of representative regions in the bulk of the scaffolds were created applying colour channel thresholds and visualised using an image processing software (CTvox).

2.3.3. Mechanical tests

Tensile strength and modulus of the PLLA and PLLA-BBG-Sr membranes were measured using a Uniaxial Universal Testing Machine (Instron 4505, USA) according to the standard ASTM D 638. The membranes were cut into strips of 50 mm length, 10 mm width and 0.1 mm thickness. The tests were conducted using a 1 kN load cell, with a gauge length of 20 mm and a crosshead speed of 5 $mm.min^{-1}$ until rupture. The tensile strenght was taken from the stress-strain curves as the maximum stress hold by the samples. Tensile modulus was estimated from the initial slope of the stress–strain curve (between 0.5% and 1% strain) using the linear regression method. The average and SD were determined using 5 specimens per composition.

2.3.4. Degradation assay

The electrospun membranes (n=3 per time point) were immersed in PBS (Sigma-Aldrich, UK) at a ratio of 10:10 (membrane (mg): PBS (ml)) for 7, 14, 21, and 28 days in a water-shaking bath at 60 rpm and 37 °C. Each immersion solution was filtered and the pH measured (Crison Instruments, Spain). Inductive coupled plasma (ICP) analysis was performed to determine the concentrations of Si, B and Sr in solution. The absorption was measure at specific wavelengths (λ= 251.611 nm for Si, λ= 249.773 nm for B and λ= 407.771 nm for Sr) and the concentrations were determined using calibration curves obtained with standard solutions (Alfa Aesar, UK) prior to the analysis of the samples.

The membranes were removed from PBS, the excess surface water was removed and the samples were immediately weighed. Afterwards, the samples were dried in the oven at 37 °C, to constant weight, recording the final mass of the membranes. The water uptake (WU) was calculated according to Eq. (1):

$$WU(\%) = (m_{tp} - m_f)/m_f \times 100 \quad \text{Eq. (1)}$$

Where m_{tp} is the wet mass of the specimen at the specific time (days), and m_f is the final mass after immersion and drying. The weight loss (WL) was calculated according to Eq. (2):

$$WL(\%) = (m_f - m_i)/m_i \times 100 \quad \text{Eq. (2)}$$

Where m_f is the mass of the dried membranes after its immersion in water, and m_i is the mass of the dried membranes before immersion in PBS.

TGA (Q500, TA Instruments, USA) was also used to quantify the changes in the weight (mass) of the membranes during the degradation process. In addition, thermal analysis was performed to determine the amount of BBG-Sr (non-combustible) glass particles that was compounded with PLLA to produce the composite membranes. Experiments were performed in platinum pans, at a heating rate of 40 $K.min^{-1}$ from 50 to 700 °C in an oxygen atmosphere.

2.4. *In vitro* culture of BM-MSCs on electrospun membranes

2.4.1. Isolation and expansion of mesenchymal stromal cells

BM-MSCs were isolated from bone marrow of 4-5 week-old male Wistar rats according to the method established by Maniatopoulos *et al.* [34] and recently used by Santocildes-Romero [31]. BM-MSCs were expanded in basal medium consisting of DMEM (Sigma-Aldrich, UK), supplemented with 100 $U \cdot ml^{-1}$ penicillin (Sigma-Aldrich, UK) and 100 $\mu g \cdot ml^{-1}$ streptomycin (Sigma-Aldrich, UK). Cells were cultured at 37 ºC in an atmosphere of 5% CO_2.

2.4.2. MSCs proliferation, viability and morphology

Prior to the *in vitro* studies, BM-MSCs, at passage 2, were harvested and seeded at a density of 3×10^4 cells per membrane of Ø = 6.5 mm held in plastic inserts (CellCrown™ 24, Scaffdex, UK). Cells were cultured for 7, 14 and 21 days under static conditions. All scaffold conditions were cultured in basal and osteogenic differentiation media (basal medium supplemented with 50 $\mu g \cdot ml^{-1}$ L-ascorbic acid, 10 mM β-glycerophosphate and 10^{-8} M dexamethasone).

2.4.3. BM-MSCs proliferation, viability and morphology

2.4.3.1. Morphological evaluation of cultured cells

After each time-point the cells cultured on the membranes were washed with PBS and fixed with 4% formalin solution (0.5 ml) for 15 min at RT. The cells were then washed with PBS, containing 0.2 % Triton X, for 2 min. After the fixation and permeation steps, the cells were washed again with PBS and stained with DAPI (1:1000, Sigma-Aldrich, UK) for 2 min at RT, and phalloidin-tetramethylrhodamine B isothiocyanate (Sigma-Aldrich, UK) for 1 h at RT. Finally, the cells were washed and observed using an Axioplan 2 imaging fluorescent microscope with a digital camera QIC AM 12-bit (Zeiss, UK).

2.4.3.2. Cell viability and proliferation (PrestoBlue® and PicoGreen® assays)

The PrestoBlue® reagent (Fisher Scientific, UK) is a resazurin-based solution that is reduced to resorufin by viable cells which can be detected flurometrically. The cell viability assay was executed according to the manufacturer's instructions. In brief, the PrestoBlue® reagent was added to a final concentration of 10% to the cell culture medium and the cultures incubated for 1 h at 37 ^{o}C. 200 µl samples of the culture medium were removed and placed in 96-well plates and the resorufin fluorescence quantified spectrophotometrically using a microplate reader (Tecan Infinite M200, UK). The fluorescence was determined at an excitation wavelength of 560 nm and emission wavelength of 590 nm. The metabolic activity was presented in fluorescence values and compared with the control (cell cultured onto PLLA membranes under basal medium conditions).

The PicoGreen® dsDNA reagent (Invitrogen, USA) is an ultrasensitive fluorescent nucleic acid dye for quantification of dsDNA in solution. This assay enables measurement of cell proliferation. After each culturing period, the cells were washed with PBS and incubated at 37 ºC for 3 h followed by a freezing step at -80 ºC for overnight in ultra-pure water (1 ml) to ensure the cell lysis. Finally, the fluorescence was determined at an excitation wavelength of 485 nm and emission wavelength of 528 nm. The DNA concentration was presented in $\mu g \cdot ml^{-1}$ and compared with the control (cell cultured onto PLLA membranes under basal medium conditions).

2.4.4. Alkaline phosphatase (ALP) quantification

The concentration of ALP was determined for all the cell culture time points, using the lysates used for the DNA quantification and the Alkaline Phosphatase, Diethanolamine Detection kit (Sigma-Aldrich, UK), which is based on the conversion of pNPP to free p-nitrophenol by ALP. In brief, a buffered pNPP solution was prepared and equilibrated at 37 ºC. Afterwards, 2% (v/v) of sample or control lysate was added. Immediately after mixing the absorbance was read at 405 nm in a microplate reader (Tecan Infinite M200, UK) for ≈ 5 min. An ALP standard solution was used as control and buffer as blank. The units were calculated according to the following Eq. (3):

$$\frac{(\Delta A_{405nm}/\min\ Test - \Delta A_{405nm}/\min\ Blank)\times df \times V_F}{18.5 \times V_E} \quad \text{Eq. (3)}$$

Where df = dilution factor; V_F = Volume of final solution; 18.5 = millimolar extinction coefficient of pNPP at 405 nm and V_E = Volume of samples/ALP standard solution.

2.4.5. RNA isolation and real-time quantitative polymerase chain reaction (rtPCR)

RNA was extracted with tri-reagent (Sigma-Aldrich, UK) according to the manufacturer's instructions. The RNA concentration was determined by microspectrophotometry (NanoDrop 1000, Germany). The cDNA synthesis was performed using the qScript cDNA synthesis kit (Quanta BioSciences, VWR, Germany) with 100 ng of RNA template in a final volume of 20 µl. Cycling was as follows: 1 cycle at 22 °C, 5 min; 1 cycle at 42 °C, 30 min; 1 cycle at 85 °C, 5 min. The amplification of the target cDNA was performed using the PerfeCTa SYBR Green FastMix (Quanta BioSciences) with 1 µl of cDNA, 200 nM of each primer (Table VII.1) in a final volume of 20 µl. Real time-PCR cycling was as follows: 1 cycle at 95 °C, 2 min; 44 cycles at 95 °C; 10 s at gene annealing temperature (Table VII.1); 30 s at 72 °C; followed by dissociation curve analysis. All the reactions were carried out on a PCR cycler Mastercycler Realplex (Hamburg, Germany). The transcripts expression data were normalised to the housekeeping gene *Gapdh* in each sample. The quantification was performed according to the Livak method ($2^{-\Delta\Delta Ct}$ method

[35]), considering as calibrator at each time point the PLLA - basal medium for PLLA-osteogenic medium and PLLA-BBG-Sr basal medium for PLLA-BBG-Sr osteogenic medium (threshold = 1).

Table VII.1 - Primers used for rtPCR

Gene	Primer sequence 5'-3' Forward/ reverse	T_m (ºC)
Osteocalcin (*Bglap*)	CATCTATGGCACCACCGTTT AGAGAGAGGGAACAGGGAGG	60.0
Osteopontin (*Spp1*)	ATCTCACCATTCCGATGAATCT CAGTCCATAAGCCAAGCTATCA	60.0
Osterix (*Sp7*)	CACTGGCTCCTGGTTCTCTC CCACTCCTCCTCTTCGTGAG	60.0
Alkaline phosphatase (*Alpl*)	TGCCTTACCAACTCATTTGTG ACGCGATGCAACACCACTC	57.4

3. Results and discussion

3.1. Characterisation of electrospun membranes

The PLLA and PLLA-BBG-Sr (10% w/w BBG-Sr/PLLA) composite membranes were successfully obtained by electrospinning. TGA analysis confirmed that we successfully incorporated 10% (w/w) of BBG-Sr microparticles in the PLLA fibres. The morphology, microstructure and fibre integrity of the electrospun PLLA and PLLA-BBG-Sr membranes was characterised by SEM and μCT. Electrospun PLLA and PLLA-BBG-Sr membranes are composed of smooth and uniform fibres. No large particles were detected (Figure VII.1a and 1c), however, the formation of small agglomerates in the membranes containing the BBG-Sr microparticles was observed [36]. Figure VII.1c highlights in red circles the BBG-Sr microparticles incorporated into the fibres. The homogeneous distribution of the BBG-Sr microparticles in the PLLA-BBG-Sr membrane could be

observed in the 2D virtual model representatively obtained using an image processing software CTvox of µCT images (Figure VII.1d), in which the red colour represents the BBG-Sr microparticles distributed into the composite membranes in green. As expected, the PLLA membranes do not present any particles in their structure (Figure VII.1b).

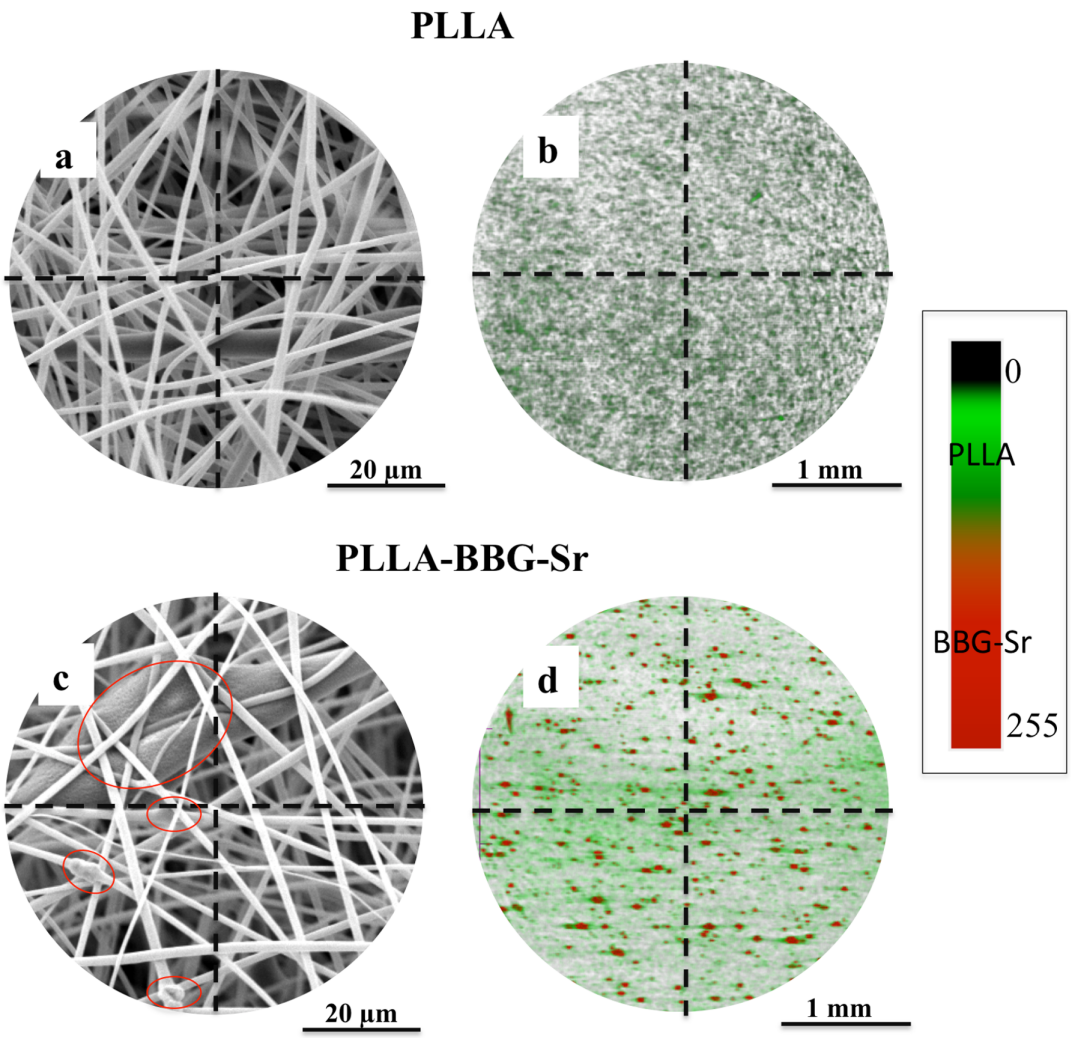

Figure VII.1 - SEM micrographs (a and c) and representative µCT 2D images (b and d) of PLLA and PLLA-BBG-Sr membranes. The areas encompassed by red lines in (c) show particles incorporated into the fibres. In (b and d) PLLA fibres are represented in green and the BBG-Sr microparticles are represented in red.

The mechanical properties of the biomaterials are important in providing physical support for cell growth and migration matching those of the tissue at the site of implantation [37]. Figure VII.2a presents the stress–strain curves obtained for the PLLA and PLLA-BBG-Sr

membranes under tensile load up to a strain of 50%. The PLLA-BBG-Sr membranes showed the highest tensile strength (0.75 ± 0.7 MPa), when compared to the PLLA membranes (0.55 ± 0.6 MPa), indicating that the incorporation of BBG-Sr reinforced the membranes. The same trend was observed for the Young's modulus (Figure VII.2b), calculated from the initial linear slope of the stress-strain curves, where the loading of BBG-Sr microparticles improved the modulus from 14.6 ± 3.8 MPa (PLLA) to 24.7 ± 5.3 MPa (PLLA-BBG-Sr). This might be due to an increase in rigidity through the filler effect, in which the microparticles encumber the movement of the polymer chains and the amount of extendable material in the membrane. On the other hand, while the incorporation of the microparticles in PLLA-BBG-Sr membranes can affect the tensile strength, where there is no interaction between fibres and particles. The availability of cations derived from the incorporated microparticles may contribute to the crosslinking of the carboxylic acid groups (that are present in the chain ends of the PLLA) through the formation of carboxylates. These carboxylate cross-links induce the interlocking of the membranes, resulting in an improvement of the Young modulus [38] As demonstrated by Thomas *et al*. [39], small concentrations of nano HA resulted in a reinforcement of PCL. It was observed by Jeong *et al*. [40] in an analogous way, that the addition of increasing concentrations of HA increasingly enhanced the mechanical properties of the composite, namely their tensile strength and Young's modulus. Therefore, our results support that, with the inclusion of BBG-Sr microparticles into the PLLA matrix, it is possible to tune their mechanical properties, contributing to be a closer match those from the living tissue at the site of surgical intervention.

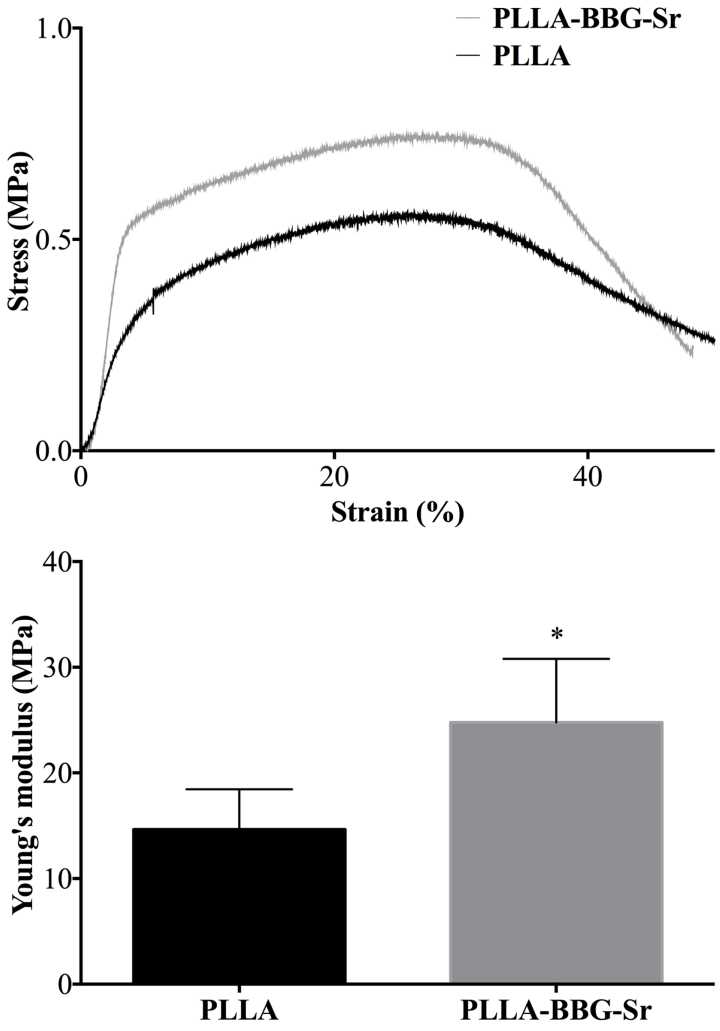

Figure VII.2 - (a) Stress–strain curves of PLLA and PLLA-BBG-Sr membranes and their respective (b) Young's modulus determined from the initial slope of the curves. The data was analysed by non-parametric statistics; data analysis using the Mann-Whitney test revealed a significance of $p<0.05$ (*).

3.2. Degradation of the electrospun membranes

A biomaterial suitable for promoting bone regeneration in a tissue engineering perspective should present an appropriate biodegradability. The BTE concept is based on the substitution of the biomaterial by new bone. This requires that the degradation rate of the biomaterial matches that of new bone formation, in order to occur a progressive substitution of the biomaterial by the new bone tissue [15, 41]. The degradation profiles of PLLA and PLLA-BBG-Sr membranes (Figure VII.3) were evaluated by weight loss and

water uptake, as well as the release of chemical species from the membranes, and pH of the immersion solutions. The water uptake and weight loss data showed differences between the PLLA and the PLLA-BBG-Sr membranes (Figure VII.3a and 3b). Both membranes presented steady and continuous water uptake and weight loss from week 2 to week 3. However, the PLLA-BBG-Sr membranes presented a more pronounced 'burst' of weight loss during the first week. The differences between the two membranes during this initial stage of degradation might be attributed to the penetration of the PBS solution through the polymer/glass interface and/or surface cracks that facilitated the degradation of the material and enhanced the water uptake. Another possibility is related with a superficial hydrolytic degradation generated by the leaching of chemical species from the glass particles [42, 43]. The pH measurements presented no significant variation of pH for both PLLA and PLLA-BBG-Sr membranes over time. An initial burst release of B, Si and Sr from the PLLA-BBG-Sr membranes into the immersion solution was observed (Figure VII.3c). The release of such chemical species can only have originated from the BBG-Sr microparticles, corroborating the possibility of the origin of the weight loss being mainly derived from the hydrolytic degradation of the glass particles. During the last week of degradation (21 to 28 days) it was also noticed that an increase in the PLLA-BBG-Sr weight loss that correlates with the reduction of glass percentage determined by TGA (Figure VII.3d) and the increased concentration of mainly B and Sr-containing chemical species, that were leached from the glass particles to the immersion medium (detected by ICP). The increase on the degradation is clear during the last week; however, the leaching observed by ICP during the first 3 weeks is not corroborated by the TGA analysis. In this case, the presence of phosphates from the solution buffer might generate a surface layer of strontium phosphate that limits the mass exchange from the glass particles to the immersion solution. In this case, the weight loss derived from the leaching of B, Si and Sr from the glass particles is partially compensated by the deposition of phosphates. The fact that the PLLA-BBG-Sr composite membranes lost twice the mass during the degradation process suggests that the incorporation of BBG-Sr into PLLA fibres increased the degradability and the degradation rate of the membranes, as well as the release of active chemical species to the surrounding medium [15].

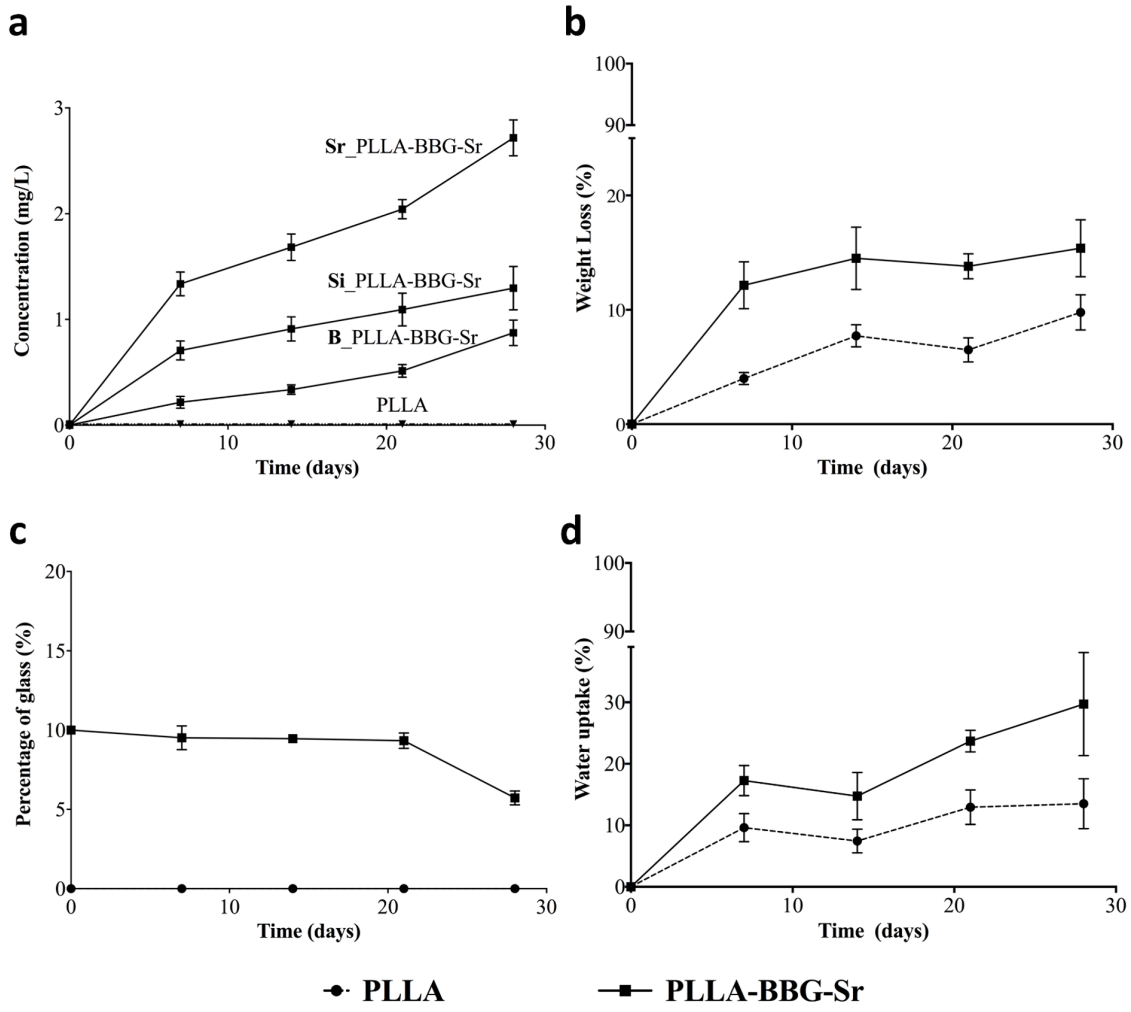

Figure VII.3 - Degradation profile of the PLLA and PLLA-BBG-Sr membranes during 30 day of degradation in PBS at 37 ºC. (a and d) WU and WL of the PLLA and PLLA-BBG-Sr membranes; (c) release profiles of chemical species from the PLLA-BBG-Sr membranes; and (d) percentage of glass (w/w) in the studied membranes.

3.3. *In vitro* biological evaluation

3.3.1. Morphology, viability and proliferation of the BM-MSCs

Apart from the suitable chemical and physical properties of the biomaterial, it is also crucial to evaluate if they are cytotoxic. To this purpose, direct contact assays are widely used as a preliminary screening for biomaterials [44]. Fluorescence microscopy images (Figure VII.4a) show the morphology of BM-MSCs cultured in the presence of PLLA

and PLLA-BBG-Sr membranes in basal or osteogenic medium (Figure VII.4a). The attached BM-MSCs displayed a well-spread morphology and several cell-to-cell contacts. As expected, the PrestoBlue® and PicoGreen® data (Figure VII.4b and 4c) demonstrated that the cells proliferated over the time course under basal conditions, which is consistent with the morphology images (Figure VII.4a). There is also and increase on their metabolic activity (day 7 versus day 21). However, under osteogenic conditions BM-MSCs did not proliferate and exhibited an increase in metabolic activity (day 7 versus day 21), which suggested the occurrence of differentiation [8, 45]. PLLA and PLLA-BBG-Sr electrospun membranes were found to be a non-cytotoxic support for BM-MSCs attachment and proliferation (Figure VII.4) without any adverse effect caused by the addition of BBG-Sr particles. In addition, the randomly distributed fibres and porous structure of electrospun membranes should enable an efficient transfer of nutrients, as well as support suitable cell penetration into the bulk of the membranes.

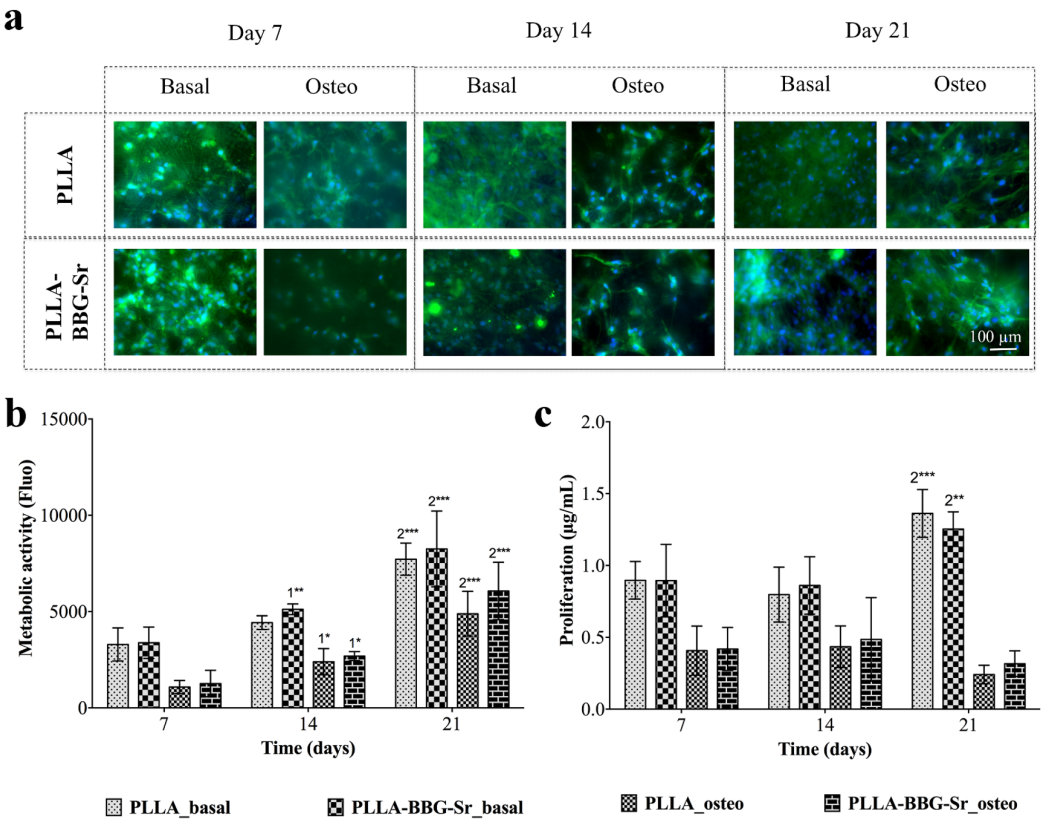

Figure VII.4 - (a) Morphology, (b) metabolic activity and (c) proliferation of BM-MSCs cultured for 7, 14 and 21 days in basal (basal) or osteogenic medium (osteo), and in the

presence of PLLA or PLLA-BBG-Sr. In the representative microscopy images (a) the nuclei of cells are stained in blue (DAPI) and the actin filaments are stained in green (Phalloidin). In Figure VII.4b and 4c, the results are expressed as means ± SD with n = 3 for each experimental data point. The data were analysed by non-parametric statistics: Kruskal-Wallis test, followed by a Dunn's multiple comparison test and were marked as: *** $p<0.001$; $^{**}p<0.01$; * $p<0.05$. On the graphs the figure '1' represents the comparison with day 7 and the figure '2' represents the comparison with day 14.

3.4. Osteogenic differentiation markers

It has been demonstrated that the release of chemical species containing Si, B or Sr from BBG-Sr glass particles could stimulate the osteoblast proliferation and differentiation. The ALP activity is commonly related with functional activity of the bone-derived cells, such as their osteogenic differentiation and the onset of mineralisation [36, 46]. In order to execute a preliminary evaluation on the capacity of the PLLA-BBG-Sr membranes to induce osteogenic differentiation, we cultured BM-MSCs onto them and quantified the ALP activity after 7, 14 and 21 days (Figure VII.5b). SEM was also used to check for mineral deposits and the mineralisation stage of the BM-MSCs (Figure VII.5a). In the SEM micrographs it is possible to confirm that the BM-MSCs create a cell layer attached to the PLLA and PLLA-BBG-Sr membranes. In the case of BM-MSCs cultured under osteogenic conditions, formation of phosphate deposits at the later time points (Figure VII.5a, day 21) were observed. In contrast, ALP activity (Figure VII.5b) of cells cultured in PLLA-Sr membranes increased during the time of culture under osteogenic conditions, suggesting that the addition of BBG-Sr microparticles increased the ALP expression levels. Therefore, the PLLA-BBG-Sr membranes stimulated the BM-MSCs to initiate their osteogenic differentiation. This stimulus is very likely to be related with the presence of the B, Si and Sr chemical species leached from the BBG-Sr glass particles to the surrounding medium [47, 48], as also shown in the ICP data (Figure VII.3a). Comparatively, some authors [31, 32] studied the effect of the release of Si and Sr chemical species from BG, and found that they stimulate cell differentiation. Other authors have also demonstrated improvements in cell differentiation and bone mineralisation by the addition of glass particles into polymeric matrices [6, 36, 49]. As an example, Santocildes-Romero [9], fabricated electrospun membranes incorporating 10% BGSr glass particles

with increasing Sr content with no cytotoxic effects on osteosarcoma cells; Rajzer and co-workers [36] verified that the addition of 20% HA ceramic particles into PDLL electrospun composites could direct HA mineralisation in cell culture; Ren *et al.* [6] also showed that PCL-SrBG electrospun scaffolds enhanced the ALP activity of MC3T3-E1 cells in the presence of osteogenic media in comparison with the glass-free PCL scaffolds after 21 days of culture. Hence, the addition of BBG-Sr glass particles to PLLA fibres accelerated the BM-MSCs osteogenic differentiation (ALP activity, Figure VII.5b), in the presence of osteogenic media after 14 days of cell culture, showing higher increase after 21 days of cell culture.

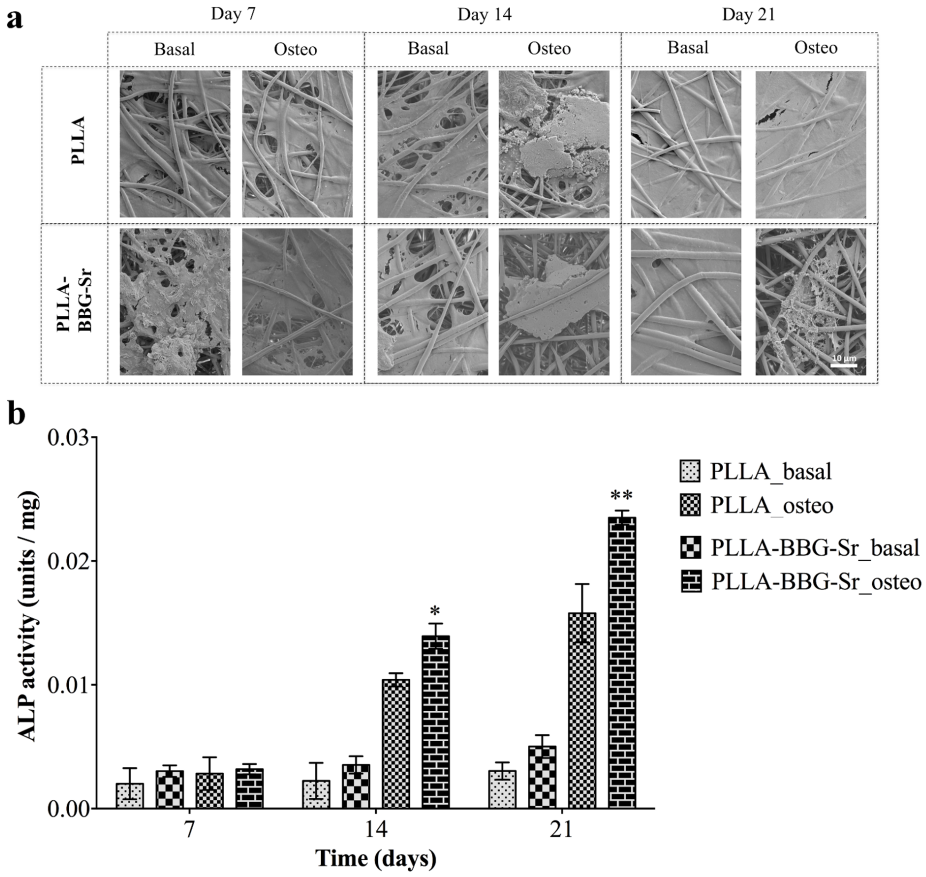

Figure VII.5 - (a) Morphology/mineralisation (SEM micrographs) of BM-MSCs and their (b) ALP activity after 7, 14 and 21 days of culture in the presence of PLLA and PLLA-BBG-Sr, in basal (basal) or osteogenic medium (osteo). ALP results are expressed as mean ± SD with n = 3 for each datapoint. The data was analysed by non-parametric statistics: Kruskal-Wallis test, followed by a Dunn's multiple comparison test. **

(p<0.01); * (p<0.05). The significance is in relation to cells cultured on PLLA (in the absence of BBG-Sr glass particles) under the same culture conditions.

Complementary to the reported viability, proliferation and ALP activity data, the differentiation level of BM-MSCs cultured onto PLLA and PLLA-BBG-Sr membranes was assessed by quantitative PCR of selected bone-specific gene transcripts. In the literature it is well described that osteogenic differentiation of BM-MSCs has three phases: the proliferative phase, which is followed by the ECM synthesis and maturation, and lastly the mineralisation phase [50, 51]. Therefore, in this study the osteogenic potential of the cells was evaluated at day 14 and 21 using the expression pattern of the representative osteogenic markers: *Alpl*, *Spp1*, *Bglap* and *Sp7* [8, 52]. The transcripts expression data were normalised against the housekeeping gene *Gapdh* and the quantification performed according to the Livak method ($2^{-\Delta\Delta Ct}$ method), considering the PLLA (basal medium) as calibrator for PLLA (osteogenic medium) and PLLA-BBG-Sr (basal medium) as calibrator for PLLA-BBG-Sr (osteogenic medium). Commonly, *Alpl* acts as early marker of the osteoblastic phenotype. This gene expression level is known to increase with the progression of osteoblastic differentiation [53]. According to the gene expression data (Figure VII.6a) there is a significant up-regulation of *Alpl* in the BM-MSCs cultured onto PLLA-BBG-Sr membranes at 14 and 21 days of culture in relation to BM-MSCs cultured onto PLLA membranes (all under osteogenic medium). Again, Ren *et al.* found the same *Alpl* gene up regulated in MC3T3 cells cultured in PCL-SrBG membranes, but only after 21 days of culture. These observations are consistent with the quantification of the ALP activity (Figure VII.5b), in which there was a significantly higher activity for the BM-MSCs cultured onto PLLA-BBG-Sr (under osteogenic medium) after 14 days of culture, when compared with the cells cultured onto PLLA [47, 48]. Regarding the maturation and mineralisation phase, we investigated the expression of the genes that encode two non-collagenous proteins present with the ECM of bone, e.g. *Spp1* and *Bglap*. *Spp1* is a protein found in bone, teeth, kidneys and epithelial lining tissue; consequently, *Spp1* cannot be considered bone-specific, although it is associated to bone related functions [8, 45]. The *Spp1* gene expression results (Figure VII.6b) showed that at 14 days of culture, BM-MSCs cultured on PLLA presents a high *Spp1* expression, which might be related with their important functions in cell adhesion, migration and survival [53]. The fact that *Spp1* expression is significantly higher when cultured on PLLA membranes might be a result of proliferation and cell spreading processes. On the other hand, *Bglap*,

which is the second most abundant protein present in bone, is exclusively secreted by osteoblastic cells at the last stage of maturation [45, 53]. When cultured on PLLA-BBG-Sr membranes, *Bglap* expression (Figure VII.6c) is significantly higher in relation to the basal medium for 14 and 21 days of culture. This suggests that the combined effect of the osteogenic factors and the dissolution products might be enhancing *Bglap* gene expression, which may be an indicator of osteoblastic differentiation. This data is in accordance with the report of Strobel *et al*. [54] showing that BM-MSCs, after 14 days of exposure to cell culture medium containing nanoparticles of Sr-substituted bioglass, increased their *Bglap* expression. Finally, *Sp7* is a well-characterised osteoblast specific gene and it is associated with the regulation of numerous other genes (e.g. osteocalcin, osteopontin, bone sialoprotein), and is acknowledged as a late bone marker that plays a key role in the differentiation of preosteoblasts into fully functioning osteoblasts [8, 53]. Our data at day 21 registered an increase of *Sp7* gene expression in the BM-MSCs cultured on PLLA-BBG-Sr membranes (under osteogenic medium) in relation to the same cells cultured on the same membranes but under basal medium, as well as the cells cultured onto PLLA (under osteogenic and basal medium). These observations are consistent with the overexpression of the other monitored gene *Alpl* and their protein expression (ALP) for PLLA-BBG-Sr membrane [55]. In fact, Isaac *et al*. [56] demonstrated that the addition of strontium to BG particles resulted in a significant up-regulation of Runx2 and Osterix of osteoblastic cells. In summary, the detected overexpression of *Alpl, Bglap* and *Sp7* genes in cells cultured onto PLLA-BBG-Sr membranes show that the incorporation of BBG-Sr glass particles into the PLLA membranes promotes the osteogenic differentiation of BM-MSCs [47].

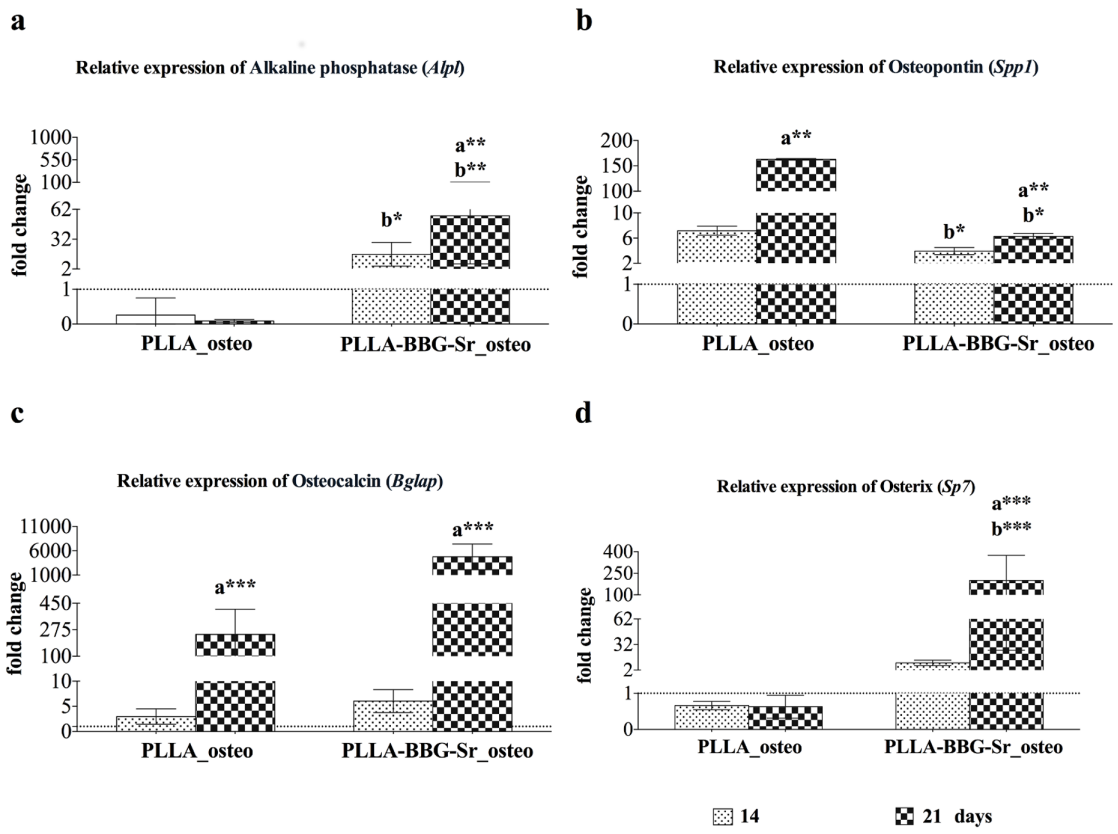

Figure VII.6 - Relative gene expression profile of BM-MSCs cultured onto PLLA and PLLA-BBG-Sr membranes during 14 and 21 days. Selected genes: *Alpl,* osteogenic mineralisation initiators (a); *Spp1 (b)* and *Bglap (c)*, extracellular matrix; *Sp7* (d), transcription factors. The transcripts' expression data were normalised against the housekeeping gene *Gapdh* and the quantification performed according to the Livak method ($2^{-\Delta\Delta Ct}$ method). For each timepoint it was used: the calibrator PLLA (in basal medium) for the experiments with PLLA (in osteogenic medium); and the calibrator PLLA-BBG-Sr (in basal medium) for the experiments with PLLA-BBG-Sr (in osteogenic medium). In all the cases the calibrator is represented as a dashed line (threshold = 1). The results are expressed as mean ± SD with n = 3 for each bar. The data was analysed by non-parametric statistics: Kruskal-Wallis test, followed by a Dunn's multiple comparison test and differences were considered: *** $p<0.001$; ** $p<0.01$; and * $p<0.05$. *a* denotes significant differences in relation to cells cultured in basal medium (PLLA or PLLA-BBG-Sr); *b* denotes significant differences in relation to cell cultured onto PLLA in osteogenic medium.

4. Conclusions

Bioactive membranes of PLLA-BBG-Sr composites were successfully prepared using electrospinning. The μCT data evidenced that BBG-Sr microparticles were homogeneously incorporated into the fibres and the membrane structure. Our data indicated that, the addition of BBG-Sr into the PLLA matrix improved the *in vitro* water uptake and degradability of the membranes. Moreover, the incorporation of the BBG-Sr microparticles improved the mechanical properties of the membranes, namely in their Young modulus and tensile strength. The *in vitro* biological evaluation confirmed that both PLLA and PLLA-BBG-Sr membranes are able to promote the attachment of BM-MSCs, without any cytotoxic effects. Furthermore, the addition of BBG-Sr microparticles to the PLLA membranes increased the ALP activity (under osteogenic conditions), as well as the BM-MSCs osteogenic differentiation as shown by up-regulation of *Alpl*, *Sp7* and *Bglap* gene expression *in vitro*. The present work suggests that the composite of PLLA membranes and BBG-Sr microparticles can be used as a strategy to prepare bioactive composite membranes for bone regeneration.

References

(1) Zhao, S.; Zhu, M.; Zhang, J.; Zhang, Y.; Liu, Z.; Zhu, Y.; Zhang, C., Three dimensionally printed mesoporous bioactive glass and poly(3-hydroxybutyrate-co-3-hydroxyhexanoate) composite scaffolds for bone regeneration. *Journal of Materials Chemistry B* **2014,** 2, (36), 6106-6118.

(2) Jiang, T.; Carbone, E. J.; Lo, K. W. H.; Laurencin, C. T., Electrospinning of polymer nanofibers for tissue regeneration. *Progress in Polymer Science* **2015,** 46, 1-24.

(3) Gentile, P.; Chiono, V.; Carmagnola, I.; Hatton, P. V., An Overview of Poly(lactic-co-glycolic) Acid (PLGA)-Based Biomaterials for Bone Tissue Engineering. *International Journal of Molecular Sciences* **2014,** 15, (3), 3640-3659.

(4) Sui, G.; Yang, X.; Mei, F.; Hu, X.; Chen, G.; Deng, X.; Ryu, S., Poly-L-lactic acid/hydroxyapatite hybrid membrane for bone tissue regeneration. *Journal of Biomedical Materials Research Part A* **2007,** 82A, (2), 445-454.

(5) Madhavan Nampoothiri, K.; Nair, N. R.; John, R. P., An overview of the recent developments in polylactide (PLA) research. *Bioresource Technology* **2010,** 101, (22), 8493-8501.

(6) Ren, J.; Blackwood, K. A.; Doustgani, A.; Poh, P. P.; Steck, R.; Stevens, M. M.; Woodruff, M. A., Melt-electrospun polycaprolactone-strontium substituted bioactive glass scaffolds for bone regeneration. *Journal of Biomedical Materials Research Part A* **2013**, n/a-n/a.

(7) Gupta, B.; Revagade, N.; Hilborn, J., Poly(lactic acid) fiber: An overview. *Progress in Polymer Science* **2007,** 32, (4), 455-482.

(8) Martins, A.; Duarte, A. R. C.; Faria, S.; Marques, A. P.; Reis, R. L.; Neves, N. M., Osteogenic induction of hBMSCs by electrospun scaffolds with dexamethasone release functionality. *Biomaterials* **2010,** 31, (22), 5875-5885.

(9) Santocildes-Romero, M. E.; Goodchild, R. L.; Hatton, P. V.; Crawford, A.; Reaney, I. M.; Miller, C. A., Preparation of Composite Electrospun Membranes Containing Strontium-Substituted Bioactive Glasses for Bone Tissue Regeneration. *Macromolecular Materials and Engineering* **2016**, n/a-n/a.

(10) Haimi, S.; Suuriniemi, N.; Haaparanta, A.-M.; Ellä, V.; Lindroos, B.; Huhtala, H.; Räty, S.; Kuokkanen, H.; Sándor, G. K.; Kellomäki, M.; Miettinen, S.; Suuronen, R., Growth and Osteogenic Differentiation of Adipose Stem Cells on PLA/Bioactive Glass and PLA/β-TCP Scaffolds. *Tissue Engineering Part A* **2008,** 15, (7), 1473-1480.

(11) Bhakta, S.; Faira, P.; Salata, L.; de Oliveira Neto, P.; Miller, C.; van Noort, R.; Reaney, I.; Brook, I.; Hatton, P., Determination of relative *in vivo* osteoconductivity of modified potassium fluorrichterite glass–ceramics compared with 45S5 bioglass. *Journal of Materials Science: Materials in Medicine* **2012,** 23, (10), 2521-2529.

(12) Hench, L., The story of Bioglass. *Journal of Materials Science: Materials in Medicine* **2006,** 17, (11), 967-978.

(13) Mofokeng, J. P.; Luyt, A. S., Morphology and thermal degradation studies of melt-mixed poly(lactic acid) (PLA)/poly(ε-caprolactone) (PCL) biodegradable polymer blend nanocomposites with TiO2 as filler. *Polymer Testing* **2015,** 45, 93-100.

(14) Carrasco, F.; Pagès, P.; Gámez-Pérez, J.; Santana, O. O.; Maspoch, M. L., Processing of poly(lactic acid): Characterization of chemical structure, thermal stability and mechanical properties. *Polymer Degradation and Stability* **2010,** 95, (2), 116-125.

(15) Niu, Y.; Guo, L.; Liu, J.; Shen, H.; Su, J.; An, X.; Yu, B.; Wei, J.; Shin, J.-W.; Guo, H.; Ji, F.; He, D., Bioactive and degradable scaffolds of the mesoporous bioglass and poly(l-lactide) composite for bone tissue regeneration. *Journal of Materials Chemistry B* **2015,** 3, (15), 2962-2970.

(16) Hench, L. L., Bioceramics: From Concept to Clinic. *Journal of the American Ceramic Society* **1991,** 74, (7), 1487-1510.

(17) Barros, A. A. A.; Alves, A.; Nunes, C.; Coimbra, M. A.; Pires, R. A.; Reis, R. L., Carboxymethylation of ulvan and chitosan and their use as polymeric components of bone cements. *Acta Biomaterialia* **2013,** 9, (11), 9086-9097.

(18) Gomes, F. O.; Pires, R. A.; Reis, R. L., Aluminum-free glass-ionomer bone cements with enhanced bioactivity and biodegradability. *Materials Science and Engineering: C* **2013,** 33, (3), 1361-1370.

(19) Rabiee, S. M.; Nazparvar, N.; Azizian, M.; Vashaee, D.; Tayebi, L., Effect of ion substitution on properties of bioactive glasses: A review. *Ceramics International* **2015,** 41, (6), 7241-7251.

(20) Rahaman, M. N.; Day, D. E.; Sonny Bal, B.; Fu, Q.; Jung, S. B.; Bonewald, L. F.; Tomsia, A. P., Bioactive glass in tissue engineering. *Acta Biomaterialia* **2011,** 7, (6), 2355-2373.

(21) Pan, H. B.; Zhao, X. L.; Zhang, X.; Zhang, K. B.; Li, L. C.; Li, Z. Y.; Lam, W. M.; Lu, W. W.; Wang, D. P.; Huang, W. H.; Lin, K. L.; Chang, J., Strontium borate glass: potential biomaterial for bone regeneration. *Journal of The Royal Society Interface* **2010,** 7, (48), 1025-1031.

(22) Huang, W.; Day, D.; Kittiratanapiboon, K.; Rahaman, M., Kinetics and mechanisms of the conversion of silicate (45S5), borate, and borosilicate glasses to hydroxyapatite in dilute phosphate solutions. *Journal of Materials Science: Materials in Medicine* **2006,** 17, (7), 583-596.

(23) Pires, R. A.; Abrahams, I.; Nunes, T. G.; Hawkes, G. E., Multinuclear magnetic resonance studies of borosilicate glasses for use in glass ionomer cements: incorporation of CaO and Al2O3. *Journal of Materials Chemistry* **2006,** 16, (24), 2364-2373.

(24) Pires, R. A.; Abrahams, I.; Nunes, T. G.; Hawkes, G. E., The role of alumina in aluminoborosilicate glasses for use in glass-ionomer cements. *Journal of Materials Chemistry* **2009,** 19, (22), 3652-3660.

(25) Wang, H.; Zhao, S.; Xiao, W.; Xue, J.; Shen, Y.; Zhou, J.; Huang, W.; Rahaman, M. N.; Zhang, C.; Wang, D., Influence of Cu doping in borosilicate bioactive glass and the properties of its derived scaffolds. *Materials Science and Engineering: C* **2016,** 58, 194-203.

(26) Fernandes, J. S.; Martins, M.; Neves, N. M.; Fernandes, M. H. F. V.; Reis, R. L.; Pires, R. A., Intrinsic Antibacterial Borosilicate Glasses for Bone Tissue Engineering Applications. *ACS Biomaterials Science & Engineering* **2016**.

(27) Marie, P. J.; Ammann, P.; Boivin, G.; Rey, C., Mechanisms of Action and Therapeutic Potential of Strontium in Bone. *Calcified Tissue International* **2001,** 69, (3), 121-129.

(28) Hoppe, A.; Güldal, N. S.; Boccaccini, A. R., A review of the biological response to ionic dissolution products from bioactive glasses and glass-ceramics. *Biomaterials* **2011,** 32, (11), 2757-2774.

(29) Hesaraki, S.; Gholami, M.; Vazehrad, S.; Shahrabi, S., The effect of Sr concentration on bioactivity and biocompatibility of sol–gel derived glasses based on CaO–SrO–SiO2–P2O5 quaternary system. *Materials Science and Engineering: C* **2010,** 30, (3), 383-390.

(30) Wu, C.; Fan, W.; Gelinsky, M.; Xiao, Y.; Simon, P.; Schulze, R.; Doert, T.; Luo, Y.; Cuniberti, G., Bioactive SrO–SiO2 glass with well-ordered mesopores: Characterization, physiochemistry and biological properties. *Acta Biomaterialia* **2011,** 7, (4), 1797-1806.

(31) Santocildes-Romero, M. E.; Crawford, A.; Hatton, P. V.; Goodchild, R. L.; Reaney, I. M.; Miller, C. A., The osteogenic response of mesenchymal stromal cells to strontium-substituted bioactive glasses. *Journal of Tissue Engineering and Regenerative Medicine* **2015,** 9, (5), 619-631.

(32) Gentleman, E.; Fredholm, Y. C.; Jell, G.; Lotfibakhshaiesh, N.; O'Donnell, M. D.; Hill, R. G.; Stevens, M. M., The effects of strontium-substituted bioactive glasses on osteoblasts and osteoclasts *in vitro*. *Biomaterials* **2010,** 31, (14), 3949-3956.

(33) Brooke, G.; Cook, M.; Blair, C.; Han, R.; Heazlewood, C.; Jones, B.; Kambouris, M.; Kollar, K.; McTaggart, S.; Pelekanos, R.; Rice, A.; Rossetti, T.; Atkinson, K., Therapeutic applications of mesenchymal stromal cells. *Seminars in Cell & Developmental Biology* **2007,** 18, (6), 846-858.

(34) Maniatopoulos, C.; Sodek, J.; Melcher, A. H., Bone formation *in vitro* by stromal cells obtained from bone marrow of young adult rats. *Cell Tissue Research* **1988,** 254, (2), 317-330.

(35) Livak, K. J.; Schmittgen, T. D., Analysis of Relative Gene Expression Data Using Real-Time Quantitative PCR and the 2−ΔΔCT Method. *Methods* **2001,** 25, (4), 402-408.

(36) Rajzer, I.; Menaszek, E.; Kwiatkowski, R.; Chrzanowski, W., Bioactive nanocomposite PLDL/nano-hydroxyapatite electrospun membranes for bone tissue engineering. *Journal of Materials Science: Materials in Medicine* **2014,** 25, (5), 1239-1247.

(37) Chan, B. P.; Leong, K. W., Scaffolding in tissue engineering: general approaches and tissue-specific considerations. *European Spine Journal* **2008,** 17, (Suppl 4), 467-479.

(38) Liang, S.-L.; Cook, W. D.; Thouas, G. A.; Chen, Q.-Z., The mechanical characteristics and *in vitro* biocompatibility of poly(glycerol sebacate)-Bioglass® elastomeric composites. *Biomaterials* **2010,** 31, (33), 8516-8529.

(39) Thomas, V.; Jagani, S.; Johnson, K.; Jose, M. V.; Dean, D. R.; Vohra, Y. K.; Nyairo, E., Electrospun Bioactive Nanocomposite Scaffolds of Polycaprolactone and Nanohydroxyapatite for Bone Tissue Engineering. *Journal of Nanoscience and Nanotechnology* **2006,** 6, (2), 487-493.

(40) Jeong, S. I.; Ko, E. K.; Yum, J.; Jung, C. H.; Lee, Y. M.; Shin, H., Nanofibrous Poly(lactic acid)/Hydroxyapatite Composite Scaffolds for Guided Tissue Regeneration. *Macromolecular Bioscience* **2008,** 8, (4), 328-338.

(41) Shakya, A. K.; Holmdahl, R.; Nandakumar, K. S.; Kumar, A., Polymeric cryogels are biocompatible, and their biodegradation is independent of oxidative radicals. *Journal of Biomedical Materials Research Part A* **2014,** 102, (10), 3409-3418.

(42) Liao, G.; Jiang, S.; Xu, X.; Ke, Y., Electrospun aligned PLLA/PCL/HA composite fibrous membranes and their *in vitro* degradation behaviors. *Materials Letters* **2012,** 82, 159-162.

(43) Navarro, M.; Ginebra, M. P.; Planell, J. A.; Barrias, C. C.; Barbosa, M. A., *In vitro* degradation behavior of a novel bioresorbable composite material based on PLA and a soluble CaP glass. *Acta Biomaterialia* **2005,** 1, (4), 411-419.

(44) Zonari, A.; Novikoff, S.; Electo, N. R. P.; Breyner, N. M.; Gomes, D. A.; Martins, A.; Neves, N. M.; Reis, R. L.; Goes, A. M., Endothelial Differentiation of Human Stem Cells Seeded onto Electrospun Polyhydroxybutyrate/Polyhydroxybutyrate-Co-Hydroxyvalerate Fiber Mesh. *PLoS ONE* **2012,** 7, (4), e35422.

(45) Amorim, S.; Martins, A.; Neves, N. M.; Reis, R. L.; Pires, R. A., Hyaluronic acid/poly-l-lysine bilayered silica nanoparticles enhance the osteogenic differentiation of human mesenchymal stem cells. *Journal of Materials Chemistry B* **2014,** 2, (40), 6939-6946.

(46) Marie, P. J.; Fromigué, O., Osteogenic differentiation of human marrow-derived mesenchymal stem cells. *Regenerative Medicine* **2006,** 1, (4), 539-548.

(47) Peng, S.; Zhou, G.; Luk, K. D. K.; Cheung, K. M. C.; Li, Z.; Lam, W. M.; Zhou, Z.; Lu, W. W., Strontium Promotes Osteogenic Differentiation of Mesenchymal Stem Cells Through the Ras/MAPK Signaling Pathway. *Cellular Physiology and Biochemistry* **2009,** 23, (1-3), 165-174.

(48) Yang, F.; Yang, D.; Tu, J.; Zheng, Q.; Cai, L.; Wang, L., Strontium Enhances Osteogenic Differentiation of Mesenchymal Stem Cells and *In Vivo* Bone Formation by Activating Wnt/Catenin Signaling. *STEM CELLS* **2011,** 29, (6), 981-991.

(49) Kim, H.-W.; Lee, H.-H.; Knowles, J. C., Electrospinning biomedical nanocomposite fibers of hydroxyapatite/poly(lactic acid) for bone regeneration. *Journal of Biomedical Materials Research Part A* **2006,** 79A, (3), 643-649.

(50) Reis, A. M. S.; Ribeiro, L. G. R.; Ocarino, N. d. M.; Goes, A. M.; Serakides, R., Osteogenic potential of osteoblasts from neonatal rats born to mothers treated with caffeine throughout pregnancy. *BMC Musculoskeletal Disorders* **2015,** 16, (1), 1-11.

(51) zur Nieden, N. I.; Kempka, G.; Ahr, H. J., *In vitro* differentiation of embryonic stem cells into mineralized osteoblasts. *Differentiation* **2003,** 71, (1), 18-27.

(52) Munisso, M. C.; Kang, J.-H.; Tsurufuji, M.; Yamaoka, T., Cilomilast enhances osteoblast differentiation of mesenchymal stem cells and bone formation induced by bone morphogenetic protein 2. *Biochimie* **2012,** 94, (11), 2360-2365.

(53) Ashammakhi, N.; Reis, R.; Chiellini, E., Chapter 13: Genes and Proteins Involved in the Regulation of Osteogenesis. In *Topics in Tissue Engineering*, G., K.; S., C.; N., A., Eds. 2007; Vol. 3.

(54) Strobel, L. A.; Hild, N.; Mohn, D.; Stark, W. J.; Hoppe, A.; Gbureck, U.; Horch, R. E.; Kneser, U.; Boccaccini, A. R., Novel strontium-doped bioactive glass nanoparticles enhance proliferation and osteogenic differentiation of human bone marrow stromal cells. *Journal of Nanoparticle Research* **2013,** 15, (7), 1-9.

(55) Tu, Q.; Valverde, P.; Chen, J., Osterix enhances proliferation and osteogenic potential of bone marrow stromal cells. *Biochemical and biophysical research communications* **2006,** 341, (4), 1257-1265.

(56) Isaac, J.; Nohra, J.; Isaac, J.; Jallot, E.; JNedelec, J.; Berdal, A.; Sautier, J., Effects of strontium-doped bioactive glass on the differentiation of cultured osteogenic cells. *European Cells and Materials* **2011,** 21, (2011), 130-143.

4. SECTION

VIII. CHAPTER

General Conclusions and Final Remarks

VIII. CHAPTER

General Conclusions and Final Remarks

Degenerative and inflammatory joint and bone diseases, including osteoporosis, anorexia nervosa, rheumatoid arthritis affects millions of people worldwide. Due to its nature, bone diseases often require surgical intervention with partial or total bone removal, which causes severe limitations to the patient's life. In addition, accidents may require the removal of a significant volume of bone fragments that compromise its complete regeneration. Under these medical scenarios it is necessary to provide a scaffold for the bone tissue to regenerate and recover its functionality, usually refereed as a bone tissue engineering (BTE) strategy. Therefore, medical devices for BTE must be designed to be degradable upon implantation, functioning as a short-term template while bone defects regenerate. More recently, the huge numbers of joint and bone surgeries parallels that to medical-device associated infections (MDAI), which often results in the failure of the medical devices. Moreover, the prescription of intravenous or oral antibiotic therapies after bone and joint surgeries have been increasing in number and time of treatment; while the risk of the wide spreading of antibiotic-resistance bacteria are increasing.

This thesis was outlined to address these problems through the development of glass and glass-biodegradable matrix composites with multifunctional properties to address the pressing clinical needs in orthopaedic surgeries. The driving force behind this thesis was to prevent or reduce MDAI, through the appropriate design of the materials that are used in BTE, while maintaining their capacity to promote bone regeneration. Due to its unexplored potential, the emphasis of the work was on the development of borosilicate bioactive glasses (BBGs) and their compounding into a glass-polymer composite structure. In this context, BBGs should be biologically active, strongly bonding to bone tissue. Based on the tissue engineering and regenerative medicine (TERM) concepts, the glass-polymer composites porous structures were designed to support the growth of bone cells and promote new bone formation under a complete regeneration approach. Therefore, the experimental work present in this thesis can be broadly divided into 2 main parts: 1) the design and synthesise of BBGs and extensively characterise them *in vitro*; and 2) incorporate those BBGs into a suitable polymeric matrix (PLLA), to act as a template able to support bone regeneration. Under the first part, numerous bioactive

glasses (BGs) were synthesised and screened for their bioactivity. Afterwards, the selected BBGs (i.e. Mg, Ca and Sr-containing) were studied for their biological response, antibacterial activity and osteointegrative properties, such as, the formation of a bone-like hydroxyapatite (HA) layer that is required for the establishment of a strong interfacial bond between the medical devices and the bone. BBGs are known to possess a dissolution rate compliant with the timeframe observed during bone regeneration, while including tissue bonding properties (i.e. conversion rate of HA and controlled release of potentially bioactive inorganic components). Therefore, the impact of different divalent cation (i.e. Mg^{2+}, Ca^{2+} and Sr^{2+}) in the BBGs activity was studied, relying on the possibility that they can release different ionic species that might induce a series of biological responses, such as: cell adhesion; cell proliferation; cell differentiation; and antibacterial activity. In the second part of the thesis (development of glass-polymer composite structures), the biodegradable poly-L-lactic (PLLA) was chosen as the matrix for the BBG-polymer composites, due to its ability to adjust itself to the shape of the bone defect and to support cell ingrowth, as well as the enormous approval rate of PLLA-based medical devices by the Food and Drug Administration (FDA). Regarding the type of cells used during this project, they followed a line of increasing relevance from cell lines to primary cultures of differentiated and undifferentiated cells, namely mouse lung fibroblast-like cell line (L929), human osteosarcoma cell line (SaOs-2), rat bone marrow mesenchymal stem cells (BM-MSCs) and human adipose-derived stem cells (hASCs).

Three BBG compositions of general formula $0.05Na_2O{\cdot}0.35x{\cdot}0.20B_2O_3{\cdot}0.40SiO_2$ (molar ratio, where x = MgO or CaO or SrO) were prepared by melt quenching and were investigated for the effect of crystallisation on their cytotoxicity towards L929 and SaOs-2 cells (chapters III and IV). The L929 and SaOs-2 cells actively proliferated in the presence of glass-ceramics produced from BBG at concentrations up to 50 $mg{\cdot}ml^{-1}$, supporting that a controlled BBGs crystallisation can be used to influence the biocompatibility of their glass-ceramics (Chapter III). The overall results were positive and the work was continued by the study of the fabricated BBGs regarding their antibacterial and osteogenic capacity in Chapter IV and Chapter V, respectively. In Chapter IV it is demonstrated the antibacterial potential of BBGs: BBG-Mg (9 to 72 $mg{\cdot}ml^{-1}$) exhibited bacteriostatic activity against *S. epidermidis*; while BBG-Sr was able to eradicate *P. aeruginosa* at concentrations $\geq$ 18 $mg{\cdot}ml^{-1}$. Additionally, BBGs were immersed in SBF and it was possible to confirm their ability to form their bioactivity,

with BBG-Ca and BBG-Sr exhibiting the capacity to form apatite-like structures with a cation/P ≈ 1.7 upon 7 days of immersion. In Chapter V, BM-MSCs were cultured with medium conditioned with BBGs for 21 days of culture to induce their osteogenic differentiation. An overexpression of bone-specific proteins was observed, including alkaline phosphatase (ALP), osteopontin (OP) and osteocalcim (OC), as well as a high mineralisation of BM-MSCs under BBG-Mg and BBG-Sr conditioned osteogenic media for concentrations of 20 and 50 $mg \cdot ml^{-1}$ of the glass particles. Outstandingly, BBG-Sr at a concentration of 50 $mg \cdot ml^{-1}$ showed an increase on the mineralisation and expression of ALP, OP and OC, even under basal media conditions. Moreover, when comparing BBG glasses with 45S5 bioglass® (a common standard in BTE), the results showed that both BBG-Mg and BBG-Sr promoted a higher expression of ALP, OP and OC than 45S5 bioglass®. Hence, the great performance demonstrated by the BBGs studied in Chapter III to V led us into the following step of this thesis: to fabricate a composite material of BBG glass incorporated into a PLLA matrix, that provides a structural support for cellular attachment and proliferation, and to promote the regeneration of bone. This composite was designed to present a porous structure and appropriate interconnectivity to allow cell ingrowth. Chapter VI reports the fabrication of this porous PLLA scaffolds compounded with ≈ 25% of BBGs (w/w) by wet spinning and fibre bonding techniques, endowing them with bioactive properties (PLLA-BBGs). Cellular *in vitro* studies showed that the developed fibres are not cytotoxic, as well as suitable for hASCs adhesion and cell ingrowth through the scaffolds (randomly interconnected porous with mean pore diameters higher that 100 μm). The PLLA-BBGs presented a faster degradation rate with a constant release of inorganic species, which were able to stimulate the deposition of calcium phosphate structures at the surface of the composite after 7 days of immersion in SBF (Ca/P ratio of ~1.7). Overall, we showed that the proposed scaffolds present a tailored kinetics on the release of inorganic species and controlled biological response under conditions that mimic the bone physiological environment. The results presented in Chapter VI, encouraged the selection of BBG-Sr to fabricate electrospun PLLA membranes loaded with 10% (w/w) of BBG-Sr (i.e. PLLA-BBG-Sr). In Chapter VII we evaluated the capacity of these PLLA-BBG-Sr electrospun membranes to promote the differentiation of BM-MSCs. The homogeneous incorporation of the BBG-Sr particles into the microfibres (1 to 3 μm) enhanced their mechanical properties (69% higher Young modulus and 36% higher tensile strength). It also promoted an increase in the activity of alkaline phosphatase (ALP) and up-regulated BM-MSCs osteogenic gene expression (i.e.

Alpl, *Sp7* and *Bglap*) *in vitro*. Hereupon, these results showed that the developed PLLA-BBG-Sr electrospun membranes are able to promote the osteogenic differentiation of the BM-MSCs supporting their used as a biomaterial capable of promoting bone regeneration.

The work herein described highlights the possible use of biomaterials' design (chemical, physical, morphological, etc.) to create multifunctional approaches that address several relevant aspects in the TERM strategies. Therefore, with the manipulation of the chemistry of the biomaterial, it is possible to provide predictable, local delivery of biological and biochemical cues to the site of injury, promoting faster bone regeneration. This thesis not only demonstrated that, manipulating the chemical composition of glasses it is possible to generate bioactive glass and glass-ceramics that are capable of supressing the growth of pathogenic microorganisms along with increased bone regeneration; as well as demonstrated that a synergistic combination of inorganic and polymeric biomaterials can support and guide cells through the bone differentiation process, augmenting their potential to promote bone regeneration.

This thesis reports a significant progress in the development of multifunctional biomaterials able to combine antibacterial activity and bone regeneration capacity. However, many crucial challenges remain before the developed biomaterials become a clinical reality. The ability of the glasses or glass/polymer composites to induce blood vessel formation at the defect site is essential for a perfect vascularisation and faster healing. Future studies can be done either by studying the incorporation of other ions species related with vascularisation process or by grafting growth factors directly on the scaffold surface to promote the vascularisation on site. It is also relevant to validate the PLLA-BBG systems under clinical application, by performing *in vivo* studies. Newly developed medical devices must be assessed for the requirements of biocompatibility, mechanical stability and safety prior to be used clinically. The most characteristic and promising feature of the proposed glasses and multifunctional composites is the ability to tailor different properties in one single device. It is thus expected that the multifunctional composite structures incorporating BBG microparticles will find great applicability in the complex domain of BTE.